The effect of atmospheric turbulence on the performance of terrestrial digital optical line of sight communication systems.

Thesis

THE EFFECT OF ATMOSPHERIC TURBULENCE ON THE PERFORMANCE OF TERRESTRIAL DIGITAL OPTICAL LINE OF SIGHT COMMUNICATION SYSTEMS

by

Christopher John Lilly DMS, C.Eng, MIERE, MIEEE

A THESIS SUBMITTED TO THE FACULTY OF TECHNOLOGY,
THE OPEN UNIVERSITY
FOR THE DEGREE OF
DOCTOR OF PHILOSOPHY (Ph.D)

OCTOBER 1986

Date of Submission: October 1986
Date of Award: 24 February 1987

ABSTRACT

This thesis considers the theory, application, and design principles of atmospheric optical line of sight communication systems and in particular the effect of atmospheric turbulence on the error rate performance of digital terrestrial systems is considered in some detail. In order to aid understanding of the physical processes involved, a qualitative model is presented which is followed by a quantitative analysis and model. These models utilise the atmospheric refractive index structure parameter which is shown to be a measure of atmospheric turbulence. A hypothesis is proposed which relates the atmospheric refractive index structure parameter to the error rate performance of terrestrial optical communication systems. Practical data obtained on a typical link as part of this research work is reported which shows that there is indeed a relationship between the atmospheric refractive index parameter and error rate performance as proposed in the hypothesis. The degree of correlation of the practical data with the theory is such that the hypothesis is readily validated. Techniques for alleviating the effects of atmospheric turbulence are also considered.

HYPOTHESIS

It is contended that, whilst there are many parameters in an atmospheric digital optical communication system which will affect the overall error rate performance of the system such as path length, lens aperture diameter etc, they are invariably systematic in nature and can usually be readily taken into account in the system's design in order for a given steady-state error performance to be achieved. Increased path attenuation due to non-systematic atmospheric effects such as rain, fog, snow etc has been much studied by other workers and with the benefit of the wealth of data obtained on these effects due allowance can be made for them in the system's design. It is postulated in this thesis that another major non-systematic effect is atmospheric turbulence, which is generally measured as a function of the atmospheric refractive index structure parameter, C_n^2, which can give rise to significant variations in the error performance of the system. The thesis gives, both qualitatively and quantitatively, a relationship between the atmospheric refractive index structure parameter and the error rate performance for terrestrial digital optical communication systems having path lengths of up to about 1000m in length. The crux of the hypothesis is the proposal that the signal to noise ratio is degraded by a factor $(e^{4\sigma_x^2} - 1)$, where σ_x^2 is the log amplitude variance of the received signal which is itself related to the level of atmospheric turbulence as measured by the parameter C_n^2.

****
* CONTENTS *
****

INDEX OF FIGURES

INTRODUCTION

> "Basic research is what I am doing when I don't know what I am doing!"
>
> Wernher von Braun

The basic object of the research project presented in this thesis is to assess the effect of atmospheric turbulence on the error rate performance of terrestrial line of sight digital optical communications systems. This assessment has been carried out theoretically and a much simpler approach has been developed in Part II of this thesis compared with those adopted by other workers. In order to verify the hypothesis a practical measurement programme spanning an 18 month period has been completed which also forms part of this research project. The results are presented in Part III of this thesis.

Performance degradation of terrestrial optical line of sight digital optical communication systems can also occur as a result of effects other than atmospheric turbulence and these are addressed theoretically in Part I of this thesis.

The reason for studying the effect of atmospheric turbulence in some considerable detail is that most of the other effects which result in performance degradation are of a systematic nature and can be readily accommodated in system design calculations. The only major non-systematic effect other than atmospheric turbulence is that resulting from increased attenuation due to atmospheric conditions such as rain, fog, snow etc. These particular atmospheric conditions are discussed in this thesis, but they have been the subject of considerable study by other workers, unlike atmospheric turbulence, and hence have not been considered in any great detail in this thesis. Comprehensive references are provided for the benefit of those readers wishing to pursue these aspects further.

This thesis also considers the general principles involved in the design and application of terrestrial digital optical line of sight communication systems. The thesis will therefore enable designers and users of such systems to gain an understanding of the mechanisms giving rise to performance degradation arising from turbulence (as well as other effects) and will enable systems to be designed and/or employed with the effects of atmospheric turbulence in particular being better understood.

The thesis commences in Part I Chapter 1 with a general review of optical communication systems and then considers a generalised system model. In order to obtain an understanding of the mechanisms and effect of atmospheric turbulence at an early stage Chapter 2 proposes a qualitative model for the turbulent atmosphere. Turbulence gives rise to a number of effects in optical communications systems which include scintillation, beam spread, and beam wander. Owing to their close relationship to scintillation, which is considered in some detail in later chapters, beam spread and beam wander warrant a chapter to themselves, Chapter 3, in the hope that any confusion between the different mechanisms can be avoided at an early stage. The existing theories relating to atmospheric turbulence are reviewed in Chapter 4. Atmospheric turbulence is usually measured in terms of the refractive index structure parameter, a very important parameter which is considered in Chapter 5.

Chapter 6 in Part II contains the crux of the thesis, namely the hypothesis that error rate performance is directly linked to the magnitude of atmospheric turbulence.

In Part III the practical measurements and results carried out as part of the research work are presented. In Chapter 7 the technique employed in the measurement of the atmospheric turbulence is described together with a review of the results and in Chapter 8 measurements on an actual optical

line of sight link are described along with the results of the simultaneous measurement of the magnitude of atmospheric turbulence.

Finally, Part IV, Chapter 9 presents the conclusions from the work, and Chapter 10 makes some recommendations, and itemises some areas for further study.

The work which has constituted this research project has resulted in the investigation and study of many related and sometimes spurious avenues of activity. To have recorded every single aspect of the research work would have resulted in a massive tome comprising many volumes. The view has been taken that only the mainstream activities, together with those side issues which are especially relevant or are necessary for an adequate understanding of the main body of the thesis, are included in this text. Where appropriate, references and in some instances appendices, have been included in order to enable the interested reader to pursue these side issues should this be so desired.

The work which has culminated with the publication of this thesis commenced in the latter half of 1981 and with formal support of the Open University in early 1982. The project was undertaken as part of the professional activities of the author with the support of what is now British Telecommunications plc.

PART I

THEORY

CHAPTER 1

OPTICAL LINE OF SIGHT COMMUNICATION

CHAPTER 1

OPTICAL LINE OF SIGHT COMMUNICATION

1.1 INTRODUCTION

Optical communication has existed for many centuries. Well known examples are the use of bonfires on hilltops for the signalling of the approach of the Spanish Armada in the 16th Century and red indians' smoke signals in the Wild West. The heliograph has been widely employed, the principle of the reflexion of the sun's rays being readily utilised. Morse code principles have been applied to optical communications resulting in the well-known Aldis lamp system being widely used during the two World Wars, particularly by the Royal Navy. Alexander Graham Bell demonstrated his photophone, the first known demonstration of the transmission of speech over a beam of light as long ago as 1880 [1.1].

Some atmospheric line of sight optical communication systems employed during World War II are described by Huxford and Platt [1.2]. One such German system had a transmission range of 4.2 km and a speech band transmission capability of about 3 kHz.

Optical communication received an enormous impetus with the invention of the laser by Maiman [1.3] in 1960. Helium-neon, argon and carbon dioxide lasers have been used in a variety of practical and experimental non-guided optical communication systems, but the development of the semiconductor injection laser in 1962 [1.4] was a spur to work in this field. During the 1960s considerable research effort was expended on both guided and non-guided optical communications techniques. The work of Kao and Hockham of Standard Telecommunications Laboratories on guided wave optical communication was published in their now famous paper in 1966 [1.5]. This paper initiated the current interest in optical fibre guided-wave communication and this particular technology has now been

developed to the point where numerous operational systems have been installed [1.6] and we are already into the third generation of such systems. The design and performance of optical fibre systems is exceedingly well documented and references [1.7-1.11] provide a good overview.

Non-guided optical communication systems received considerable attention during the 1960s mainly as a result of potential military uses and applications in space. Non-guided optical communication systems do however suffer from certain drawbacks, which resulted in the systems not being fully developed nor generally deployed for terrestrial applications. The advantages and disadvantages of non-guided systems are discussed later in Section 1.3. In the main, alternative transmission techniques were employed to meet the communications requirements of the 1960s and 1970s. The level of research effort into non-guided optical communication during the 1970s has been minimal, as witnessed by the relatively small number of papers published on the subject in the last 10 years or so. Inevitably publication of a certain amount of research work funded by military agencies has had to be withheld for national security reasons, particularly in the USA.

Despite the disadvantages of non-guided optical communications systems there are a number of distinct advantages which warrant further study of the technique. Interest is currently being shown by various military agencies, particularly in the US, who have placed research contracts with major American research organisations. The current emphasis of this research appears to be in developing specialised communications links between satellites, between space shuttles and between satellites and submerged submarines [1.12-1.14].

In recent times major telecommunications network operators (eg British Telecom), in response to market pressures, have felt the need to

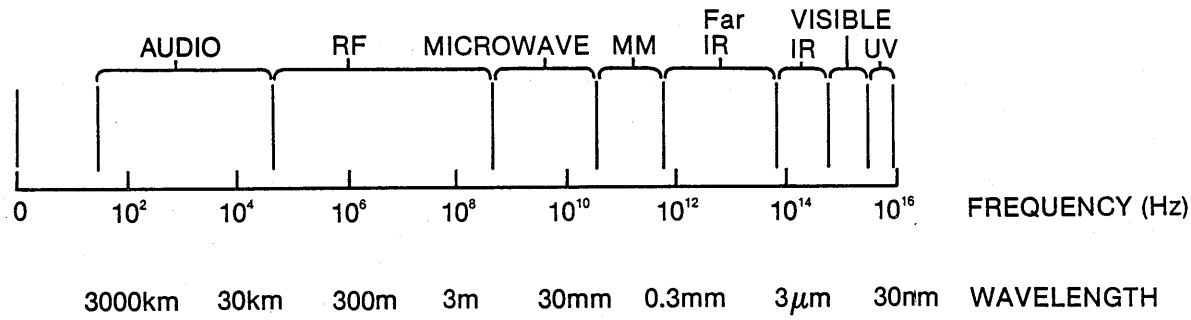

Figure 1.1 The electromagnetic spectrum

investigate various 'fringe' transmission techniques and atmospheric line of sight terrestrial optical links represent one such technique. The particular application of interest to British Telecom is the rapid provision of service to major customers without the need to instal underground cables. It is sometimes the case that the underground ducts, which would normally be used to provide service, are all full, and that the construction of new duct ways would introduce intolerable delays in the provision of service. Optical line of sight systems are thought to be a possible alternative to microwave systems in such cases where a line of sight path is available. Consequently some interest is being shown by organisations, such as British Telecom, in the development and optimisation of line of sight systems for use in particular terrestrial applications.

1.2 THE OPTICAL DOMAIN

High capacity and/or wideband transmission systems generally employ some form of electro-magnetic wave or carrier. Throughout the history of telecommunications there has been a steady trend towards the use of higher and higher carrier frequencies. The trend has applied to both landline cable systems and radio systems. The reason for this trend is simply that the traffic carrying ability of any system is directly related to the bandwidth (frequency extent) of the modulated carrier, which is generally limited to a fixed portion of the carrier frequency itself. It follows therefore that increasing the carrier frequency theoretically increases the available transmission bandwidth, and therefore the information capacity of the overall system. The electromagnetic spectrum is shown in Figure 1.1. It can be seen that the optical region extends from a frequency of 10^{12} Hz (or 1 THz) to 10^{16} Hz. An optical system having a carrier frequency of 10^{14} Hz, (corresponding approximately to a wavelength of 3 micron), would have a potentially usable bandwidth many

times greater than a microwave radio system operating at 1 GHz. Potential increases in traffic carrying ability of this order of magnitude are very attractive to systems engineers concerned with high capacity transmission. It is also worth noting that, as the operating frequency is increased the ability of antennae to collimate the beam is increased, resulting in improved overall system performance. This is discussed in more detail in Section 1.4.2 in which optical transmitter gains are discussed. These amongst other advantages, have stimulated research into all aspects of optical communications over the last two decades.

1.3 ADVANTAGES AND DISADVANTAGES OF OPTICAL COMMUNICATIONS SYSTEMS

The advantages of line of sight optical systems may be summarised as follows:-

- Potentially very high traffic capacity
- Relatively secure
- High immunity to electromagnetic interference
- No interconnecting cable rquired
- Long path lengths (in the case of free space systems)
- Complete electrical isolation
- Negligible crosstalk
- Relative ease of installation (for fixed path terrestrial links)
- High resistance to jamming
- Small equipment size

Unfortunately there are some major disadvantages associated with atmospheric optical communications which should also be noted. The most serious drawback is the effect of the atmospheric propagation path on the optical carrier wave. This arises because the sizes of the molecules and particles in the atmosphere are comparable with optical wavelengths (ie about 1 micron) resulting in propagation effects which are not found at

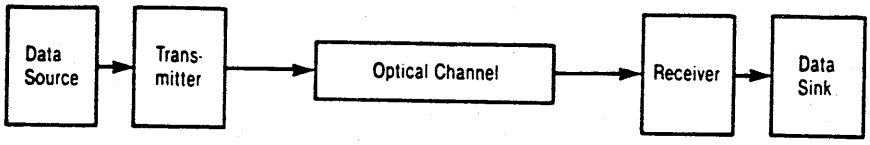

a) Basic block diagram

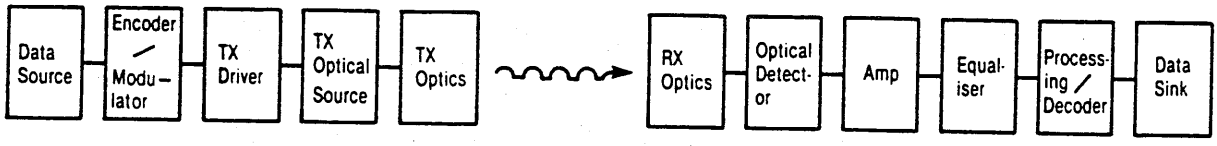

b) More detailed block diagram

Figure 1.2 System block diagrams

radio and microwave frequences (ie wavelengths of greater than about 30 mm). In particular significant fading during adverse weather conditions such as snow, rain, fog etc often results in complete loss of transmission and this thesis also shows that atmospheric turbulence can also be a major cause of system performance degradation. These effects are aggravated by the fact that they are of a random nature, both spatially and temporarily, which of course makes modelling of the propagation path much more difficult [1.16].

1.4 THE SYSTEM MODEL

1.4.1 The Basic System

A diagram of a simple system model is shown in Figure 1.2(a), in which the transmitter and a receiver are indicated, in between which is the optical communication channel. Figure 1.2(b) shows the system in somewhat more detail. In this diagram the data to be transmitted, which may be in either analogue or digital form, is fed to the encoder. In the case of a digital system the data may, in some instances, be fed directly to the transmitter driver, or it may be encoded to make it suitable for transmission over the link. The encoding techniques employed are generally aimed at maximising the signal to noise ratio at the receiver. Most of the common modulating techniques employed on any transmission system have been utilised on optical communication systems [1.15] including:-

a. frequency modulation

b. phase modulation

c. amplitude (intensity) modulation

d. polarisation modulation

The data signal, encoded as necessary, is fed to the transmitter driver which powers the transmit device (optical source) the

particular type of optical source employed depending on the particular system requirements. Both gas and semiconductor lasers have been successfully employed. Gas lasers are generally employed when high optical output power is required, eg greater than 1 mW, and when it is desired to operate at wavelengths at which there are no semiconductor sources currently available. Semiconductor laser sources have the advantage of small size and low power consumption, which makes them very attractive, particularly for portable systems. Semiconductor light emitting diodes are also employed with acceptable results, when their lower radiated optical output powers can be tolerated.

External modulation is generally needed for gas lasers but in the case of semiconductor devices the optical source converts the modulating electrical signal directly to a modulated optical signal. The optical signal is then transmitted via suitable launch optics as an optical light field or beam, through the optical channel, which in the case considered in this work, is the turbulent atmosphere.

If the optical channel were a free space channel then the signal would only be attenuated in accordance with the inverse square law [1.16] (for a divergent beam). Propagation of signals in the atmosphere however results in attenuation of the signal due to absorption, scattering and turbulence. Signal dispersion effects can normally be ignored since the dispersion for all but very high bit rate systems (operating in excess of 1 Gbit/s) is usually negligible.

The optical signal is received by the receiver optics and focussed onto a suitable detector. Associated with the receiver lens system are spatial and bandpass frequency filters which are used to minimise the effects of background illumination noise. The optical detector

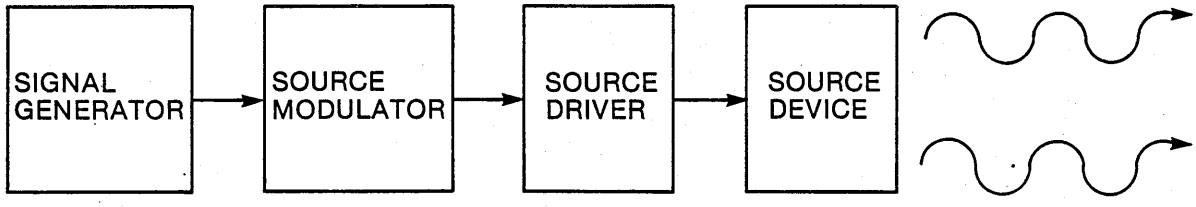

a) Direct modulation

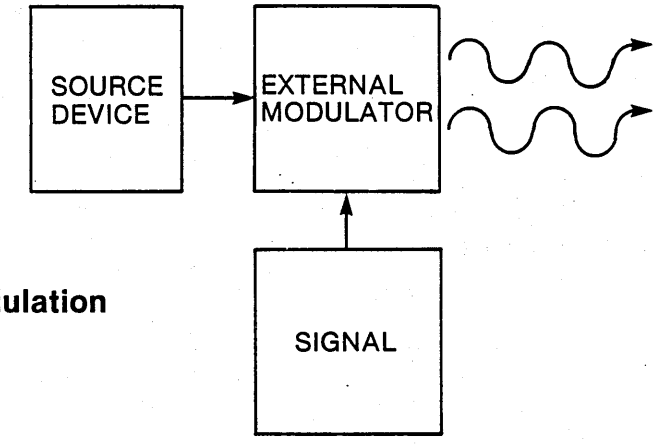

b) External modulation

Figure 1.3 Transmitter modulation techniques

can be either a semiconductor photodiode, a photomultiplier or photoconductor, and is employed to convert the optical signal back into the electrical domain. Post-detection circuitry is then used to amplify, equalise, and re-generate if necessary, the detected optical signal.

It is appropriate to consider the constituent parts of the system in more detail.

1.4.2 The Optical Transmitter

There are two basic models for optical transmitters, one for optical sources which can be directly modulated and the other for sources which are externally modulated. The two models are shown diagrammatically in Figure 1.3. The arrangement in Figure 1.3(a) is generally utilised for semiconductor sources which can be directly modulated such as semiconductor lasers and light emitting diodes. Gas lasers cannot readily be directly modulated and hence a suitable external modulator is usually employed as shown in Figure 1.3(b). The typical characteristics of the various source types are indicated in Table 1.1 below:-

Parameter	Gas Lasers	Semiconductor Lasers	Semiconductor Light emitting diodes
Wavelengths	632 nm (HeNe) 1060 nm (HeNe) 10,000 nm (CO_2)	850 nm (GaAlAs) 1300 nm (InGaAsP)	900 nm (GaAs) 1300 nm (InGaAsP)
Output power	1-500 mW	Up to 1 mW	Up to 0.5 mW
Beam shape	Circular	Oval	Circular (Burrus type)
Beam divergence	0.5-1.0 mrad	< 20 mrad	> 20 mrad
Lifetime	> 1000 hrs	> 100,000 hrs	> 100,000 hrs
Cost	£300-10,000	£300-500	£50-300

Table 1.1 Comparison of the most Common Optical Sources

Various techniques have been employed in order to provide an adequately stable optical carrier, generally employing some form of feedback arrangement with detection of the optical signal. Such detection when using gas lasers is carried out by sampling the laser output. When semiconductor lasers are employed the output from the back facet may be monitored, a technique which does not reduce the output power significantly and which can readily be incorporated into the transmitter source package.

The transmitter optics can be considered in principle in two ways. One is to adopt optical ray theory and the other is to apply the approach adopted by radio engineers in the design of antennae for radio-frequency (and in particular microwave frequency) systems. This thesis considers the former approach on the basis that it is more readily applicable although some of the results of the latter approach will be mentioned in order to highlight some salient points.

Now the transmitter is essentially a lens system as shown in Figure 1.4. In the first instance the source is assumed to be an LED having a diffuse radiation pattern and a radiating area A_S. The radiant intensity is I_o and is assumed to be constant for all the light collected by the transmitter lens. The latter has an effective area A_T and a focal length f. In order to carry out some calculations it is necessary to include the receiver with its effective aperture A_R located a distance L from the transmitter. L is of course much greater than f. In a well designed receiver all the light incident on A_R will be focussed onto the active region of the detector. Obviously in order to maximise the received power an image of the source should be formed on the plane of the receiver lens aperture.

Using basic thin lens optical theory [1.28] the distance from the source LED to the centre of the transmitter lens, u, is given by:

$$\frac{1}{u} = \frac{1}{f} - \frac{1}{L} \simeq \frac{1}{f} \tag{1.1}$$

The area of the image is given by:

$$A_{im} = \frac{A_s L^2}{u^2} \simeq \frac{A_s L^2}{f^2} \tag{1.2}$$

Now the power collected by the transmitter lens, P_T, is given by:

$$P_T = \frac{I_o A_T}{u^2} \simeq \frac{I_o A_T}{f^2} \tag{1.3}$$

Now in practice the image of the source at the receiver lens invariably more than fills the effective receiver lens operature area, A_R. The fraction of transmitted power P_T, which actually reaches the detector, is therefore given as $\frac{A_R}{A_{im}}$ and hence the received optical power, P_R, is given by:

$$P_R = \frac{P_T A_R}{A_{im}} \tag{1.4}$$

Substituting for A_{im} in this equation we obtain:

$$P_R = \frac{P_T \cdot A_R u^2}{A_s L^2} \simeq \frac{P_T \cdot A_R f^2}{A_s L^2} \tag{1.5}$$

If we now substitute for P_T we obtain:

$$P_R = \frac{I_o A_T}{u^2} \cdot \frac{A_R u^2}{A_s L^2} \simeq I_o A_T \cdot \frac{A_R}{A_s L^2} = \frac{R_s A_T A_R}{L^2} \qquad (1.6)$$

where $R_s = \frac{I_o}{A_s}$ which is the radiance of the source.

It follows from equation (1.6) that if the received optical power is to be maximised, which is the usual objective, then the source needs to be high powered and the effective lens apertures of both the transmitter and the receiver should be as large as possible.

It is useful to obtain a feel for the orders of magnitude involved and if, as an example, one takes a system having an LED with a radiance of $0.1 W/mm^2/sr$ and transmit and receive apertures of diameter 35 mm then with a path length of 1 km the receive power would be 100 nW.

Of course the derivations and calculations given thus far do not take account of any aberrations arising from imperfect optical systems, but they may be applied equally well to mirror, and mixed mirror and lens (catadioptric) systems.

Now the discussion so far has not taken any diffraction limitations into account. These can occur when the source emission area becomes less than a particular size. Diffraction patterns are produced when, for instance, an aperture is uniformly illuminated resulting in a set of concentric rings. The radius of the first ring of a diffraction pattern is given by:

$$(1.22 \lambda f/d_a) \qquad (1.7)$$

where d_a is the diameter of the aperture.

The diffraction limited situation occurs in an optical system when the radius of the first intensity minimum (ie dark ring) of the diffraction pattern becomes comparable in size with the diameter d_{im} of the normally focussed image. That is when

$$d_{im} = \frac{d_s}{u} < \frac{1.22\ \lambda\ L}{d_a} \tag{1.8}$$

where d_s is the diameter of the source.

Re-arranging equation (1.8) we obtain:

$$d_s < \frac{1.22\ u\ \lambda}{d_a} \simeq \frac{1.22\ f\ \lambda}{d_a} \tag{1.9}$$

In order to understand when the diffraction limited condition might occur in practice if one takes, as before, the example where d_T = 35 mm, λ = 1 μm and the focal length of the lens system f = 100 mm then using equation (1.9) it can be calculated that diffraction would occur only if the active source diameter was less than 3 μm. Surface emitting LEDs have active areas of tens of microns and their use is unlikely to result in diffraction limited operation. Edge-emitting LEDs with active areas of just a few microns could be subject to diffraction and the light from semiconductor lasers, being highly collimated and coherent, normally produces a diffraction limited image.

In the diffraction limited case the radiant intensity, I_o, at the centre of the diffraction pattern is given by:

$$I_o = \frac{P_T A_T}{\lambda^2} \tag{1.10}$$

The total power collected at the receiver, assuming perfect alignment, will be:

$$P_R = \frac{P_T A_T}{\lambda^2} \cdot \frac{A_R}{L^2} \tag{1.11}$$

As before this assumes a perfect system with no aberrations or optical losses. Equation (1.11) is not the complete answer because it assumes that the transmitter aperture is uniformly illuminated. In practice semiconductor lasers have an intensity distribution which is Gaussian and it can be shown that, by considering the mathematical expression for the optical power density distribution for the laser, equation (1.11) becomes, for the case of a diffraction limited laser system:

$$P_R = \frac{P_T \pi r^2}{\lambda^2} \cdot \frac{A_R}{L^2} \tag{1.12}$$

where r = radius of the power density distribution (to the 1/e points).

Comparison of equations (1.11) and (1.12) indicates that they are identical if one regards πr^2 as the effective transmitter aperture area, A_T.

The foregoing has discussed the optical approach. An alternative approach which might be used employs the principles developed for radio systems. Owing to the directionality of non-isotropic antennae each such antenna is assumed to have some measure of gain when compared with an isotropic antenna.

The optical lens system employed on optical communication links is analogous to a microwave radio antenna system in that the modulated

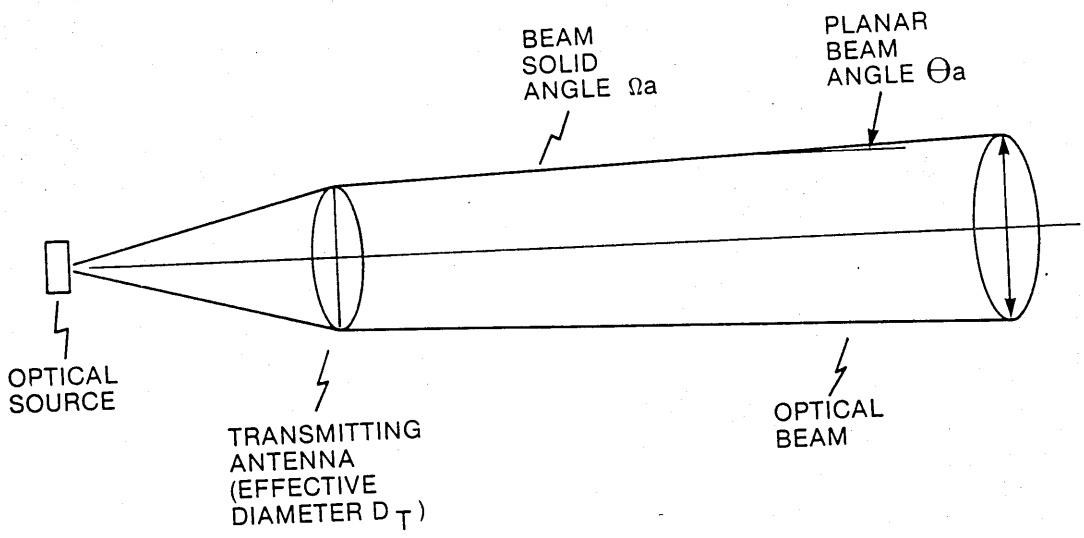

Figure 1.4 Typical transmitter optical antenna arrangement

optical carrier signal is focussed into an optical beam suitable for transmission through the optical channel. Radio-frequency principles are sometimes employed in which case the two main features used to define the performance of the optical antenna are the antenna gain, G_a, and the beam angle, Ω_a. From classical electromagnetic field theory for antennae [1.17], the antenna gain is defined by:-

$$G_a = \frac{P_{TX_{max}}}{P_{ISO}} \tag{1.13}$$

where $P_{TX_{max}}$ is the maximum power per unit solid angle radiated by the antenna and P_{ISO} is the power per unit solid angle which would be radiated by a lossless isotropic antenna with the same power applied at its terminals. It follows that if a power of P watts is available to be transmitted then, in the case of an isotropic antenna, the transmitted optical power density will be:-

$$P_{ISO} = \frac{P}{4\pi} \quad \text{watts/unit solid angle} \tag{1.14}$$

Substituting (1.14) in (1.13) we obtain:-

$$G_a = \frac{P_{TX_{max}} \cdot 4\pi}{P} \tag{1.15}$$

Simple rearrangement of (1.15) yields an expression which will assist in deriving the antenna beam angle.

$$P_{TX_{max}} = \frac{G_a \cdot P}{4\pi} \tag{1.16}$$

The beam angle Ω_a was shown in Figure 1.4, and is defined as the solid angle in steradians (measured at the antenna) into which the

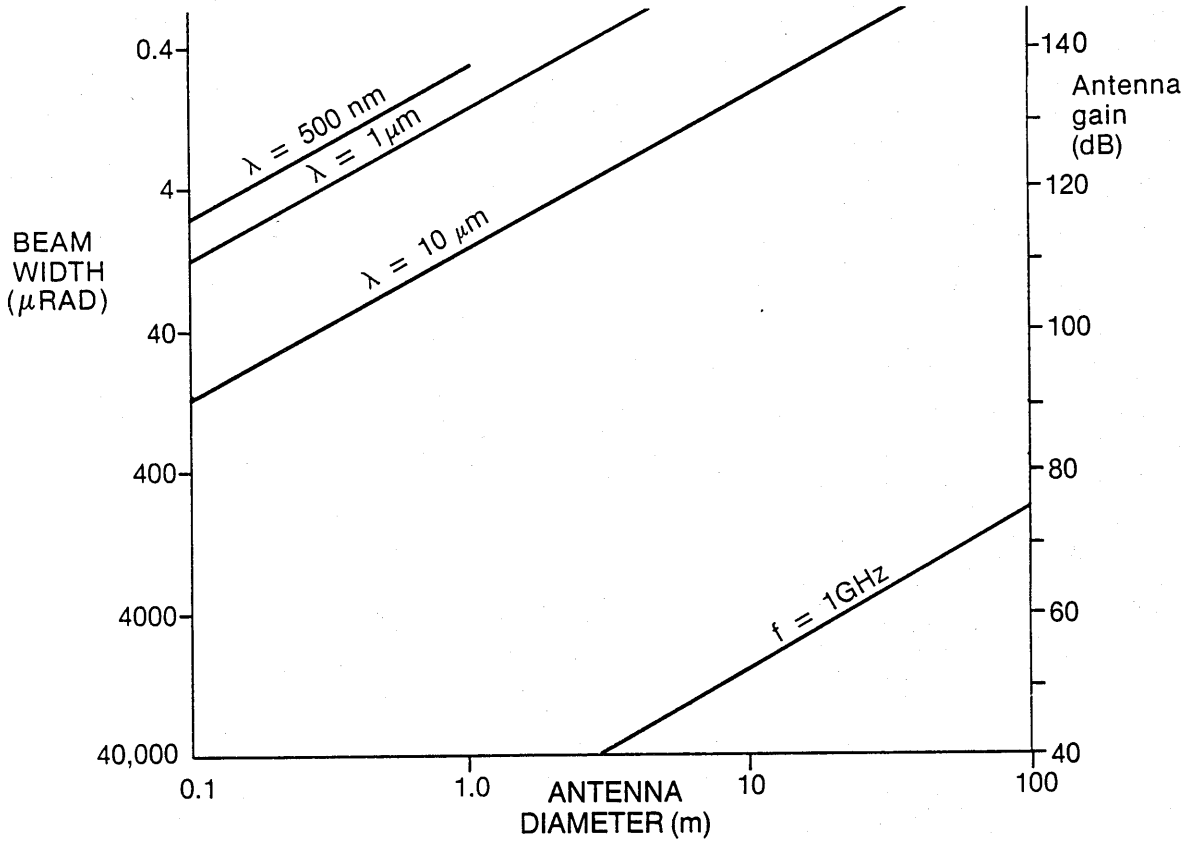

Figure 1.5 Beamwidth and antenna gain as a function of antenna diameter

(Note: 40,000 μrad = 2.2°)

maximum power density must be concentrated in order to have the same total power, P. It follows therefore using equation (1.16) that:-

$$G_a \cdot \frac{P}{4\pi} \cdot \Omega_a = P \qquad (1.17)$$

$$\text{hence} \qquad \Omega_a = \frac{4\pi}{G_a} \quad \text{steradians} \qquad (1.18)$$

Equation (1.18) indicates that the beam solid angle is inversely proportional to the antenna gain, that is the higher the antenna gain (and by definition higher directionality) the narrower the beam solid angle. It is often more convenient in design calculations to use the planar beamwidth, θ_a, as indicated in Figure 1.4. This can be derived from the complex mathematical expression for the far field pattern. On the assumption that the optical lens/aperture is circular, and has an effective diameter of d_{TX} and is diffraction limited, then an optical signal of wavelength, λ, transmitted through the antenna will have a planar 3 dB beamwidth, θ_a of approximately [1.16]:-

$$\theta_a \simeq \frac{\lambda}{d_{TX}} \text{ radians} \qquad (1.19)$$

Figure 1.5 indicates this interrelationship for typical values of λ and d_{TX} and also shows the relationship with antenna gain [1.16].

Figure 1.5 indicates that the planar beamwidth for an optical system operating at one micron and having an effective lens aperture diameter of 150 mm is about 4 μrad (microradians). This extremely narrow beamwidth is advantageous in that beam spreading due to the transmit antenna is minimal, but it does give rise to difficulties in alignment on installation of fixed terrestrial links. There are even

greater problems for extra-terrestrial links, eg, to and from (or between) satellites and aeroplanes, resulting in the need for highly sophisticated tracking equipment. The alignment problems of terrestrial fixed links can usually be minimised by employing accurately aligned telescopes incorporated in the transmitter and receiver assemblies.

It is perhaps useful to note how the radio-frequency approach is used in practice. Given the transmitter and receiver antenna gains in decibels (dBs) together with the optical channel losses (also in dBs), then simple summation of these parameters will provide the overall channel gain or loss [1.28]. This is completely analogous to the approach employed by radio systems designers.

Of the two approaches discussed above each has its merits. In practice it depends on exactly what one is requiring to calculate or prove as to which technique might actually be adopted. Whichever technique is employed a number of significant points can be clearly discerned viz:

i The larger the effective transmit aperture the narrower the beam for a given wavelength.

ii The narrower the beam the greater the receive power.

iii The narrower the beam the greater the difficulty in alignment of the transmitter and receiver.

iv The larger the effective transmit aperture the larger the antenna gain for a given wavelength.

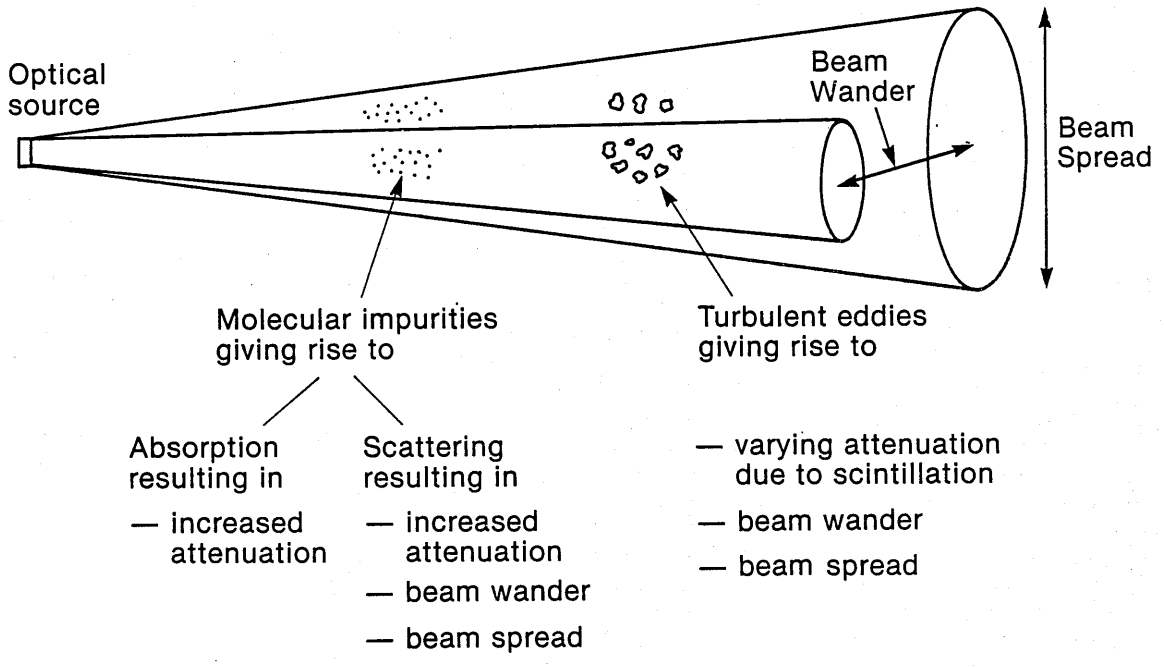

Figure 1.6 Illustration of the degradation mechanisms present in an atmospheric optical channel

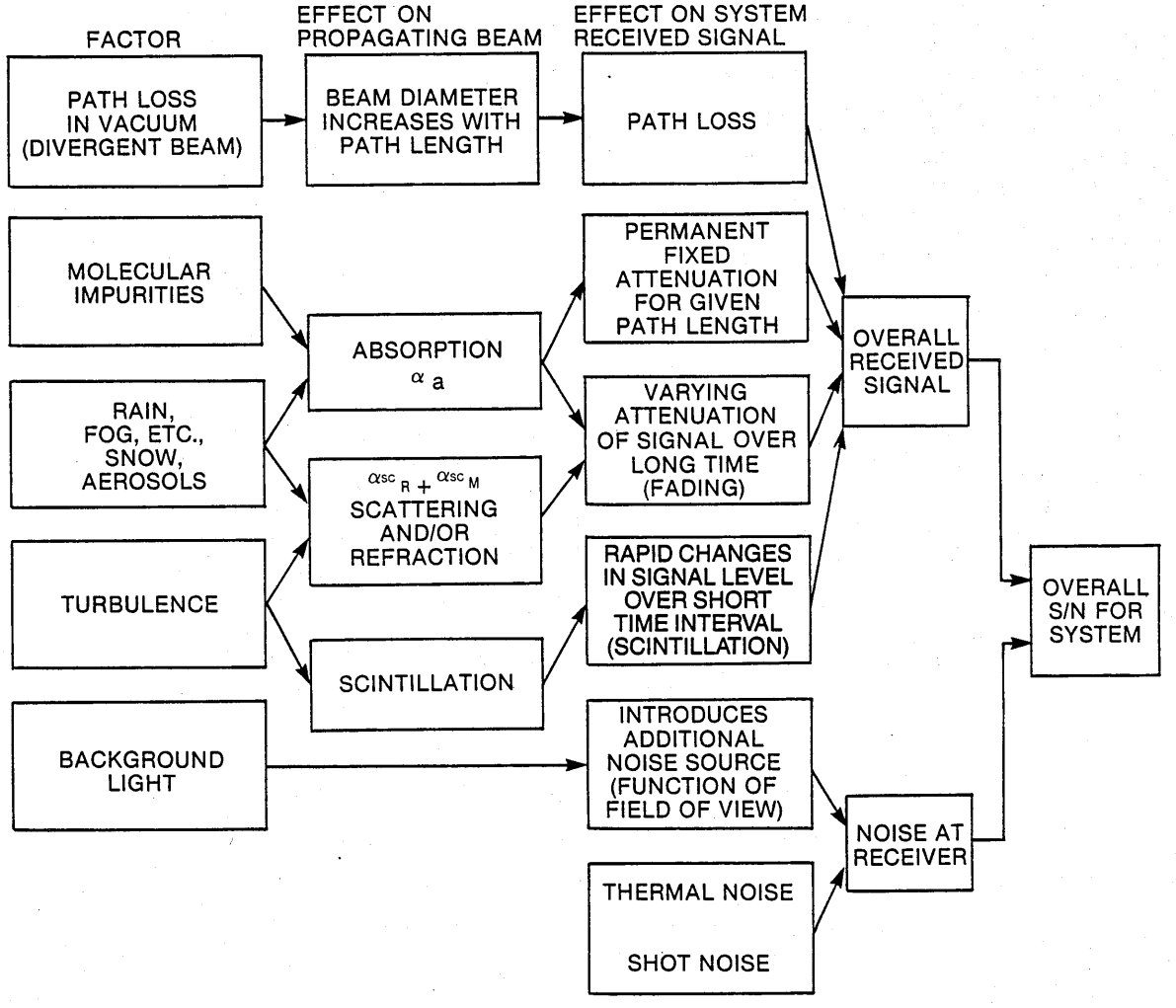

Figure 1.7 Model of atmospheric optical line of sight system in block schematic form

1.4.3 The Optical Channel

1.4.3.1 General

The free space optical channel is readily modelled since atmospheric effects such as turbulence are non-existent. The only major parameter of interest in such channels is the free space loss whereas in terrestrial atmospheric systems it is but one of a number of significant parameters. The free space loss parameter arises as a result of the optical beam being divergent and emanating from a point source and it is proportional to the inverse square of the path length [1.16].

Unfortunately in an atmospheric optical channel there are additional degradation mechanisms present which give rise to attenuation and dispersion of the transmitted signal.

These degradation mechanisms may be categorised as:

- scattering effects
- turbulent effects
- material effects (eg absorption)

These effects are illustrated in Figure 1.6 and presented as a diagrammatic model in Figure 1.7.

These effects arise because, when an electromagnetic wave propagates through a non-free space channel, its wave front is altered. These alterations are a function of the wavelength of operation and are caused by interactions of the wave with inhomogeneities, aerosols and impurities in the atmospheric medium. These effects become more severe as the wavelength decreases and becomes comparable with the size of the inhomogeneities, aerosols and impurities, and hence optical

signals, having wavelengths in the micron region are more susceptible than say microwave radio signals, which have wavelengths on the order of millimetres.

Each of these effects will be discussed briefly with the object of highlighting the nature of the resultant systems performance degradation and the order of magnitude of the effect.

1.4.3.2 Scattering Effects

There are two major scattering effects which occur in the atmosphere known as:-

- Rayleigh scattering, and
- Mie scattering.

Rayleigh scattering is primarily due to inhomogeneities in the molecular structure of the atmosphere. It has been shown [1.18] that the loss due to Rayleigh scattering is proportional to the inverse of the fourth power of the wavelength of the optical signal:-

$$L_{sc_{Rayleigh}} \propto \frac{1}{\lambda^4} \qquad (1.20)$$

where λ = wavelength of the optical signal.

Rayleigh scattering in a clear atmosphere at, for instance, a wavelength of one micron is fairly minimal at less than 0.1 dB/km, and decreases rapidly as the wavelength is increased.

Mie Scattering on the other hand is scattering due to the presence of large particles such as fog, smoke, water droplets etc in the atmosphere. Scattering of this type can be quite severe and can contribute as much as 1-10 dB/km to the path loss

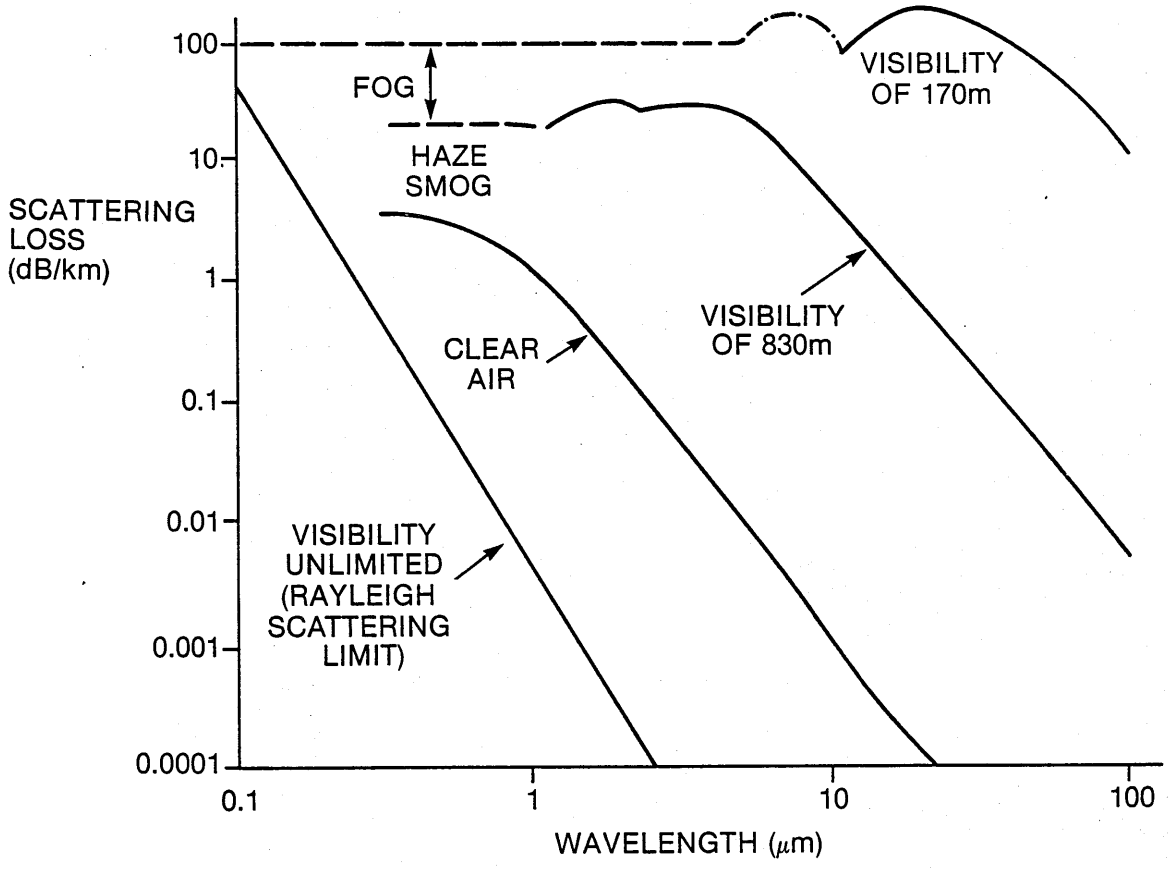

Figure 1.8 Atmospheric scattering loss as a function of wavelength.

in particularly bad cases, and can result in complete shut down of the system if insufficient margins are available.

Data on the magnitude of the scattering coefficients (for both Rayleigh and Mie Scattering) as a function of both wavelength and altitude has been derived from various empirical studies [1.19], and typical results are shown in Figure 1.8.

It follows from the foregoing that the scattering of an optical beam results in distortion of the beam wavefront and its beamwidth leading to a reduction in received optical power level at the receiver.

Scattering which gives rise to these effects may be broadly divided into two categories:-

- weak scattering
- strong scattering.

With weak scattering there is beam movement but the beam wavefront is substantially unaffected. This is usually known as beam wander. In addition the orientation of the plane wavefront can change, known as wave tilt, and also the beamwidth can increase, known as beam spreading. Such effects generally occur when the beamwidth is much narrower than the cross-section of the inhomogeneities.

Strong scattering on the other hand occurs when particles in the optical channel such as fog, smoke, rain etc are particularly dense and the beamwidth is much larger than the cross-section of the impurities. In this instance each particle acts as a discrete scatterer for different points along the beam-front and hence in a dense medium the scattering becomes quite acute

resulting in the break-up of the beam wavefront. It follows that since the location, movement, and density of the scattering particles is random, the distortion of the beam wavefront will also be random in nature, resulting in a randomly varying amplitude and phase across the beam. These effects can be minimised by increasing the effective diameter of the receiver aperture, a technique known as 'aperture averaging' [1.20].

Scattering of an optical signal can also give rise to signal (pulse) dispersion. In other words a transmitted rectangular optical signal pulse will become dispersed in time as it propagates through the atmospheric optical communications channel giving rise to an overall reduction in bandwidth of the optical channel for a given optical carrier.

Pulse dispersion occurs in strong scattering channels due to multipath effects. The various multipath signals arrive at the optical detector in the receiver at different times resulting in dispersed pulses in the case of digital communications systems. Fortunately such dispersion is only normally a major problem in systems design if the delay dispersion is a significant portion of the bit period.

For a clear air turbulent (scattering) channel the pulse dispersion is typically a few pico seconds, implying a channel bandwidth of hundreds of Gigahertz, which is not troublesome for the vast majority of communications systems.

1.4.3.3 Turbulent Effects

Turbulent eddies in the atmosphere are produced as a result of small temperature differences between adjacent volumes of air. Turbulence is particularly acute near the ground and its

magnitude is affected by retained ground heat and heat emissions from buildings such as ventilation outlets. The turbulent eddies cause variations in the refractive index structure of the atmosphere which, despite being small, typically only a few parts in 10^6, can have a profound cumulative effect upon the performance of atmospheric communication systems giving rise to beam wander, angle of arrival fluctuations, beam broadening and intensity fluctuations known as scintillations. Conventionally this refractive index structure is given by a parameter usually represented as C_n^2, which is considered in more detail in Chapter 5.

The variations in the refractive index structure give rise to constructive and destructive interference effects which result in fluctuations in the received signal level. Such effects are normally referred to as 'scintillation'. It has been established by various workers [1.16] that these signal level fluctuations decrease with increasing wavelength, with height above the ground, and with increasing receiver aperture size. As an indication of the order of magnitude of the scintillations, a 1 km link located 10-20 m above ground level may experience fluctuations of 10 dB or more when turbulence effects are particularly large. The frequency of the fluctuations (or scintillations), depends on the wind speed normal to the optical path, but dominant frequency components in the range 20-100 Hz are typical with lower magnitude components extending up to 1 kHz. The problem in modelling these scintillations is that they are random (stochastic) in nature and can only be described statistically. Various theories on turbulence are considered in Chapter 4 and the effect of

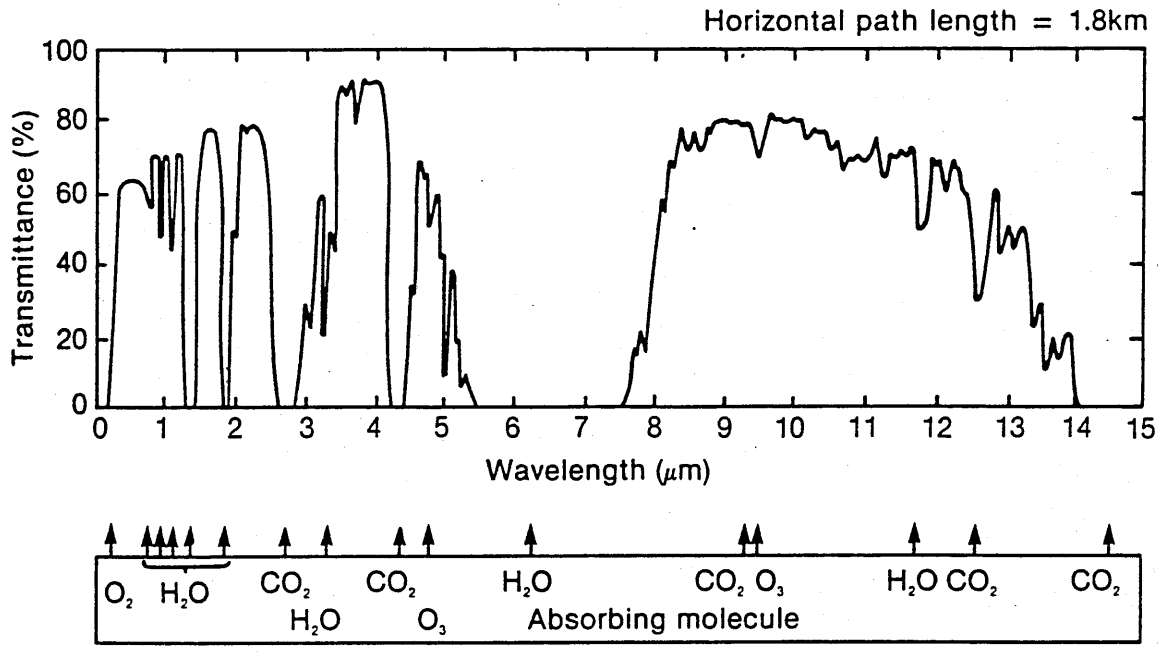

Figure 1.9 Atmospheric transmittance
(after Gower (1.28))

turbulence on system performance is quantified in the hypothesis given in Chapter 6. Detailed consideration of the atmospheric refractive index structure parameter is given in Chapter 5.

1.4.3.4 Material Effects

Absorption is one of the major loss mechanisms in atmospheric optical communication systems and occurs as a result of absorption of energy at the frequency (wavelength) of vibration of the particular molecules present in the atmosphere.

A typical plot of atmospheric absorption against wavelength is given in Figure 1.9. It can be readily seen that there are certain wavelengths at which it would be most inappropriate to operate any optical systems. These undesirable wavelengths are commonly those at which absorption peaks occur for many of the main constituents of the atmosphere such as oxygen, carbon dioxide and the OH radical and these are shown in the figure. Major absorption peaks occur at wavelengths of 2.7 (H_2O and CO_2), 6.1 (H_2O) and 15.0 (CO_2) μm. Most optical communications systems operate at those common laser operating wavelengths which coincide with minimal absorption wavelength regions in the absorption spectral plot. Typical wavelengths are in the 800-900 nm region where semiconductor sources are readily available and at wavelengths of around 10 μm in which region CO_2 gas lasers typically operate. Typical clear air losses are on the order of 0.1- 1.0 dB/km at wavelengths around 850 nm (see also Figure 1.8).

Of course any impurities in the air, and/or atmospheric ingredients such as rain, fog, snow etc, will all increase the attenuation of an optical channel tremendously, typically by

10 dB or more depending on the concentration of rain, snow, fog etc and on the path length. These atmospheric effects are a major consideration in the design and utilisation of atmospheric optical communication systems and are probably the biggest factors which have prevented such systems being universally adopted, since they can easily render a terrestrial optical communication system unworkable.

1.4.4 Overall Optical Channel Model

Bringing the previous parts of Section 1.4.3 together it is possible to derive a simple model for the atmospheric optical channel. The total optical attenuation coefficient of an atmospheric channel, α_t, is given by:-

$$\alpha_t = \alpha_{fs} + \alpha_a + \alpha_{sc} \tag{1.21}$$

where α_{fs} = free space loss coefficient.

α_a = absorption loss coefficient.

α_{sc} = scattering loss coefficient.

As already discussed in Section 1.4.3.2 the scattering loss coefficient is given by:

$$\alpha_{sc} = \alpha_{sc_R} + \alpha_{sc_M} \tag{1.22}$$

where α_{sc_R} = Rayleigh scattering attenuation coefficient.

α_{sc_M} = Mie scattering attenuation coefficient.

The total path loss, L_t of an optical link is given by:-

$$L_t = e^{-\alpha_t \cdot L} \tag{1.23}$$

where L = the path length

α_t = total attenuation coefficient as given in (1.21) above.

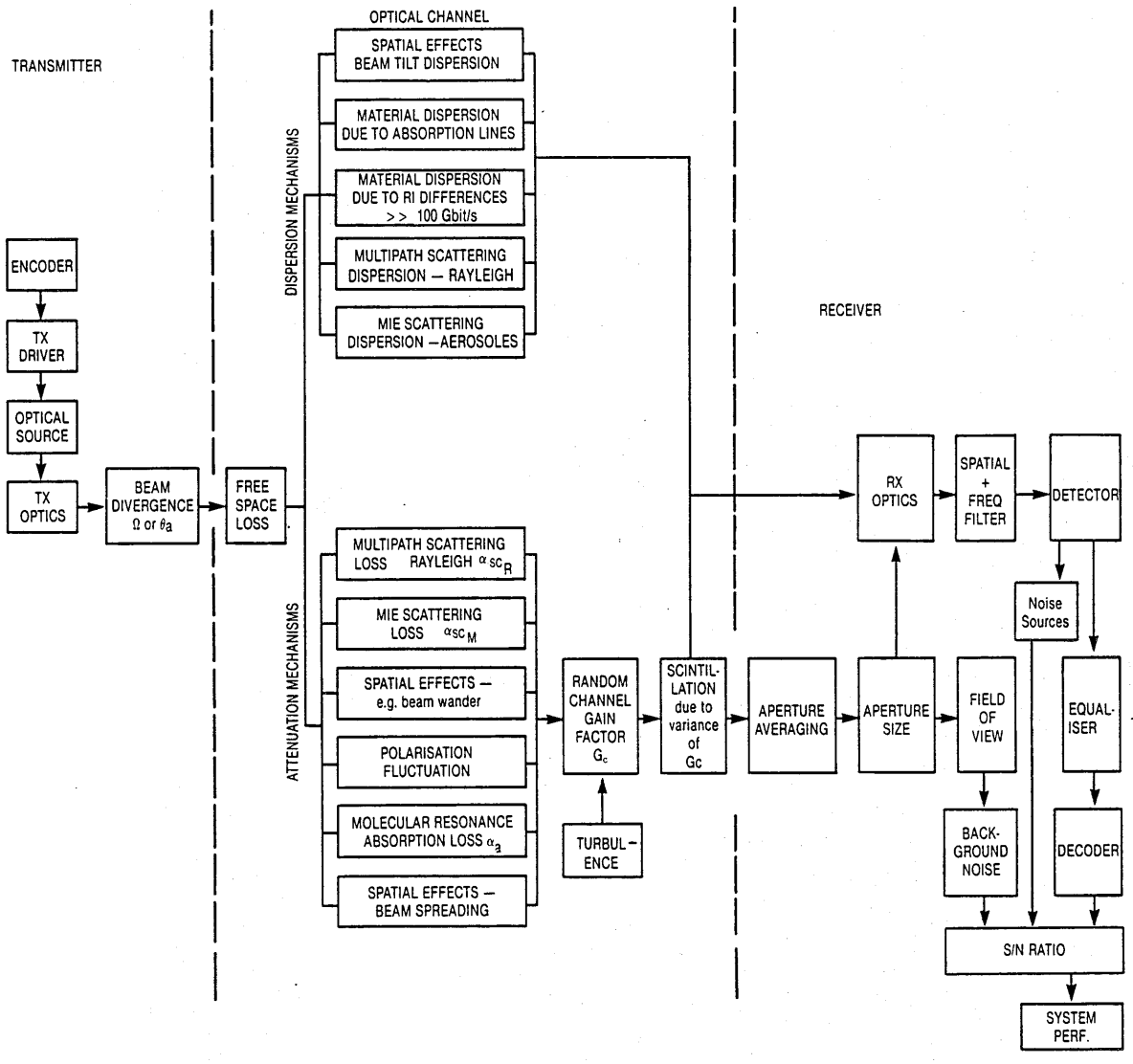

Figure 1.10 Overall system model for optical channel

The variation of path loss with time, ie amplitude fluctuations at the receiver due to scintillation effects can be taken into account by employing a factor for the random channel gain (or loss) G_c [1.16], such that the overall path loss is given by:-

$$L_{ov}(t) = G_c(t)L_t \tag{1.24}$$

It is important to note that all the above expressions are wavelength dependent and are therefore a function of the wavelength, λ, of the optical signal.

The model for dispersion effects is given by:-

$$t_{tot}^2 = t_{sc}^2 + t_{mat}^2 \tag{1.25}$$

where t_{tot} = total dispersion over the complete optical channel.

t_{sc} = dispersion due to multipath effects in a scattering channel.

t_{mat} = material dispersion.

t_{sc} itself is given by:-

$$t_{sc}^2 = t_{sc_R}^2 + t_{sc_M}^2 + t_{bt}^2 \tag{1.26}$$

where t_{sc_R} = dispersion due to Rayleigh scattering.

t_{sc_M} = dispersion due to Mie scattering.

t_{bt} = dispersion due to beam tilt at the receiver.

A schematic diagram of the optical channel model is given in Figure 1.10. The effects giving rise to varying channel gain are considered in more detail in subsequent chapters.

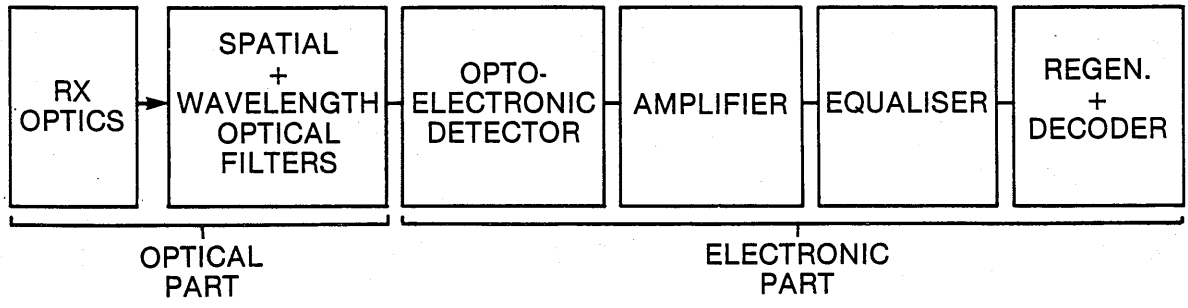

Figure 1.11 Block diagram of optical receiver

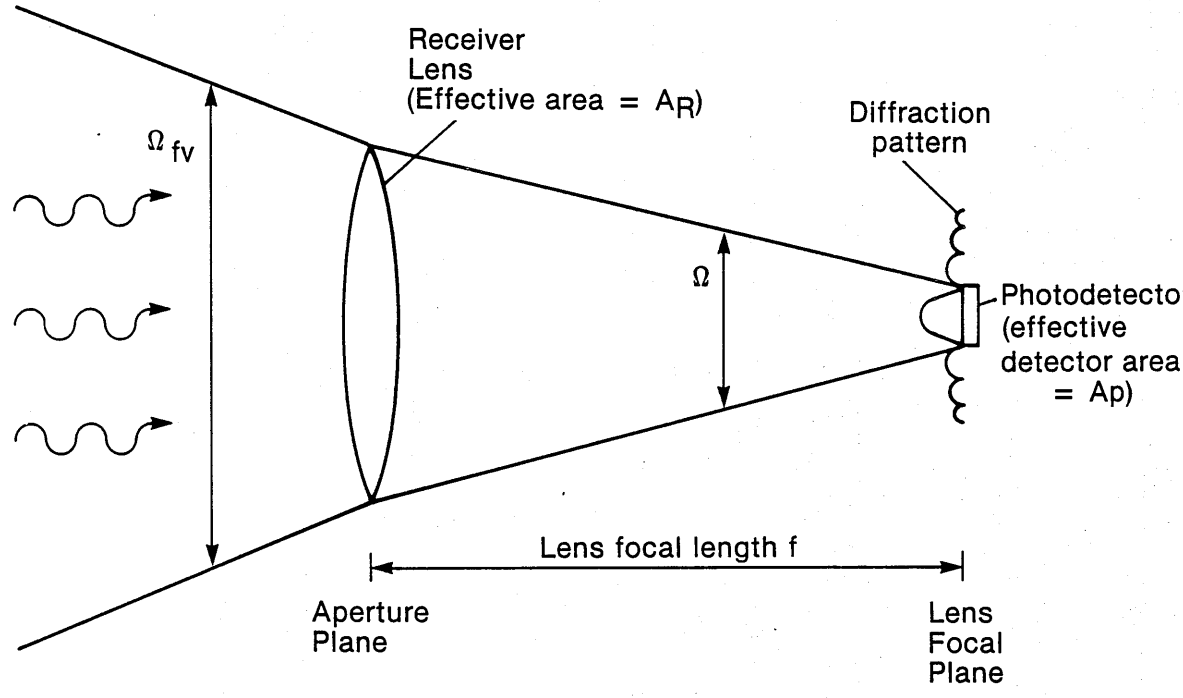

Solid angles $\Omega = \frac{A_R}{f^2}$ $\Omega fv = \frac{A_p}{f^2}$ $\Omega_{dl} \simeq \frac{\lambda^2}{A_R}$

Figure 1.12 Optical receiver lens system

1.4.5 The Optical Receiver

1.4.5.1 The Optical Receiver Model

Figure 1.11 shows a block diagram of a typical optical receiver and the optical receiver lens system is shown in more detail in Figure 1.12. Although a convex lens system is shown in this figure concave lenses can be used. Typical arrangements consist of a focussing lens or lens system, a spatial filter, a frequency (wavelength) filter (desirably a bandpass filter) and a photo-detector. The optimum aperture size for the lens is a function of a number of parameters. It should be large in order to benefit from aperture averaging effects in order to maximise the received optical signal power (see Chapter 4), to minimise the effects of beam wander etc, and to facilitate alignment on installation. On the other hand the larger the lens diameter becomes, the more unwieldy is the equipment in terms of both size and weight, and the greater the amount of background radiation which is received. The focal length, f, of the lens is usually a compromise between desired system performance and equipment size. The photo-sensitive optical detector having a sensitive area, A_p, is located in the focal plane.

The optical power received, P_R, at the receiver was deduced using thin lens theory in equation (1.12). In the case of an atmospheric channel absorption and scatter effects need to be included such that equation (1.12) becomes:-

$$P_R(t) = P_T \cdot \frac{\pi r^2}{\lambda^2} \cdot \frac{A_r}{L^2} \cdot T_a \qquad (1.27)$$

where T_a = atmospheric transmittance factor due to absorption, scattering and scintillation etc.

The detected optical power is also a function of the receiver field of view. Off-axis signals within the design field of view will fall on the active surface area of the detector. It follows that the receiver field of view is a major design parameter since too small a value would result in scattered off-axis signals not being detected. On the other hand too large a value would permit a larger amount of background radiation to be detected.

The receiver field of view is the solid angle looking out from the receiver within which all arriving plane waves must occur in order for their diffraction pattern to be projected onto the active area of the detector.

Geometric analysis of Figure 1.12 reveals that, assuming relatively small angles, the field of view Ω_{fv} is given by:-

$$\Omega_{fv} = \frac{A_p}{f^2} \qquad (1.28)$$

where A_p = effective detector area.

f = focal length of the receiver lens.

The field of view is obviously related to the size of the detector active area. In principle it would be desirable to have quite a large detector active area, since this would permit aperture averaging [1.20] and also increase the receiver field of view. This would also facilitate the manufacturing process in respect of the alignment of the receiver lens to the detector, and also alignment of the transmitter to the receiver on installation of the link. In practice there has to be a compromise since the larger the detector sensitive area the larger is the junction capacitance, which tends to restrict the

channel bandwidth and hence the maximum digital capacity of the link.

The smallest satisfactory field of view is known as the diffraction limited field of view as shown in Figure 1.12. The diffraction limited field of view, Ω_{dl} is given by:-

$$\Omega_{dl} = \frac{(\lambda f)^2/A_R}{f^2} = \frac{\lambda^2}{A_R} \qquad (1.29)$$

where $(\lambda f)^2/A_R$ = Area of main hump of diffraction pattern.

A_R = effective receiver lens area.

It follows therefore that the diffraction limited field of view is a direct function of the effective lens area of the receiver. It is seldom practicable to arrange for the area of the detector to be such that the receiver field of view is equal to the diffraction limited field of view. Indeed in practice Ω_{fv} is usually much larger than Ω_{dl}.

1.4.5.2 Background Radiation

Reference has already been made to background radiation. This radiation is, of course, undesirable since it appears as an additional noise source, effectively degrading the system signal to noise ratio (and error rate in digital systems). The design of the receiver optics will affect the amount of background radiation detected. Background radiation from whatever source falling within the receiver field of view will be detected although the receiver field of view can be limited by inserting a spatial filter in between the receiver lens and the detector. In addition the insertion of a frequency (or wavelength)

bandpass filter, also between the receiver lens and the detector, will reduce the detected level of background radiation still further.

Background radiation can be divided into two basic types [1.23] viz:-

i diffuse background radiation, such as the sky,

ii point sources such as stars, the sun, artificial terrestrial lights etc.

It is usual [1.16] to describe background radiation sources in terms of a spectral radiance function N(f) which is defined as the power radiated at a frequency f per unit bandwidth into a solid angle per unit of source area. For instance if the receiving antenna has an effective lens area of A_R, which is located a distance, L, from the source of the background noise, then the spectral radiance function is the solid angle measured from the source of A_R/L^2 steradians.

Between the background noise source and the receiver the background radiation is affected by the transmittance of the atmosphere, T_a, and the transmittance of the receiver optics, T_{RX}. In addition an optical frequency (wavelength) filter, if provided, will pass radiation over an optical bandwidth of B_o microns.

In practice the receiver field of view, Ω_{fv}, is fairly narrow and if it is assumed that the surface of the background noise source is normal to the receiver axis then the received background noise power, P_b, is given by [1.16]:

$$P_b = N(f) \cdot \Omega_s \cdot A_R \cdot B_o \quad \text{watts} \tag{1.30}$$

where Ω_s is that part of Ω_{fv} which is subtended by the background noise source at the receiver.

This expression gives the background noise power for a point source.

When the background noise source is extended and completely fills the receiver field of view, as is the case for the diffuse background radiation from the sky then:

$$\Omega_{fv} = \Omega_s = \frac{\pi}{4} \cdot \theta_{fv}^2 \tag{1.31}$$

where θ_{fv} is the plane angle radian measure of Ω_{fv}, for a conically shaped field of view.

The expression for the background noise power due to diffuse background radiation derived from Equation (1.30) is then [1.16];

$$P_b = \frac{N(f) \cdot \pi \cdot \theta_{fv}^2 \cdot A_R \cdot B_o}{4} \quad \text{watts} \tag{1.32}$$

Measured data on the irradiance functions of background noise sources is given in reference [1.24].

1.4.5.3 Detection

There are two main detection methods employed on optical communications systems:-

- Non-coherent (direct) detection
- Coherent detection.

In non-coherent detection systems the optical signal is focussed onto the detector which converts it into an electrical signal. If the detector was perfect, and had a quantum efficiency of 100%, then each photon falling onto the detector sensitive area would result in the release of one electron. In practice quantum efficiencies of 50-70% are typical. The electrical signal produced at the detector is a replica, although in adverse cases a somewhat vague one, of the electrical signal used to drive the optical source at the transmitter. The detected electrical signal will be severely reduced in amplitude due to the attenuation of the optical channel resulting in a degraded signal to noise value. In addition signal dispersive effects in the optical channel may result, in the case of digital systems, in pulse tails appearing in zero time slots, giving rise to intersymbol interference. Intersymbol interference causes closing of the 'eye' patterns resulting in a degraded signal to noise ratio, and hence a poorer error rate performance [1.15].

Equalisation circuitry following a post detection amplifier is often used to compensate for the dispersive effects of the optical channel and the detector/amplifier combination. After equalisation the signal may be further amplified and regenerated as necessary. A block schematic diagram of a typical receiver was shown in Figure 1.11.

Coherent detection is somewhat different to direct detection in that the received optical signal is mixed with a locally generated optical signal. The combined signal is then detected as for the direct detection systems. There are two principle coherent detection techniques:-

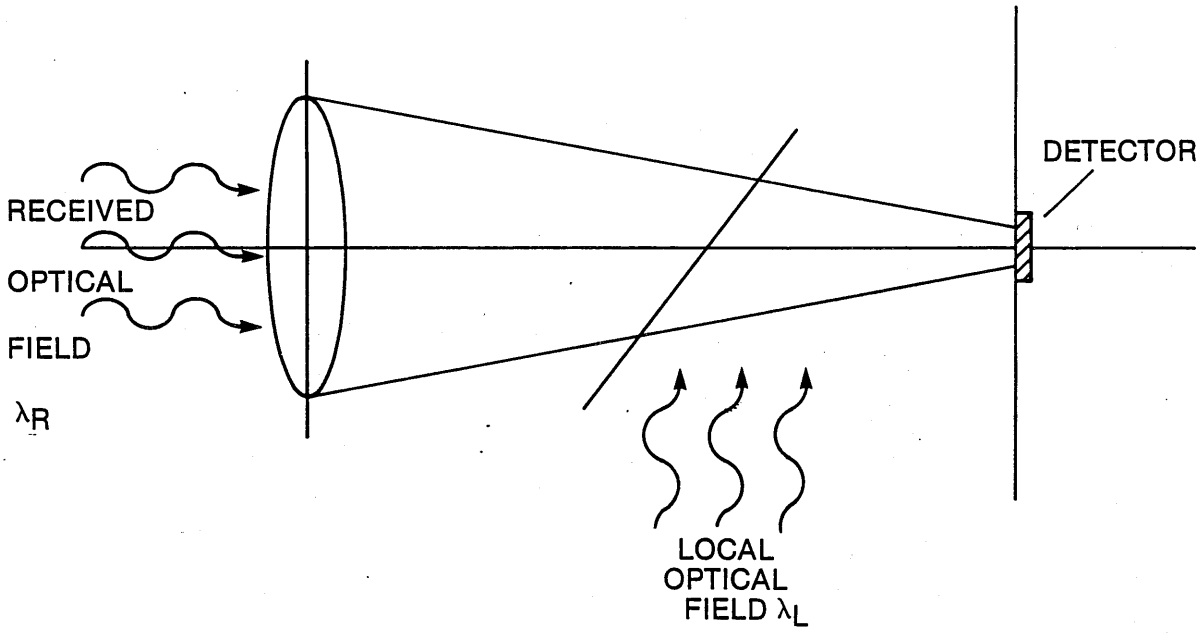

a) HETERODYNE DETECTION $\lambda_R \neq \lambda_L \Rightarrow$ DETECTED IF SIGNAL

b) HOMODYNE DETECTION $\lambda_R = \lambda_L \Rightarrow$ DETECTED BASEBAND SIGNAL

Figure 1.13 Principles of coherent detection

- homodyne detection
- heterodyne detection.

A diagram showing the principle of coherent detection arrangements is shown in Figure 1.13. With homodyne detection the local oscillator generates an optical signal which has the same nominal frequency as the received optical signal. After mixing and detection the difference signal represents the required baseband signal. With heterodyne detection the local oscillator frequency is somewhat different to that of the received optical signal resulting in an intermediate frequency (IF) signal being detected. This IF signal is then demodulated to baseband using standard radio circuit techniques.

Each detection technique has its merits and de-merits. The direct detection arrangement has to combat the effects of background radiation and the internal receiver thermal noise while attempting to recover the intensity modulation of the transmitted signal. It has the advantage of being simple to implement and therefore relatively cost effective and does not involve all the problems which come with the use of local oscillators. On the other hand the signal to noise ratio at the receiver is somewhat better for coherent systems than for non-coherent systems and one can either take advantage of this by accepting an improved error rate performance or alternatively the same signal to noise ratio can be maintained, but the system reach increased proportionately. Models for signal to noise ratio for the various detection techniques using various modulation formats are given in the literature [1.25].

For the purposes of this work the emphasis will be on direct detection systems since it is this technique which is currently generally employed on terrestrial optical line of sight communications links since they are much easier to implement and are therefore more cost effective than coherent systems.

1.4.5.4 Detectors

The purpose of the detector is to convert, in as efficient a manner as possible, the optical energy impinging upon its surface to electrical energy so that the signal can be amplified, equalised and if necessary regenerated - all in the electrical domain.

There are three main types of device which may be employed viz:-

- Photomultipliers
- Photoconductors
- Photodetectors.

Photomultipliers are not generally favoured for use in terrestrial communications line of sight links because they are generally fairly large in size, are expensive and less reliable than semiconductor photodiodes. Photoconductors are not normally sensitive enough for most systems applications. Semiconductor photodiodes on the other hand are very suitable for use in the near infra-red region and have the advantages of being:-

- highly sensitive
- small in size
- comparatively cheap
- easily utilised

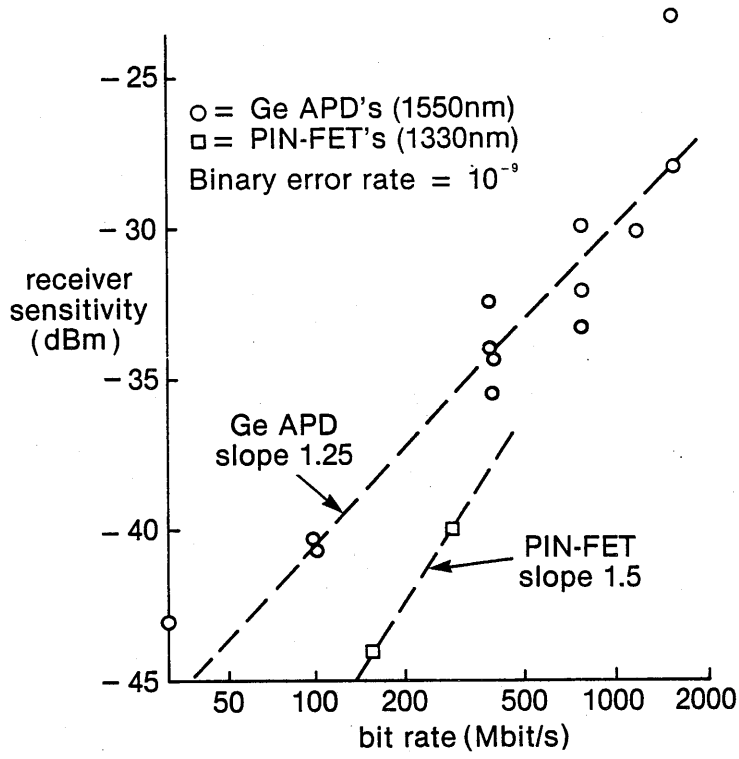

Figure 1.14 Typical published receiver sensitivities

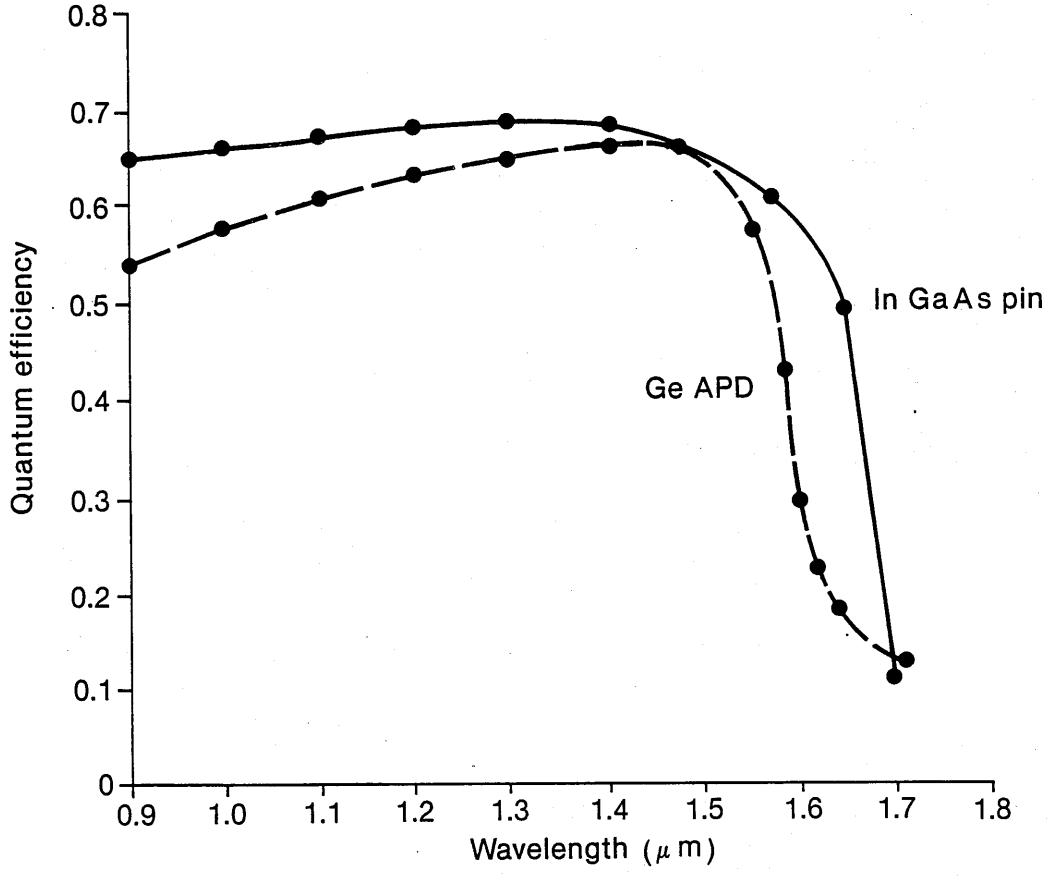

Figure 1.15 Quantum efficiencies for photodiodes

Avalanche photodiodes (APD's) have been employed for many years, since they are highly sensitive eg a minimum received power level of -66 dBm has been achieved at 2 Mbit/s with an error rate of 10^{-9} [1.26]. They do however suffer from the need to have high bias voltages applied to them, of the order of 300-400V and moreover the bias supply voltage has to be varied to compensate for the anticipated temperature excursions to which the device is likely to be subjected. PIN diodes have proved to be very popular, since they are much cheaper than APD's, and do not require the high bias voltages, for instance 15-20V is usually adequate. However, when used as discrete devices their sensitivity is some 10 dB worse than that of APD's [1.27]. In the last few years considerable research has been carried out into the use of PIN photodiodes and in particular into increasing their sensitivity so as to make them comparable or even superior to avalanche photodiodes. This work has resulted in the development and commercial availability of what is now commonly known as the PIN-FET detector [1.27]. Such detectors work on the principle of minimising the capacitances between the PIN diode and the FET and by optimising the individual devices for interconnection purposes. For these reasons the PIN-FET combination is assembled into a dual in line package for direct mounting onto a printed circuit board.

Figure 1.14 compares the sensitivities of the different detectors at two different wavelengths in the near infra-red region as a function of bit rate.

Different materials are optimum for different wavelengths as the quantum efficiency graph in Figure 1.15 shows.

Much of the recent device development work is a direct result of the need for practical, sensitive detectors for use with optical fibre systems, but much of the work can, and indeed has already been readily applied to optical line of sight communications systems.

The foregoing has pre-supposed the use of just a single detector. There are however advantages in employing a detector array in certain circumstances. For instance each individual detector of the detector array will detect a different angle of the receiver field of view. Thus it can be said that the optical signal arriving at the receiving lens aperture is spatially sampled, each of the detectors producing signal output or not, depending on the spatial position and angle of entry of the beam. Parallel processing of the electrical detector outputs is then employed to recover the wanted signal. The use of photodetector arrays is a form of diversity reception and can be employed to advantage in situations where atmospheric turbulence causes strong and variable scattering effects.

1.5 CONCLUSIONS

This chapter has given an introduction to the basic principles of optical line of sight communication. Subsequent chapters will consider the significance of atmospheric turbulence on the performance of such systems.

CHAPTER 2

A QUALITATIVE MODEL OF THE TURBULENT ATMOSPHERE

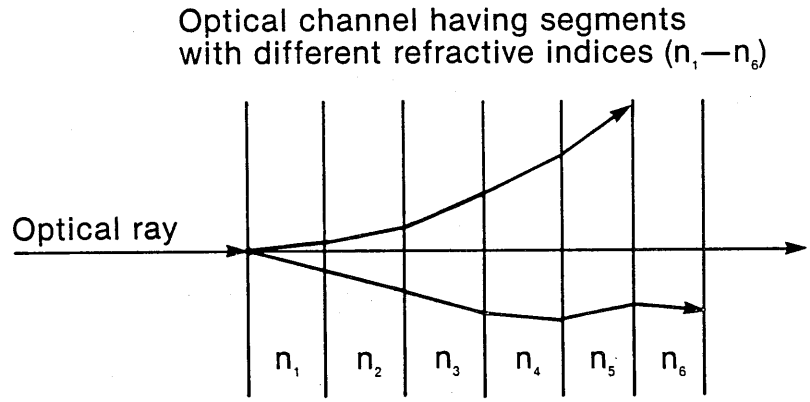

Figure 2.1 Successive planar segments model

CHAPTER 2

A QUALITATIVE MODEL OF THE TURBULENT ATMOSPHERE

2.1 INTRODUCTION

In considering the effect of turbulence in the atmosphere on optical beams it is convenient to establish a suitable model for the various mechanisms involved. This chapter describes a qualitative model which is used as a basis for the more detailed quantitative analyses given in subsequent chapters.

2.2 THE QUALITATIVE MODEL

A very basic model is that of successive planar segments as shown in Figure 2.1. If one assumes that each segment has a different value of refractive index then it follows that a plane wave incident at the first segment will be refracted according to Snell's Law. The beam will be further refracted as it passes through each boundary between successive segments resulting in beam shift. If the values of the refractive index of each of the segments $n_1 - n_n$ all increased by small amounts in a linear manner, then the optical ray would be continually refracted in the same direction. In practice the values of n do not increase or decrease in a regular linear manner and hence the optical ray will be refracted in a rather random manner as shown in the lower part of Figure 2.1. A further complication is that turbulence is not stationary, indeed the air temperature, height above ground and wind velocity, all result in the value of the refractive index in each segment varying significantly with time. The variations are generally regarded as being stochastic in nature and it follows that the optical beam at the receiver will wander, the magnitude of the wander being a function of the amount of turbulence.

So far the model has merely assumed segmentation along the propagation path of the optical beam, with the segments extending some distance either

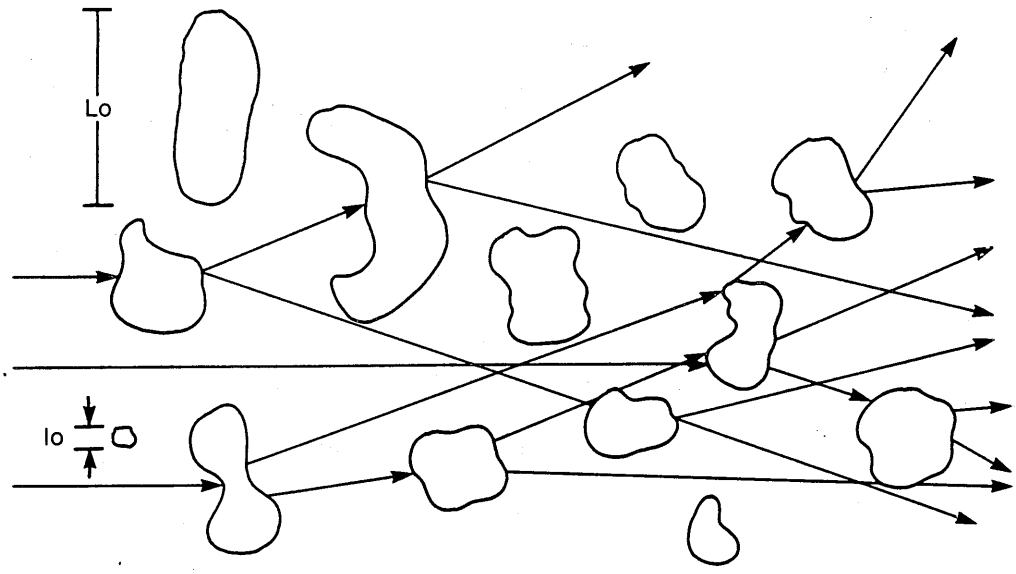

Figure 2.2 Scattering of optical beam due to presence of turbulent eddies

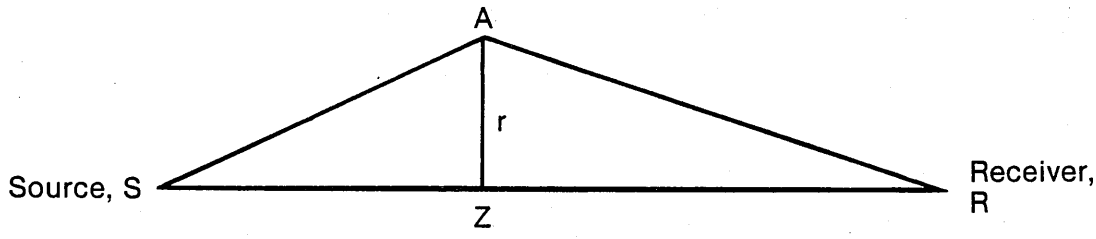

Figure 2.3 Basic turbulent eddy model

side of the beam such that the segment boundaries are all parallel to each other and normal to the axis of the propagating beam. It follows from what has been said above about the stochastic nature of turbulence that in practice the segments are most unlikely to comprise of such parallel boundaries.

An improved model is one in which the planar segments are in fact replaced by 'blobs' or 'eddies' having a different refractive index to the surrounding atmosphere as shown in Figure 2.2. Obviously the turbulent atmosphere would consist of numerous eddies each affecting the propagation of the optical beam as the beam passes through the atmosphere. The sizes of the eddies are characterised in terms of 'scale sizes':the inner scale signified by l_o represents the diameter of the smallest eddy and the outer scale signified by L_o which represents the maximum diameter of the largest eddy. It will be established below that the size of the eddy will determine the effect on the optical beam ie beam wander or beam spread.

Now consider an eddy in the path of an optical beam launched at point S and received at point R as shown in Figure 2.3. The light source at S emits a spherical wave of wavelength λ.

The receiver at R detects a proportion of the emitted radiation . If one now assumes that a turbulent eddy having a diameter of 2r exists at point Z, then a diffraction pattern will be observed at R whose size and contrast are determined by Z, r and λ and by the refractive index fluctuations, Δn, of the eddy.

For an eddy at position Z, the eddy which is most effective in producing scintillation is that which results in the two rays SR and SAR destructively interfering. This occurs when the path lengths are such that:-

$$SAR - SR = \frac{\lambda}{2}$$

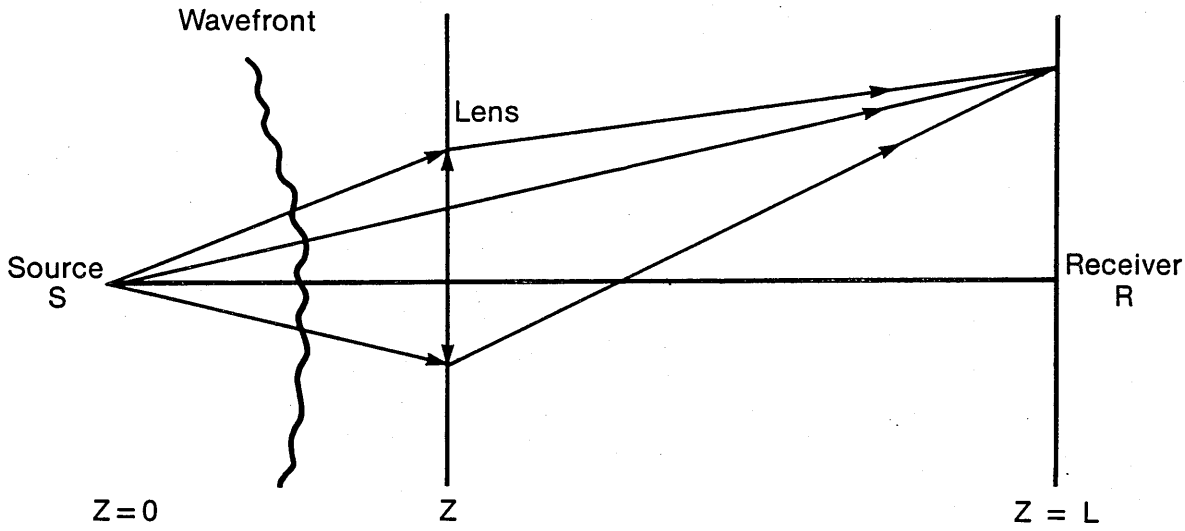

Figure 2.4 Propagation geometry with distorted wavefront

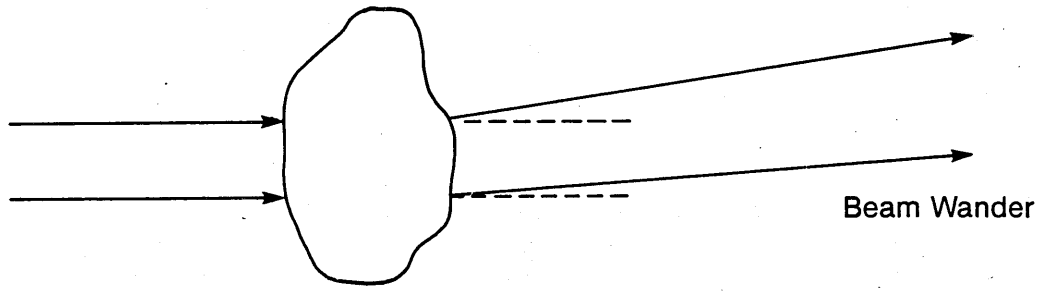

a) Beam diam. < eddy size

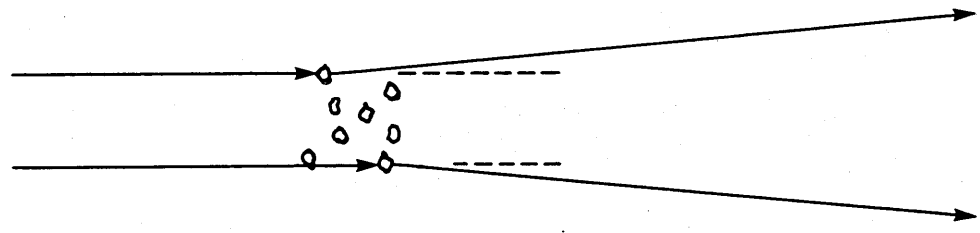

b) Beam diam. > eddy size

Beam spread

Figure 2.5 Beam wander and spread in relation to turbulent eddy size

The above simple model just considers an eddy at point Z. Simple superposition of the effects of supposed independent eddies located all along the path gives a basic theory for the effect of scintillation at R.

The next step is to suppose that the eddy at Z is illuminated by a wavefront which is no longer spherical but is distorted by preceding eddies. In addition succeeding eddies lying between Z and R will affect the wave and will modify the scintillations which would otherwise have been produced due to the eddy at Z.

In order to understand the effect of turbulent eddies between S and Z on the diffraction pattern of the eddy at Z it is convenient to consider the eddy at Z as a lens focussing the light on a screen at location R. As the wavefront passes through the turbulence before reaching the lens its wavefront is distorted in a random manner as shown in Figure 2.4. Those distortions which are smaller than the lens (ie the eddy), will cause the resolving power of the lens to diminish and will thus increase the size of the spot observed at R (ie beam spread). Those distortions larger than the size of the lens will cause wave tilts and will move the spot on the screen without changing its size (ie beam wander). Exactly the same effects will be caused by turbulent eddies lying between the lens and the screen at R. These effects are represented diagramatically in Figure 2.5. It follows from the foregoing that it is the size of the eddy rather than the location of the eddy which is important and which determines whether beam wander and/or beam spread occur in any particular instance.

It is also important to consider the relative lifetimes of the eddies of various sizes. Large eddies persist for longer than small eddies, both because of their intrinsic lifetimes and because, for a given crosswind velocity, they take longer to pass through the optical beam. The small scale fluctuations in the wavefront change in detail many times during the

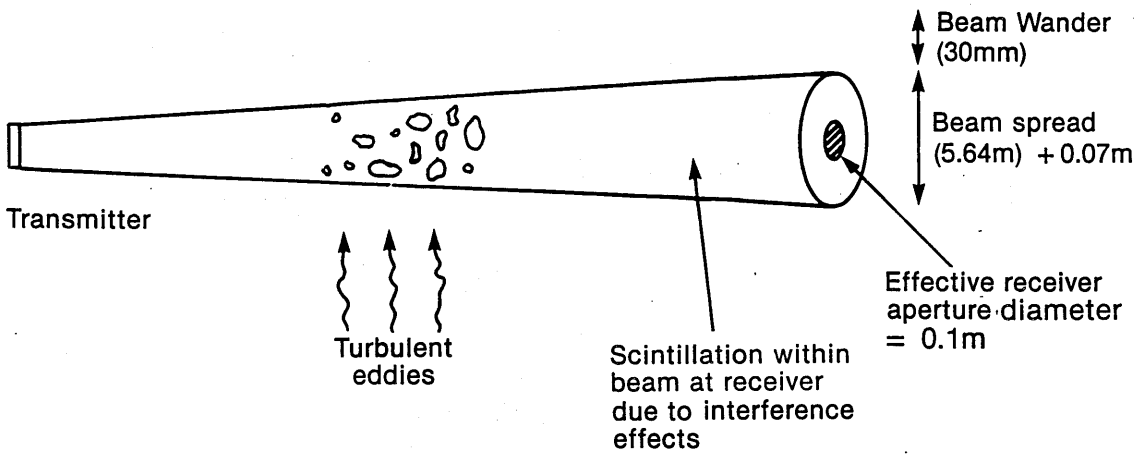

Turbulence induced effect	Magnitude for $Cn^2 = 10^{-12} m^{-2/3}$ and path lengths of L=500m	Corresponding SNR degradation
Beam spread (due to turbulent eddies being small compared with beam diameter)	70 mm (140 μrad or 0.008°)	< 2dB
Beam wander (due to turbulent eddies being large compared with beam diameter)	30 mm (std dev.)	<1 dB
Scintillation	55dB change in SNR for P (e)= 10^{-9}	c. 55dB

Note: Beam spread in absence of turbulence = 5.64 m due to finite source area (assuming source area = 1 mm², Lens focal length = 0.1m, path length = 500m)

Figure 2.6 Summary of turbulence induced effects

lifetime of the eddy, so that they cause a smearing of the diffraction pattern of the Fresnel zone size eddy. In contrast the large scale distortions do not change appreciably during the lifetime of the eddy. Thus although the fluctuations may displace the diffraction pattern, they have no effect on the statistics of the scintillations produced by the eddy. Even the smallest details in the scintillation pattern arrive at R unaffected, ie unsmeared, by the large scale distortions.

It follows that, at a given point, the optical power will be the summation of the energies of the different waves reaching that point, with consequential constructive and destructive interference. Since the turbulent eddies are forever changing, the optical power at the given point will also vary. It is these variations which are known as scintillations.

It will be shown in more detail in the subsequent chapters that the optical power variations at the receiver in a typical optical line of sight communication system are due predominantly to turbulence induced scintillation effects rather than turbulence induced beam spreading and beam wander, but for information purposes the typical orders of magnitude for each have been calculated and are shown in Figure 2.6.

2.3 CONCLUSIONS

The qualitative model described above attempts to explain the effect of turbulence on the propagation of optical beams passing through the atmosphere.

It is concluded that the magnitude of the turbulence and hence the size of the resultant turbulent eddies determines the precise effect at the receiver. That is small fluctuations will give rise to a smearing of the beam (ie beam broadening) and larger fluctuations give rise to a physical shift of the diffraction pattern (ie beam wander). In addition

interference effects will give rise to scintillation. All of these effects will give rise to a variation in the received power level but scintillation is invariably the major cause of such variations. The significance of beam spread and wander for typical systems is discussed in Chapter 3 and of scintillation in Chapters 4 and 6-8.

CHAPTER 3

BEAM SPREAD AND BEAM WANDER OF OPTICAL BEAMS PROPAGATING THROUGH THE TURBULENT ATMOSPHERE

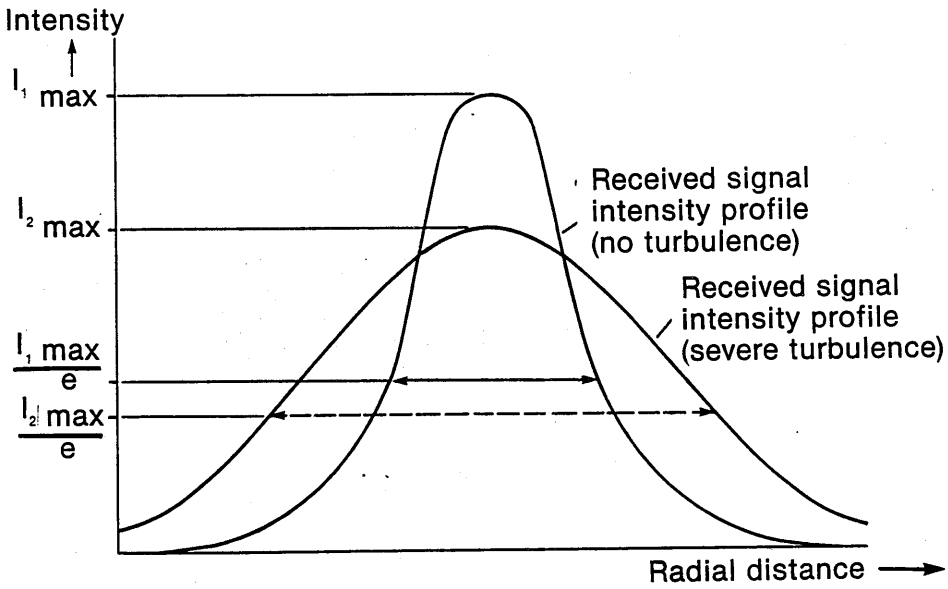

Figure 3.1A Beam spread

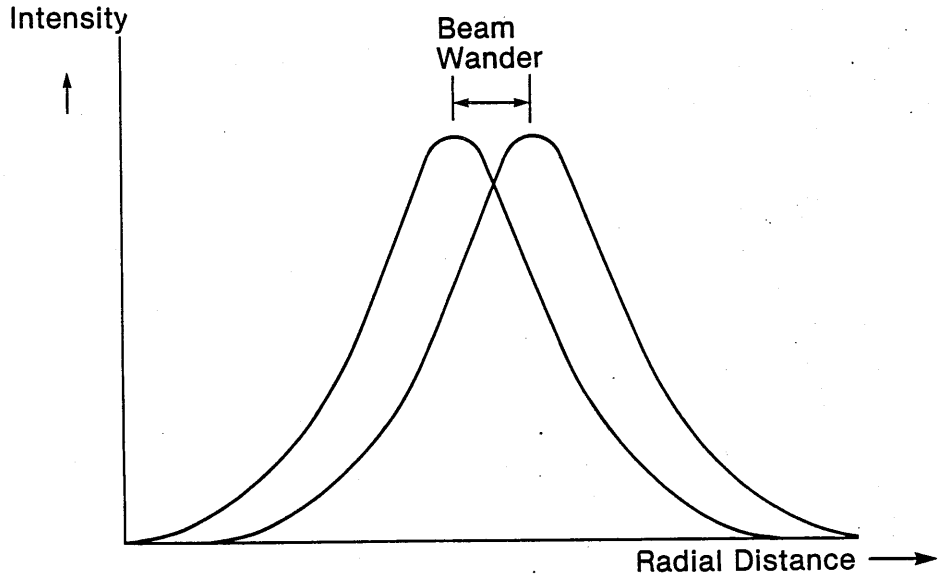

Figure 3.1B Beam wander

CHAPTER 3

BEAM SPREAD AND BEAM WANDER OF OPTICAL BEAMS PROPAGATING THROUGH THE TURBULENT ATMOSPHERE

3.1 INTRODUCTION

Optical beams propagating through the atmosphere are commonly subjected to atmospheric turbulence effects which give rise to:-

- Beam spread
- Beam wander.

Beam spread in this instance is the effect whereby the diameter of the beam, having traversed an atmospheric path of length, L, increases due to turbulence by an amount over and above that which can be attributed to normal atmospheric scattering and/or non-focussing and transmit aperture effects. The beam width is usually measured at the 1/e amplitude (equivalent to the $1/e^2$ power) points in the beam profile.

Similarly, beam wander is the effect whereby the maximum point on the received beam power profile moves from its original position as a result of atmospheric turbulence. Figure 3.1 illustrates the two effects diagramatically.

It is very important that the mechanisms which give rise to beam spread and beam wander are adequately understood since they are closely linked to the effect of scintillation and often confused with it. This chapter therefore addresses beam spread and wander in order to facilitate understanding of the subsequent more detailed analyses of the effects of turbulence in the atmosphere.

The basic principles of beam spread and beam wander are described in Section 3.2 of this chapter. The practical implications are discussed in Section 3.3, and a review of some practical data is given in Section 3.4.

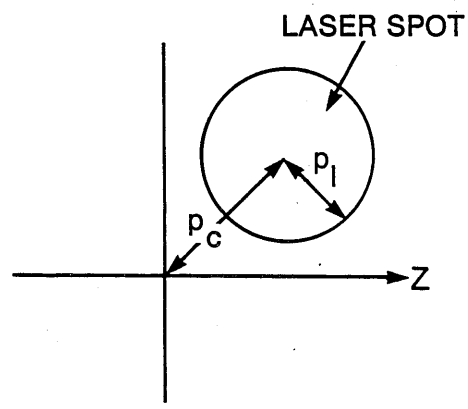

Figure 3.2 Short exposure time broadening and deflection of a laser spot on a receiver in a turbulent medium.

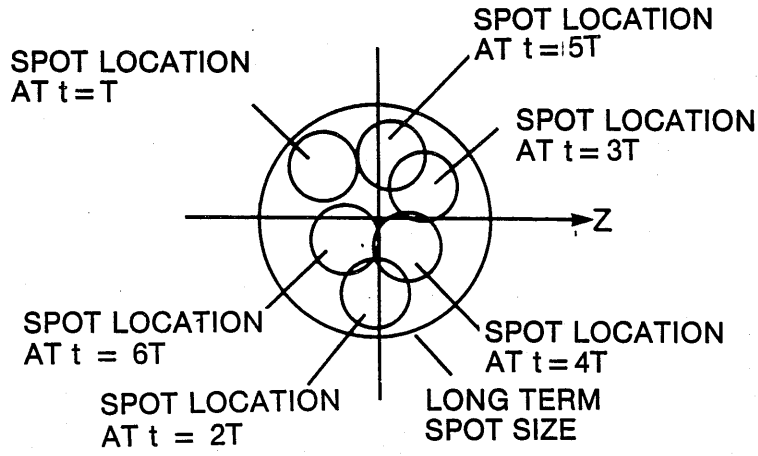

Figure 3.3 Time history of the wander of a laser beam on a receiver in a turbulent medium

3.2 Beam Spread and Wander

In the absence of turbulence, a laser beam exiting from an aperture of diameter d_T would, in the far field, have an angular spread θ_a of order λ/d_T, where λ is the signal wavelength (from equation 1.19). When turbulence is present the situation becomes much more complex because the beam is scattered by the moving turbulent eddies. This gives rise to an angular beam spread which may be much greater than θ_a; in addition other effects such as beam wander or even break-up of the beam into an ensemble of individual beams may occur.

When discussing the radius of a beam propagating in a turbulent medium it is necessary to distinguish between its short and long term spread. In general, when a laser beam interacts with the turbulent eddies it is found that those eddies which are large compared with the diameter of the beam tend to deflect the beam, whereas those eddies which are small compared with the beam diameter tend to broaden the beam, but do not deflect it significantly. Consequently, if a photographic plate was placed at a distance x into the random medium and a very short exposure picture was taken a broadened laser spot (due to the small eddies) of radius ρ_s which is deflected (due to the large eddies) by a distance ρ_c, would be observed, as indicated in Figure 3.2. Now, because the turbulent eddies are flowing across the beam, the beam will be continually deflected in different directions in time intervals of order $\Delta t = d/|V|$, where V is the transverse flow velocity of the turbulent eddies. The time history of the beam wander is shown in Figure 3.3. Because the spot dances from position to position in times of order Δt, it is clear from Figure 3.3 that a picture of the received spot taken with an exposure time much longer than Δt, would show a broadened spot with a mean square radius (ρ_L^2) given by:-

$$\langle \rho_L^2 \rangle = \langle \rho_s^2 \rangle + \langle \rho_c^2 \rangle \qquad (3.1)$$

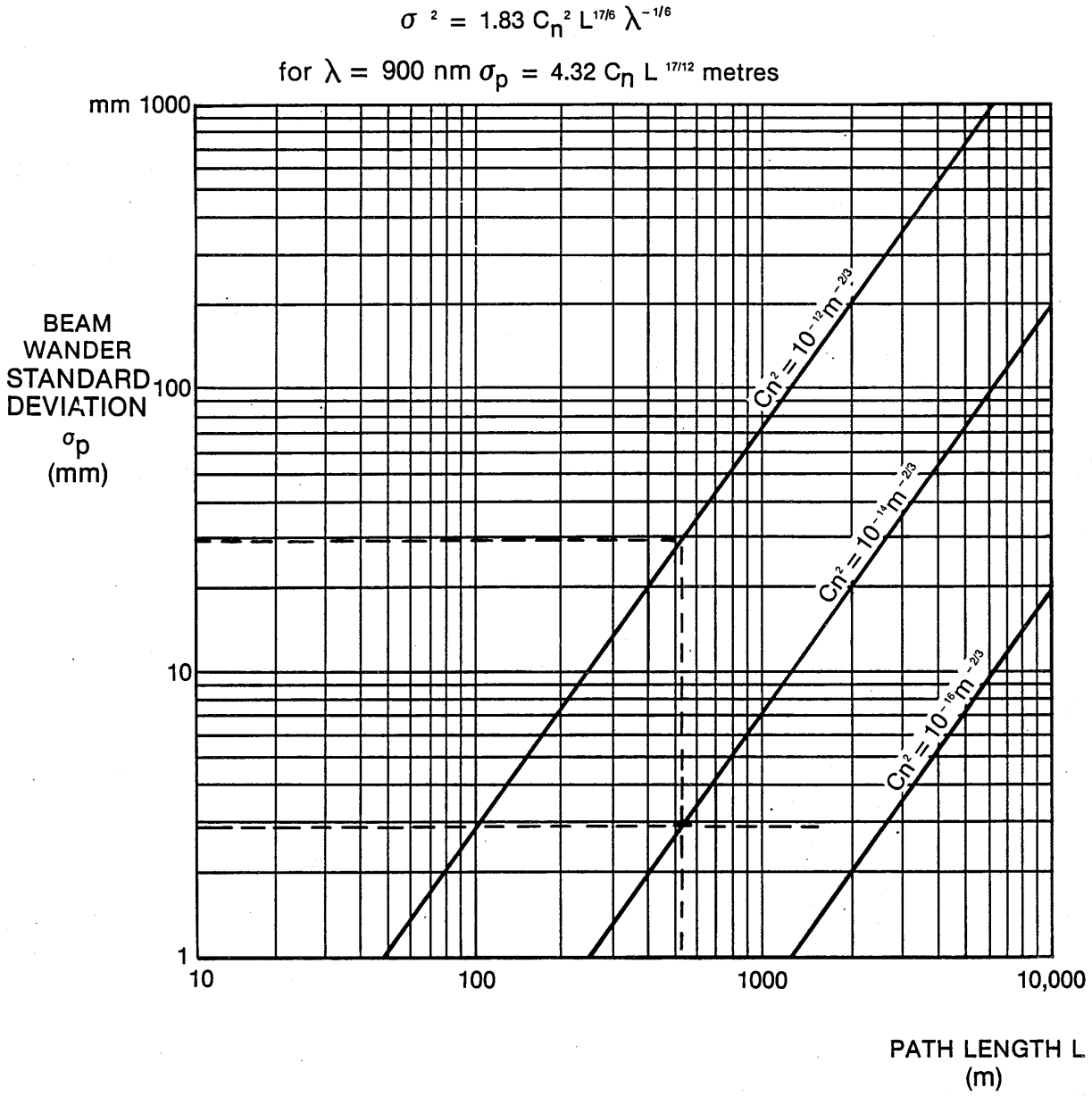

Figure 3.4 Beam wander vs. path length

where ρ_s is the short-term beam spread and ρ_c is the long-term beam spread.

When the turbulence is strong the beam no longer wanders significantly, but rather breaks up into multiple beams. In this case a short exposure picture of the received spot would consist not of a single spot, but of a multiplicity of spots at random locations on the receiving aperture. The long exposure picture, however, would be a blurred version of the short exposure, but with approximately the same total diameter.

3.3 SUMMARY OF PRACTICAL IMPLICATIONS

3.3.1 Beam Wander

Various workers [3.1] have produced theories for the magnitude of beam wander as a function of the atmospheric turbulence, represented by the atmospheric refractive index structure parameter C_n^2. This parameter is fundamental in studies involving atmospheric turbulence since it is the prime parameter for determining its magnitude. It is considered in some detail in Chapter 5 but typical values lie within the range $10^{-12}m^{-2/3}$ to $10^{-16}m^{-2/3}$ representing high and low levels of turbulence respectively.

Owing to the non-stationary and stochastic nature of the atmosphere the generally accepted models are based on the theoretical models as modified by empirical results. The generally accepted expression for beam wander [3.1] is given in terms of the empirically derived beam wander variance, σ_ρ^2 where:-

$$\sigma_\rho^2 = 1.83\ C_n^2\ L^{17/16}\ \lambda^{-1/6} \qquad (3.2)$$

Figure 3.4 shows the standard deviation for beam wander σ_ρ, versus path length L for various magnitudes of C_n^2 and a wavelength

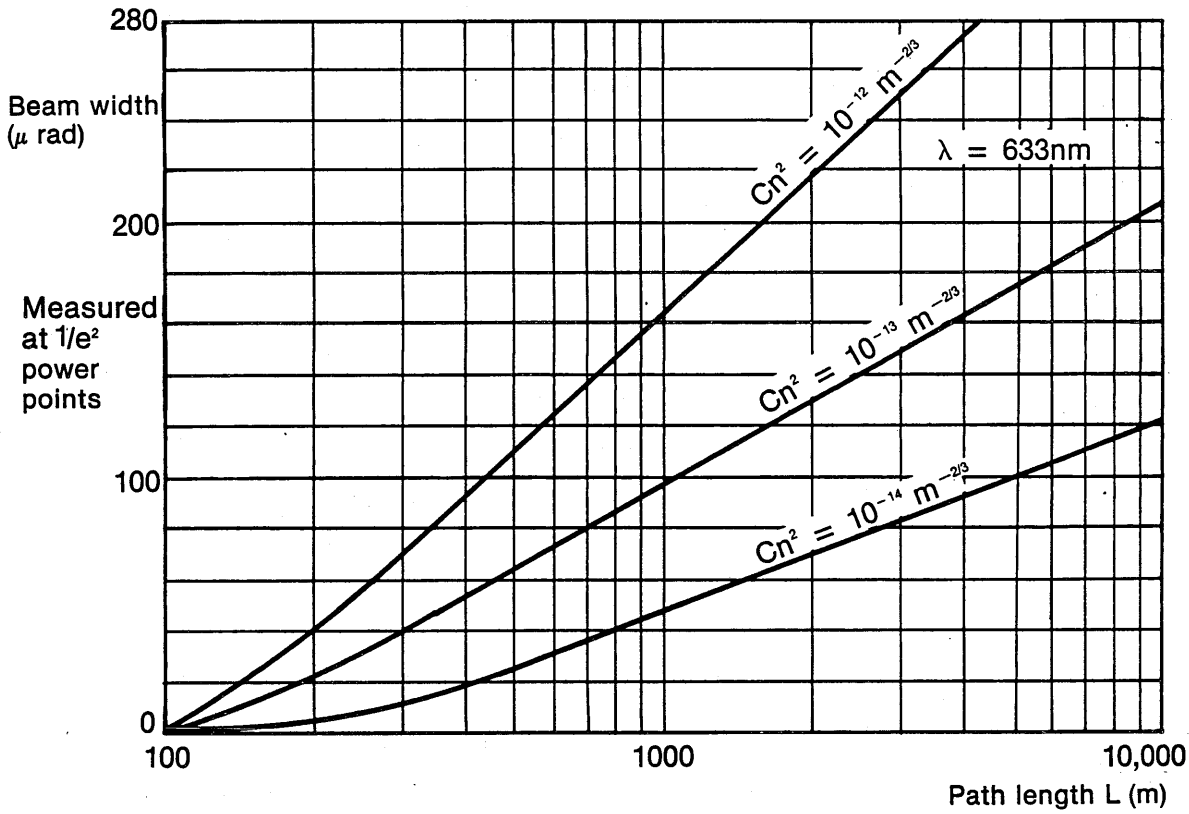

Figure 3.5 Beamwidth vs. path length for varying levels of turbulence

of λ = 900 nm. It can be seen that the beam centroid will move by up to 60 mm with a probability of 95% for path lengths of L = 500m if the value of C_n^2 increases to $C_n^2 = 10^{-12} m^{-2/3}$. However, the latter represents intense turbulence and more typical values of σ_ρ which would be experienced for a path length of L = 500 m would be in the range up to about 10 mm (λ = 900 nm; $C_n^2 = 10^{-14}$ to $10^{-16}\ m^{-2/3}$).

3.3.2 Beam Spread

Beam spread has been investigated in some detail by Dowling and Livingstone [3.2], amongst others, who have established various predictions for beam spread. Multiple regression analysis of their practical measured data has yielded the following empirically derived expression for beam width (spread) θ, as determined at the $1/e^2$ power points:

$$\theta = (1.44 \times 10^{-9} C_n^{0.85} L^{0.62} (2\pi/\lambda)^{0.65} - 1.7 \times 10^{-9})^{\frac{1}{2}} \qquad (3.3)$$

where C_n^2 = atmospheric refractive index structure parameter

L = path length

k = wavenumber of propagating energy = $2\pi/\lambda$

The constant of 1.44 has been proposed [3.2] based on practical results and multiple regression analysis. A correlation co-efficient of 0.85 suggests that the expression is a reasonably good fit to the empirical data.

Figure 3.5 shows the beam spread versus path length for different values of C_n^2 derived from equation (3.3) [3.2].

[3.2]

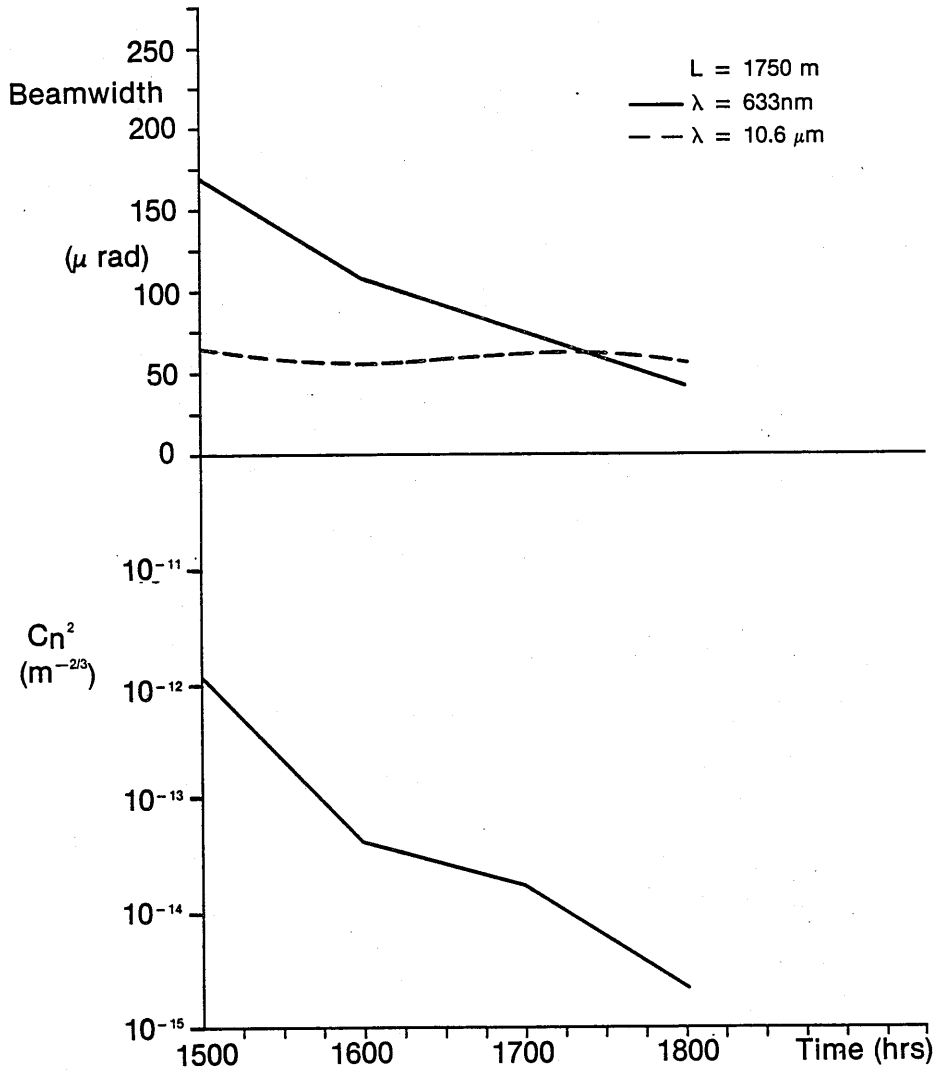

Figure 3.6 Variations of beamwidth with C_n^2 and with time

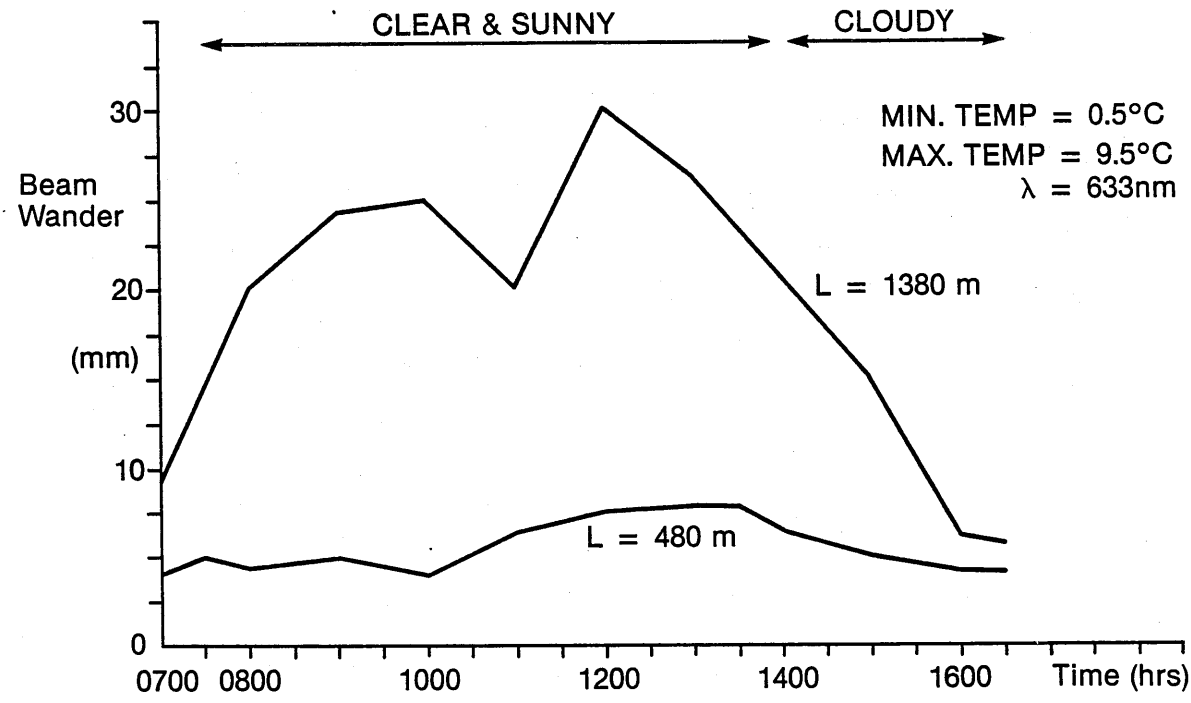

Figure 3.7 Beam wander variation with time (after ref. 3.1)

3.4 PRACTICAL DATA

Dowling et al [3.2] have published results giving the variation of short term average beam width with time and also the corresponding value of C_n^2. The measurements were made using a transmit lens aperture of 400 mm over various path lengths. Typical results for a path length of 1750 m are shown in Figure 3.6. There seems to be generally a very good correlation between C_n^2 and the beam width for wavelengths in the visible and near infra-red regions but the measurement at a wavelength of 10.6 μm (mid infra-red region) in contrast shows very little correlation between beam width and C_n^2, the beam width remaining fairly constant with time at this wavelength.

Buck [3.3] and Ochs and Lawrence [3.4] have also published results which are in general agreement with those of Dowling et al [3.2].

Cordray et al [3.5] and Chiba [3.1] have published results of beam wander measurements. The latter used a television camera to measure the beam wander and values of up to 30 mm were measured in strong turbulence ($C_n^2 = 10^{-13} m^{-2/3}$) on a test range of path length 1380 m.
Figure 3.7 gives some of Chiba's results for path lengths of 480 m and 1380 m. Various measuring techniques were employed including the use of a movie camera and use of a photodetector, whose position could be precisely adjusted, and data recorder.

In all cases a high correlation between the magnitude of beam wander and C_n^2 was observed, more than adequately supporting the theoretical predictions.

3.5 CONCLUSIONS

This chapter has indicated the strong influence of turbulence as measured by the refractive index structure parameter (C_n^2) on beam width and beam wander. Empirically derived expressions have been derived by various

workers to permit the prediction of the magnitude of the various beam broadening and beam wander effects and the expressions appear to be supported by practical data.

Beam width and beam wander measurements have not been made to validate the previous data generated by other workers as part of this research work, partly because there appears to be adequate existing evidence to support the theoretical predictions and partly due to the availability of a test range having only a maximum length of 500 m. The data discussed in this chapter suggests that, for systems having a path length of 500 m, the magnitude of beam broadening and wander is small and hence not the dominant cause of received signal power variations. In addition measurement error could be a significant source of error in any measurements made over this limited distance. Figure 2.6 in Chapter 2 compared the magnitudes of these effects with that of scintillation and suggested that the latter is the main cause of turbulence induced system performance degradation. The results from this chapter would appear to endorse this conclusion.

CHAPTER 4

ATMOSPHERIC TURBULENCE - A REVIEW OF EXISTING THEORIES

CHAPTER 4

ATMOSPHERIC TURBULENCE - A REVIEW OF EXISTING THEORIES

4.1 INTRODUCTION

Chapter 1 discussed the principles of atmospheric line of sight optical communication and highlighted some of the problems associated with this particular transmission medium. Turbulence in the atmosphere was noted as being especially troublesome. Turbulent eddies, produced as a result of ground-air and air-air temperature differentials, give rise to very small variations in temperature (of the order of 0.1-1°C), which in turn cause small changes in the refractive index of the atmospheric medium, of the order of 10^{-6}.

Although these refractive index variations are very small in magnitude, in a practical atmospheric communications link the transmitted optical signal propagates through a large number of refractive index differentials, resulting in a significant cumulative effect.

The cumulative effect of these refractive index differentials results in beam wander and beam broadening, which were discussed in Chapter 3, and scintillation at the receiver which was considered qualitatively in Chapter 2 and which will be considered quantitatively in Chapter 6. As already mentioned, these intensity fluctuations, or scintillations, are one of the major causes of transmission performance degradation in atmospheric optical communication systems.

4.2 HISTORICAL REVIEW

A comprehensive survey of the literature has revealed that, although high speed atmospheric communication was not technically feasible prior to the invention of the laser by Maiman [4.1] in 1960, a great deal of the theoretical work and some experimental work had already been carried out,

albeit usually aimed at investigations into wave propagation for reasons other than atmospheric communications.

Probably the most well-known example of the effect of turbulence in the atmosphere is the twinkling or, in more technical terms, the scintillation of stars when observed from the earth. In the early 1950's there was considerable scientific interest in the twinkling and quivering of stellar images in astronomical telescopes. Various papers were published on the effects of scintillation at about this time by Mikesell [4.4], Nettlebald [4.5], Butler [4.6, 4.7], Ellison et al [4.8] and Protheroe [4.9]. The irregular displacements of the image of a star in random directions is known as quivering and is related to the fluctuations in angle of arrival of the received light wave. This particular subject has been fairly thoroughly reviewed by Kolchinski [4.10, 4.11] and the effects of speckle phenomena have been reviewed by Dainty [4.12].

The effect of turbulence on acoustic propagation (ie sound waves) was studied as early as 1941 by Obukhov and others [4.13]. Various approaches appear to have been adopted, for instance Krasilnikov used a geometrical approach [4.14, 4.15] as did Bergmann [4.16] and the limitations of this approach were discussed by Ellison [4.17] and Tatarskii [4.18].

In principle the problem with the geometrical approach is that it is only valid for relatively short path lengths and in the case of optical waves it is restricted to distances of just a few tens of metres.

As a consequence wave theory then began to be considered during the early 1950's by workers such as Mintzner [4.19-4.21], Obukhov [4.22] and Tatarskii [4.23].

However, both ray theory (geometrical optics) and wave theory were based on perturbation theory, in which gradual incremental changes along the

propagation path are assumed. In these approaches it was assumed that scintillations were small in magnitude compared with the mean value of signal. This is something of a restriction as will be indicated in subsequent discussion of experimental results in Chapters 7 and 8. Obukhov [4.22] overcame this restriction by employing a technique, suggested by Rytov [4.24], which involved taking the logarithm of the optical intensity field, and this technique is now referred to as the 'Rytov' method.

Two major theoretical works were published by Chernov [4.2] and Tatarskii [4.3], both Russians, in English in the United States in 1960 and 1961, respectively. The interest of Chernov and Tatarskii was not in optical communication as such, but in the general aspects of the propagation of waves in a turbulent medium. These works were aimed primarily at gaining an understanding of effects such as the propagation of starlight through the atmosphere, and the propagation of sound waves through the atmosphere and the sea. They were also of value in studying the propagation of microwave signals through planetary atmospheres and the propagation of radio waves through the ionosphere and interplanetary space.

In the mid 1960's Gracheva and co-workers [4.25, 4.26] demonstrated that the theory for the variance of the logarithm of the irradiance did not appear to be applicable to long path lengths above a certain critical value. This effect is now known as the 'saturation effect' and is discussed in detail in Section 4.5.

4.3 REVIEW OF THE VARIOUS THEORIES

4.3.1 Classical Theory

It has been shown by various workers [4.3, 4.27, 4.28] that the refractive-index fluctuations are proportional to the temperature fluctuations. The temperature fluctuations originate from large-scale

phenomena, such as heating of the earth's surface, but are broken down and mixed by the wind until they exist at all scales. Since wind velocity fluctuations control the temperature variations, the statistics of the random velocity field have had to be studied. The two books by Tatarskii [4.3], [4.27] on turbulence include aspects particularly relevant to propagation.

The kinetic energy of turbulence is usually introduced by such large scale phenomena as wind, or convection from solar heating, and/or man-made heat sources from the ground. Therefore, it is reasonable to assume that the turbulent energy is introduced through the action of scale sizes larger than some minimum value L_0 called the outer scale of turbulence, which corresponds to a wavenumber $k_0 = 2\pi/L_0$. For scale sizes having wavenumbers smaller than k_0 the form of the energy spectrum cannot be so easily specified since it depends on surface geography and local meteorological conditions. Near the ground, the value of the outer scale is thought to be comparable with the height above ground. In the upper atmosphere L_0 is often 100 metres or more, but in the presence of stratified layers, perhaps as thin as a few metres, L_0 cannot greatly exceed the layer thickness.

As the spatial wavenumber increases above k_0 and the scale size becomes smaller than the distance to the ground, or to the nearest inversion layer, the turbulence tends to become homogeneous. Under these conditions, both theory and experiment indicate a $k^{-11/3}$ dependence for the spectrum. The theory of this dependence, originally proposed by Kolmogorov [4.29], is based on the assumption that the energy is input at small wavenumbers and dissipated at much larger wavenumbers, and the scale sizes are small enough so that buoyancy effects are negligible. In this wavenumber range known as the inertial subrange, the large eddies are unstable and break apart.

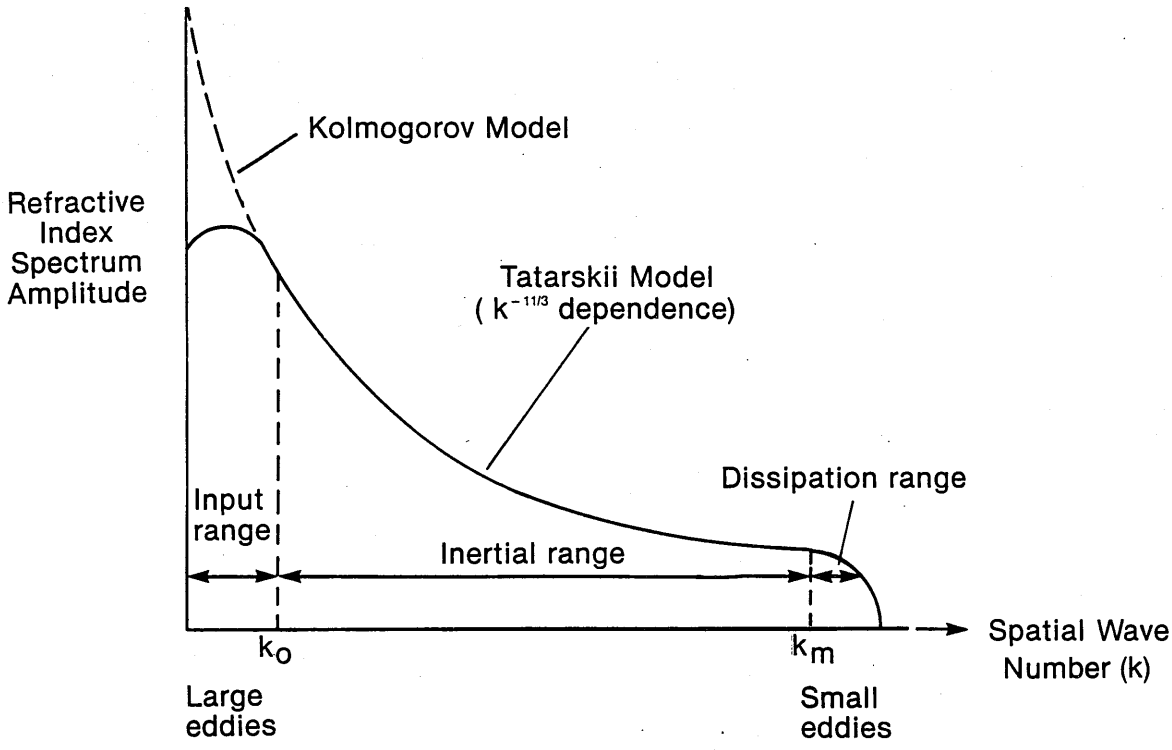

Figure 4.1 Kolmogorov and Tatarskii models for fluctuations of refractive index

Note: $k_o = \frac{2\pi}{L_o}$ and $k_m = \frac{2\pi}{l_o}$ where typically L_o = 1–10m and l_o = 1–30 mm)

Thus they transfer energy to smaller scales (higher wavenumbers) down to the "inner scale of turbulence" l_0, a scale of only a few millimetres, where the energy is dissipated into heat. Figure 4.1 illustrates this diagrammatically.

Tatarskii [4.27] proposed the following model for the atmospheric refractive index spectrum based on the statistical model of Kolmogorov [4.29]:-

$$\emptyset(k) = 0.033\, C_n^2\, k^{-11/3} \exp(-k^2/k_m^2) \qquad (4.1)$$

where C_n^2 = refractive index structure parameter

k = wavenumber

k_0 = wavenumber corresponding to the outer scale of turbulence L_0 where $k_0 = 2\pi/L_0$

k_m = wavenumber corresponding to the inner scale of turbulence, l_0 where $k_m = 2\pi/l_0$

The adjustable parameters of the atmospheric refractive index model are as follows:

i C_n^2, the refractive-index structure parameter (sometimes optimistically called the structure "constant") which is a measure of the magnitude of the refractive-index fluctuations;

ii l_0, the inner scale of turbulence, below which viscous dissipation steepens the spectrum;

iii L_0, the outer scale of turbulence, above which the energy is presumed to be introduced into the turbulence.

The effects of beam spread, beam wander and scintillation on optical communications systems are determined to a large extent by the "large

scale" and "small scale" turbulent variations. Large scale variations are those phenomena that affect the average position of a light beam measured over a period of, say, 10 seconds; small scale variations are those irregularities that, for example, distort an image, broaden a laser beam, or cause rapid twinkling and dancing of a star (see Figure 2.5). The physical dividing line between these scales is about a metre or less.

The largest scales in the atmosphere are due to the general decrease with height of atmospheric density and the curvature of the atmospheric layer as it clings to the spherical earth. It is for this reason that an optical ray arriving at the earth from a star bends down-ward as it passes through an atmosphere of steadily increasing refractive index. This effect is particularly significant for stars near the horizon or for near-horizontal ground-to-ground optical paths.

The refractive index n of the atmosphere is conveniently and customarily characterised in terms of the refractivity, N, measured in parts per million. These N units are related to n by $N = (n-1)10^6$. For optical wavelengths $N = 79\ P/T$, where P is the atmospheric pressure in millibars and T is the temperature in degrees Kelvin. N is roughly equal to 290 at sea level, varying with wavelength by about 10 per cent over the visible band and with humidity by about one per cent. The details of these variations have been reviewed by Owens [4.30].

The actual atmosphere is usually less smooth than the ideal model of the atmosphere. Particularly characteristic are layers having great horizontal extent and a vertical temperature gradient that changes abruptly. Their structure is usually measured with standard balloon-

borne radiosonde equipment having time constants that limit the spatial resolution to about 15 metres. Thus, there is only a limited knowledge of how sharply defined such layers may be.

The work of Lane [4.31] and Richter [4.32] suggests that there are thin sharp gradients of refractive index, often well above ground, extending horizontally for many kilometres and persisting for hours at a time. Visual observation from aircraft passing through the boundary of a haze layer occasionally discloses a more or less regular undulation of the layer. Ludlam [4.33] suggested that the breaking of such waves produces much of the turbulence that occurs a kilometre or more above ground.

The 'classical' theory of atmospheric line-of-sight optical communication is usually attributed to Chernov [4.2] and Tatarskii [4.3], who solved the wave equation directly using perturbation techniques.

This work by Chernov and Tatarskii is formally known as the 'Method of Small Perturbations' and involves the expansion of the magnitude of the electric field into a series of ever-decreasing terms which may or may not converge. When the series converges a finite number of terms will accurately describe the propagation path. As the strength of the refractive index fluctuations increases the series does not converge resulting in an imperfect representation of conditions portraying the saturation effect and the model cannot then be applied.

Lawrence and Strohbehn [4.34] and Fante [4.35] have produced excellent reviews of the classical approach. However, the fundamental problem with the classical approach is that it does not adequately explain the saturation effect, which occurs at high levels of turbulence and/or longer path lengths.

4.3.2 Modern Theories

The 'classical' approach has been built on in more recent years by various 'modern' theories which were aimed at quantifying the saturation effect etc.

In order to make progress in the solution of the wave equation in this most difficult area most workers have made certain approximations which include the assumptions that:-

a. The fluctuating part of the dielectric constant is much smaller than the mean value,

b. the wavelength is very small compared with the size of a typical dielectric constant inhomogeneity,

c. the path length is large compared with the wavelength and size of inhomogeneity.

These approximations, either individually or combined, yield a number of different simplified forms of the wave equation. The various approaches are reviewed in some detail by Strohbehn [4.36] but three main approaches have been identified from the literature each of which yields the same overall result. They are all extremely complex and are beyond the scope of this thesis; the interested reader is referred to the various references for a detailed appraisal.

The so-called Diagram method was proposed by Bourret [4.37, 4.38] in which graphical techniques were applied in order to simplify the wave equation for the received optical field. The technique leads to reasonable solutions for the mean field similar to those for the classical approach. However, the mathematics are still extremely cumbersome particularly when endeavouring to establish the effects of

high levels of turbulence and/or long path lengths as is the case in the saturation region.

Tatarskii [4.39, 4.40] and Klyatskin [4.41-4.43] both developed similar techniques which used the Markov random process. In these techniques fluctuations in the atmospheric refractive index were assumed to be completely uncorrelated in the direction of propagation and as a consequence the equations for the moments of the electro-magnetic field could be derived using the Markov random process. The Markov approximation technique yields the same ultimate equations as the Diagram method and hence has the same drawbacks.

The classical approach, often known as the 'method of small perturbations' has been further developed by the 'modern' theorists by making similar assumptions to those made by Tatarskii in the Markov random process technique together with the assumptions that depolarisation and backscatter effects are negligible. The technique involves working on thin slabs of the atmospheric medium orientated perpendicular to the propagation axis. The thickness of each slab was assumed to be large compared with the largest inhomogeneity but small enough so that a perturbation method may be employed to calculate the field as it propagates through the slab. This method yields the same overall result as obtained for the other two 'modern' methods.

4.3.3 Usefulness of the 'Classical' and 'Modern' Theories

Both the classical and the modern theories are invariably extremely mathematically complex. The classical theory appears to be adequate for systems having short path lengths in which turbulence is not too severe. The modern theories which were developed in an endeavour to open up their applicability to include long path lengths and high levels of turbulence have not been particularly successful in this

respect, and as such do not currently have much to offer over and above the original classical approach.

4.4 IMPORTANT MATHEMATICAL MODELS

Following the Rytov premise that the log amplitude fluctuation, x, is normally distributed, Tatarskii [4.3] was able to deduce expressions for the log amplitude and log irradiance variances. The logarithm is taken in order to overcome the problem that the amplitude fluctuations can in practice be very large compared with the mean amplitude level. Assuming plane wave propagation and the Kolmogorov-Obukhov model for atmospheric turbulence [4.29] Tatarskii postulated that, for horizontal plane wave propagation through the atmosphere, the log amplitude variance σ_x^2 is given by:

$$\sigma_x^2 = 0.31\, C_n^2\, k^{7/6}\, L^{11/6}$$

$$\text{for } L_o >> (\lambda L)^{1/2} >> l_o \qquad (4.2)$$

To avoid any confusion it should be noted that $\sigma_l^2 = 4\sigma_x^2$ where σ_x^2 is the log amplitude variance and hence it follows that the log irradiance variance σ_l^2 is given by:

$$\sigma_l^2 = 1.24\, C_n^2\, k^{7/6}\, L^{11/6} \qquad (4.3)$$

where L = path length

L_o = outer scale of turbulence, typically 1 m.

l_o = inner scale of turbulence, typically a few mm.

$k = 2\pi/\lambda$

Expression (4.3) is sometimes referred to as the Rytov approximation since it employs an approach originally proposed by Rytov [4.24]. Although based on theoretical concepts it is in fact an empirically derived expression.

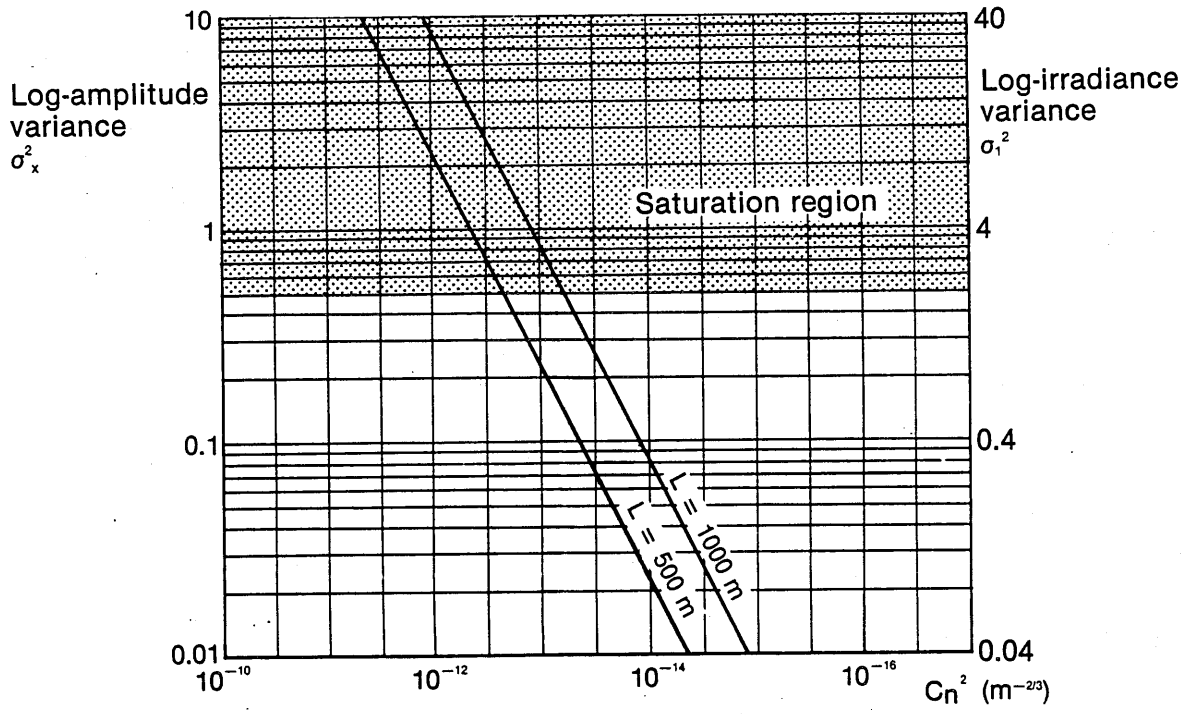

Figure 4.2 Log-amplitude and log-irradiance variances versus C_n^2 for different path lengths (for $\lambda = 1\mu m$)

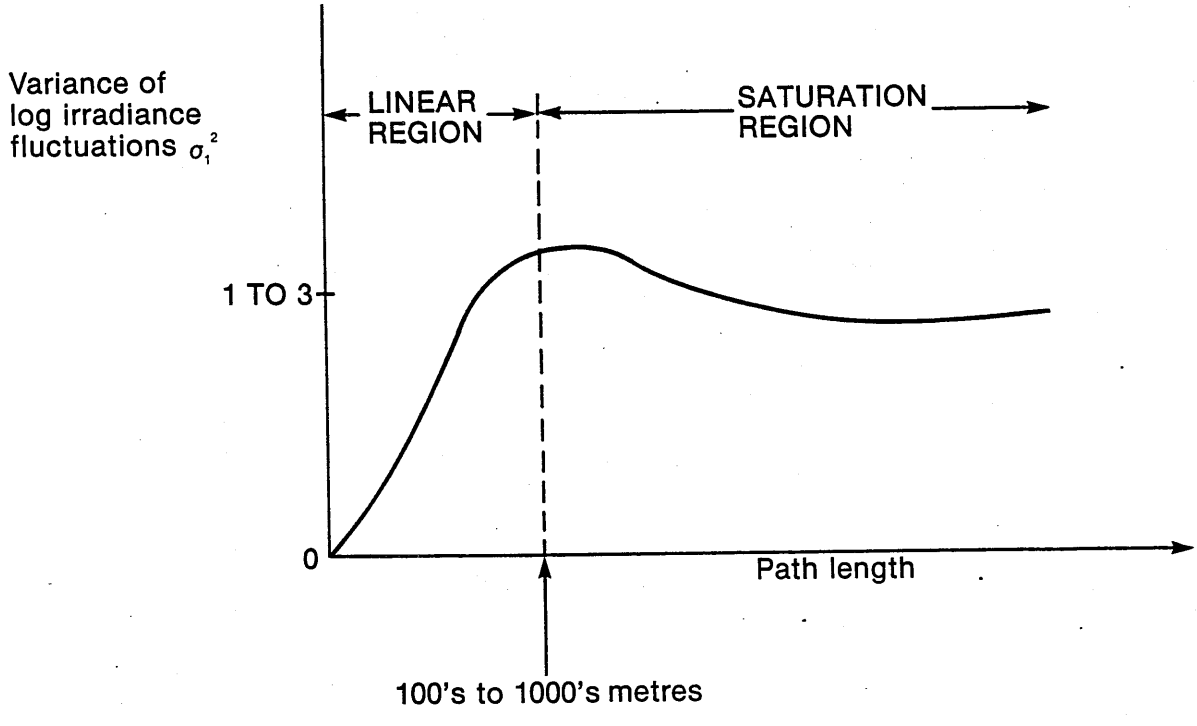

Figure 4.3 The variation of σ_1^2 with path length

For a system operating at a wavelength of one micron over a path length, L, of 1000 m, σ_1^2 becomes:-

$$\sigma_1^2 = 1.24\ C_n^2\ [2\pi \times 10^6]^{7/6} \times 1000^{11/6}$$
$$= 33.4 \times 10^{12} \times C_n^2$$

Figure 4.2 shows the relationship between σ_x^2, σ_1^2, and C_n^2 for path lengths of 500 and 1000 m and a wavelength of 1 micron.

4.5 THE 'SATURATION EFFECT'

4.5.1 General

It has been shown theoretically, and also physically observed for some time [4.44], that the variance of the logarithm of the optical signal amplitude (and hence irradiance) fluctuations increases with path length up to a certain distance. Physical measurements have shown that beyond this critical path length, σ_1^2 remains nominally constant, ie it has 'saturated'. This effect is extremely significant in the design of terrestrial line of sight optical communication systems since the maximum value of σ_1^2 for the maximum design path length for the system determines the required dynamic range of the receiver. A typical characteristic illustrating the saturation effect as path length is increased is shown in Figure 4.3.

The diagram illustrates the variation of the variance of the log irradiance with increase in path length. In the pre-saturation region the increase in value of variance is fairly linear with increase in path length. However, at path lengths of a few hundred metres saturation begins to occur such that further increases in path length do not result in any further increase in σ_1^2. Indeed in many instances σ_1^2 actually decreases a little to form a slight 'trough' in the saturation region.

Equation (4.3) indicates that the log irradiance variance σ_1^2 is proportional to $L^{11/6}$ and this appears to be applicable on shorter path lengths of a few hundred metres or less. However, as the path length is increased and 'saturation' of σ_1^2 occurs, the equation no longer holds [4.45]. Clifford et al [4.45] suggest that from their measurements the equation does not hold for values of σ_1^2 in excess of about 1.0.

Other workers suggest that saturation does not occur until σ_1^2 reaches a value of nearly 3.0 and that expression (4.3) applies up to this value. (Note that $\sigma_1^2 = 4\ \sigma_x^2$ ie the log irradiance variance equals four times the log amplitude variance.)

4.5.2 Theories to Explain the 'Saturation Effect'

The saturation effect, whereby the variance of the logarithm of the optical signal amplitude (or irradiance) fluctuations saturates as a critical path length is reached, has been the subject of various studies aimed at deriving some form of model to describe the effect.

It is noteworthy that to date there have been no theories published which fully adequately explain or quantify the saturation phenomenon [4.44, 4.46]. The most applicable model produced to date is that of Philips et al [4.47] who have developed a universal empirically derived mathematical model which appears to fit the practical data to an acceptable degree of accuracy. The model assumes log-normal statistics for short path lengths, a Rayleigh type distribution for the region around maximum variance of log irradiance fluctuations, and a negative exponential distribution beyond the maximum variance (see Figure 4.3). The model has yet to be verified by other workers.

The approaches mentioned in Section 4.3 were aimed at solving the wave equations for optical propagation in the atmosphere, and all yielded

extremely complex expressions which to date have not been solved in a manner which has been completely useful for comparison with experimental results over the full range of operational conditions. Moreover the approaches have not so far permitted an adequate understanding of the basic physical mechanism underlying the saturation process.

4.6 TECHNIQUES FOR ALLEVIATING SCINTILLATION EFFECTS

Scintillation in atmospheric digital communication systems gives rise to error rates greatly in excess of those which would be obtained if the medium was free space. In principal this degradation in system performance can be alleviated by:-

a. increasing the transmitted power,

or b. increasing the receiver sensitivity and/or the received power.

The following particular techniques are noteworthy:-

i Spatial Diversity Reception

This technique is a derivation of that commonly employed on fixed point to point microwave radio transmission systems, in which a number of receivers, say n, are utilised, each separated by more than a log-amplitude coherence length from the others. In this way n times the optical signal energy is received with n different scintillation values and hence improved error rate performance can be obtained.

ii Detector Arrays

This technique may be regarded as a variation of spatial diversity whereby a number of detectors provide spatial diversity reception but within the receiver and, of course, after the receiver lens aperture. This technique is of particular value in overcoming the effects of beam wander, and to a lesser extent beam spread.

iii Aperture Averaging

Equation (4.3) applies only to a point-sized receiver in which the fluctuations are correlated over the size of the receiver. As the receiver becomes bigger, the signal fluctuations become uncorrelated and are averaged over the aperture, with the overall effect of decreasing the total intensity fluctuation at the detector.

Shapiro [4.48] has established an aperture-averaging factor, F, which quantifies the amelioration of the fading that results from spatial-averaging of the scintillation within the receiver optics. The factor is given by:

$$F = \frac{\lambda L / A_R^2}{1 + (\lambda L / A_R^2)} \qquad (4.4)$$

where λ = wavelength

L = path length

A_R = effective area of receiver lens.

This expression was derived using the Tatarskii theory [4.39].

It has been suggested by Brookner [4.49] that for many applications a well designed direct detection system may not be significantly more sensitive to background radiation than for instance a heterodyne receiver system. Moreover, since direct detection is simpler to implement than heterodyne detection it tends to be a more practical proposition for many applications, especially terrestrial line of sight systems.

iv Coding and Messaging Techniques

Message repetition may be employed either in addition to the above or as an alternative. If a message of N bits is transmitted M times at intervals separated by more than the atmospheric coherence time, the

probability that all M repetitions are received with one or more bits in error is such that:-

$$P_e(M) = P_e^M$$

where P_e is the error probability for a single message transmission (ie when M = 1).

This technique is, of course, not particular to optical communication systems but can be of value in certain applications, particularly those where high system integrity and demanding performance is required eg military systems.

In addition or as an alternative to message repetition there are various error-correcting codes [4.50] which can be used in order to overcome the problems of poor or temporarily degraded error rate performance occuring as a direct result of turbulence induced scintillation.

4.7 CONCLUSIONS

There have been various theories produced to explain and quantify the saturation effect but none have been completely successful and not for the want of using some exceedingly complex mathematical procedures. It has to be concluded therefore that for atmospheric optical communication systems the theories hitherto derived are only really accurate for short path lengths and/or low levels of turbulence. Further research is clearly required for a fuller understanding of the physical processes involved for systems having long path lengths and/or high levels of turbulence.

CHAPTER 5

THE ATMOSPHERIC REFRACTIVE INDEX STRUCTURE PARAMETER

CHAPTER 5

THE ATMOSPHERIC REFRACTIVE INDEX STRUCTURE PARAMETER, C_n^2

5.1 INTRODUCTION

This chapter introduces and discusses the concept of the atmospheric refractive index structure parameter, designated C_n^2, which provides a measure of the magnitude of atmospheric turbulence. Results of C_n^2 measurements obtained by other workers are presented and discussed. Methods of measurement of C_n^2 are compared and the optimum technique for use in the practical part of this research is deduced.

5.2 MATHEMATICAL FORMULATION FOR C_n^2

The refractive index of air at optical frequencies is given by [5.1]:-

$$n = 1 + \frac{77.6P}{T}\left[1 + \frac{7.52 \times 10^{-3}}{\lambda^2}\right] \times 10^{-6} \qquad (5.1)$$

where P is the atmospheric pressure in millibars

T is the temperature in degrees Kelvin

λ is the wavelength of interest in micrometres (microns)

At sea level n = 1.0003 typically. It should be noted that equation (5.1) above does not include a term which introduces the effect of water vapour pressure but on land this term can be neglected since it contributes significantly less than 1% to the result. More precise formulae which include the water vapour term are given by Owens [5.2].

The turbulence induced refractive index variations of interest occur principally as a result of naturally occurring random fluctuations in wind velocity. The latter can be aggravated by man made sources of heat such as building ventilation outlets etc which can be particularly troublesome if an optical line of sight link passes directly over such an outlet. The

theory of turbulence is covered extensively in the literature [5.3-5.6] and has also been addressed in Chapters 2 and 4 of this thesis.

In turbulence theory the term 'structure' is used to describe dimensionless properties of the turbulence, such as spectrum or correlation shapes or ratios of stress components [5.6].

Most optical phenomena depend on differential rather than absolute path lengths and hence the statistics of random index fluctuations and of random wavefronts can be given in terms of structure functions. The structure function, $D_R(r)$, for an arbitrary spatially distributed random variable $R(r)$, can be defined as:-

$$D_R(r) = \langle [R(r_1) - R(r_2)]^2 \rangle \qquad (5.2)$$

where $r = r_1 - r_2$ = a vector quantity

$\langle\ \rangle$ = represents an ensemble average

If the random process generating R is isotropic, then $D_R(r)$ is a function only of $r = |r|$. Thus, for instance, the structure function for temperature functions may be represented as $D_T(r) = \overline{(t_1 - t_2)^2}$.

Kolmogorov [5.7] proposed a mathematical model for fluid velocity turbulence which was discussed in Chapter 4. It will be recalled that the fundamental feature of this model was the hypothesis that the kinetic energy associated with the larger turbulent eddies is redistributed, without loss, to successively smaller and smaller eddies, until finally dissipated by viscosity (see Figure 4.1).

In the open atmosphere solar heating generates atmospheric kinetic energy over scale sizes (L_o) that extend from a few to many metres. Kinetic energy leaves the air by frictional generation of heat over scales, l_o, which are generally less than a few millimetres in size at the earth's

surface. The intervening range is called the inertial sub-range, and typically ranges from a few millimetres to a few metres.

Kolmogorov suggested that for most practical applications over this sub-range, where $l_o << r << L_o$, the structure function for temperature fluctuations $D_T(r)$ obeys a two-thirds power law [5.7] such that:-

$$D_T(r) = C_T^2 r^{2/3} \tag{5.3}$$

where C_T^2 = temperature structure parameter

Re-arranging expression (5.3) gives:

$$C_T^2 = \frac{D_T(r)}{r^{2/3}} = \frac{\overline{(t_1-t_2)^2}}{r^{2/3}} \tag{5.4}$$

For the case where $r << l_o$, $D_T(r)$ varies as r^2.

The Kolmogorov suggestion that equation (5.3) is valid has been supported by experimental evidence from Myrop [5.9] and Kaimal et al [5.10]. Equation (5.3) is the basis for the modelling of optical propagation through the turbulent atmosphere, but for it to be really useful it still needs to be related to the refractive index of the atmosphere.

The Kolmogorov theory predicts that, since C_T^2 and C_n^2 are of the same form, the two-thirds power law may also be applied to the structure function of the refractive index, D_n, [5.7]. Hence by analogy it may be stated that:-

$$D_n(r) = C_n^2 r^{2/3} \tag{5.5}$$

where C_n^2 = refractive index structure parameter, the dimensions of which are (length) $^{-2/3}$ (from equation 5.5).

The next step is to relate equation (5.5) to the refractive index of the atmosphere. Equation (5.1) gives the refractive index of the atmosphere, n, in terms of temperature, T, and pressure, P.

The structure function for n can be determined by differentiating equation (5.1) with respect to T such that [5.31]:

$$\frac{\delta n}{\delta T} = \frac{-77.6P}{T^2}\left[1 + \frac{0.00753}{\lambda^2}\right] \times 10^{-6} \qquad (5.6)$$

It follows from equation (5.6) that:

$$C_n^2 = \left[\frac{77.6P}{T^2}\right]^2 \left[1 + \frac{0.00753}{\lambda^2}\right]^2 \times 10^{-12}\, C_T^2 \qquad (5.7)$$

and in particular:

$$C_n^2 = \left[\frac{(79.06P)10^{-6}}{T^2}\right]^2 C_T^2 \quad \text{for } \lambda = 0.633\ \mu m \qquad (5.8)$$

and:

$$C_n^2 = \left[\frac{(78.32P)10^{-6}}{T^2}\right]^2 C_T^2 \quad \text{for } \lambda = 0.9\ \mu m \qquad (5.9)$$

Using the expression for C_T^2 in expression (5.4) and inserting in equation (5.9) we obtain for wavelengths of typical system operation of 0.9 μm:

$$C_n^2 = \left[\frac{(78.32P)10^{-6}}{T^2}\right]^2 \cdot \frac{\overline{(t_1-t_2)^2}}{d^{2/3}} \qquad (5.10)$$

Using equation (5.10) values for C_n^2 may be calculated from measured values of P and T and knowing the temperature structure parameter C_T^2.

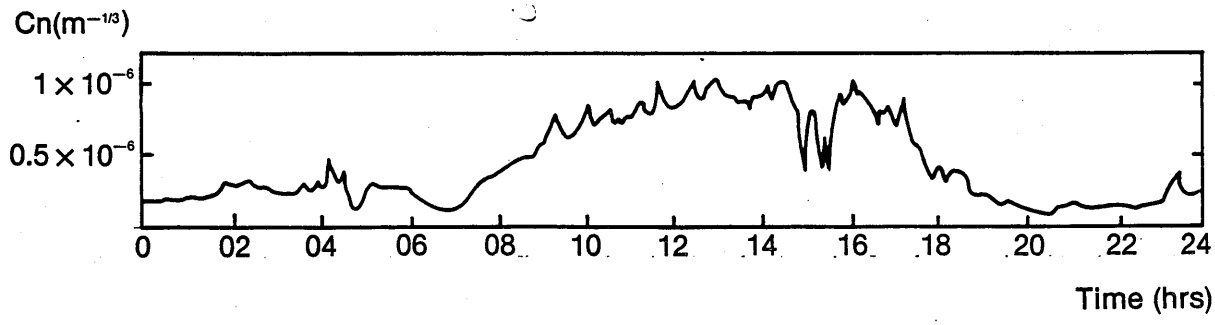

Figure 5.1 Plot of the behaviour of the refractive index structure parameter for a 24 hour period on a clear sunny day (from ref 5.11)

Techniques for measuring C_T^2 are considered in Section 5.4. It should be noted that C_n^2 has the dimensions $m^{-2/3}$.

The foregoing analysis has indicated that the refractive index fluctuations due to turbulence, have the same statistical properties (ie have the same structure function law) as velocity turbulence. In particular it has been noted that variations in the refractive index of the atmosphere are caused predominantly by variations in temperature.

5.3 EXPERIMENTAL ARRANGEMENTS AND PUBLISHED MEASURED C_n^2 DATA

Clifford [5.11] has published details regarding the behaviour of C_n^2 as a function of altitude and time of day, and a typical plot for a clear sunny day is given in Figure 5.1. [Note: For a reason which is not particularly clear to the author, Clifford has presented his results showing C_n rather than C_n^2. The principles and associated comments are still valid however.] This plot was obtained at a height of 2 m above the ground and measured near the National Bureau of Standards, Boulder, Colorado, USA.

The measurements were made using two fine-wire thermometers as described by Lawrence [5.12] and then computing the value of C_T^2 by dividing the mean square temperature difference of the two thermometers by the thermometer spacing to the two-thirds power. C_n^2 was then obtained using equation (5.10).

From Figure 5.1 it can be seen that there is a distinct diurnal variation which is typical for measurements made at heights of up to about 100 m above the ground. The general level of C_n^2 and the magnitude of its fluctuations is low at night-time but as the sun rises and solar heating of the ground commences, air convection currents occur which result in a gradual increase in the value of C_n^2, and in the magnitude of the fluctuations of C_n^2.

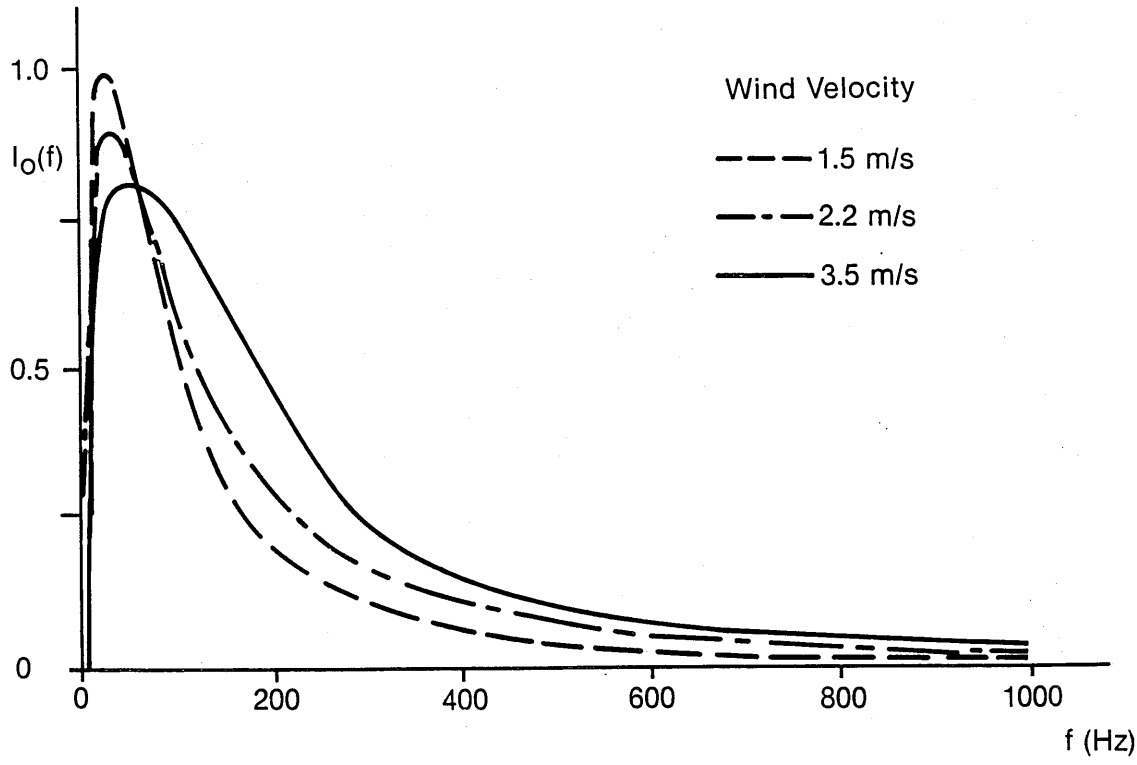

Figure 5.2 Normalised frequency spectrum of optical intensity and hence C_n^2 fluctuation for different wind speeds

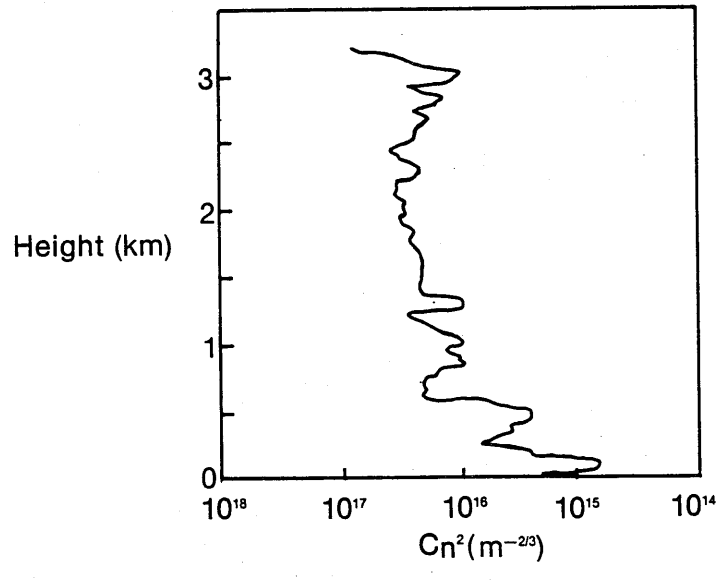

Figure 5.3 Variation of C_n^2 with altitude (after ref 5.15)

Clifford [5.11] has explained the effect as follows: the sun's rays warm the surface of the earth which in turn warms the layer of air adjacent to the earth. If air parcels from the layer become displaced upwards, they find themselves warmer and hence less dense and more buoyant than the ambient air. They therefore continue to accelerate upwards and it is the mixing of the rising hot air parcels with cool descending air which produces the observed temperature differences. Clifford reports typical values of C_n^2 for a sunny day as being in the range 10^{-16} to $10^{-12} m^{-2/3}$ with the smaller (first) value representing weak turbulence and the other extreme representing severe turbulence.

It is interesting to note in Figure 5.1 that the sharp dips in C_n^2 occurring between 1400 and 1600 hrs are due to intermittent cloud cover which caused the ground to cool rapidly and convection to be reduced resulting in somewhat lower values of C_n^2 being measured.

The C_n^2 fluctuations for different wind speeds have been reported by Tatarskii [5.12] and Figure 5.2 shows the measured results for the normalised frequency spectrum of received optical intensity which corresponds to the C_n^2 fluctuations for wind speeds of up to 3.5 m/s.

It has been found that C_n^2 varies with altitude above the ground and various measurements have been made by means of tower mounted sensors [5.14], aircraft mounted sensors [5.13, 5.15] and balloon borne sensors [5.14].

Oochs and Lawrence [5.15] in particular have shown the complicated behaviour of C_n^2 with increase in altitude and typical results which they obtained are shown in Figure 5.3, from which it can be seen that the variations are somewhat random but with a generally decreasing mean value of C_n^2 with height. Neff [5.14] has proposed that the mean value of C_n^2 decreases in proportion to (height above ground)$^{-4/3}$,

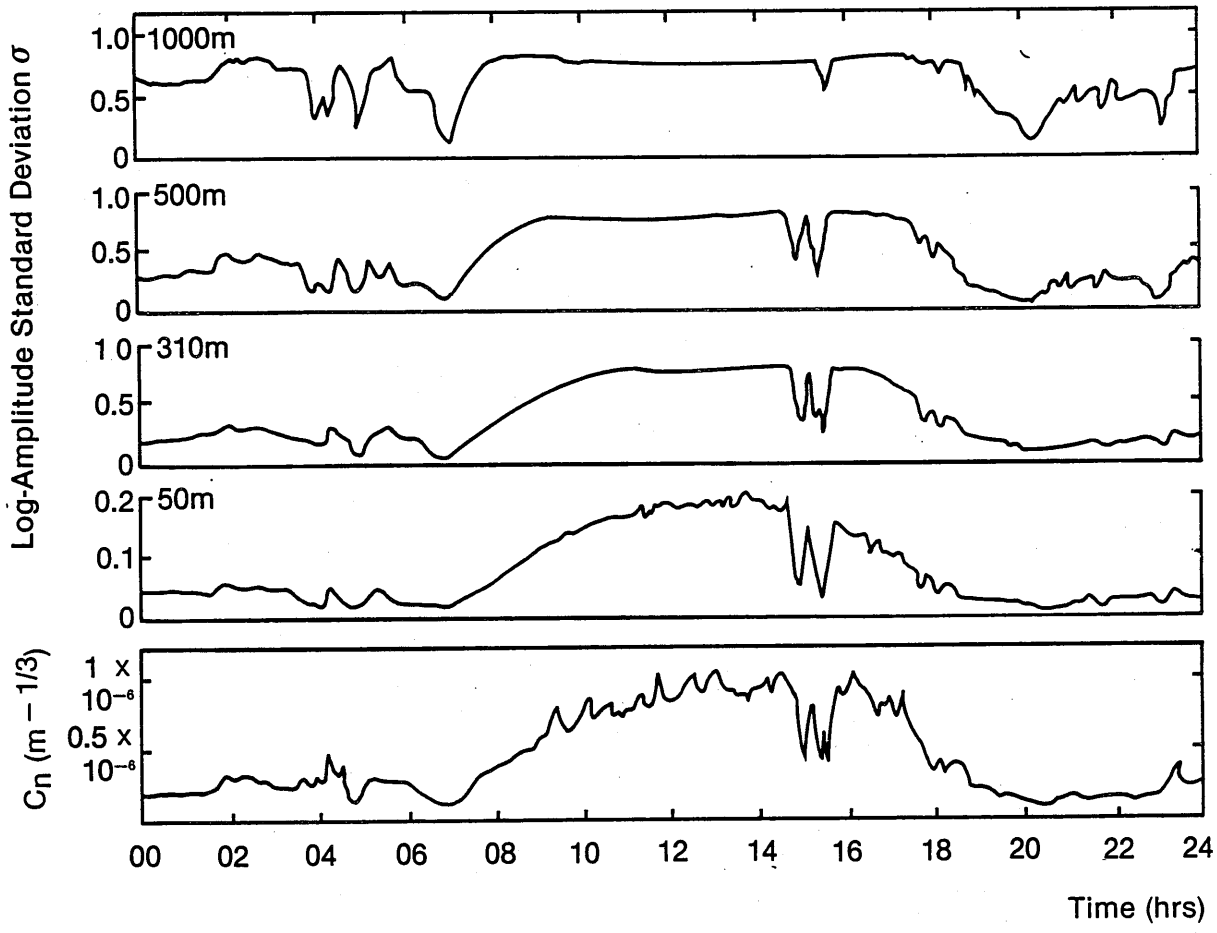

Figure 5.4 Variation of the log-amplitude standard deviation σ for each of 4 path lengths and the corresponding refractive index structure parameter C_n measured at Boulder USA over a 24 hour period (from ref 5.11)

and this has been supported by data obtained by Frisch and Oochs [5.16]. This reduction in mean value with height can be accounted for by the reduced effect of convection as the height above ground is increased, and hence a corresponding reduction in turbulent effects. A more detailed review of this particular aspect is given by Clifford [5.11].

Clifford [5.11] has also published results which clearly show the saturation effect as in Figure 5.4. The results show the flattening of the peak levels of log amplitude standard deviation as the path length increases despite a continued increase in C_n^2.

5.4 TECHNIQUES FOR MEASUREMENT OF C_n^2

5.4.1 General

In any practical studies of turbulence in the atmosphere it is necessary to consider and to measure the atmospheric refractive index structure parameter known as C_n^2. As has already been discussed C_n^2 is the most important single parameter in considering atmospheric turbulence and is a direct measure of the magnitude of such turbulence. The study of turbulence in general, and turbulence in the atmosphere in particular, tends to be a rather esoteric subject. As a result the number of researchers around the world who have actually measured C_n^2 is exceedingly small. As a consequence it is perhaps not surprising that there is not a generally agreed technique for measuring C_n^2. Three approaches are considered in this thesis based on:-

i the use of microthermometers;

ii measurement of the amount of scintillation at the receiver;

iii deduction of C_n^2 from the amount of beam wander and spreading.

In each case the theoretical basis and the practical design implications are considered.

5.4.2 Microthermometer Approach

5.4.2.1 General

Turbulence in the atmosphere is due to variations in temperature between adjacent 'volumes' of air, where these 'volumes' can be in the order of l_o (known as the inner scale of turbulence), where $l_o << (\lambda L)^{\frac{1}{2}}$. Thus for $\lambda = 10^{-6}$ m and L = 1000 m then $l_o << 32$ mm. These small temperature differences are characterised by the atmospheric temperature structure parameter, C_T^2, which can be fairly readily measured using two small temperature probes having a fast response time spaced such that the spacing, d, is given by $l_o < d < L_o$ (l_o and L_o being the inner and outer scales of turbulence respectively. Note that L_o is typically of the order of 1 m or more.). The refractive index structure parameter C_n^2 is a direct function of C_T^2, which is given by the mean of the square of the difference in temperature measured by the sensors, divided by the sensor spacing to the 2/3 power. Thus the value of C_n^2 can be readily established (see equation 5.7).

5.4.2.2 Theory

In Section 5.2 an expression for C_n^2 was derived in terms of the temperature difference between two sensors spaced a distance d apart. The expression applicable for wavelengths of 900 nm, is given as:

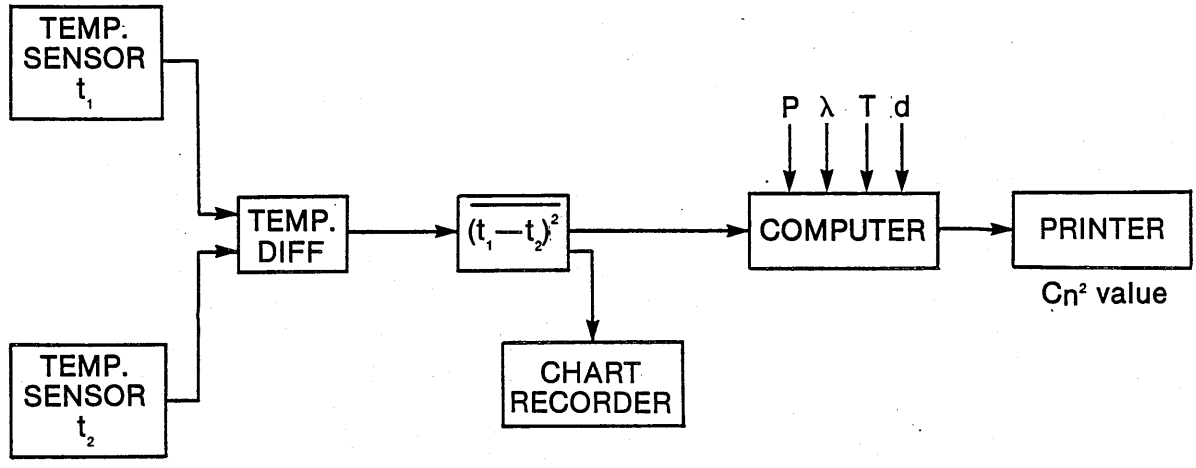

Figure 5.5 Block schematic of temperature sensor arrangement

$$C_n^2 = \left[\frac{78P}{T^2} \times 10^{-6}\right]^2 \cdot \frac{\overline{(t_1 - t_2)^2}}{d^{2/3}} \qquad (5.11)$$

where P = mean atmospheric pressure in millibars

T = mean atmospheric temperature in degrees Kelvin

$t_1 - t_2$ = temperature difference between temperature sensors 1 and 2

d = separation of temperature sensors 1 and 2

5.4.2.3 Practical Design Considerations

5.4.2.3.1 General

The theory in Paragraph 5.4.2.2 above indicates that the temperatures at two points spaced d mm apart must be sensed. The difference temperature must then be obtained and the mean square value determined. A measure of the value of C_n^2 is thus obtained; the precise value of C_n^2 is deduced knowing the values for mean pressure, mean temperature, wavelength of interest and the spacing of the two temperature probes. A block diagram of an arrangement is given in Figure 5.5.

5.4.2.3.2 Temperature Sensors

The temperature difference to be measured is of the order of 0.002 to 2°K [5.17] and the fluctuations may be at a rate of up to 1000 Hz. It follows therefore that the temperature probes must desirably:-

a. be highly sensitive - being capable of sensing differences of as little as 0.002°K;

b. have a fast response time - that is desirably less than 1 ms;

c. be no greater in size than the inner scale of turbulence l_o, ie < c.30 mm.

The possibilities are:-

i Fine Wire Temperature Probes

The most suitable material for use as fine wire temperature probes is platinum because of its high stability and purity [5.18]. It also has a highly linear resistance temperature coefficient.

In order that accurate measurements of the temperature of a given 'volume' of air can be made, the probe needs to be the same size or preferably smaller than the diameter of the said volume. The diameter of concern is the inner scale of turbulence l_o which for $\lambda = 10^{-6}$ m and L = 1000 m is approximately 32 mm. Thus the length of the sensitive part of the probe must be <32 mm.

For a wire to have a response time of 2 ms or better it should have a diameter, d_w, of less than typically 0.02 mm (see Appendix 3).

Hence the need is for a platinum wire no greater than 0.020 mm in diameter and < 32 mm in length. Such wire is not readily obtainable but it can be produced by using 'Woolaston' wire, which is platinum wire coated with silver. The latter can be etched away using dilute nitric acid to reveal the required length and diameter of platinum. The silver either side of the exposed platinum provides

a useful means of terminating what would otherwise be an extremely delicate and fine wire.

An alternative yet highly practical method is the use of light bulb filaments. For instance a miniature christmas tree light bulb with its glass bulb removed, yields a tungsten filament of typically 0.05 mm in diameter and up to about 5 mm in length. Whilst these dimensions are less than perfect the technique presents a highly practical approach to the problem. Keeping the filaments in the light bulb base, but without the glass, greatly facilitates the probe mounting problem which, with other approaches, is certainly non-trivial. However, this alternative approach does have the major drawback that fast temperature variations will not be detected.

ii Thermocouples

Thermocouples are a distinct possibility for use as temperature difference sensors in this application due to their inherent relative measurement capability.

The use of a reference and a sensor junction spaced apart by an appropriate amount gives a direct indication of the temperature differential between the sensors. Thermocouples have sensitivities of the order of 50 microvolts/°C or so, which means that careful design of subsequent voltage amplifiers is very necessary in order to avoid thermal noise, and external and mains interference problems.

The only real drawback of thermocouples is their response time of up to 1-2 seconds. This is somewhat longer than is really desired for really precise and versatile C_n^2 measurements, although not totally unacceptable.

iii Thermistors

Thermistors make good temperature sensors in principle having as they do a good temperature sensitivity (typically 100 ohms/°C). Moreover they are relatively simple to use and are highly accurate.

Unfortunately owing to their physical structure they have a rather long time constant of not less than 5 seconds and they suffer from self-heating effects, which can give rise to significant erroneous results especially when temperatures of less than 1°C are to be measured.

iv Integrated Circuit Bandgap Temperature Sensors

These devices are not generally sufficiently sensitive for the small temperatures to be measured in C_n^2 measurements and they normally have a response time of 5 seconds or more, which completely rules them out for this application.

v Quartz Crystal Temperature Sensors

These devices are exceedingly accurate to 0.0001°C and clearly would be highly desirable for use in this application. Regrettably owing to the relatively large mass of the quartz crystal sensors used, the response

time is of the order of 9s [5.19], which makes them unsuitable for C_n^2 measurements.

It follows from the foregoing that the really important temperature sensor parameters for C_n^2 measurements are:-

- high accuracy, ie accurate to better than 0.01°C;
- fast response time, ie much less than 1s.

Appendix 2 compares the common types of temperature sensor and they are summarised in Table A2.2 of Appendix 2. Appendix 3 gives some data on the use of fine wire sensors and requisite electronics and Appendix 4 considers a design using thermocouples. All the sensors can be considered to be adequately responsive and acceptably accurate. However, only the wire resistance technique has a fully acceptable response time, and even then only if the wire is no greater than a few microns in diameter. Unfortunately, such wire is not readily available largely due to lack of demand but also because of its fragility.

It is concluded that, for microthermometric measurements of the type required in this project, although the use of platinum wire resistance temperature sensors is the ideal option, a practical alternative is the thermocouple approach which is fairly readily implemented, albeit with a slight loss of performance in respect of measured response time of the higher frequency temperature fluctuations. The significance of this is that the measurement accuracy is dependent on the rate of temperature fluctuations which in truth is a function of the mean ambient temperature and wind velocity. Wind fluctuations of the order of 500

Hz and more have been experienced [5.20], but the magnitude of these fluctuations is about one tenth of those measured in the range 20-80 Hz. Figure 5.2 shows typical frequency spectra for different wind velocities. In view of this data fast acting thermocouples are therefore considered to be adequate and the technique is thought to be well worth adopting in addition to or instead of the wire resistance approach.

Details concerning the actual measurement of the refractive index structure parameter as part of this project are given in Chapter 7 and the apparatus actually employed which utilised thermocouples in the thermometric approach is detailed in Appendix 4.

5.4.3 Scintillometer Approach

5.4.3.1 General Theory

This approach is based on the measurement of the received scintillating optical signal. The optical signal is detected and then processed electrically in order to derive the log irradiance variance. The latter is related to the refractive index structure parameter by the empirically derived expression:-

$$\sigma_1^2 = 1.24\ k^{7/6}\ L^{11/6}\ C_n^2 \qquad (5.12)$$

This expression which was considered in Chapter 4, was derived by Tatarskii [5.21] as part of his massive tome on the subject of atmospheric turbulence. Various workers including Dowling et al [5.22] and Ochs et al [5.23] have obtained results which have supported the validity of equation (5.12) provided that one does not enter the saturation region, ie the expression is only valid for values of σ_1^2 up to about 1.

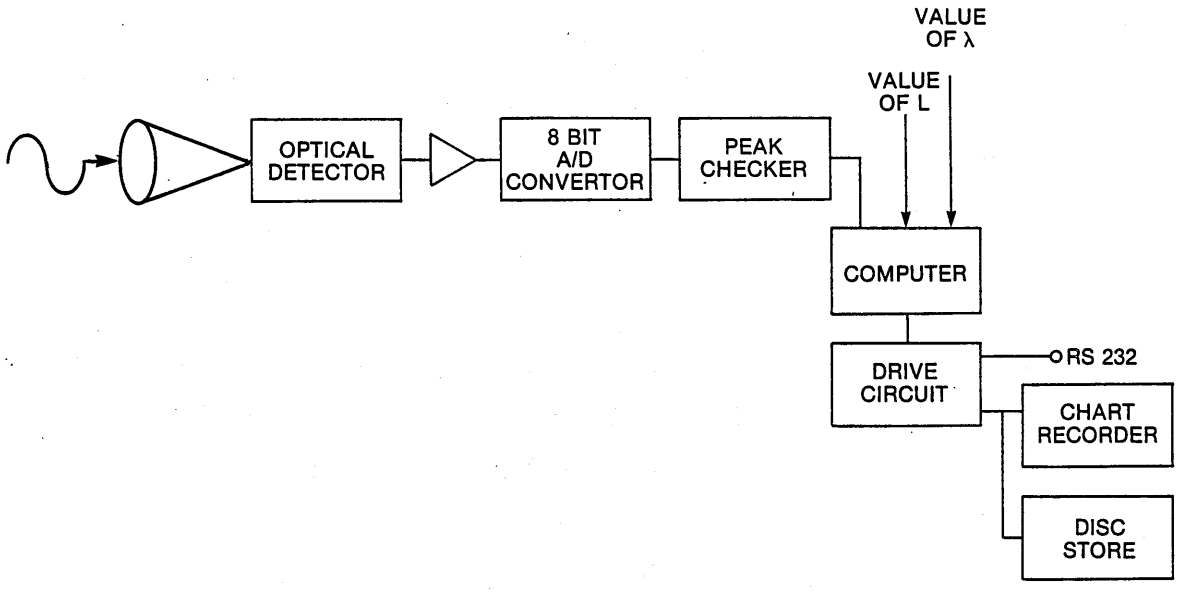

Figure 5.6 Scintillation equipment for $C_{n_1}^2$ measurement

A diagram showing the fundamental measuring arrangement is given in Figure 5.6.

There are two variations of this technique defined by the use of:-

a. large aperture receivers;

b. small aperture receivers.

The merits of each are discussed below.

One other approach which has been employed by Wesely et al [5.24] involves the assessment of visual resolution.

5.4.3.2 Practical Techniques

5.4.3.2.1 Determination of C_n^2 using Large Aperture Receivers

Wang et al [5.25] have proposed a single receiving aperture scintillometer in which the effective diameter D_R of the receiver is such that :-

$$D_R >> (\lambda L)^{\frac{1}{2}} \qquad (5.13)$$

Wang proposed an empirically based theory which introduced the effective lens diameter into equation (5.12) resulting in Expression (5.14):

$$\sigma_1^2 = 0.9\ C_n^2\ L^3\ D_R^{-7/3} \qquad (5.14)$$

Re-arranging (5.14) yields:

$$C_n^2 = \frac{\sigma_1^2\ D_R^{7/3}}{0.9\ L^3} \qquad (5.15)$$

For a given receiver the value of effective diameter of the receiver is fixed and known, as is the path length L. Thus

measurement of the variance of the log irradiance of the received signal enables a measure of C_n^2 to be obtained.

Hill et al [5.26] have suggested that $D_R > 20\ l_o$, where l_o = inner scale of turbulence, for best results.

5.4.3.2.2 Determination of C_n^2 using Small Aperture Receivers

Using a small aperture receiver ensures that the effects of aperture averaging can be ignored and, provided the system is operated at a point beneath the saturation level of the scintillating signal then the expression in (5.12) can be directly employed. Re-arrangement of equation (5.12) yields:-

$$C_n^2 = \frac{\sigma_l^2}{1.24\ k^{7/6}\ L^{11/6}} \qquad (5.16)$$

Thus with knowledge of the path length and wavelength, measurement of the variance of the logarithm of the received signal irradiance can be used to obtain information on C_n^2.

5.4.4 Beam Wander and Beam Spread Approach

5.4.4.1 Theory

Beam wander and beam spreading are a function of the angular variations of the light beam as it travels along a given path and in this instance these angular variations due to atmospheric turbulence are of prime concern. It is therefore necessary to consider as a starting point the angular variations.

Various workers have addressed themselves to the problem including Chernov [5.27], Beckmann [5.28], Hodara [5.29] and Chiba [5.30]. The latter in particular gives a theoretical

analysis using the ray equation which is particularly useful, albeit rather complex. The approach involves the calculation of the mean square deviation of the ray, $\Delta\theta^2$, from its initial direction after travelling a distance ΔL. Integration and substitution of the Kolmogorov relationship between the refractive index structure parameter and the corresponding correlation function yields an expression for the variance of the angular variation, σ_θ^2, given by:-

$$\sigma_\theta^2 = 5.7\ C_n^2\ L\ w_o^{-1/3}\ (1 \pm \theta L/6w_o) \qquad (5.17)$$

where: θ = planar beam angle

W_0 = beam diameter

Beam wander can be considered as the differential coefficient of the angular variation along the path multiplied by the distance from the point in question to the receiving point when projected on the receiving plane. Since the angular variation through the atmosphere is small and its differential coefficients with respect to the path are statistically independent of each other, following Chiba's approach [5.30] and substituting for W_0 and θ, equation (5.17) can be used as a basis for deriving an expression for the variance of beam wander σ_p^2, such that:

$$\sigma_p^2 = 1.83\ C_n^2\ \lambda^{-1/6}\ L^{17/6} \qquad (5.18)$$

For $\lambda = 1000\ nm = 10^{-6}\ m$

$$\sigma_p^2 = 18.3\ C_n^2\ L^{17/6} \qquad (5.19)$$

Equation (5.19) clearly indicates that beam wander is a direct function of C_n^2 for a given path length L. Figure 5.7

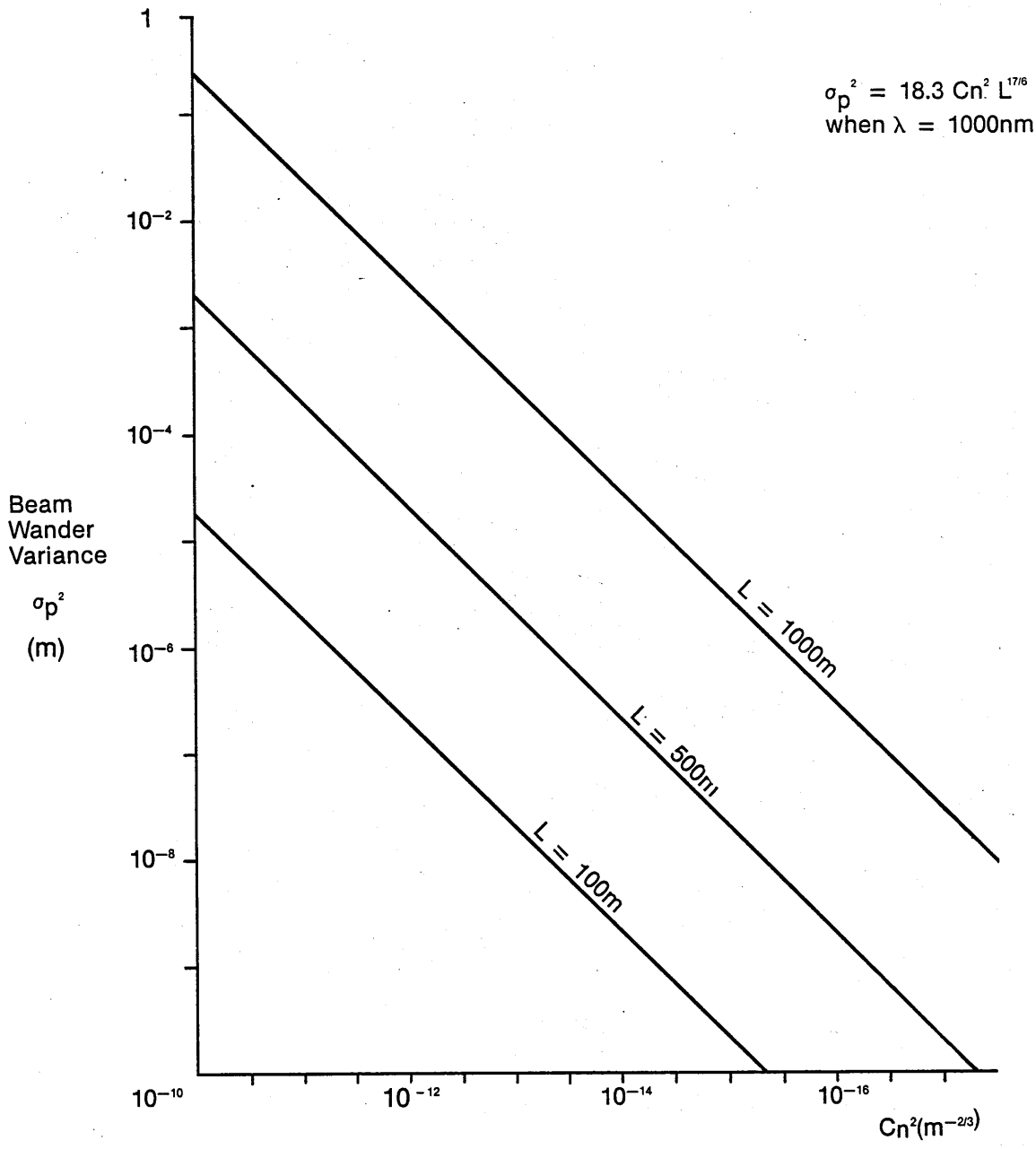

Figure 5.7 Beam wander variance vs C_n^2 (derived from equation 5.19)

illustrates the order of magnitude of beam wander in terms of its variance for a given path length for different values of C_n^2.

5.4.4.2 Practical Approaches

5.4.4.2.1 Visual Resolution Technique

This technique used by Wesely et al [5.24] is probably the simplest of all the techniques for the determination of C_n^2. In effect the technique consists of the visual observation of the atmospheric blurring of point sources. An incoherent light source, typically a quartz-halogen lamp is placed behind a screen which has a number of apertures located in it. The diameter of the aperture is desirably about 10% of the spacing between the apertures. The light issuing from the apertures is then observed from a distance (ie a few hundred metres). Wesely [5.24] has suggested that the estimate of angular resolution of the point sources when observed from a distance L is given by:-

$$\theta_e = 3.4\ \lambda^{-1/5}\ L^{3/5}\ (C_n^2)^{3/5} \qquad (5.20)$$

where the constant of 3.4 is empirically derived.

Field experiments by Wesely have indicated that measurements of C_n^2 can be taken by visual observation of the atmospheric blurring of two point sources of light. For lines of sight at about 1-2 m above ground level the response of the human eye is slow enough for use of long exposure estimates of image degradation, but fast enough to detect and ignore image dancing caused by spatial inhomogeneities larger than the outer scale of turbulence.

The equipment necessary for estimates of C_n^2 is limited to a suitable telescope and light sources. On the assumption that the atmosphere's limiting resolution angle is at least 4 λ/D (where D is the effective lens diameter) for a typical portable astronomical telescope with Cassegraine optics, the effects of the telescope can be ignored and a simple calculation of C_n^2 from θ_e, L and λ can be made from Expression (5.21) (derived from Equation (5.20)):

$$C_n^2 = (0.3\ \theta_e)^{5/3}\ \lambda^{1/3}\ L^{-1} \qquad (5.21)$$

5.4.4.2.2 Photodetection of optical signal and analysis of beam spread and beam wander in electrical domain.

In this arrangement the received optical signal is detected by a matrix of opto-electronic detector photodiodes. The electrical signals so derived, after amplification, can then be analysed to yield a measure of beam spread and beam wander. The ideal arrangement would employ a large matrix array of photodiodes, say 100 x 100, in order to provide detailed data on the variation of the characteristics of the received optical signal. In practice such an arrangement obviously results in some considerable circuit complexity and signal analysis capacity problems. Clearly reducing the number of photodetectors reduces the accuracy of the data in proportion.

Chiba [5.30] has shown that beam wander is not just in a vertical direction, but does in fact 'dance' around quite considerably (see Figure 3.3), hence the need for a two dimensional matrix rather than just a linear array. He has

shown that the magnitude of this 'spot dancing', as it is sometimes known, can be as much as 30 mm for a path length of 1380 m and at a wavelength of 632 nm during periods of high values of C_n^2 (see Figure 3.7).

The biggest problem with this approach is that the magnitude of beam wander is likely to be only of the order of 10-30 mm at most even for a path length of 1000 m and consequently a precision compact matrix array of the type mentioned above would really be required if accurate and meaningful results were to be obtained.

5.5 CONCLUSIONS

Each of the three main techniques discussed in Section 5.4 above is a fairly practical method of deriving a measure of C_n^2. The scintillometer and beam wander and spread approaches are based on empirically derived expressions and as such are only suitable for giving relative changes in C_n^2 (unless otherwise calibrated). The latter in addition requires precise determination of the magnitude of beam wander in order to obtain an accurate measurement leading to a requirement for a multi-detector compact array. The microthermometric approach is an absolute measure of C_n^2 and as such is preferred over the other two approaches. As already discussed it does suffer from somewhat greater complexity than the others, and the selection of suitable temperature sensors is quite critical. In the microthermometric approach C_n^2 is measured at a single point rather than as a composite measurement over the whole path length as is the case with the other techniques, but measurements which were carried out as part of this research work and which are reported in Chapter 7 suggest that this is not in fact a problem. On balance the microthermometric approach is considered to be the best because:-

i it provides an absolute measurement of C_n^2;

ii it is based on an adequate theoretical basis and does not rely on any empirically derived relationships;

iii it is in principle more accurate than the other methods.

Of the various microthermometric techniques which might be employed the following were considered in detail:-

a. The platinum wire sensor technique (the arrangement is given in Appendix 3).

b. The thermocouple approach which is somewhat simpler, although because the voltages being measured are of the order of tens of microvolts a low noise restricted bandwidth amplifier arrangement is necessary as described in more detail in Appendix 4. The results reported in Chapter 7 suggest that the longer time constant of the thermocouple approach, when compared with the fine-wire sensor approach, is not in fact a problem for the type of measurement required for this measurement program.

The practical difficulties encountered in the use of fine wire sensors during the practical phase of this research project are discussed in Appendix 3 and resulted in the adoption of the thermocouple approach for the practical measurements of C_n^2 which were needed for the validation of the hypothesis. The practical results are reported in Chapter 7.

PART II

HYPOTHESIS

CHAPTER 6

THE ERROR RATE HYPOTHESIS

CHAPTER 6

THE ERROR RATE VS C_n^2 HYPOTHESIS

6.1 INTRODUCTION

This chapter presents a hypothesis for the relationship between different performance parameters of an atmospheric optical communications system and in particular between the error rate performance and the level of atmospheric turbulence.

6.2 THE HYPOTHESIS

It is contended that, whilst there are many system parameters in an atmospheric optical communications system which will affect the overall error rate performance of the system, eg path length, lens aperture diameter etc, they are invariably systematic in nature, and can usually be readily taken into account in the system design in order for a given steady state error performance to be achieved. However, it is postulated here that atmospheric turbulence can give rise to significant variations in the basic error performance of a system when compared with a non-turbulent environment. The atmospheric turbulence is generally measured as a function of the atmospheric refractive index structure parameter, C_n^2, and hence it is the relationship between this latter parameter and error-rate performance which is important for the purposes of this hypothesis.

It should be particularly noted that the hypothesis considers only the effect of scintillation arising from atmospheric turbulence. Other effects due to atmospheric turbulence such as beam broadening and beam wander have been shown to be insignificant for systems having relatively short path lengths eg less than about 1 km (see Chapter 3). Moreover the hypothesis considers only the region in which log-normal statistics apply ie systems

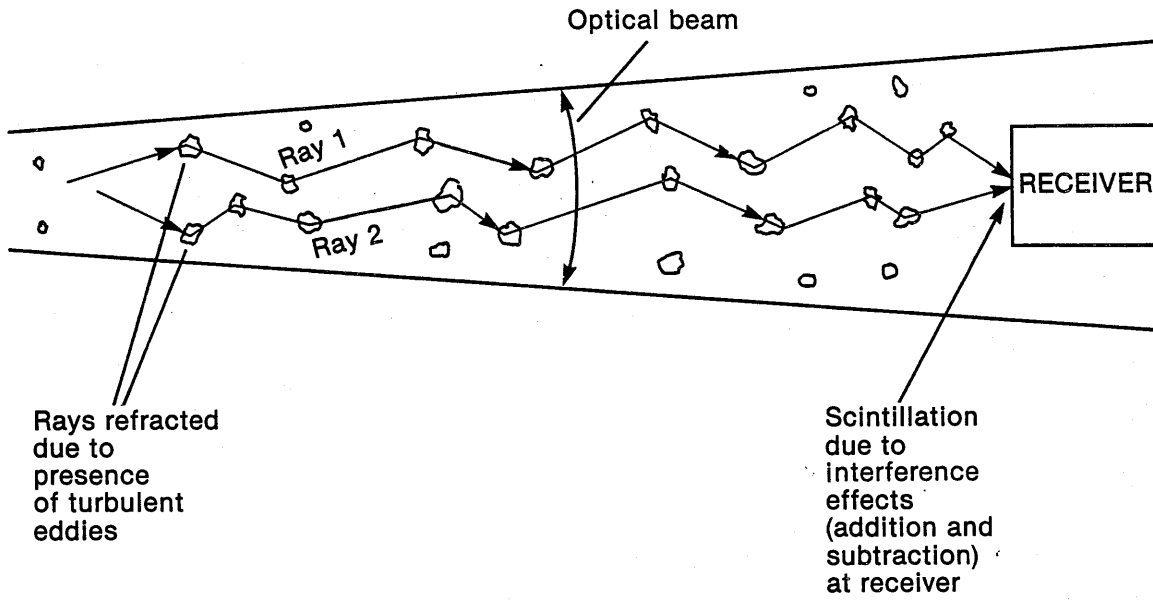

Figure 6.1 Diagrammatic representation of the scintillation effect

having path lengths which do not result in saturation of the log-irradiance variance (see Section 4.5).

Increases in atmospheric attenuation due to rain, fog, snow etc have been well researched and the increases obviously need to be allowed for in system design calculations. Since such effects are already well documented they have not been included in this hypothesis. Chapter 1 included an overview of these particular effects.

6.3 QUALITATIVE ANALYSIS OF HYPOTHESIS

Previous chapters in this thesis have indicated that for optical path lengths up to around 1000 m in length beam spread and beam wander are not significant causes of variations in the optical received power level. Optical scintillations, which arise as a result of constructive and destructive interference of optical rays within the optical beam as detected at the receiver, are however much more significant. Before obtaining a mathematical function for the scintillation effect which can be employed in system signal to noise ratio calculations it is useful to have a qualitative idea of the mechanisms giving rise to the scintillation effect.

Now consider two different rays propagating within the optical beam as shown in Figure 6.1. The rays arriving at the detector will have been scattered as a result of the various scattering mechanisms discussed in Chapter 1 and refracted due to atmospheric turbulent effects as discussed in Chapters 2 and 3. Each ray has a randomly varying optical intensity (with time) and given phase. Similarly the second ray will also have an unrelated randomly varying optical intensity and unrelated phase. Basic theory indicates that the combined effect of these two rays at a given point in the detector is determined by the straightforward additon of the optical power as a function of the phase of each signal. Such addition

results in an increase or decrease in the optical power with respect to the combined mean optical power of the two rays depending on their particular relationships. Now it must be remembered that the optical power of each ray is far from constant, indeed usually completely random. Thus we have, for two rays, two superimposed randomly varying power distributions. If we now extend the argument to consider a large number of such rays then we may apply the central limit theorem [6.1]. This theorem states that if a large number of randomly distributed functions are combined then the resultant overall distribution is normal. It follows therefore that the optical power distribution at any given point on the optical detector in the receiver, due to scintillation effects, will very likely follow a normal distribution.

6.4 RELATED THEORIES

6.4.1 Tatarskii [6.2] considered the effect of the summation of optical powers of different optical rays in connection with the receipt of light from planets and stars. In his monograph he considered the propagation of light from stars and planets through free space and finally through the earth's atmosphere. It is the passage of light through the turbulent atmosphere which gives rise to the well known twinkling stars effect. Tatarskii goes into considerable detail and mathematical complexity which cannot be repeated here. Nevertheless his work indicates that the variation of irradiance will be normally distributed which is supportive of the premise in this thesis.

6.4.2 Shapiro has carried out an analysis which may be applied to terrestrial systems but which is mathematically extremely complex [6.3, 6.4]. This analysis is based on the Huygens-Fresnel principle model for atmospheric propagation [6.5] wherein the statistics of a field received from an arbitrary extended source are derived from the

statistics of a spherical wave. The interested reader is referred to the literature for further information on the techniques used and a detailed description of the principles involved which are too lengthy to be discussed in this thesis.

Notwithstanding the not inconsiderable complexity of Shapiro's derivation it is important to note that he arrived at exactly the same expression as obtained by the Tatarskii approach discussed qualitatively in Para 6.4.1.

6.4.3 The constructive and destructive interference effect occurring as a result of turbulence in the atmosphere and known as scintillation is not dissimilar to the speckle pattern phenomenon in optical fibres [6.6]. In the latter the energy in different optical rays propagating through an optical fibre on reaching the end of the fibre will be added or subtracted together depending on their respective optical power and phase. Hence it is postulated that turbulence in the atmosphere gives rise to scintillation in a terrestrial optical line of sight link in a similar manner to the scattering (and refraction) of rays within an optical fibre giving rise to speckle patterns at the fibre end. If one was to monitor the optical power at a given spot within a speckle pattern emanating from a fibre end one would find that the power varied in accordance with a normal distribution [6.6]. The speckle pattern phenomenon therefore represents a good analogy to the scintillation effect and supports the general premise postulated in the preceding sections that atmospheric scintillation variations are also likely to be normally distributed.

6.5 QUANTITATIVE ANALYSIS

6.5.1 Derivation of Noise Degradation Factor for use in SNR Calculations due to Turbulence Induced Scintillation Effects

The noise degradation factor which is needed in order to determine the effect of turbulence on the signal to noise ratio and ultimately the system error rate can be given by the relative irradiance variance.

This relative variance is expressed as:

$$\text{Relative irradiance variance} = \text{Noise degradation factor} = \frac{\sigma_1^2}{\langle I \rangle^2} \qquad (6.1$$

Where $\langle I \rangle$ = mean level of irradiance.

Hence the objective is to express the relative irradiance variance in a form which both facilitates practical measurement of the relevant parameters and in particular provides a relationship with the atmospheric refractive index structure parameter, C_n^2. Contrary to the expositions of Tatarskii [6.2] and Shapiro [6.3], which are both extremely mathematically complex, this thesis provides a relationship derived from basic principles which avoids the complex workings of these other authors. Despite being much more straightforward, the approach proposed in this thesis is considered to be just as mathematically rigorous as those of Tatarskii and Shapiro.

In the first instance amplitude and irradiance fluctuations are considered in order to derive the relative variance.

Tatarskii has shown [6.2] that the signal amplitude at the receiver is log-normal, that is the log-amplitude X is a normal variable, where:

$$X = \ln A \tag{6.2}$$

The log-amplitude has mean value:

$$\langle X \rangle = \langle \ln A \rangle \tag{6.3}$$

and mean-square value:

$$\begin{aligned} \langle X^2 \rangle &= \langle X \rangle^2 + \sigma_x^2 \\ &= \langle \ln A \rangle^2 + \sigma_x^2 \end{aligned} \tag{6.4}$$

where σ_x^2 = log amplitude variance.

The instantaneous value of irradiance, I, is defined to be the square of the instantaneous amplitude, A, such that:

$$I = A^2 \tag{6.5}$$

Now we also have the log-irradiance, Y, given by:

$$\begin{aligned} Y &= \ln I \\ &= 2 \ln A \end{aligned} \tag{6.6}$$

$$= 2X \tag{6.7}$$

Note that the magnitude of amplitude and irradiance fluctuations is so large that it has become common practice amongst workers in the field to use log-amplitude and log-irradiance functions.

If X is a normal (Gaussian) variable, then Y = 2X will also be normal. The log-irradiance has mean value:

$$\langle Y \rangle = \langle \ln I \rangle = 2 \langle \ln A \rangle \tag{6.8}$$

and mean-square value:

$$\begin{aligned} \langle Y^2 \rangle &= \langle \ln I \rangle^2 + \sigma_y^2 \\ &= 4 \langle \ln A \rangle^2 + \sigma_y^2 \end{aligned} \tag{6.9}$$

Now, from equation (6.7) we know that Y = 2X hence equation 6.9 becomes:

$$4\langle X^2\rangle = 4\langle \ln A\rangle^2 + \sigma_y^2 \tag{6.10}$$

Re-arranging equation (6.10) we obtain an expression for σ_y^2:

$$\sigma_y^2 = 4\langle X^2\rangle - 4\langle \ln A\rangle^2 \tag{6.11}$$

Also, from equation (6.4) we have:

$$\sigma_x^2 = \langle X^2\rangle - \langle \ln A\rangle^2 \tag{6.12}$$

Hence, by comparing equations (6.11) and (6.12) we can establish the relationship whereby:

$$\boxed{\sigma_y^2 = 4\sigma_x^2} \tag{6.13}$$

Given that X = lnA and Y = lnI, we can find A or I since:

$$A = e^X \; ; \; I = e^Y \tag{6.14}$$

Using the exponential form, we can continue to find the mean and mean-square value of I:

$$\langle I\rangle = \langle e^Y\rangle \tag{6.15}$$

and

$$\langle I^2\rangle = \langle e^{2Y}\rangle \tag{6.16}$$

We have noted that Y is a normal variable, hence we can use the result derived in Appendix 6 whereby:

$$\langle I\rangle = \langle e^Y\rangle = e^{\langle y\rangle} e^{\sigma_y^2/2} \tag{6.17}$$

and

$$\langle I\rangle^2 = e^{2\langle y\rangle} e^{\sigma_y^2} \tag{6.18}$$

To find $\langle I^2 \rangle$ we must evaluate $\langle e^{2y} \rangle$ using the following theory:

If $a = 2b$, then $\langle a \rangle = 2 \langle b \rangle$

and $\langle a^2 \rangle = 4 \langle b^2 \rangle$

Using this information we thus obtain:

$$\langle I^2 \rangle = \langle e^{2y} \rangle = e^{2 \langle y \rangle} e^{2 \sigma_y^2} \tag{6.19}$$

The irradiance has variance:

$$\sigma_I^2 = \langle I^2 \rangle - \langle I \rangle^2 \tag{6.20}$$

and a relative variance:

$$\sigma_I^2 / \langle I \rangle^2 = \frac{\langle I^2 \rangle}{\langle I \rangle^2} - 1 \tag{6.21}$$

Using equations (6.18) and (6.19) we deduce that:

$$\frac{\langle I^2 \rangle}{\langle I \rangle^2} = \frac{e^{2 \langle y \rangle} e^{2 \sigma_y^2}}{e^{2 \langle y \rangle} e^{\sigma_y^2}} = e^{\sigma_y^2} \tag{6.22}$$

Finally, from expression (6.13) we have the relationship: $\sigma_y^2 = 4 \sigma_x^2$. Hence, the relative irradiance variance can be expressed in the form:

$$\frac{\sigma_I^2}{\langle I \rangle^2} = e^{4 \sigma_x^2} - 1 \tag{6.23}$$

where σ_x^2 is the log-amplitude variance. The log-amplitude variance is related to the atmospheric refractive index structure constant (C_n^2), the path length (L) and wave length by the relationship given in equation (4.2), repeated here for completeness viz:

$$\sigma_x^2 = 0.31\ C_n^2\ k^{7/6}\ L^{11/6} \qquad (6.24)$$

It follows from equations (6.23) and (6.24) that the relative intensity variance is also a function of C_n^2, L and λ.

The relative irradiance variance given in equation (6.23) is analogous to the corresponding expressions derived by Tatarskii [6.2] and Shapiro [6.3], but the derivation in this thesis is considerably more straightforward than either of their derivations.

The expression for the relative irradiance variance given in equation (6.23) may be used in signal to noise calculations to increment the level of noise due to turbulence induced scintillation which, of course, will result in a decrement of the value of signal to noise ratio. This calculation is given in Section 6.6.

6.5.2 The S/N Decrementing Factor

It may be reasonably concluded that the expression for the relative irradiance variance, $(e^{4\sigma_x^2} - 1)$, as derived in the preceding sections of this chapter, is a factor which may be used to indicate quantitatively the way in which the received optical signal intensity varies as a result of turbulence induced scintillation effects ie following a normal distribution.

The expression is used in the subsequent section to show how turbulence affects the signal to noise ratio and hence the system error rate.

6.6 MATHEMATICAL DERIVATION OF RELATIONSHIP BETWEEN C_n^2 AND ERROR-RATE PERFORMANCE

The quantitative analysis given below assumes the use of a collimated beam transmitter and a diffraction limited direct detection receiver with on-off

keying intensity (amplitude) modulation. It is further assumed that the receiver employs a low-pass filter to limit the shot noise bandwidth.

The SNR is calculated for an electrical point between the photodiode and the first amplification stage and the fundamental expressions employed are given in Appendix 5 [6.7]. Now the noise term comprises thermal, shot and first stage amplifier noise terms and hence the generalised SNR expression is given by:-

$$SNR = \frac{\langle I_p^2 \rangle}{\langle I_t^2 \rangle + \langle I_{sh}^2 \rangle + \langle I_a^2 \rangle} \tag{6.25}$$

where I_p = electrical signal current

I_t = thermal noise current

I_{sh} = shot noise current

I_a = amplifier noise current

The noise terms in the denominator are given by:-

$$\text{Thermal noise term } \langle I_t^2 \rangle = \frac{4kTB}{R} \tag{6.26}$$

Shot noise arises from a number of different sources viz:-

$$\text{Shot noise due to dark current } \langle I_d^2 \rangle = 2qI_dB \tag{6.27}$$

$$\text{Shot noise due to signal current } \langle I_p^2 \rangle = 2qI_pB = \frac{2q^2 \eta BP_R}{h\nu} \tag{6.28}$$

$$\text{Shot noise due to background current } \langle I_b^2 \rangle = 2qI_bB = \frac{2q^2 \eta BP_B}{h\nu} \tag{6.29}$$

The signal current is given by I_p where:-

$$\langle I_p^2 \rangle = \left[\frac{\eta q P_R}{h\nu}\right]^2 \tag{6.30}$$

First stage amplifier noise for a bipolar input stage is given by [6.8]:-

$$\langle I_a^2 \rangle = \frac{16\pi^3}{3} \cdot q\, I_{coll} \frac{C_T^2 B^3}{g_m^2} + 2qI_{ba}B \qquad (6.31)$$

Where I_{coll} is the collector current (typically 0.1A), C_T is the total capacitance (typically 50pF), B is the electrical bandwidth, g_m is the mutual conductance (typically 40 mS) and I_{ba} is the base current (typically 1 mA). For many low performance applications this particular noise source may be ignored.

Now the shot noise term given above does not take account of any scintillation effects arising due to the presence of turbulence in the atmosphere and the term has to be suitably modified by using the relative irradiance variance $(\exp(4\sigma_x^2) - 1)$.

With this valuable input one can make considerable progress in relating error rate to the variation in the atmospheric refractive index structure parameter, C_n^2, since the latter is a function of σ_x^2.

Inserting the expressions for the signal and noise sources derived above together with the relative irradiance variance (SNR decrementing factor) due to turbulence (derived in Section 6.5) into equation (6.25) yields:-

$$SNR = \frac{\left[\frac{\eta q P_R}{h\nu}\right]^2}{\frac{4kTB}{R} + 2qB\left[I_d + \frac{\eta q P_R}{h\nu}(\exp(4\sigma_x^2)-1) + \frac{\eta q P_B}{h\nu}\right] + \langle I_a^2 \rangle} \qquad (6.32)$$

The decrementing factor in the denominator of equation (6.32) is associated with the term for the shot noise arising from the received optical signal. Turbulence may also, in certain circumstances and in some designs of optical line of sight link, give rise to scintillation of the background

optical signal. However, this is regarded as being a second order effect since it usually has a negligible effect on overall system performance and is therefore not included in the above expression.

A computer program for calculating the SNR for various values of C_n^2 (a parameter forming part of the expression for σ_x^2) was written as part of this research work [6.14] and was used in the preparation of many of the subsequent graphs. For the purposes of this calculation it is more convenient to use P_T rather that P_R. Accordingly Appendix 7 gives details of P_R as represented by source radiance, path attenuation etc.

Appendix 9 gives the derivation of the background noise power, P_B, which is needed for determining the overall shot noise, and Appendix 10 considers the overall shot noise term and its constitution.

When the system is shot noise limited, which is the case for most good system designs, the SNR expression can be much simplified and this is derived in Appendix 11. One of the parameters which is a major contributor to shot noise is quantum noise, which arises as a result of the random arrival of photons at the detector, and the quantum noise limit is calculated in Appendix 12.

In the case of a shot noise limited system the SNR expression in equation (6.32) can be reduced to:-

$$SNR = \frac{\left(\frac{\eta q P_R}{h\nu}\right)^2}{\frac{2qB\,\eta q P_R}{h\nu}\left(\exp\left(4\sigma_x^2\right)-1\right)}$$

$$= \frac{\eta P_R}{2h\nu B\left(\exp\left(4\sigma_x^2\right)-1\right)} \qquad (6.33)$$

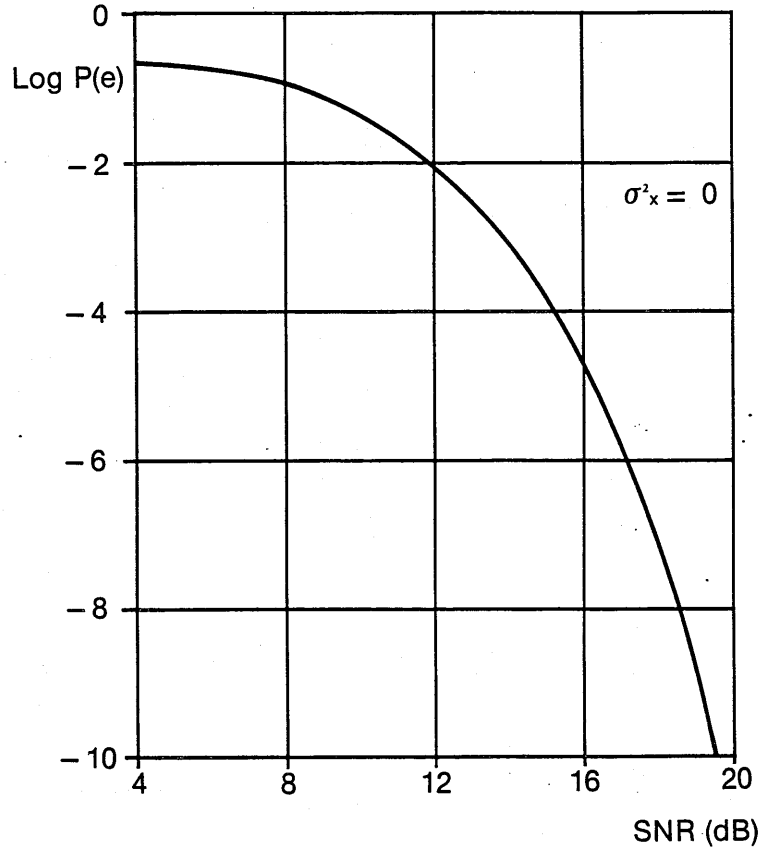

Figure 6.2 Basic theoretical relationship between SNR and P(e) for 2 Mbit/s OOK system in absence of turbulence

Equation (6.33) can be simplified further to show the relationship between SNR and σ_x^2.

$$SNR = m \cdot \frac{P_R}{(\exp(4\sigma_x^2)-1)} \qquad (6.34)$$

where $m = \frac{\eta}{2Bhv}$ = a constant for a given system of bandwidth B

Clearly from equation (6.34) it can be seen that:-

a. the SNR is a function of the received power level, P_R, as was to be expected,

b. the SNR is a function of the relative irradiance variance term $e^{4\sigma_x^2} - 1$. Previous chapters have indicated that

$$\sigma_x^2 = C_n^2 \cdot L^{11/16} \cdot (2\pi/\lambda)^{7/6} \cdot (\text{constant})$$

Hence it follows that the SNR is related to C_n^2 via an inverse exponential term.

The relationship between error probability and SNR has been well documented [6.9, 6.10] and is also addressed in Appendix 14. In the absence of turbulence the relationship for an on/off keying amplitude modulated system is given by expression (6.35) [6.3, 6.12]:

$$P(e) = 0.5 \text{ erfc } (0.5 (S/N)^{1/2}) \approx 0.5 \exp(-SNR/4) \qquad (6.35)$$

This relationship is shown in Figure 6.2 in which $\sigma_x^2 = 0$ for the case of no turbulence. In the presence of turbulence-induced scintillation the SNR has to be increased in order for a given error probability to be maintained. Following the approach proposed by Shapiro the required increase in SNR has been derived and is shown in Figure 6.3 for different values of σ_x^2, [6.3, 6.11].

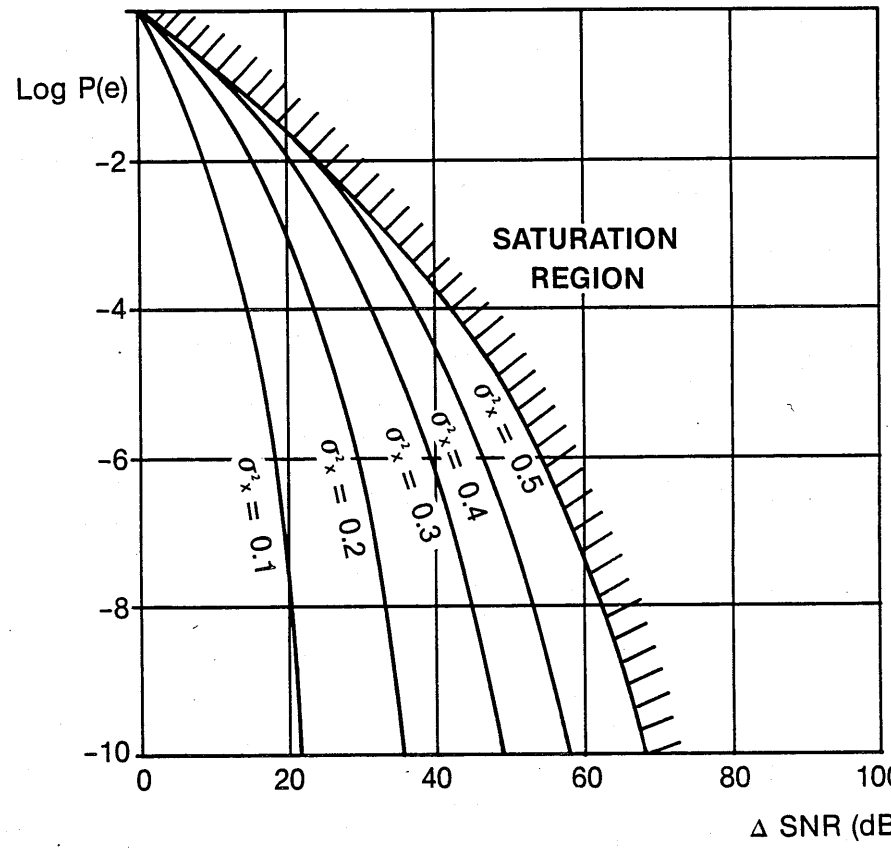

Figure 6.3 **Theoretical increase in SNR needed in order for a given P(e) to be maintained**

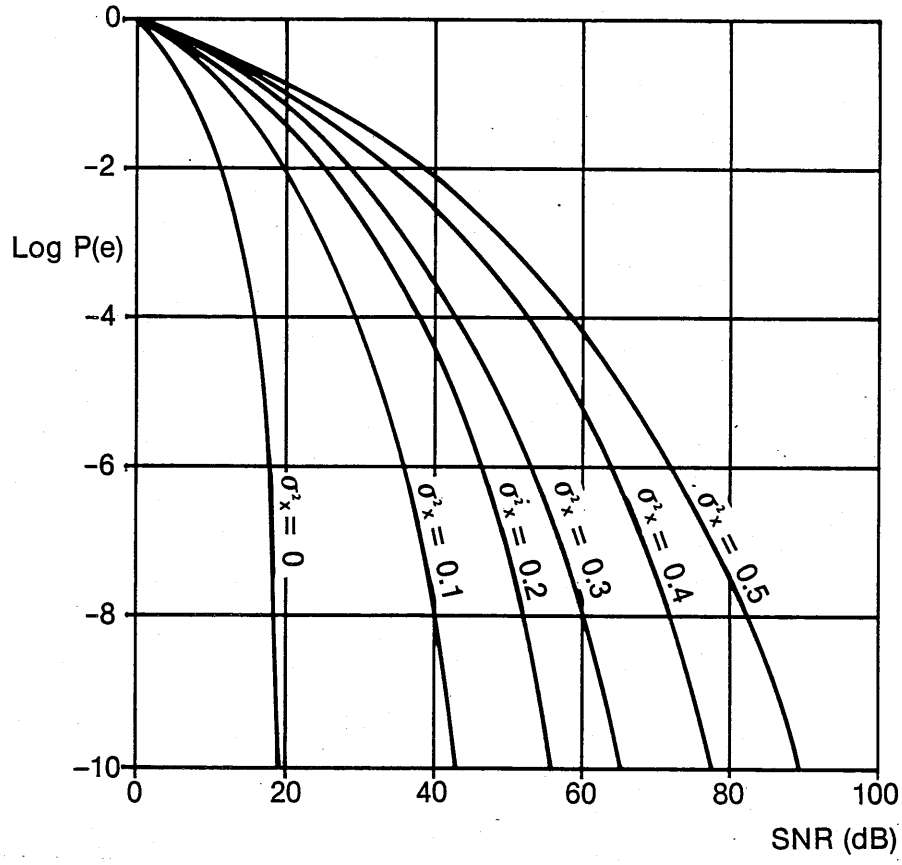

Figure 6.4 **Theoretical relationship between SNR and P(e) for 2 Mbit/s system in presence of turbulence.**

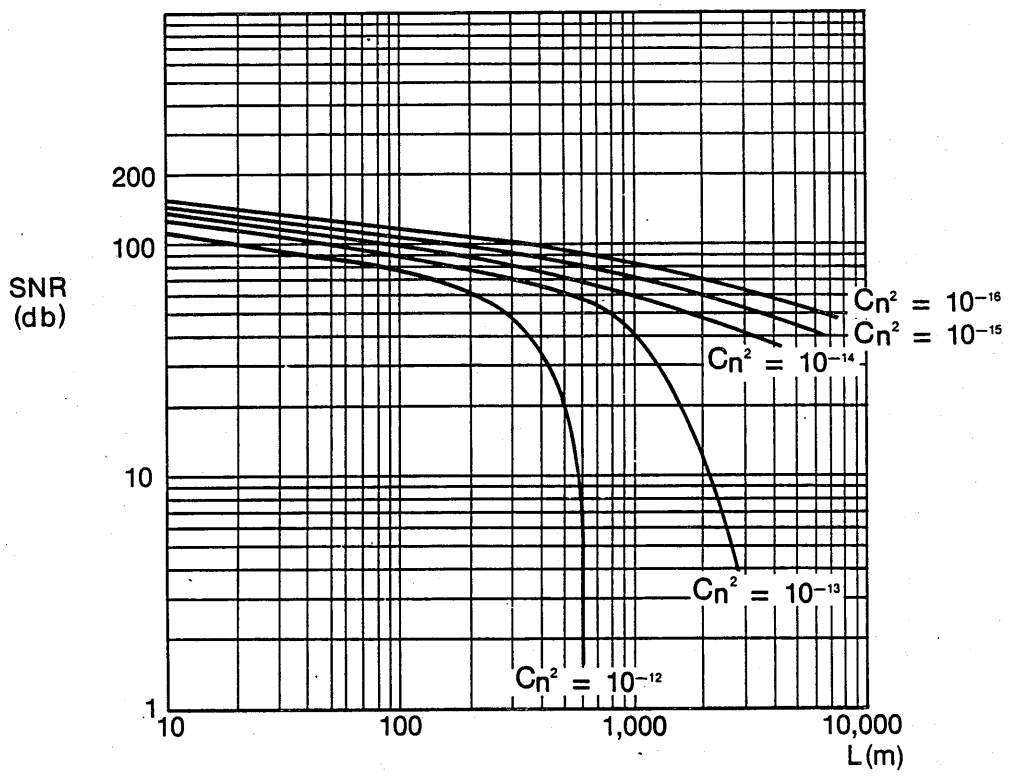

Figure 6.5 Theoretical worst case variation of SNR with path length and C_n^2 — shot noise limited system (LED radiant intensity = 10^4 W/m^2/sr)

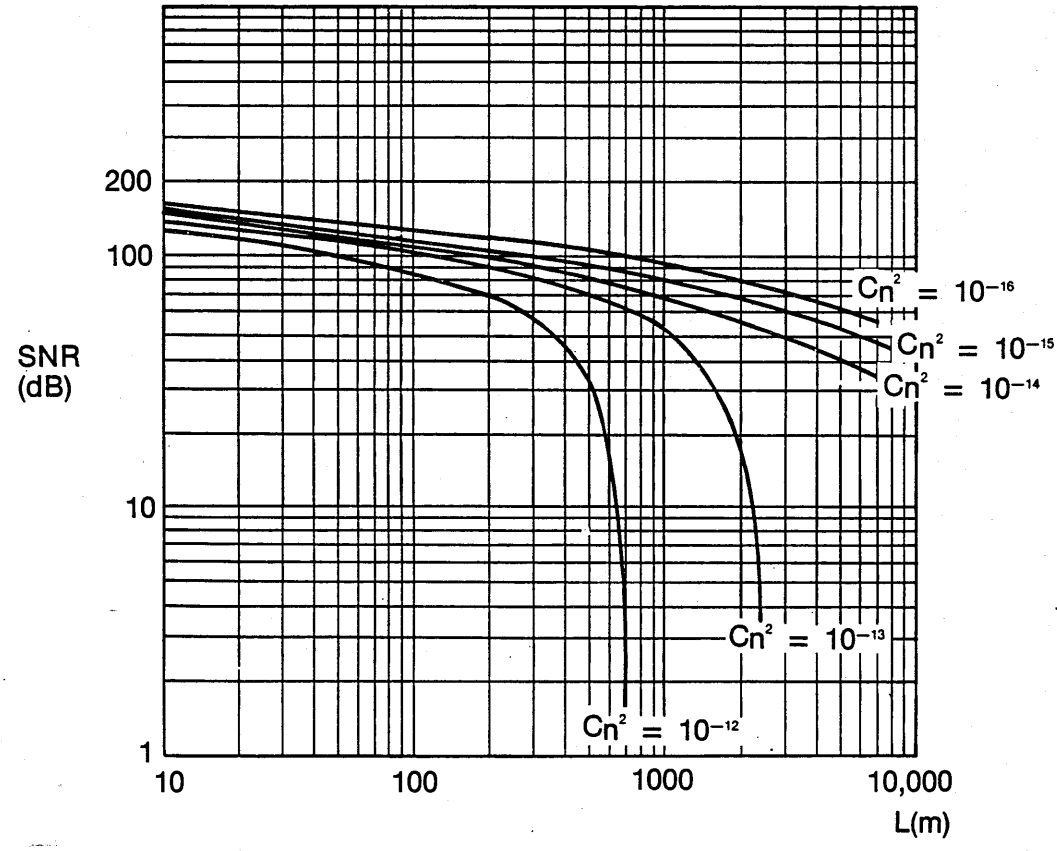

Figure 6.6 Theoretical worst case variation of SNR with path length and C_n^2 — shot noise limited system (LED radiant intensity = 10^5W/m^2/sr)

It can be clearly seen from Figure 6.3 that when the turbulence is significant, eg when $\sigma_x^2 = 0.5$, very large increases in SNR are required in order to maintain an acceptable P(e) ie up to 55 dB or even more.

The P(e) vs SNR relationship in the absence of turbulence (shown in Figure 6.2) can be combined with the data in Figure 6.3 to yield the graphs shown in Figure 6.4, which show the P(e) vs SNR relationship in the presence of turbulence for various values of σ_x^2.

Calculation of SNR in equation (6.33) for a 2 Mbit/s OOK system with different values of path length and C_n^2 yields the graphs shown in Figures 6.5 and 6.6 for LED output powers of 10^4 W/m^2/sr and 10^5 W/m^2/sr respectively. In both cases the dramatic reduction in SNR as C_n^2 increases for a given path length is quite marked, particularly for path lengths in excess of about 500m at which distance the cumulative effect of the turbulence begins to dominate significantly.

Figure 6.7 gives the data shown in Figures 6.5 and 6.6 but related in this instance to P(e) rather than SNR using the relationship shown in Figure 6.4. Figure 6.7 illustrates the main hypothesis of this paper derived from the fundamental expression in equation (6.32), ie the nature of the relationship between P(e) and C_n^2. The relationship between the error rate and C_n^2 is only too apparent. High performance systems requiring error rates of 1 in 10^9 or better and operating over path lengths of the order of 1000 m will find that the very slightest amount of turbulence will result in a dramatic degradation in the error rate. One order of magnitude change in the level of turbulence results, in the worst case, in over 2 orders of magnitude degradation in the error rate performance. As would be expected, systems operating over much shorter path lengths such as 100 m would find that, although affected by turbulence

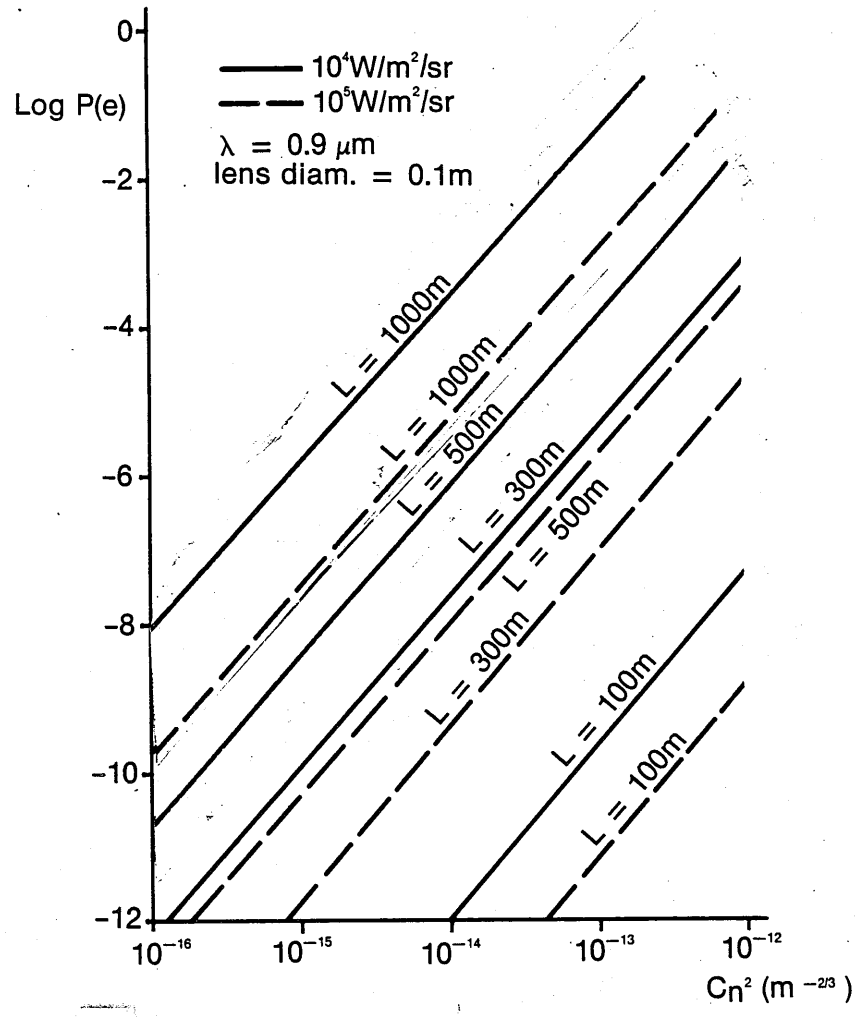

Figure 6.7 Theoretical relationship between P(e) and C_n^2 (worst case)

at about the same rate, error rate performance degradation beyond 1 in 10^9 does not occur until very severe levels of turbulence are present, represented by levels of C_n^2 approaching 10^{-12} $m^{-2/3}$. The graphs in Figure 6.7 also show that the magnitude of the error rate performance degradation is reduced as the source radiance increases.

Figure 6.8 shows the effect of various system variables on the overall signal to noise ratio for worst case turbulence of $C_n^2 = 10^{-12}$ $m^{2/3}$. There are some clear observations; for instance the performance is degraded due to:

- increase in bit rate of operation
- reduction in transmitted power
- reduced lens aperture diameters

The significance of the lens diameters is particularly worth noting. Take for instance a system operating over a path length of 500 m. For a lens diameter of 0.1 m a signal to noise ratio of 15 dB or better is achieved irrespective of the other system parameters, whereas a lens diameter of half this size ie 0.05 m would mean that the system would be wholly inoperable.

The performance of systems having other system parameters can be readily calculated from equation (6.32).

6.7 CONCLUSION

A hypothesis for the relationship between P(e) and C_n^2 has been developed. Chapter 8 gives practical results for the relationship between P(e) and C_n^2 which will enable the validity of the hypothesis to be established.

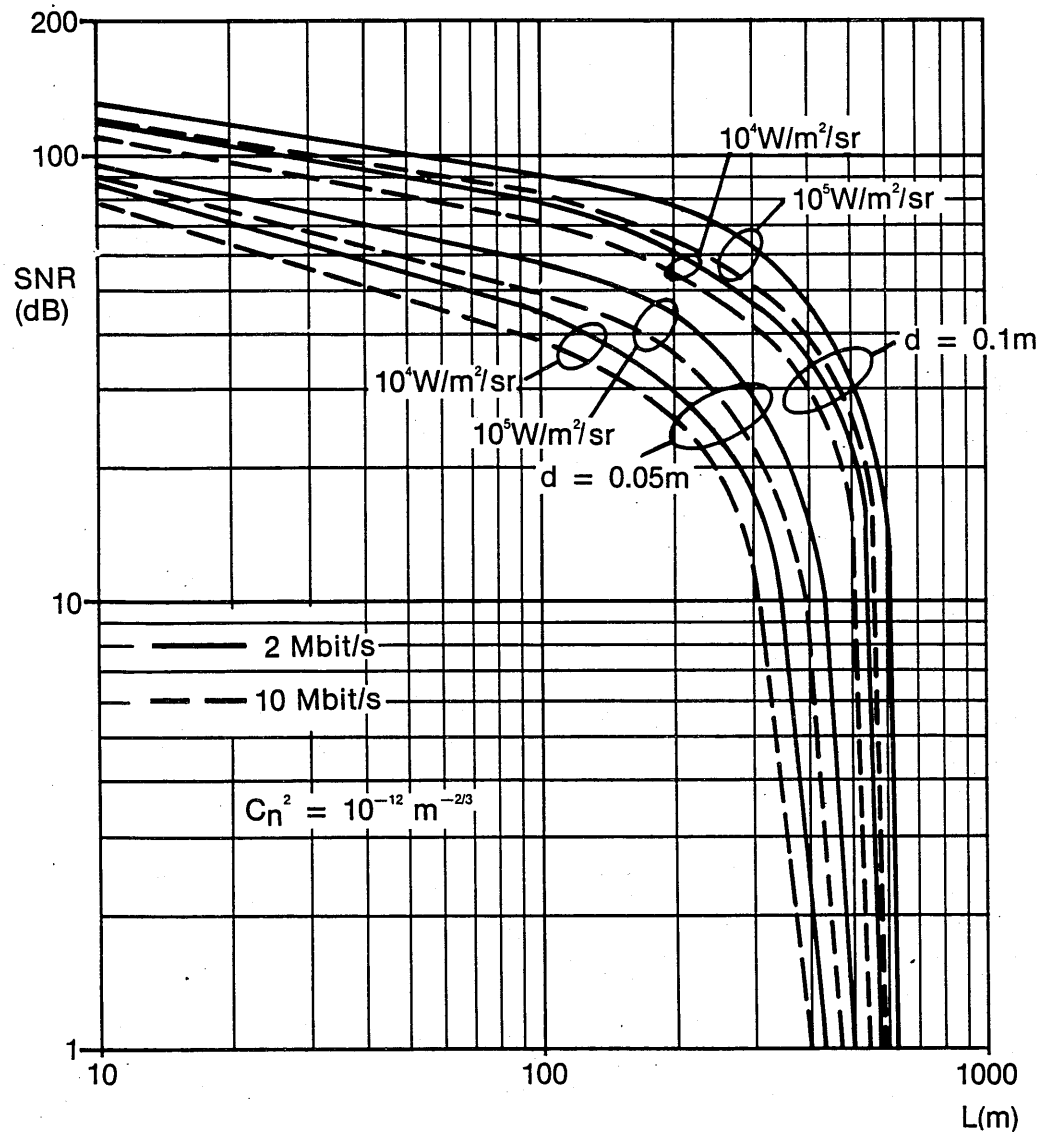

Figure 6.8 Variation of SNR with path length in severe turbulence for different system parameters

(effective transmitter lens diameter = effective receiver lens diameter = d)

From the theory developed in this chapter it is possible to say that, in order to maximise the performance of atmospheric optical communication systems, it is necessary to:

a. Employ the maximum transmitter power possible, consistent of course with any practical considerations regarding physical size, optical safety, availability of suitable sources etc.

b. Employ the maximum diameter of transmitter and receiver lenses possible which will fit into the equipment housing.

c. Operate at the lowest bit rate possible for the particular application.

Source powers of 10^5 $W/m^2/sr$ can be readily achieved using semi-conductor lasers and leds and should be the minimum power considered in design calculation if the system performance is to be maximised. In addition effective lens diameters of 0.1 m bring about a marked improvement over systems using lens diameters of half this size and there would need to be strong countermanding arguments for employing lens diameters of less than about 0.1 m if systems are to operate over path lengths of 500 m or more. Clearly the higher the bit rate of operation the greater attention which needs to be paid to all the various system parameters in order to maximise system performance.

PART III

PRACTICAL MEASUREMENTS AND RESULTS

This part of the thesis contains details of the measurement program carried out by the author as part of this research project, together with the results obtained

CHAPTER 7

THE MEASUREMENT OF THE ATMOSPHERIC REFRACTIVE INDEX STRUCTURE PARAMETER

CHAPTER 7

THE MEASUREMENT OF THE ATMOSPHERIC REFRACTIVE INDEX STRUCTURE PARAMETER

7.1 INTRODUCTION

Chapter 5 gave the theory behind the Atmospheric Refractive Index Structure Parameter, C_n^2, and explained the various techniques that, in principle, might be employed for the measurement of C_n^2. Some of the practical problems associated with the various techniques including the fine-wire measurement technique were discussed, and as a practical approach the use of thermocouples was proposed. The basic design of a thermocouple based measuring equipment was also presented in Chapter 5 and in further detail in Appendix 4.

This chapter considers the author's practical measurement of the Atmospheric Refractive Index Structure Parameter using the design derived in Chapter 5 and Appendix 4, discusses the results obtained over a period of some 18 months, and draws some conclusions.

7.2 OBJECTIVES OF EXPERIMENTS

The objectives of this phase of the experimental work were:-

a. To check that the design of the measuring equipment was adequate and that its performance gave acceptable results.

b. To assess the measured values of C_n^2 under various conditions and to compare the results with those obtained by other workers, in order to assess the validity of the results.

c. To make any conclusions which might be relevant to subsequent work concerning the variation of C_n^2 with time of day, annual variations, altitude, weather conditions etc.

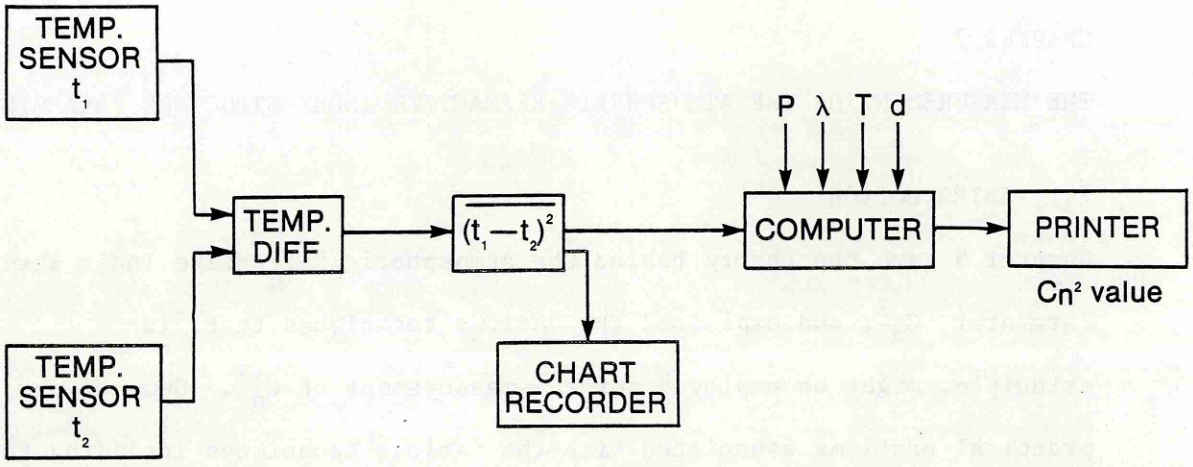

Figure 7.1 Block schematic of Cn^2 measuring equipment

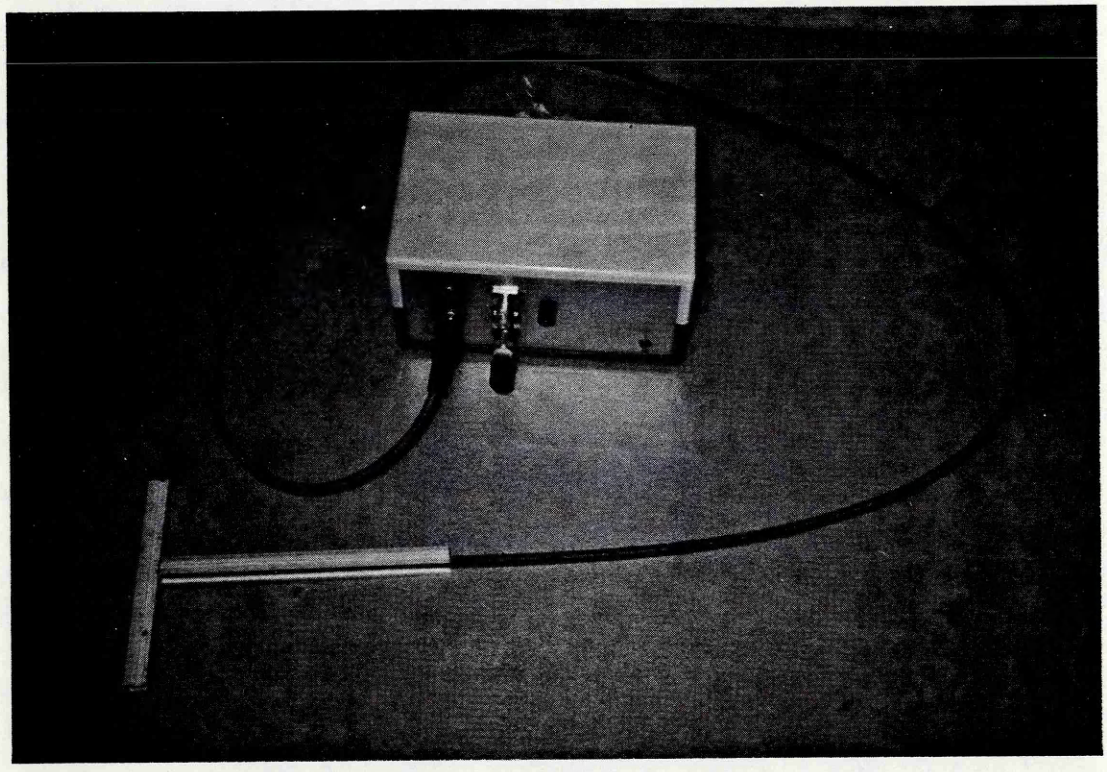

Figure 7.2 Cn^2 measuring equipment

d. To assess the effect which different sensor spacings have on the C_n^2 measurements.

e. To determine whether the sensors should be spaced horizontally or vertically.

f. To determine the time constant which should be used in order to obtain the most meaningful C_n^2 results.

7.3 MEASURING EQUIPMENT

7.3.1 C_n^2 Measuring Equipment

A block schematic diagram of the measuring equipment is shown in Figure 7.1 and the circuit arrangement for the sensors and amplification stages is given in Appendix 4. The output from the temperature sensor amplification stages was fed to a circuit which took the mean square value of the signal. The output from this stage could then be fed directly to a chart recorder from which, with appropriate calibration, the value of C_n^2 could be deduced or alternatively fed to an A/D convertor for input to a computer. The latter could be programmed with data such as wavelength, pressure etc from which the value of C_n^2 could be computed. In order to minimise extraneous noise due to power supplies etc, a $\pm$ 4.5V internal dc battery supply was used. The thermocouples used as the sensors were the exposed butt-welded type. The supply of the preferred Type E thermocouple from Omega Engineering Inc proved difficult and the more readily available Type T thermocouples (copper/copper nickel) from RS Components Type 151-259 having a sensitivity of 50 uV/°C were employed. A photograph of the equipment is given in Figure 7.2.

To facilitate analysis of the data at this stage the output from the measuring equipment was fed to a y-t chart recorder. The type employed was a J J Lloyd Instruments Type CR 600 having input ranges up to 100V and chart speeds from 1 mm/min to 100 mm/min.

7.3.2 Other Measurements

In addition to the C_n^2 measurement, the temperature and atmospheric pressure were also measured and recorded using standard instruments.

7.4 MEASUREMENTS

7.4.1 Calibration of C_n^2 Measuring Equipment

The equipment was calibrated by maintaining each of the thermocouple sensors at different, but known, temperatures and noting the output voltage. This was achieved by having one thermocouple at ambient and the other at a slightly higher temperature. The latter was achieved by placing the thermocouple above a large aluminium plate, which itself was placed above a suitable heat source. The two thermocouples were physically separated by a large thick piece of cardboard. The temperature of each thermocouple was measured using a fine point digital thermometer whose sensor could be placed in very close proximity to each of the thermocouples. The mean square temperature difference was measured.

The maximum mean square temperature difference measured was 2.25°C, which generated an output voltage of 3.5V and a corresponding reading on the chart recorder. When the two thermocouples were placed in close promixity a zero voltage was measured on the chart recorder.

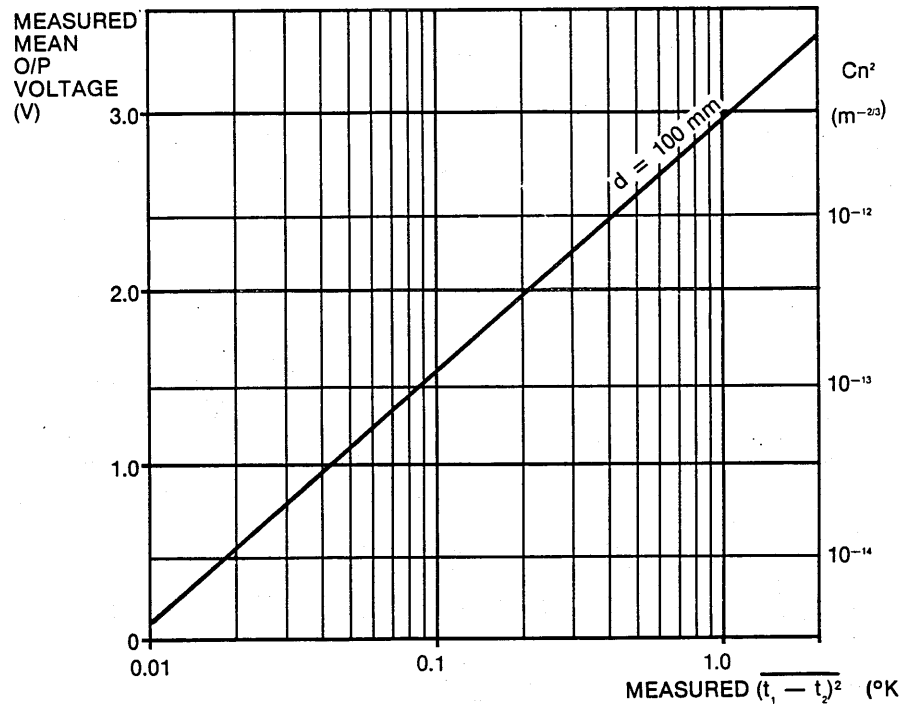

Figure 7.3 Sensor calibration chart (C_n^2 axis derived from Figure 7.4)

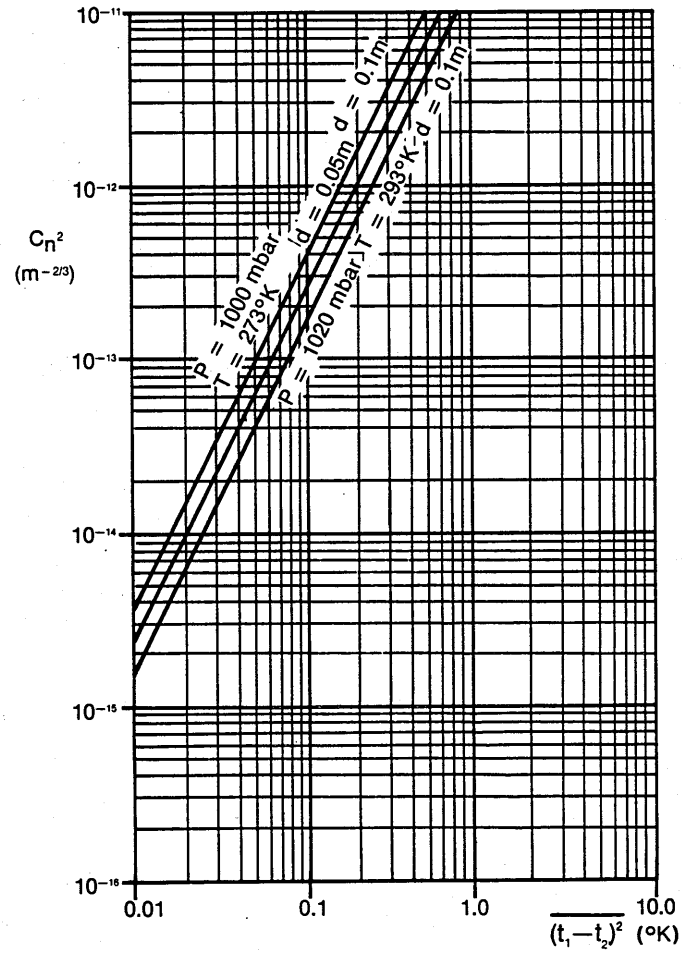

Figure 7.4 C_n^2 vs. $\overline{(t_1-t_2)^2}$

Thus a given voltage on the chart recorder represents a particular temperature difference between the two thermocouple temperature sensors. The calibration chart derived using the above technique is given in Figure 7.3.

Figure 7.4 gives a graph of temperature difference vs C_n^2 obtained from expression (7.1) originally derived in Chapter 5 (applicable for a wavelength of $\lambda = 0.9$ μm):

$$C_n^2 = \left(\frac{78.32P}{T^2} \times 10^{-6}\right)^2 \cdot \frac{\overline{(t_1 - t_2)^2}}{d^{2/3}} \qquad (7.1)$$

where P = mean atmospheric pressure in millibars

T = mean atmospheric temperature in degrees Kelvin

$t_1 - t_2$ = temperature difference between the two thermocouple sensors

From Figures 7.3 and 7.4 the x axis on the chart recorder can be calibrated.

7.4.3 Test Set Up for Determining Sensor Spacing and Configuration

In order to measure the effect of different sensor spacings the turbulent atmosphere was simulated by using an electric hot-plate whose temperature could be varied and accurately controlled. In order to ensure an even distribution of air temperature across a horizontal plane a large (one metre square) sheet of 25 mm aluminium was placed over the hot plate. Furthermore, in order to avoid crosswinds, a cardboard surround was erected 1.5 m high all around the perimeter of the horizontal aluminium plate. The sensors were positioned in the centre of the plate and at a height of 1 m above it by means of the

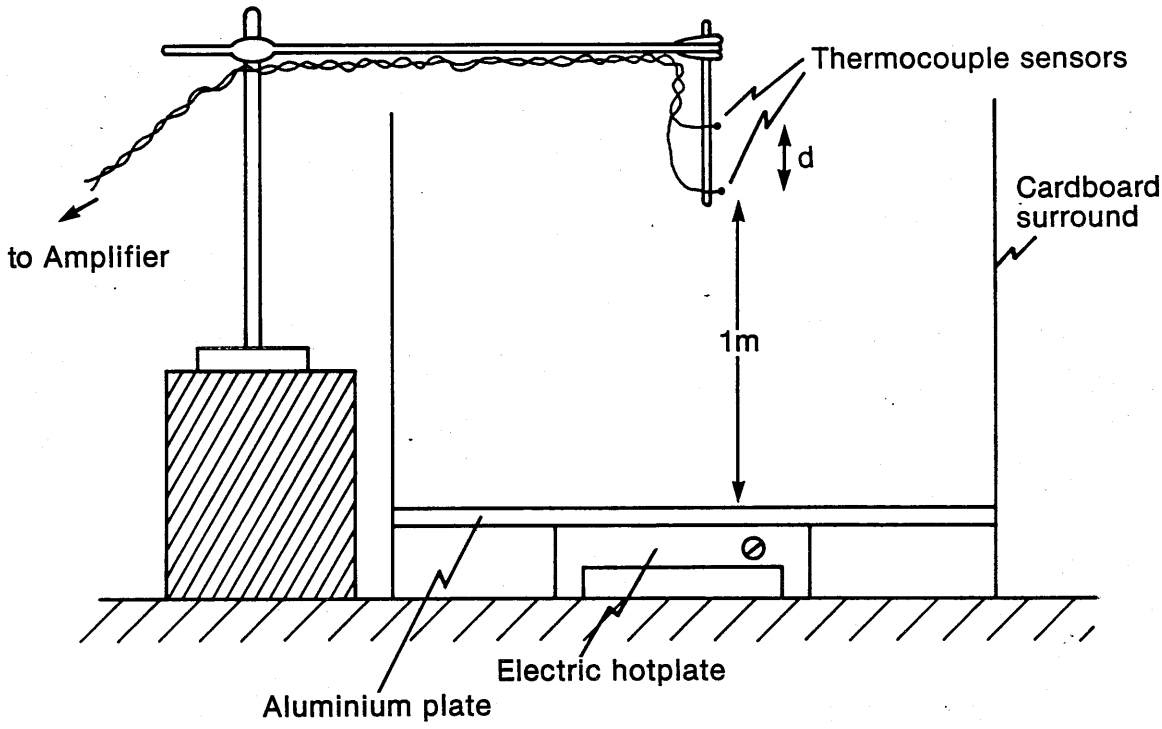

Figure 7.5 Experimental arrangement

use of a chemical retort stand and appropriate arms. A diagram of the arrangement is shown in Figure 7.5.

The thermocouple sensors were attached to a thin plastic rod such that their spacing could be altered with relative ease. The sensors were connected to the amplifier and time constant circuit via screened cable. The output from the amplifier was fed via a mean square circuit to a y-t chart recorder.

The test set-up was calibrated by using a highly sensitive electronic thermometer, the sensor of which was very small and could be located in very close proximity to the sensors used in the actual experiment. A second similar thermometer, which had previously been accurately calibrated with respect to the first, was used to measure the temperature in the vicinity of the second sensor.

With this arrangement the temperature difference between the two thermometer probes, the voltage as measured on the chart recorder and the sensor spacing could all be measured.

Sensor spacings of 10, 50 and 100 mm were chosen as being representative of typical spacings likely to be used in practice. For each sensor spacing measurements were made with and without the 100 second time constant and with the sensors spaced first vertically apart and then horizontally apart. This resulted in a total of 12 measurements, each of which was maintained for a period of 10 minutes.

7.4.4 Measurement of Variation of C_n^2 with time of day, time of year, different locations and different ground surfaces.

It is clearly important to know how C_n^2 varies during the course of the day, over an annual cycle, and also whether it makes any difference as to where along the optical communications system path

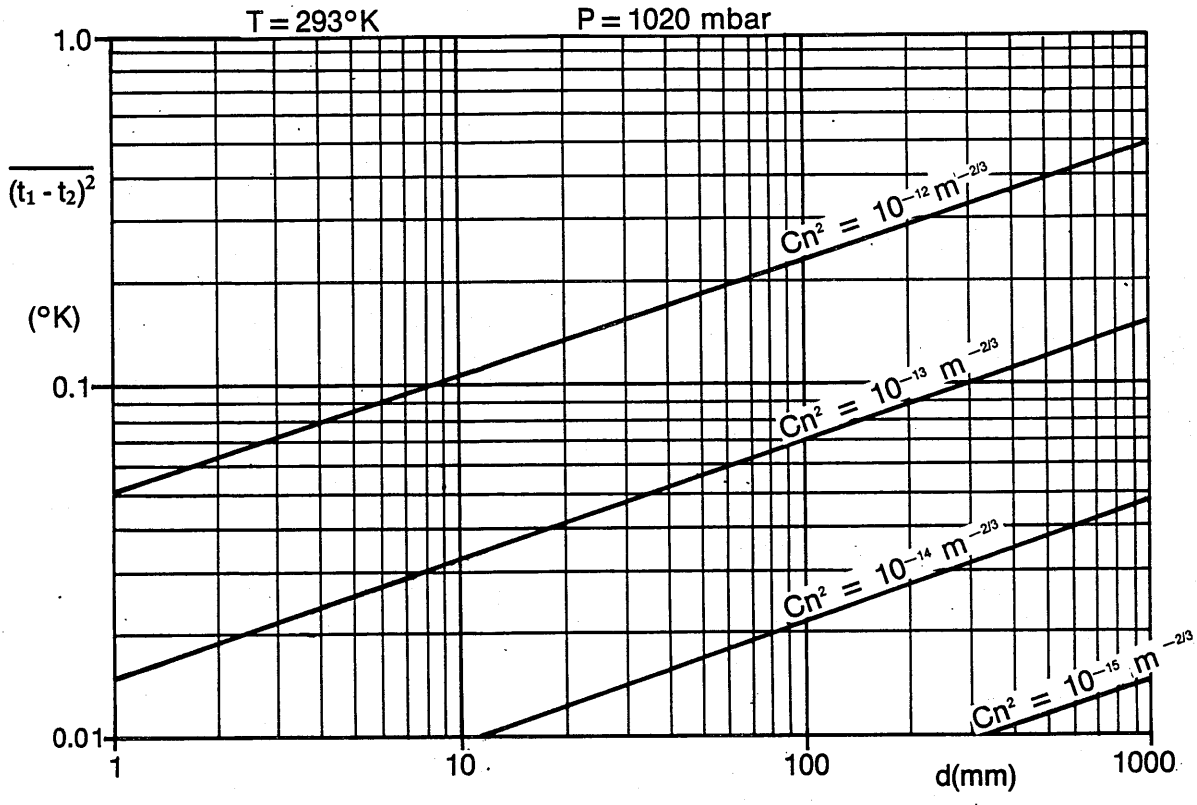

Figure 7.6 Graph for determining value of C_n^2 from knowledge of value of $\overline{(t_1-t_2)^2}$ and sensor spacing d

length the C_n^2 is measured when using single point C_n^2 measurements. In addition it is useful to know what effect different types of ground surface have on the value of C_n^2.

In order to obtain answers to these questions a range of measurement programs was established with data obtained spanning a total of 18 months from April 1984 to October 1985. The measurements made included the following:

i Measurement of C_n^2 variation during the day.

ii Measurement of C_n^2 during the day at different heights above ground.

iii Measurement of peak C_n^2 values at intervals over 18 months period.

iv Measurement of C_n^2 at different points along a 500 m test range.

v Measurement of C_n^2 for different path lengths during the day.

vi Measurement of C_n^2 above different ground surfaces during the day.

All the measurements were made with the same measuring equipment as previously described. The measurements were made at two locations; one was a central city location in London (the BT Headquarters at 2-12 Gresham Street) and the other was a greenfield site at Langton Green in Kent. Periodic calibration of the measuring equipment was made in order to ensure consistency of results over the whole period of the measurement programme.

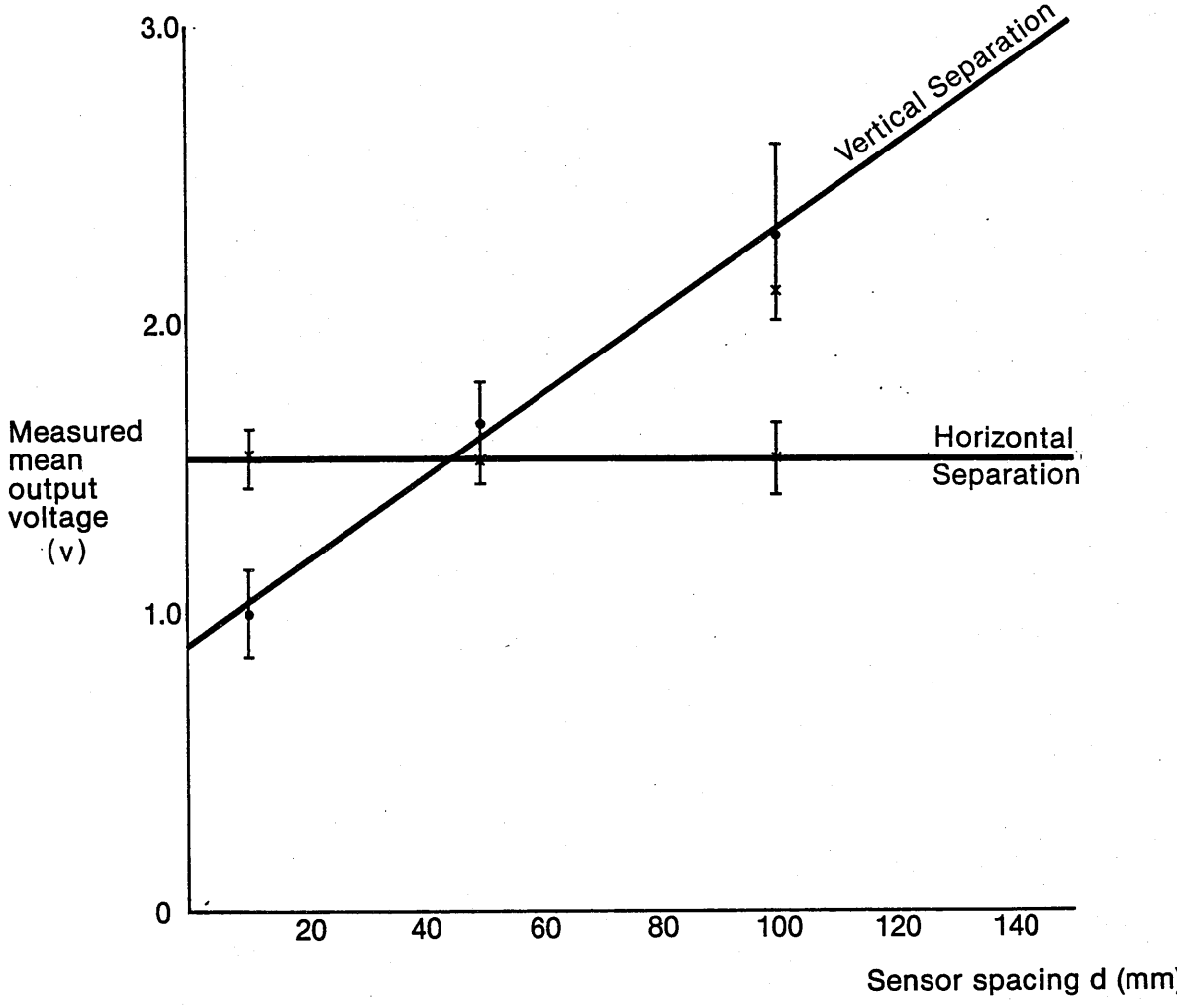

Figure 7.7 Measured mean value of output voltage for different sensor spacings

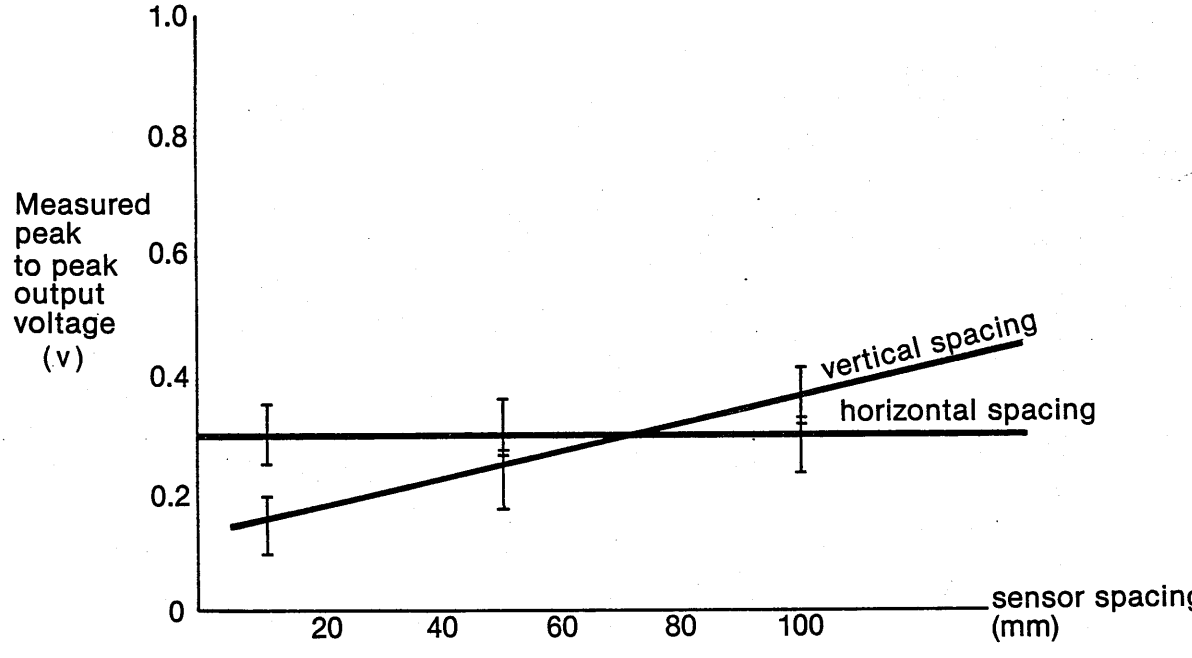

Figure 7.8 Measured peak to peak value of output voltage for different sensor spacings

7.5 RESULTS

7.5.1 General

Figures 7.6 and 7.4 show the calculated relationship between the sensor temperature difference and the sensor spacing and C_n^2 respectively. This data is used for determining the value of C_n^2 for a given temperature difference and sensor spacing.

The results of the calibration exercise are shown in Figure 7.3. From this graph a given voltage measured with a given sensor spacing could be equated to a particular temperature difference $(t_1 - t_2)$, which in turn corresponds to a particular value of the atmospheric refractive index structure parameter.

Data from the measurements made to assess sensor separation is shown in Figure 7.7 in respect of the mean levels measured. No significant difference was measured with the 100 s time constant applied compared with the no time constant arrangement. The peak to peak measurements are shown in Figure 7.8.

Representative plots from the y-t chart recorder for different sensor spacings are shown in Figures 7.9 and 7.10 for vertical and horizontal sensor spacings respectively.

The results from the various chart recorder plots are tabulated in Table 7.1.

7.5.2 Discussion of Results with Respect to Sensor Spacing and Configuration

The results show that, within the ranges of measurement employed, the change in temperature difference of the two sensors when separated vertically is linearly related to the sensor spacing, but that when

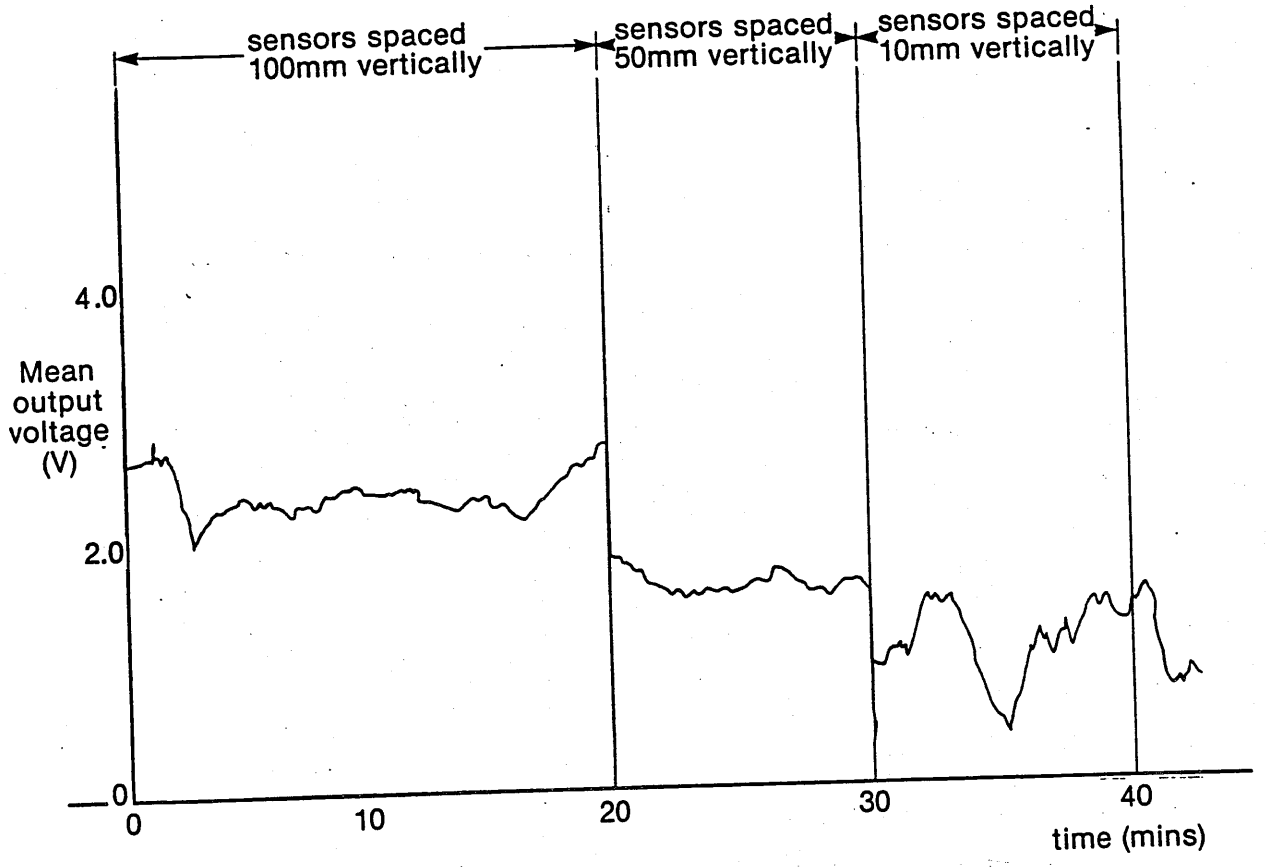

Figure 7.9 MEAN OUTPUT VOLTAGE WITH SENSORS SPACED VERTICALLY

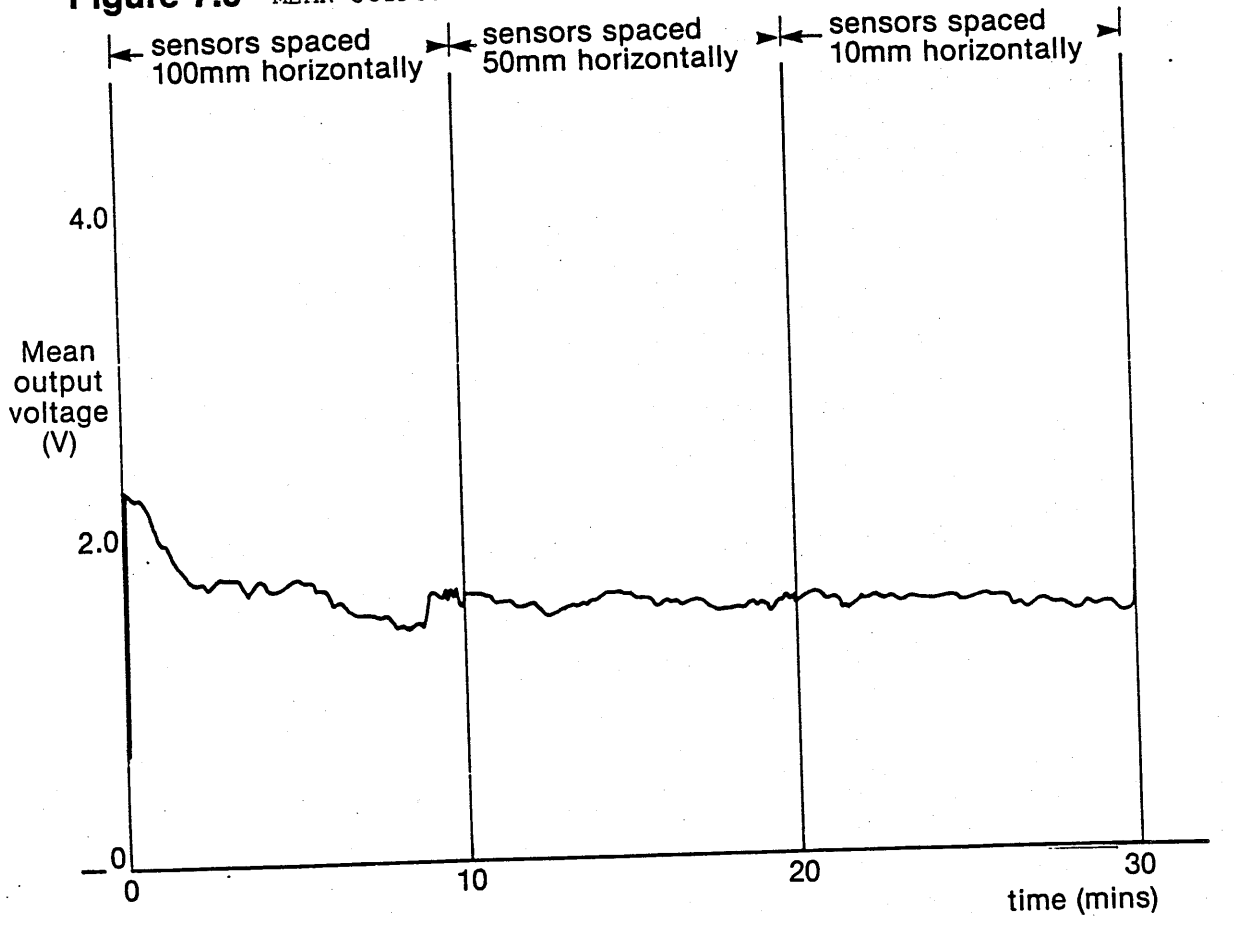

Figure 7.10 MEAN OUTPUT VOLTAGE WITH SENSORS SPACED HORIZONTALLY

TABLE 7.1 SUMMARY OF MEASURED DATA

CONFIGURATION	SPACING mm	TIME CONSTANT s	MEAN O/P VOLTAGE VOLTS	PEAK TO PEAK O/P VOLTAGE VOLTS
Vertical	200	0	2.75	0.32
		100	2.68	0.31
	100	0	2.30	0.30
		100	2.28	0.31
	50	0	1.64	0.14
		100	1.65	0.12
	10	0	1.02	0.12
		100	1.00	0.13
Horizontal	200	0	2.10	0.33
		100	2.18	0.37
	100	0	1.56	0.30
		100	1.56	0.32
	50	0	1.54	0.28
		100	1.53	0.29
	10	0	1.56	0.30
		100	1.57	0.31

horizonally separated there is little change. The results when using the 100 s time constant show less high frequency activity, as would be expected, although the long term mean level and the peak to peak variations are nominally the same as for when no time constant is employed.

One can hypothesise that there is a gradient of the refractive index structure with height above the ground (or heat plate in the case of this experiment) and that in each finite stratum above the ground the refractive index structure parameter is sensibly constant. (This is decidedly the case in the experiment since it was arranged to be so by employing the one metre square aluminium plate and the avoidance of

crosswinds.) It follows therefore that one would not expect any significant difference in temperature when the sensors are spaced horizontally.

For vertical separation of the sensors it was observed that the peak variation of $\overline{(t_1 - t_2)^2}$ decreased with decreasing sensor spacing in a similar manner to the mean value of $\overline{(t_1 - t_2)^2}$. However in the case of horizontal separation of the sensors there was no significant change observed in the magnitude of the peak to peak variations of $\overline{(t_1 - t_2)^2}$.

7.5.3 Time Constant

It was to be expected that as the time constant was increased the peaks and rapid high frequency fluctuations would be averaged out resulting in a much smoother characteristic. The time constant employed on any particular occasion is a function of the particular C_n^2 characteristic being studied.

Irrespective of whether the peaks are averaged out or not, the results show that both the mean level and the peak to peak variations of C_n^2 remained much the same as those shown in Figures 7.7 and 7.8. In practice a 100 s time constant was considered to be a good compromise in that it was sufficiently long to suppress the high frequency fluctuations but short enough for the C_n^2 fluctuations to be adequately correlated with the worst case error rate measurements (see Chapter 8).

7.5.4 Field Measurements - The Nature of C_n^2 Variations

A whole range of measurement results were obtained during the course of an 18 month measurement programme running from April 1984 to October 1985. For the purposes of logical presentation of the results

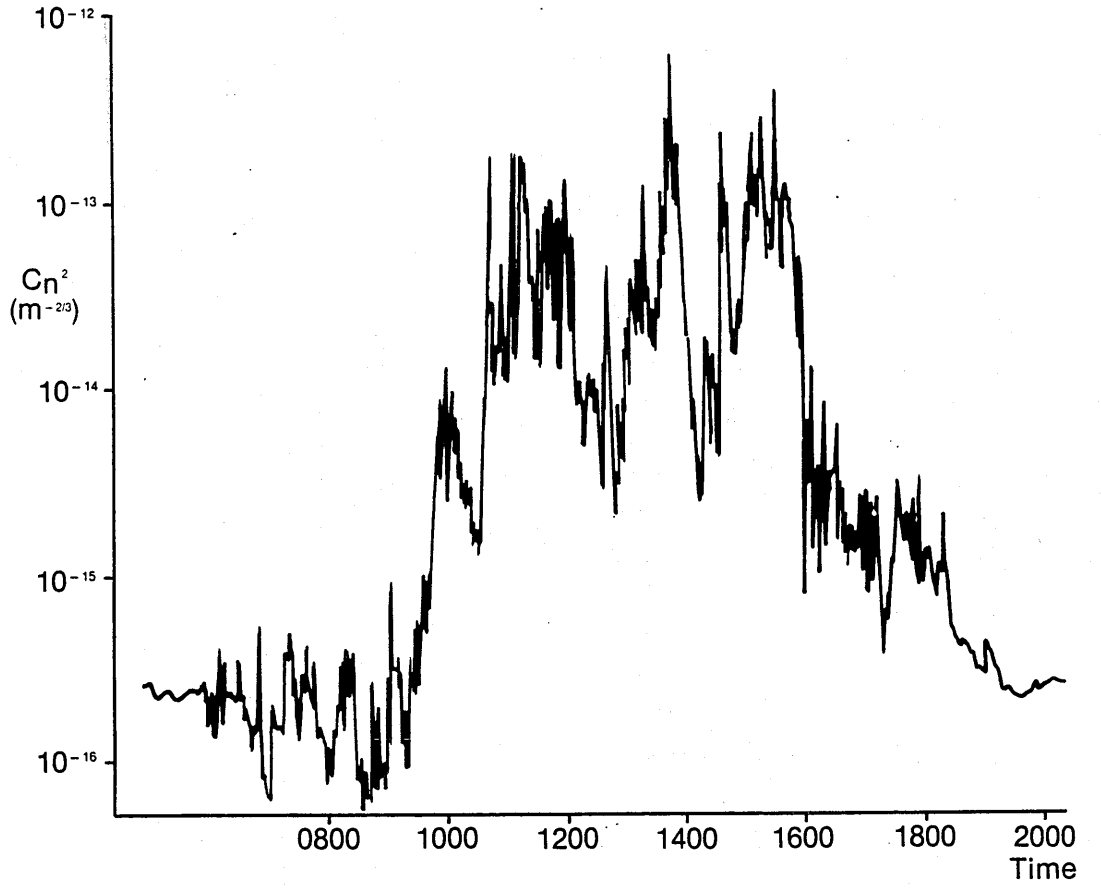

Figure 7.11 Field measurements of Cn^2

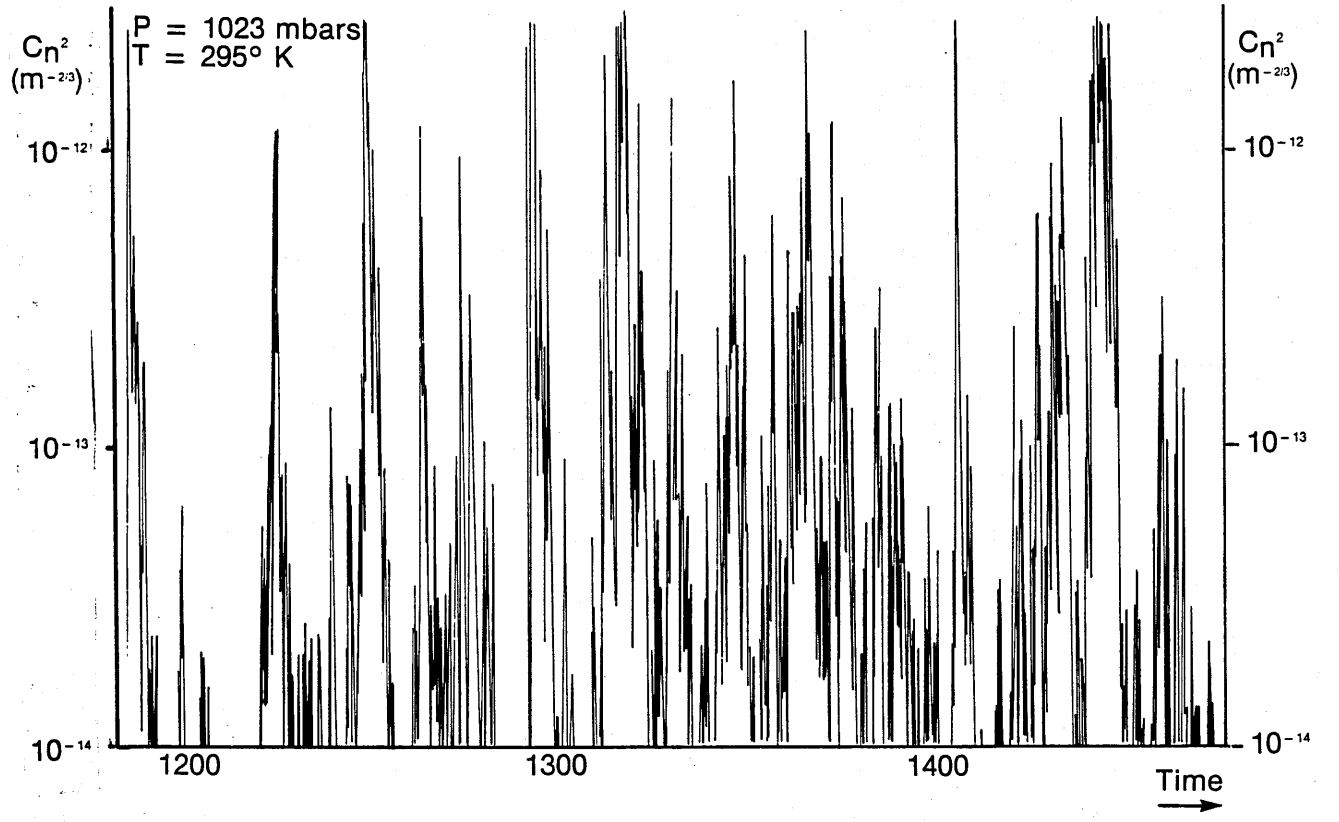

Figure 7.12 Cn^2 Measurement results — during a period of maximum turbulence (probes spaced 100mm apart vertically and 0.75 m above surface)

the measured data has been categorised so as to provide answers to specific questions.

The arrangements were as follows:

Equipment located at 2-12 Gresham Street, London, with the sensors mounted 0.75 m above the ground surface on the east side of the building. Measurements were made at various times of the year. The results shown are the worst case data ie maximum measured turbulence - the object being to show the dramatic variations which clearly can occur even in the UK.

Nominal temperature at 1200 hrs	= 295°K
Nominal atmospheric pressure	= 1023 millibars
Weather conditions	warm, clear sky, no wind

Chart recorder settings of 10 mm/min(t) and 10V/200 mm (x) were employed.

The worst case results measured are shown in Figure 7.11. It can be seen that they are quite dramatic with considerable activity throughout the day albeit to a lesser extent as the sun moved around such that there was no direct sunlight on the thermocouple probes (ie after 1350 hrs). A typical detailed section of the output from the chart record on another day during a period of maximum turbulence is given in Figure 7.12. There are clearly periods of intense turbulence with C_n^2 reaching values in excess of 10^{-12} $m^{-2/3}$ for short periods as much as 8 times an hour. Activity at $C_n^2 = 10^{-12}$ $m^{-2/3}$ appears to be common for as much as 30 minutes in any hour during the period up to 1350 hrs. On the other hand there are also periods of complete calm, ie no turbulence as represented by $C_n^2 = 10^{-15}$ $m^{-2/3}$, for up to about 20 minutes in an hour.

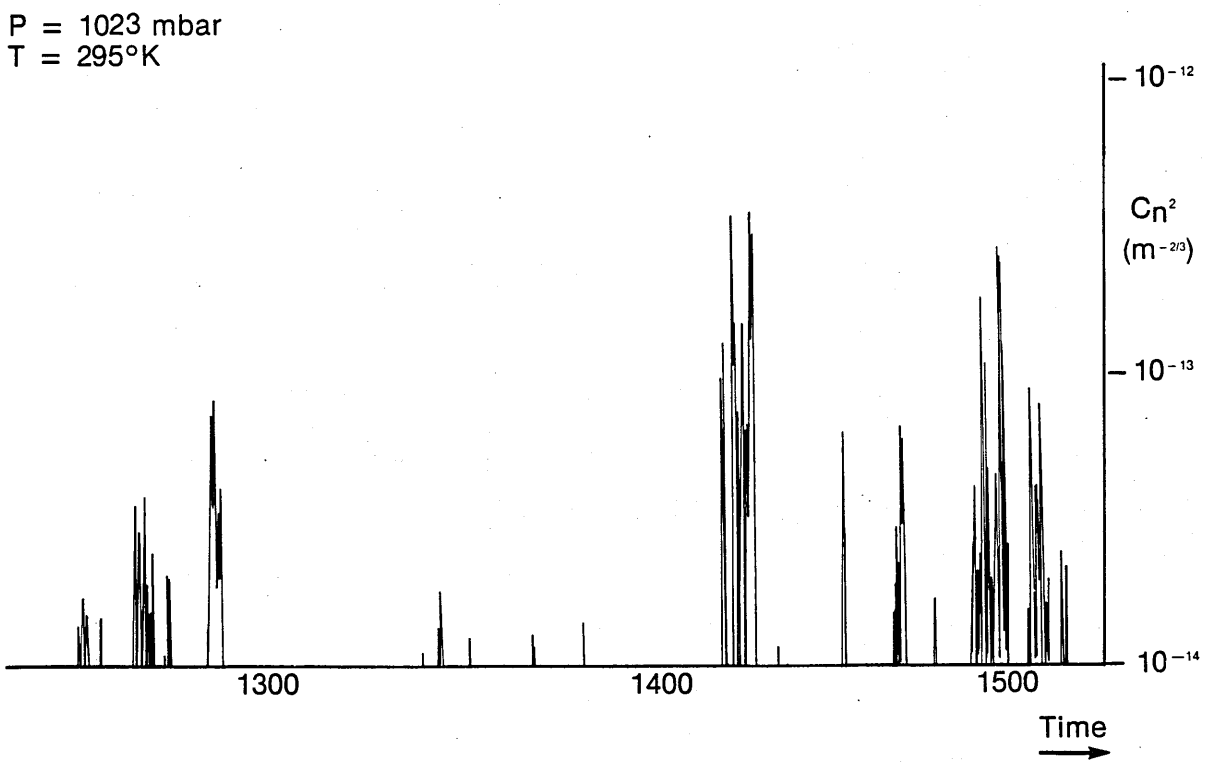

Figure 7.13 C_n^2 measurement results — (probes 20 m above surface)

As the sun disappears off the sensors and the surface of the ground, the amount of turbulence gradually decreases, with the level of activity becoming minimal with only a relatively few periods of activity up to 5 x 10^{-13} $m^{-2/3}$ for just a few minutes in any hour. Almost 6 m of printout was obtained per day with the chart recorder running at 10 mm/minute.

7.5.5 The Variation of C_n^2 with Altitude

Equipment was as for Para 7.5.4 but located on 6th floor of 2-12 Gresham Street with the sensors protruding 0.3 m out of a window. Altitude above the ground was 20 m.

Nominal temperature at 1200 hrs	= 293.5°K
Nominal atmospheric pressure	= 1020 millibars
Weather conditions	warm, slightly cloudy (5 octares) slight breeze
Duration of measurement	0900-1610 hrs

Due to the reduced activity slower chart recorder settings of 2 and 5 mm/min(t) were used. The (y) sensitivity was as for results in Para 7.5.4.

The results obtained at an altitude of 20 m above ground are significantly different to those discussed in Para 7.5.4 with very little activity over the whole of the day. Activity is typified by a few peaks of 2-4 x 10^{-15} $m^{-2/3}$ for about a second or so during an hour, with very occasional peaks to around 6 x 10^{-12} $m^{-2/3}$. Figure 7.13 shows a typical portion of the output from the chart recorder. The chart recorder was run at 5 mm/min up until 1310 and thereafter at 2 mm/min generating a total of 2 m of printout for the day. The results suggest that there is some altitude dependence of C_n^2 but it was not possible to pursue investigation of this aspect

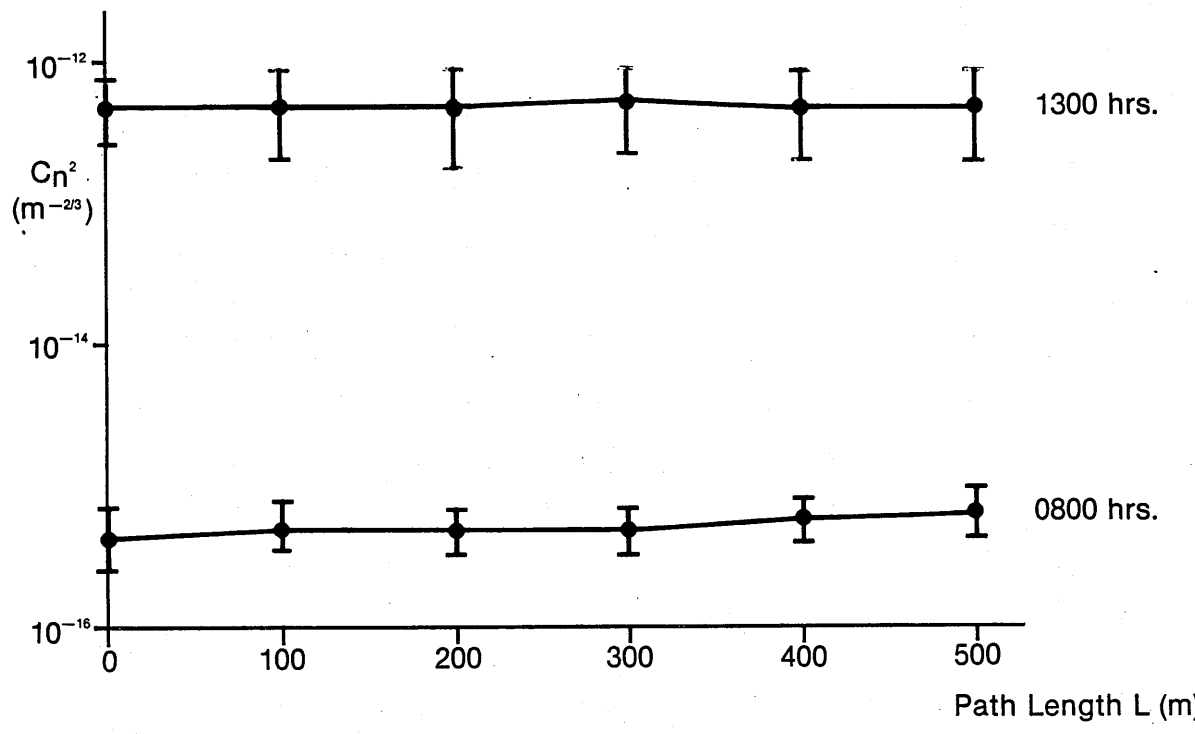

Figure 7.14 Variation of C_n^2 with path length (uniform grass surface)

as part of this thesis due to the unavailability of measuring points at different altitudes. Various researchers have already published results on this topic as already discussed in Chapter 5 and the limited results obtained from this particular measurement appear to support the generally accepted premise that there is an altitude dependence factor in C_n^2.

7.5.6 Field Measurements - The Variation of C_n^2 Along the System Path Length

For the comparison of the variation of error rate with C_n^2 to be considered in Chapter 8 it is obviously necessary to measure the value of C_n^2. The question arises as to whether C_n^2 needs to be measured all along the system propagation path or whether a single point measurement of C_n^2 is acceptable. Accordingly in this particular series of measurements the value of C_n^2 was measured at different points along the propagation path all within a few minutes of each other and then repeated at intervals during the course of the day. The measurements were made at the Speeds Farm test site at Langton Green, Kent, over a test range of 500 m comprising a uniform grass surface.

A summary of the measurements at two particular time instants, 0800 and 1300 hrs, is shown in Figure 7.14. The value of C_n^2 measured at any particular time fluctuates somewhat as indicated in the results discussed in Para 7.5.4. Nevertheless all the measurements were made at each of the measurement points 0, 100, 200, 300, 400 and 500 m from the transmitter, taking the average value in each case within approximately a timespan of just 15 minutes. The results shown in Figure 7.14 show that for a uniform ground surface (in this case short cut grass) the value of C_n^2 remains almost constant (within normal

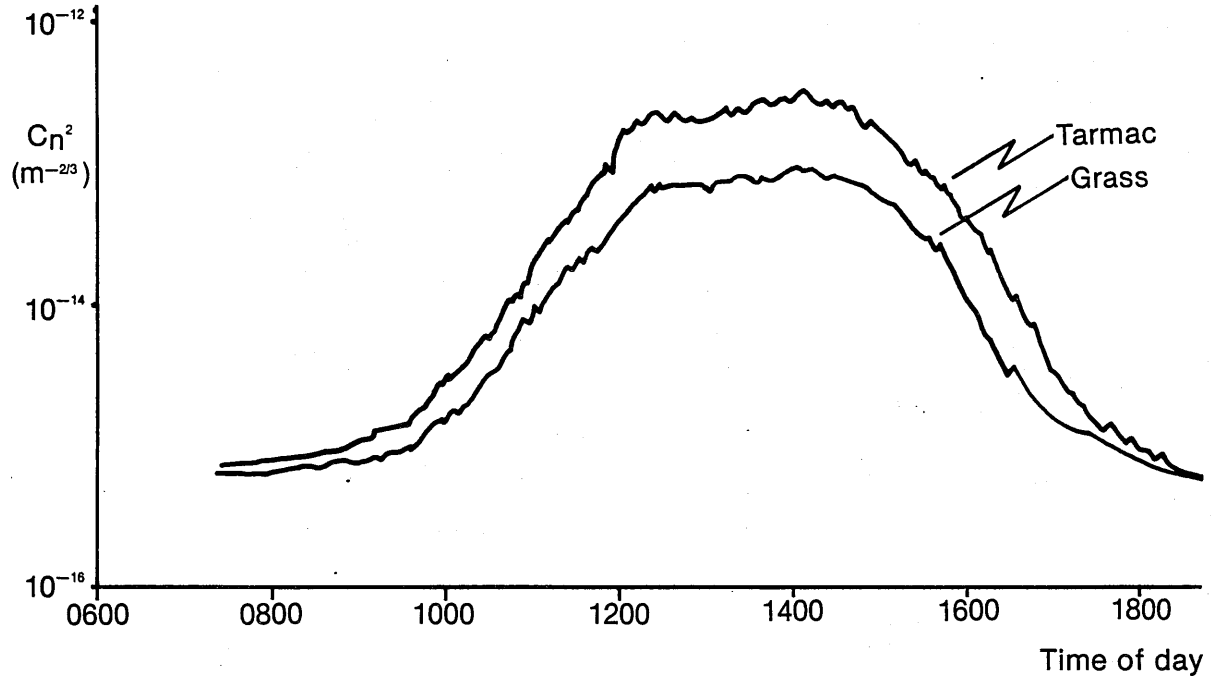

Figure 7.15 Variation of C_n^2 with time measured 1m above tarmac and grass surfaces.

limits of experimental error). Moreover, this appears to be the case irrespective of the time of day and magnitude of C_n^2.

The implication is therefore that, for a uniform surface, it does not matter where along the propagation path C_n^2 is measured, and that one measurement at any reasonable point along the path would be representative of the value of C_n^2 anywhere along the path (albeit within the limits of normal experimental error). Sufficient measurements were made at different points along the path and on different ground surfaces, to suggest that the type of ground surface, provided it is the same throughout the propagation path length, does not affect the conclusion that C_n^2 remains sensibly constant irrespective of where measured along the propagation path (see Para 7.5.7).

7.5.7 Field Measurements - Effect on Variation of C_n^2 of Different Ground Surfaces

It is necessary to know what effect the type of ground surface has on the value of C_n^2. Obviously there are many types of ground surface which might appear beneath the propagation path of an optical line of sight system. Measurements were made, however, over two types of ground surface commonly encountered in practice namely tarmac and grass. The results for the measurement of C_n^2 1 m above each of these surfaces was measured during the course of the same day and the data is shown in Figure 7.15.

It can be clearly seen that there is a distinction between the two ground surfaces. Tarmac has a greater capacity for retaining heat than grass, with the consequential result that the value of C_n^2 is generally greater when the surface is tarmac rather than grass. The maximum difference measured at any time as part of this program was 5×10^{-13} $m^{-2/3}$, but this should only be regarded as being typical

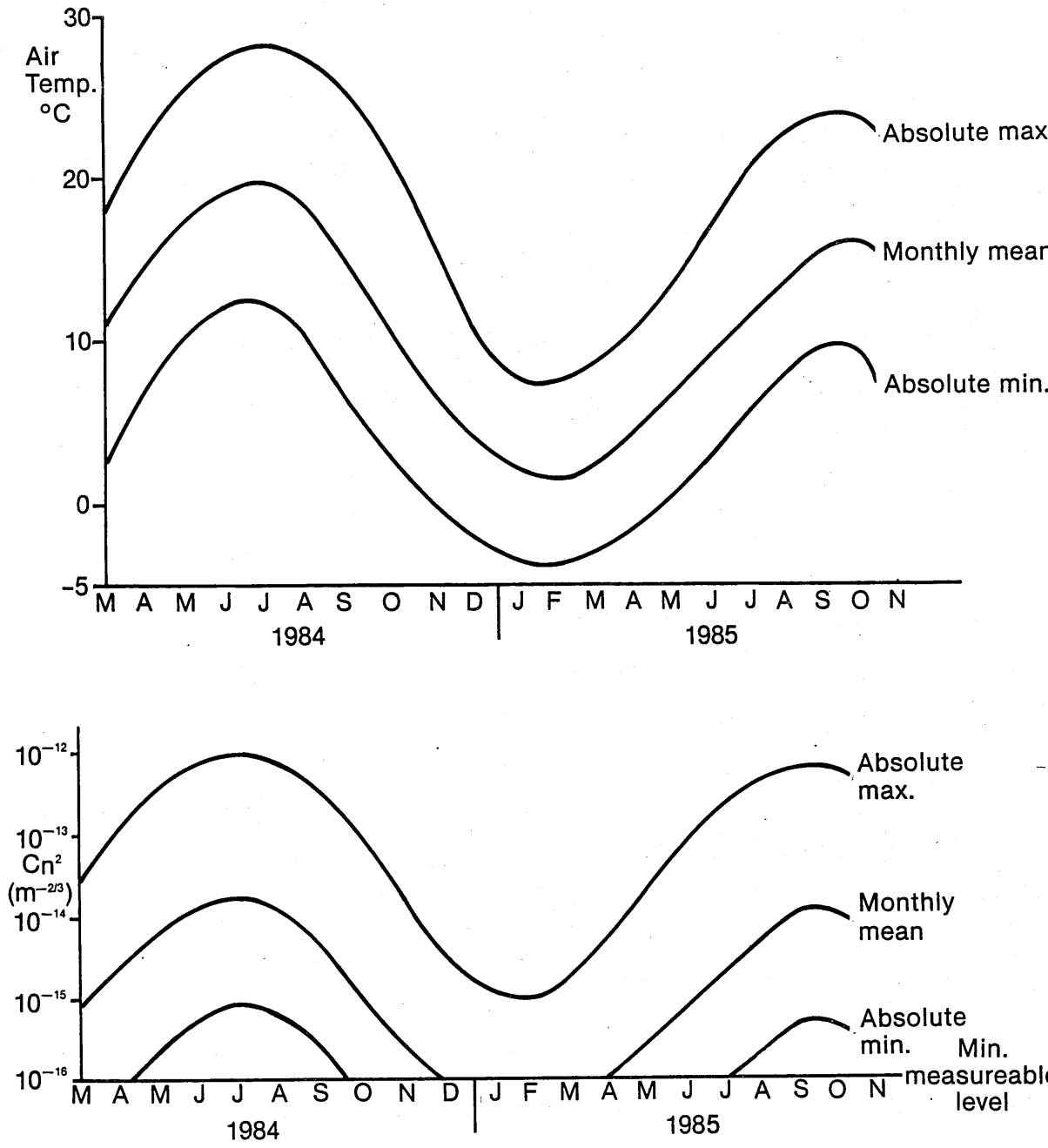

Figure 7.16 Measured monthly data for C_n^2 and temperature

of the order of magnitude of difference. In any case the results appear to confirm that surfaces which have a high thermal mass give rise to a greater degree of turbulence and hence higher value of C_n^2. This assessment is purely qualitative; full quantification of the difference arising from different types of ground surface is outside the scope of this research activity.

7.5.8 Field Measurements - Effect of Variation of C_n^2 with Time of Year

It is readily apparent from the discussion in previous chapters that the level of turbulence is primarily a function of the temperature difference between adjacent 'parcels' of air and that these in turn are a function of the ambient air temperature. In order to determine this correlation and the order of magnitude of the variation in C_n^2 during the course of a year, measurements of C_n^2 and temperature were made over a period of 18 months from April 1984 through to October 1985. The results are shown in Figure 7.16. The upper part of the figure shows the variation in air temperature measured at a height of 1 m above the ground. In particular three temperature plots are shown representing the absolute maximum measured at any time during the month, the absolute minimum and the daily average value averaged over the whole month. The lower part of the figure shows the corresponding variations in C_n^2. As for temperature, the absolute maximum and minimum values of C_n^2 measured during each month are shown, together with the daily mean value of C_n^2 averaged over a month.

The temperature results show the expected annual cyclical variation in temperature. Of particular note are the particularly cold months of January and February 1985 and the less than hot summer in July and August 1985. Obviously within the absolute maximum and minimum

temperature values shown are the normal diurnal temperature variations.

The C_n^2 variations during the course of the measurement program also followed an annual cycle peaking in July/August and being at a minimum in January/February. In the latter the value of C_n^2 is so low at 10^{-16} $m^{-2/3}$ that one can say that the level of turbulence is almost trivial such that it can almost be ignored. As was the case with the temperature measurements there is also a diurnal variation of C_n^2 as already discussed in Para 7.5.4 which means that at any particular instant on any particular day in a given month the value of C_n^2 may be anywhere between the absolute maximum and minimum values shown.

The relationship and correspondence between the variation of temperature and C_n^2 during the course of a year is clear to see from Figure 7.16, although in view of the theory and other data already discussed, it is not particularly surprising. The significance of the variation with respect to atmospheric optical communication systems performance is discussed in Chapter 8.

7.6 CONCLUSIONS

It is concluded that for C_n^2 measurements the sensors should generally be spaced vertically. The optimum spacing is considered to be of the order of 100 mm, not because shorter spacings would give intrinsically erroneous results, but because the larger the spacing the greater is the value of $\overline{(t_1 - t_2)^2}$ and hence the greater the signal/noise ratio with consequential reduced demands on the sensitivity of the associated electronics. Spacings much greater than 100 mm could exceed the outer scale of turbulence whereupon the C_n^2 formula would be less likely to

apply. The measuring equipment described appears to be capable of measuring values of C_n^2 right across the whole range 10^{-16} to 10^{-12} $m^{-2/3}$.

The use of a time constant of the order of 100 s gives a smoothed output and is therefore advantageous especially in determining the mean value of C_n^2 at any particular time, but the use of a time constant does not appear to be essential if only magnitudes of variations are to be monitored. This accords with the findings of Tatarskii [7.2].

The conclusions which can be drawn from the results obtained during the 18 month measurement programme are:-

a. The amount of turbulence decreases with the distance above ground or other surface, eg roof top, supporting the findings of other workers such as Oochs and Lawrence [5.14].

b. The general value of C_n^2 corresponding to minimal turbulence varies considerably depending on the time of year but is typically of the order of 10^{-15} to 10^{-16} $m^{-2/3}$.

c. Close to the ground, ie within 1 m, and at times of high ambient temperature, turbulence can be considerable - such that $C_n^2 = 10^{-12}$ $m^{-2/3}$ on occasions.

d. Intense turbulence gives rise to considerable activity and C_n^2 fluctuations between 10^{-15} and 10^{-12} $m^{-2/3}$. This is in contrast to the results of many other workers eg Clifford et al [7.1], who have published their results showing gradual changes, but fully in accord with those of Tatarskii [7.2]. This is thought to be solely due to the time constant/averaging techniques employed; few workers have actually given any great detail on this aspect in their published papers.

The gradual diurnal variation observed by Clifford et al is manifested as a reduction in the number of peaks in the results reported in this chapter. It may be that most other workers have integrated their results over much greater time periods thus yielding gradual changes. Clearly consideration must be given to whether the intense fluctuations need to be recorded for some reason - if they do not then a long time constant may be employed.

e. Given a uniform surface in a particular locality it appears that the value of C_n^2 is sensibly constant at all points along propagation paths of up to 500 m in length. Clearly this may not be the case if there are any reasons why the level of turbulence should vary, for instance, due to local wind speed variations, increased heat sources (eg heating and ventilating plants), variation of type of ground surface etc.

f. The nature of the ground surface affects the measured value of C_n^2. For instance differences of as much as 5.10^{-13} $m^{-2/3}$ were measured between tarmac and grass surfaces when peak levels of turbulence are being experienced. This reflects the point made in the previous paragraph regarding different ground surfaces giving rise to different magnitudes of turbulence.

g. During the course of a year the maximum measured value of C_n^2 averaged over a month varies considerably. Maximum values of C_n^2 of the order of 10^{-12} $m^{-2/3}$ are observed during the hot summer months, typically June, July and August, whereas the minimum values of the order of 10^{-16} $m^{-2/3}$ occur during the coldest months, typically December, January and February.

h. The design of measuring equipment employed and the use of Type T thermocouples appears to be more than adequate in terms of sensitivity and temporal resolution for the purpose of this thesis.

CHAPTER 8

MEASUREMENTS OF ERROR RATE AND REFRACTIVE INDEX STRUCTURE PARAMETER ON A 2 MBIT/S ATMOSPHERIC OPTICAL LINE OF SIGHT LINK

CHAPTER 8

MEASUREMENTS OF ERROR RATE AND REFRACTIVE INDEX STRUCTURE PARAMETER (C_n^2) ON A 2 MBIT/S ATMOSPHERIC OPTICAL LINE OF SIGHT LINK

8.1 INTRODUCTION

Chapter 6 gave a hypothesis for the relationship between the error rate of a digital atmospheric optical communication system and the atmospheric refractive index structure parameter. This chapter gives details of practical measurements made over the period April 1984-October 1985, the object of which was to check the validity of the above-mentioned hypothesis.

8.2 OPTIMUM BIT RATE OF SYSTEM OPERATION FOR THE MEASUREMENT PROGRAM

Factors taken into account in deciding at what bit rate the line of sight system should operate, in the first instance were:-

a. likely error rate of system and availability of test equipment to measure the error rate

b. time for detection of errors

c. duration of transient activity of C_n^2.

It was observed from the preliminary results reported in Chapter 7 that, during highly active periods of turbulence, the variation of C_n^2 with time is considerable. In particular it was observed that the value of C_n^2 could change from a value of around 10^{-15} to around 10^{-12} $m^{-2/3}$ in as little as 0.5 sec and that it might stay as high as 10^{-12} $m^{-2/3}$ for as little as 0.5 sec.

Now in order to be able to correlate the C_n^2 activity with error rate variations it is essential that, during the periods of rapid C_n^2 change, an adequate number of errors should be detected (it has to be assumed that the original hypothesis is correct in order for this statement to be made).

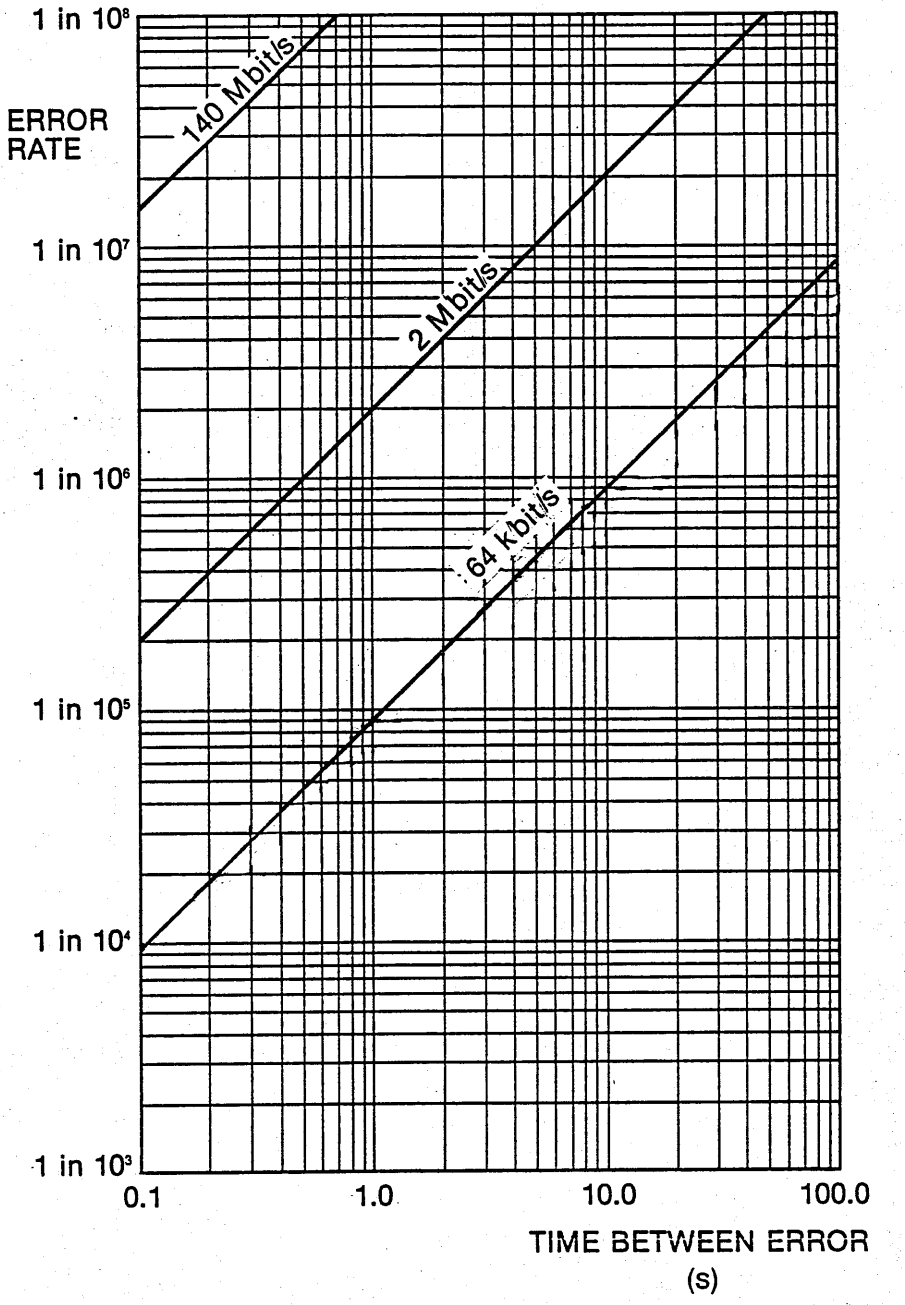

Figure 8.1 Error rate vs. time duration between errors for systems operating at different bit rates

Now if, for the sake of argument, it is assumed that the minimum number of errors to be counted in order to be able to obtain reasonably accurate results is 5 for a change of C_n^2 from 10^{-15} to 10^{-12} $m^{-2/3}$, and let it also be assumed that the minimum duration for such a change is 0.5 secs. It follows therefore that 5 errors in 0.5 seconds corresponds to 10 errors in 1 second and therefore the time between errors, assuming linear error distribution with time, is 0.1 sec.

Figure 8.1 shows the time between errors assuming equal time distribution between them for different systems operating with various error rates and operating bit rates. It can be readily observed that a 64 kbit/s system would have an error rate of 1.10^{-4} if the time interval between errors was 0.1 sec. Table 8.1 gives representative examples for three different systems.

System Bit Rate	Error Rate	No. of Errors per Second	Time Between Errors
140 Mbit/s	1.10^{-3}	1.4×10^{5}	7.14 μs
	1.10^{-6}	140	7.14 ms
	1.10^{-9}	0.14	7.14 s
2 Mbit/s	1.10^{-3}	2×10^{-3}	0.5 ms
	1.10^{-6}	2	0.5 s
	1.10^{-9}	0.002	500 s
64 kbit/s	1.10^{-3}	64	15.6×10^{-3} s
	1.10^{-6}	0.064	15.6 s
	1.10^{-9}	6.4×10^{-5}	15.6×10^{3} s

Table 8.1 Errors per second and time between errors for different systems and varying error rates

For the purposes of this measurement program the background error rate whilst C_n^2 is minimal at around 10^{-16} $m^{2/3}$ does not necessarily have to be negligibly small. The choice of bit rate of operation depends partly on the number of errors it is desired to measure during periods of low C_n^2 activity (eg $C_n^2 = 10^{-16}$ $m^{-2/3}$). It also follows that the higher the error count for a given error rate for a given period of time the more accurate are the overall measurements likely to be. It may be concluded therefore that, for the purposes of relating error rate performance to variation in C_n^2, it is advantageous to operate at the highest bit rate possible consistent with any practical/operational considerations.

The internationally agreed standard digital hierarchical levels are defined up to 565 Mbit/s, however in practice optical line of sight systems operating at speeds of 140 or 565 Mbit/s are not commonly employed since:-

- such high capacities are not normally required for short haul applications

- the spacing between the transmitter and receiver becomes unacceptably short at such bit rates if an adequate system availability is to be obtained.

In considering the standard bit rates lower down in the hierarchy it is concluded that a system operating at 2 Mbit/s represents a good compromise because:-

- such systems are fairly readily available (or can be readily developed)

- 2 Mbit/s is a popular bit rate for the provision of links which might be provided using line of sight optical communications

- the system reach of a 2 Mbit/s optical line of sight system is acceptable for many applications in local telecommunications networks etc

- the analysis of variation of the value of various system parameters as illustrated in Figure 6.9 suggests that systems operating at 2 Mbit/s have a greater range than systems operating at higher bit rates.

It is therefore concluded that, for the purposes of this thesis, the C_n^2 measurements should be correlated with the error rate of an optical line of sight system operating at 2 Mbit/s.

8.3 TEST ARRANGEMENT

A diagram of the complete test arrangement is shown in Figure 8.2. The constituent parts are described below:-

8.3.1 Optical Communication System

The optical communication system employed was constructed as part of this project and was designed to operate at a nominal digital bit rate of 2 Mbit/s over path lengths of up to nominally 1 km in length. One of the terminals mounted on a tripod is shown in Figure 8.3. The system has standard HDB 3 interfaces and operates at the hierarchical rate of 2048 kbit/s. The transmitter comprised an optical source which was a light emitting diode (led) emitting at a nominal wavelength of 900 nm. In the particular design used for these measurements the HDB 3 input interface signal was converted to a binary signal with the coding arrangement as shown in Table 8.2. The binary input signal was then simply amplified and used to directly drive the led ie optical amplitude modulation/on-off keying (OOK). The transmitter utilised a 100 mm diameter Fresnel lens with focal length also of 100 mm and the whole assembly was tripod mounted as shown in Figure 8.3.

HDB 3 SIGNAL	BINARY OUTPUT
+ ve	10
- ve	01
zero	00

TABLE 8.2 CODING ARRANGEMENT FOR 2 MBIT/S SYSTEM

The receiver was physically similar to the transmitter with a 100 mm diameter receiving Fresnel lens having a focal length of 100 mm. The received optical beam was focussed onto a pin photodiode which converted the optical signal to an electrical signal. The latter was then amplified and equalised using a simple matched RC low pass filter. The output signal was then reconverted back to HDB 3 format as per the coding algorithm in Table 8.2. The relevant system parameters are given in Appendix 13.

8.3.2 Error Measuring Equipment

A standard pattern generator and an error rate detector operating at 2 Mbit/s were used for generating the HDB 3 signal and measuring the received error rate respectively. The error rate detector had an output which could be connected to a chart recorder and the voltage measured could be related to the measured error rate. In addition the measured error rate was averaged over a period of 30 minutes in order to obtain a smoother and more accurate profile for data comparison purposes. Further data on the measuring equipment is given in Appendix 13 and Reference [8.1].

8.3.3 C_n^2 Measuring Equipment

The C_n^2 measuring equipment employed was the same as that described in Appendix 4 using a vertical sensor separation of 100 mm. The output from the equipment was fed directly to the chart recorder.

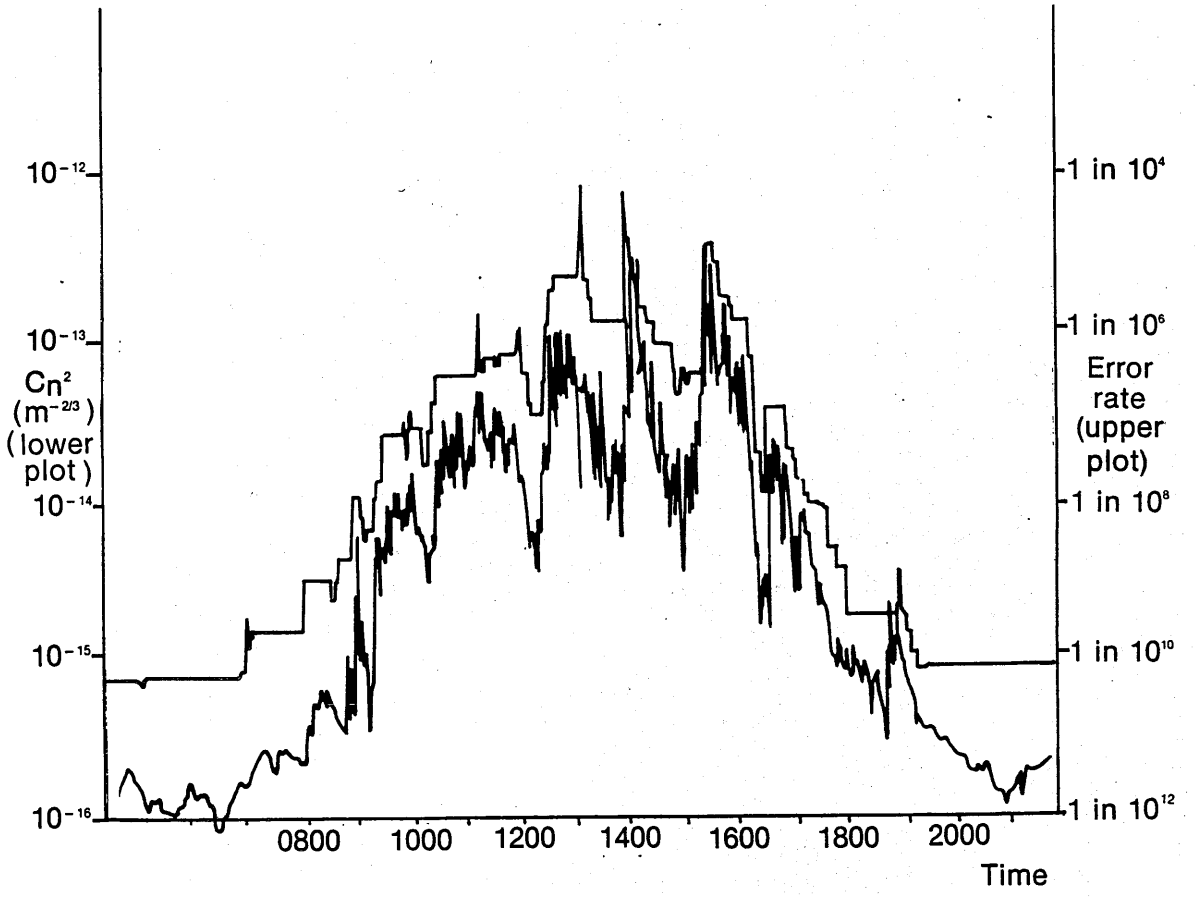

Figure 8.4 Field measurements of C_n^2 and error rate (Typical worst day measurement — 15.8.84)

8.3.4 Location

The measurements were made at Speeds Farm, Langton Green, Kent. This site was chosen for its convenience in respect of physical location and the convenient location of electricity mains supplies to power the optical system and various items of test equipment. The land over which the measurements were made was nominally flat pasture land with the grass no greater than 25 mm in length, having been regularly cut and/or grazed.

The location of the electricity mains supplies and nature of the terrain was such that a maximum optical path length of 500 m could just be achieved.

8.4 MEASUREMENTS AND RESULTS

The total measurement program during which field measurements were made extended over an 18 month period from April 1984 to October 1985. This period was preceded by a period of nearly 12 months during which internal experimentation, design work and calibration of measuring equipment took place. Data obtained from the early phases of the external work together with those measurements associated with the long term measurement of C_n^2 was considered in Chapter 7. This chapter considers those results pertaining to the measurement of C_n^2 data as it relates to system error performance.

Considerable experimental data has been obtained during the course of the measurement program. Much of the data is repetitive in nature tending to underline the general conclusions which will be debated later in this chapter.

As an example of some typical worst case results obtained, data for three different days obtained in August 1984 is shown in Figures 8.4-8.6. These figures show the data for the simultaneous measurement of C_n^2 and error

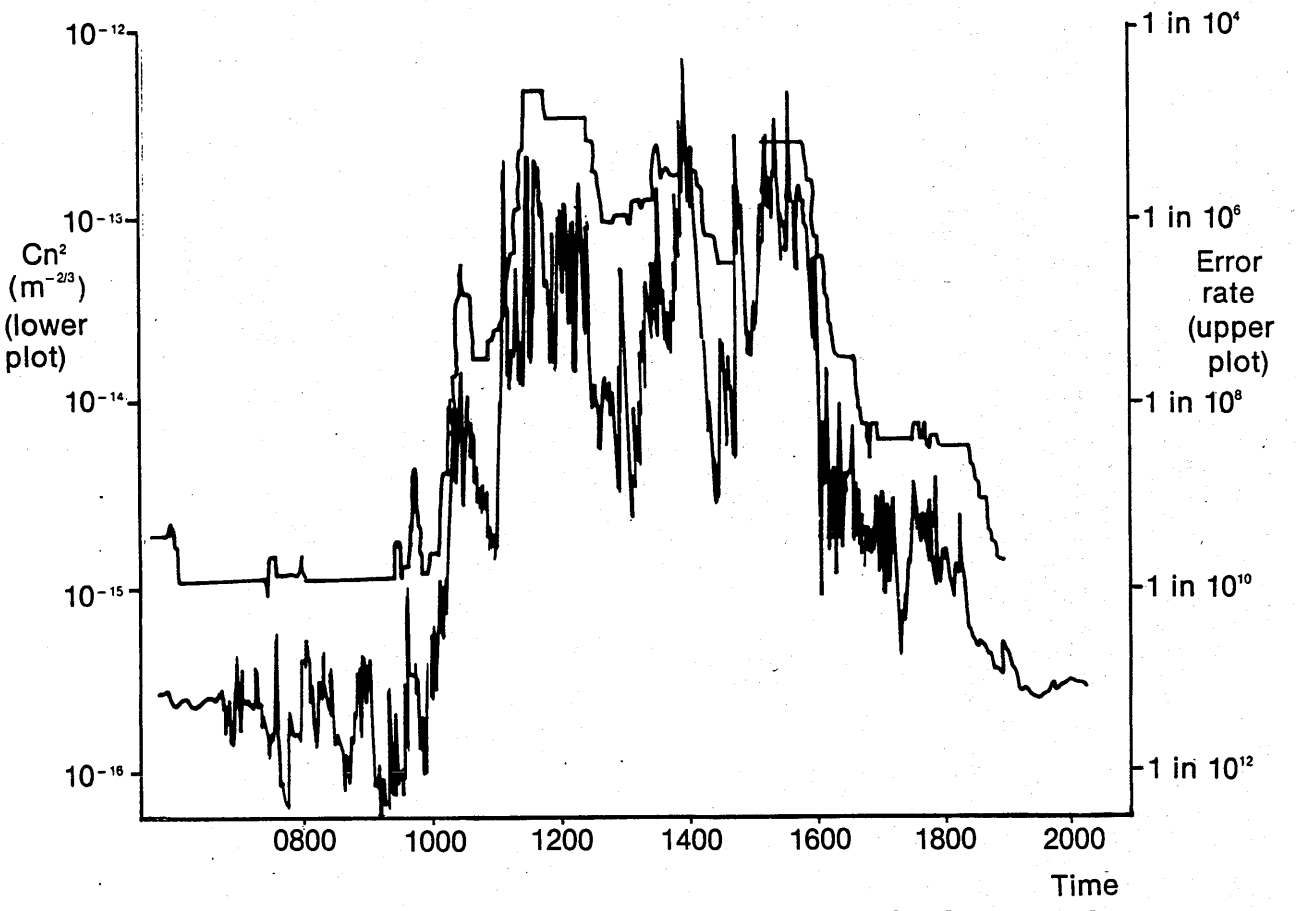

Figure 8.5 Field measurements of C_n^2 (Typical worst day measurement — 16.8.84)

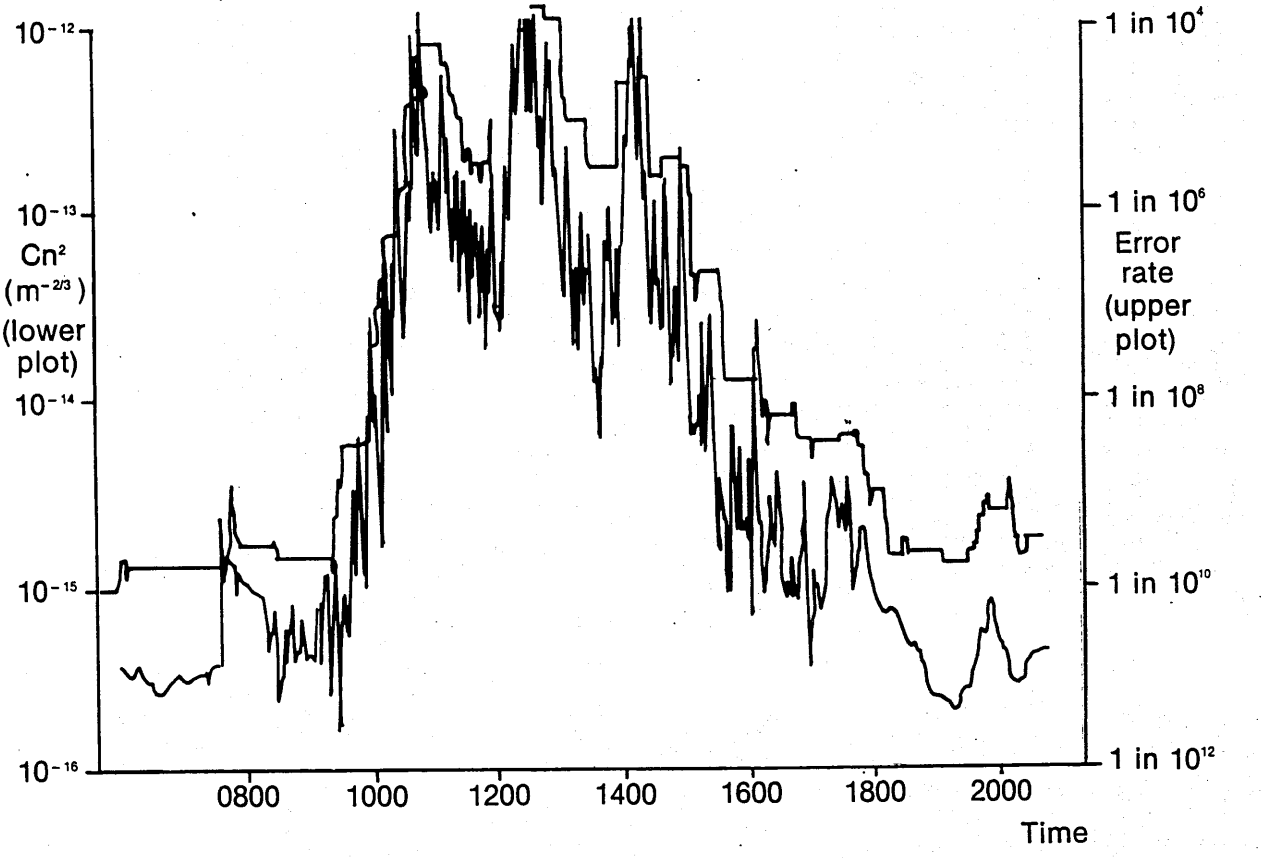

Figure 8.6 Field measurements of C_n^2 (Typical worst day measurement — 17.8.84)

rate with the test set-up as described earlier in this chapter, that is the 2 Mbit/s system with path length of 500 m.

The correlation between C_n^2 and error rate is only too apparent for each of the days chosen. The C_n^2 characteristic throughout the course of each of the three days is similar to those obtained at other times of the year and other test arrangements as discussed in Chapter 7 although the peak values of C_n^2 are lower in the colder months. In general the value of C_n^2 varies from a night-time value of around 5.10^{-15} $m^{-2/3}$ increasing rapidly during the course of the morning as the sun heats up both the air and the ground itself. The mean value of C_n^2 usually peaks somewhere between 10^{-12} and 10^{-13} $m^{-2/3}$ during the midday period when ambient temperatures are of the order of 20-25°C. On fine days the value of C_n^2 remains high for much of the afternoon due to the retained ground heat and only drops as the sun's heat reduces towards late afternoon and early evening. By about 1800-2000 hours the C_n^2 value has returned to the night-time value.

As is the case with all the C_n^2 measurements the data does indicate very large fluctuations despite the averaging function included in the C_n^2 measuring apparatus. Nevertheless despite these fluctuations the variation of the mean value of C_n^2 can be clearly discerned. Owing to the nature of the error detection process error rate measurement accuracy will be greater the worse the error rate becomes. This is because a larger number of errors will be counted for higher levels of C_n^2. For low levels of C_n^2, and hence low error rates, the time between errors for a 2 Mbit/s system is very low, typically 10 minutes, which means that the accuracy of the error rate measurement is a function of the averaging time used in the error rate detector. The Hewlett Packard set employed had a running average of 30 minutes and it follows that the error rate plots will

not reflect any particularly rapid changes in error rate at the lower error rate levels.

Measurements made at other times of the year reflect the characteristics noted previously in Chapter 7, namely that as the average air temperature for the month decreases so does the corresponding value of C_n^2. The data shown in Figures 8.4-8.6 are the worst case examples measured during the 18 month period in that they indicated the highest value of C_n^2 measured, which as might be expected was for the month of August.

The error rate plots in each case in Figures 8.4-8.6 show a satisfactory correspondence with the variation in C_n^2. Any lag that there might be would appear to be minimal indicating that any change in C_n^2 results in an almost immediate corresponding change in the error rate. The actual value of error rate will vary depending on a number of factors as previously discussed, but including path length, source power etc quite apart from any variation of C_n^2. For the system type and measurement conditions in this instance (as given in Para 8.3) and in particular a 2 Mbit/s system operating over a path length of 500 m, the error rate varied between a background error rate of about 10^{-10} to a peak error rate of about 10^{-6}-10^{-4}. Obviously different error rates would apply for other arrangements of path length, bit rate etc.

The meteorological conditions for the days for which the figures apply are shown in Table 8.3.

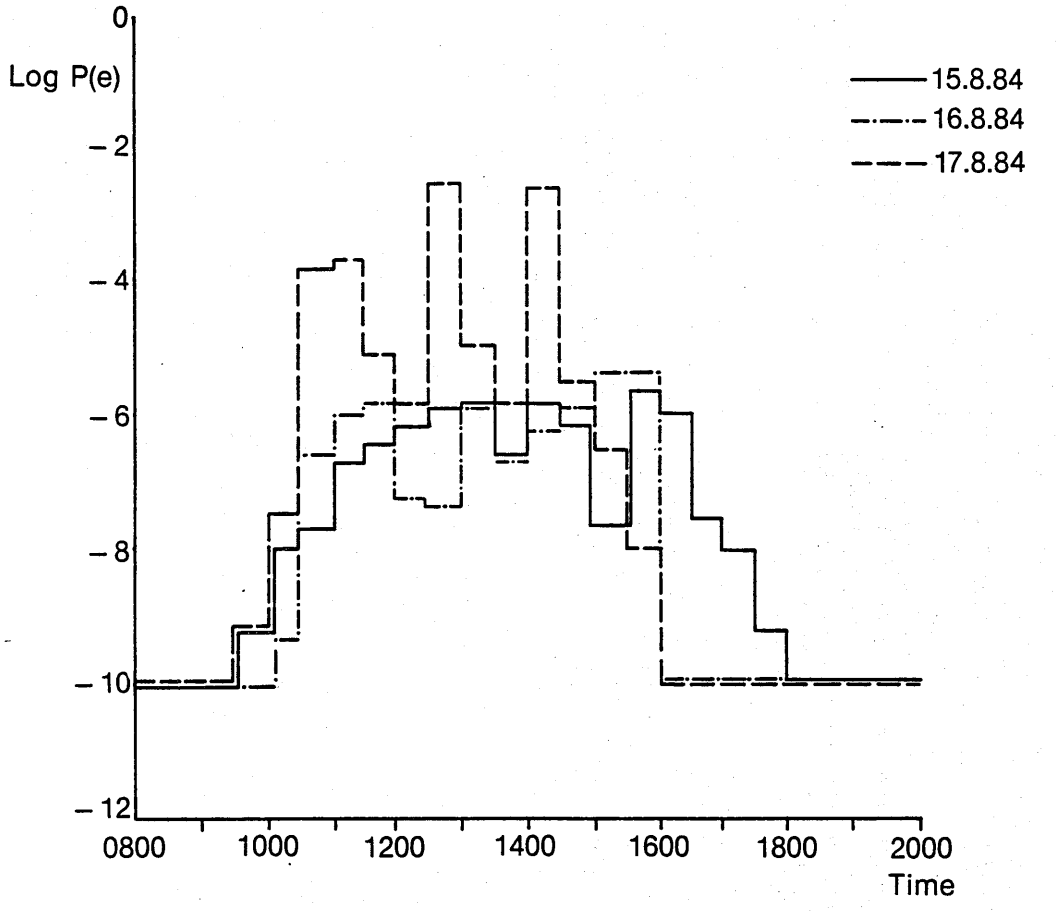

Figure 8.7 Summary of variation of error rate measurements with time of day for 2Mbit/s test link on three worst case days

TABLE 8.3 METEOROLOGICAL CONDITIONS DURING MEASUREMENTS

Day	Date	Temp °C		Wind	Cloud cover (max)
		Min	Max	m/s (est)	octas (estimated)
1	15.8.84	15.6	21.8	≤ 5	3
2	16.8.84	13.8	23.2	≤ 5	3
3	17.8.84	14.7	22.4	≤ 5	3

The variations of error rate with time for each of the three days in question averaged over 30 minute time periods are given in histogram form in Figure 8.7. This histogram presents a clearer picture of the variation. The general shape of the variation is clearly apparent and corresponds with that of C_n^2. There are unmistakeable occasional large fluctuations particularly on the last of the three days considered at about 1100, 1300 and 1430 hours. These fluctuations are a reflexion of the corresponding particularly large variations in C_n^2 on the same day (see Figure 8.6).

Also of interest is the increased duration of the degradation of the error rate in the late afternoon clearly shown in Figure 8.7 for the first of the three days reflecting the longer period of sunshine during the afternoon on that day.

The significance of these results with respect to variation of path length was established by making measurements of P(e) and C_n^2 over three path lengths of 100, 300 and 500 m.

The results from Chapter 7 indicated that for a uniform ground surface it is generally sufficient for C_n^2 to be measured at any reasonable point along the system path length. In this instance a point 50 m from the transmitter was chosen - this being the mid point of the shortest path length employed for this particular part of the measurement program. The

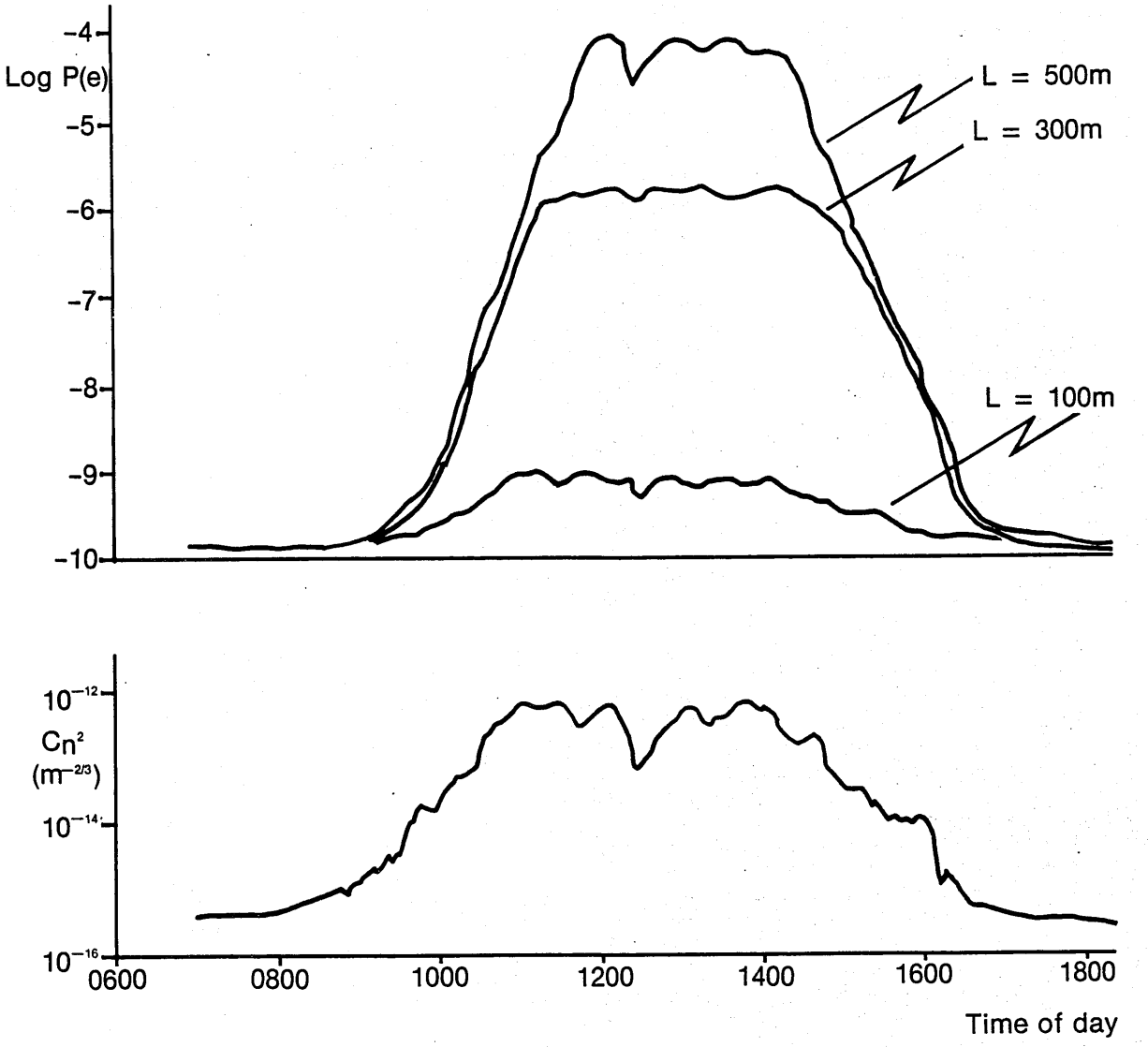

Figure 8.8 Variation of error rate with time for different path lengths (2 Mbit/s 00K system)

results for error rate variation with path length are shown in Figure 8.8 for three different path lengths of 100, 300 and 500 m. In order to permit direct comparison the results were all obtained on the same day and were achieved by moving the receiver and associated measuring equipment approximately every 15 minutes to the required location.

The results shown in Figure 8.8 clearly indicate the degradation of error rate performance with increased path length and furthermore the degradation for any particular path length as the value of C_n^2 increases particularly during the midday period. The degradation due to turbulence is observed to worsen with increased path length, confirming the length dependency of the expression for the log amplitude variance given in expression (4.2) and as shown in Figures 6.6 and 6.7.

The relevant results obtained throughout the 18 month measurement program, for path lengths of 300 and 500 m and system operation at 2 Mbit/s (OOK) are shown in Figure 8.9.

This figure shows the clear relationship between error rate and C_n^2 for both path lengths (over six decades of error rate and three decades of C_n^2). The relatively large variations in values of error rate for any given value of C_n^2 are note worthy and not surprising considering the major fluctuations in C_n^2 shown in Figures 8.4-8.6. Nevertheless the mean value of error rate in each case follows the linear relationship very closely. A plot showing the theoretical relationship calculated using the relationship for C_n^2 and error rate derived in Chapter 6 (Figure 6.8) is also given in Figure 8.9 for each of the two path lengths (but modified for the actual led radiance employed of 2.7 $W/m^2/sr$). The graphs clearly indicate the close agreement between the practical measured data and theory. The correlation co-efficient has been calculated as being 0.93 and

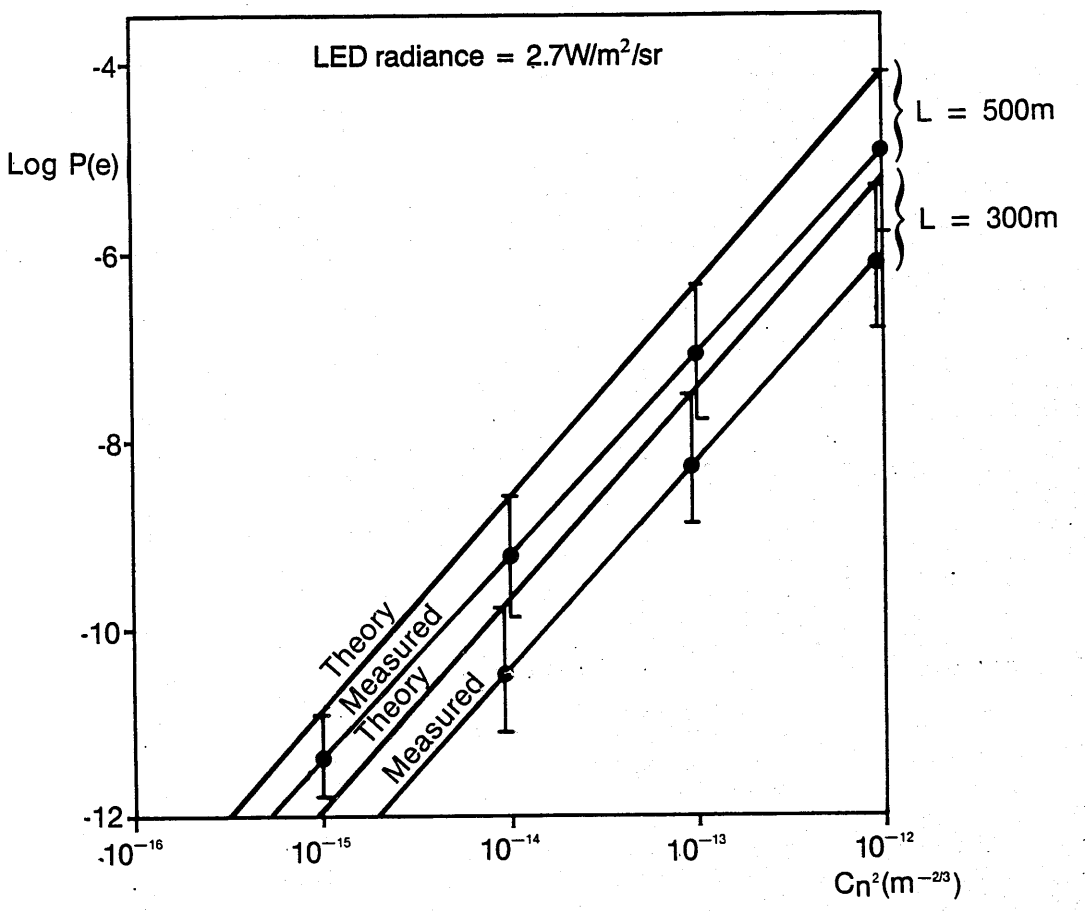

Figure 8.9 Comparison of measured results with theory for relationship between P(e) and Cn^2

(2 Mbit/s OOK system; lens diameter = 0.1m)

0.90 for the 300 and 500 m path lengths respectively, quantitatively confirming the good agreement.

Figure 8.9 shows the measured data as being consistently a little less than that predicted by the theory, but in terms of the error rate varies at worst by little more than an order of magnitude. This is due to the fact that the theory is based on worst case predictions which were not encountered continually during the period of the measurement program.

The variation of error rate and C_n^2 throughout the year is obviously of great importance. The data obtained during the whole measurement program and presented in Figures 8.4-8.6 and 8.9 has been analysed with a view to assessing the effect of time of year and ambient temperature on the overall results and the ensuing conclusions. It has been found that, at cooler times of the year eg October through to May, the mean air temperature is less than that for the August measurements considered here in some detail (as would be expected) and that as a direct consequence the values of C_n^2 are correspondingly lower. This in turn means that the error rate is not degraded to the same extent. In terms of Figure 8.9 the annual variations in temperature mean that during the winter months the performance will be low down on the practical results line (ie bottom left) and that with the advent of the warmer weather in the summer, degradation will occur with operation further up the line. The measured data in Chapter 7 gives data on the ambient temperature variations during the course of a typical year, which in turn is indicative of the variation in error rate likely to be experienced over a year.

Of course even in the winter months a daily variation is seen in the value of C_n^2, except that, because the total temperature variation on a winter's day is less than that for a summer's day, the variation of C_n^2 is correspondingly less.

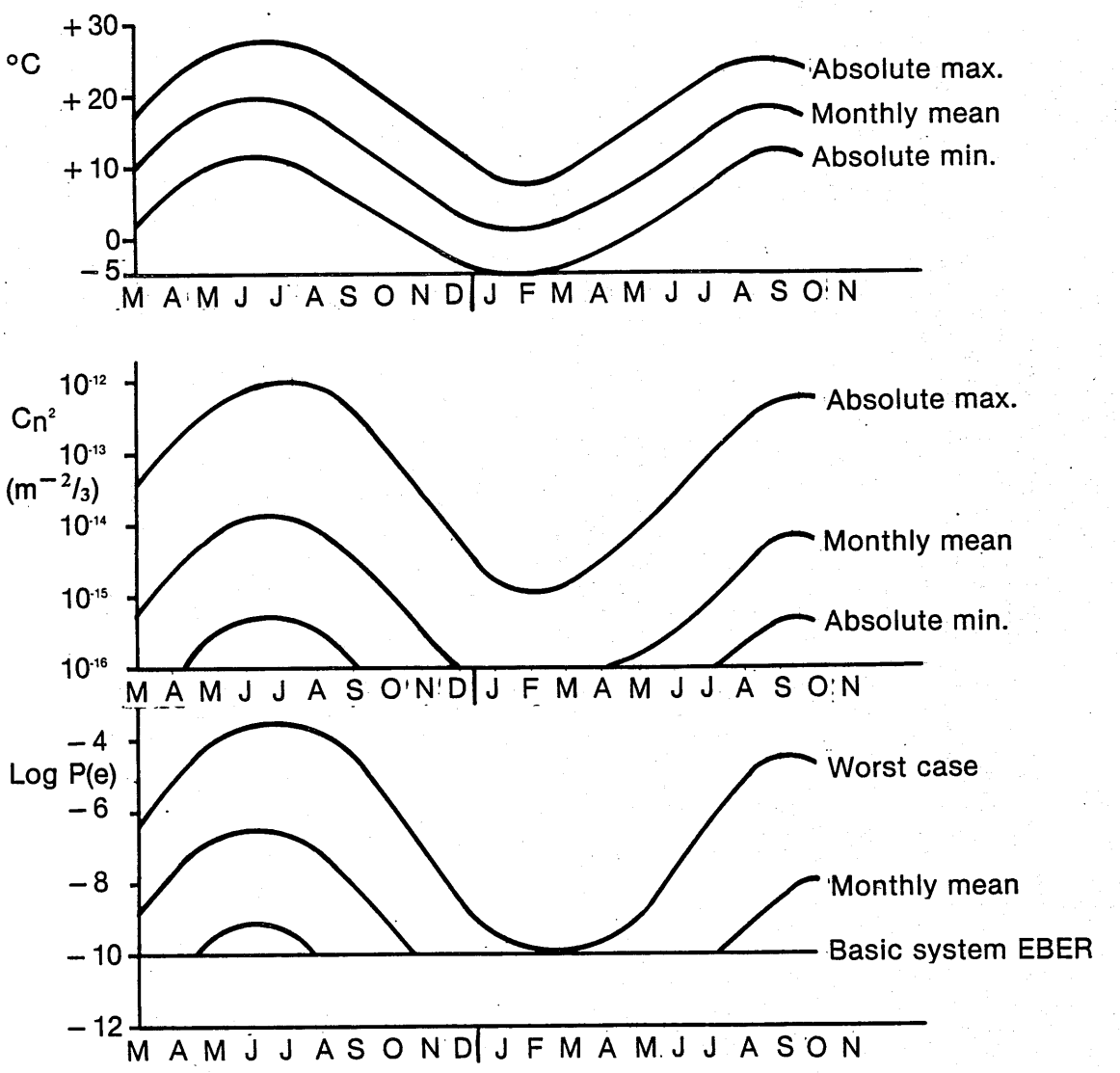

Figure 8.10 Relationship between error rate and C_n^2 with time of year (2 Mbit/s 00K system; L = 500m)

From the point of view of being able to assess the performance of the optical communication system it is useful to know the worst case during each working day and hence the measured results for C_n^2 during the course of the 18 month experimental period have been analysed with the object of quantifying the likely degradation of error rate during the course of a year. Figure 8.10 shows the measured results. Clearly the mean air temperature, the measured value of C_n^2, and the error rate for the 2 Mbit/s systems operating over a path length of 500 m are all related. The maximum monthly averaged air temperature ranged from 7°C to 27°C, the maximum value of C_n^2 ranged from 10^{-15} to 10^{-12} $m^{-2/3}$ and the error rate was degraded from 1 in 10^{-10} in the winter to 2 in 10^{-4} in the summer. The annual variations in C_n^2 data have already been discussed in Chapter 7.

8.5 CONCLUSIONS

There are a number of conclusions which may be drawn from the results of this major part of the project:

i There is a clear relationship between the value of C_n^2 and error rate as indicated in Figures 8.4-8.8. Moreover there is a good correlation for over six decades of error rate and over three decades of C_n^2 which suggests that the results are not insignificant.

ii The practical results obtained for the particular system configuration employed showed a very close correlation with the theoretical prediction (see Figure 8.9). The calculated correlation co-efficients were 0.90 and 0.93 for a path length of 500 and 300 m respectively (a perfect match would give a correlation co-efficient of 1.0).

iii The very high correlation between the practical data and theoretical prediction suggests that the theory in the form of the SNR

degradation factor ($e^{4\sigma_x^2} - 1$) is fully supported by the practical results. Such a high correlation would be less likely with simpler degradation factors which might have proposed a more basic mathematical relationship between error rate and C_n^2.

iv Such deviation as there is between the measured and theoretical data is due to the fact that worst case turbulent conditions were not endured for the whole duration of the 18 month measurement program as suggested by the spread of results for any given value of C_n^2. The discrepancy is reduced at lower levels of turbulence reflecting the overall variation of C_n^2 throughout the whole year and the fact that peak levels of C_n^2 are only usually measured in the hottest summer months in the UK.

v Although the spread of results (as indicated in Figure 8.9) is fairly large, typically nearly 1½ orders of magnitude, such a spread is not considered unusual or exceptional in view of the stochastic nature of the fundamental processes involved. Notwithstanding the large spreads the mean values are such that the linear fit applies well and correlates closely with the theoretical prediction.

vi The characteristic shown in Figure 8.9 appears to be applicable for all typical air temperatures normally experienced in the UK throughout the year, for 2 Mbit/s systems using on-off keying over path lengths of 500 and 300 m. Other characteristics will apply for different path lengths, and different source intensities as discussed in Chapter 6 and illustrated in Figure 6.9.

vii The system error performance is increasingly degraded as the path length increases due to the increased fundamental path losses and the presence of turbulence.

Having established the above conclusions it is necessary to consider their significance in practice. There is no doubt that the performance of terrestrial optical line of sight communication systems is affected by the presence of atmospheric turbulence. Clearly the worse the level of turbulence the more the performance of the optical communication system is affected. It has been clearly established that the performance will be degraded most in hot weather (ie summer months) and especially during the daylight hours (typically 1000-1600 hrs).

In fact C_n^2 values in excess of 10^{-13} $m^{-2/3}$ are only measured in the UK during the hours of approximately 1200-1400 on warm and hot days from April through to October. Thus major degradation of system performance due to turbulent effects is likely to occur during the midday period for 2-3 hours, on warm and hot days (particularly sunny ones) between the months of April through to October. During the winter months turbulent effects are normally minimal and the corresponding effect on system performance is therefore usually negligible.

Furthermore the performance of the system when turbulence is a problem will be degraded the closer to the ground the system operates, to some extent by the nature of the terrain, and the longer the path length. In respect of the latter point it has been established that for very severe levels of turbulence the system would become almost inoperable at path lengths of around 500 m with error rates of the order of 1 in 10^4 and the duration of inoperability would increase as the path length increased beyond 500 m. Obviously the shorter the path length the less is the effect of any turbulence on system performance.

It is fairly obvious that systems should not be designed to operate over paths where man-made sources of turbulence are likely to be produced, for

instance, heating and ventilating plants on the roofs of office blocks, factories and power stations etc.

The deleterious effects of turbulence on the error rate performance of systems may be ameliorated to some extent by the use of error-correcting codes and aperture averaging effects as already discussed in previous chapters.

PART IV

CONCLUSIONS

AND

RECOMMENDATIONS

CHAPTER 9

CONCLUSIONS

CHAPTER 9

CONCLUSIONS

This chapter draws together the various conclusions which appear at the end of each of the previous chapters.

The main hypothesis propounded in this thesis is that there is a direct link between the magnitude of atmospheric turbulence and the error rate performance of terrestrial digital optical line of sight communication systems.

A qualitative model has been proposed which appears to be a reasonable representation of the physical processes involved. Furthermore a quantitative relationship has also been derived between the level of turbulence and error rate performance which involves the relative intensity variance ($\exp(4\sigma_x^2) - 1$), a factor which is employed in calculating the degradation in signal to noise ratio and hence error rate performance.

Turbulence in the atmosphere gives rise to broadening and wandering of an optical beam. The greater the level of turbulence the greater the amount of broadening and wander. In addition to these effects turbulence also gives rise to scintillation at the receiver which is the result of the interference effects of the received rays having been refracted many times as they pass through the turbulent atmosphere and the numerous turbulent eddies contained therein. It has been concluded that scintillation effects are much more significant than beam broadening or beam wander for terrestrial systems having path lengths of up to 500-1000 m.

A small number of researchers in both the USA and Russia have proposed various theories with a view to explaining the effects of atmospheric turbulence. Perhaps the most noteworthy of these is Tatarskii whose monographs are discussed in some detail in Chapter 4. All the theories

tend to be mathematically complex. They appear to be supported by practical data except for when the saturation region is reached, that is when either long path lengths and/or intense turbulence conditions are present. A meaningful model which includes the saturation region has not yet been successfully derived by any workers to date, although Philips et al [4.47] have generated a mathematical expression which appears to fit the log irradiance variance/path length relationship.

Various techniques for overcoming the effects of turbulence induced scintillation have been considered. In particular aperture averaging, whereby the receiver lens aperture is increased to such a size that the signal fluctuations become uncorrelated and averaged over the lens area, is shown to be a particularly simple yet effective technique. Other standard techniques such as the use of error correcting codes can also be employed to ameliorate the situation.

The refractive index structure parameter, C_n^2, has been shown to be an effective measure of the magnitude of the level of turbulence in the atmosphere. The theoretical derivation of C_n^2 forms the basis for the chosen method of measurement of C_n^2, namely the microthermometric approach. Although other approaches were considered the microthermometric approach has the advantage that it yields an absolute measure of C_n^2 which is accurate and which is based on a sound theoretical mathematical derivation. Various practical techniques were evaluated but that using thermocouples was found to be the optimum. The longer time constant of thermocouples as against fine wire sensors was not found to present any particular practical constraints.

The main hypothesis of this research project (given in Chapter 6) is that the signal to noise ratio for an atmospheric optical communication system

is degraded by a factor ($e^{4\sigma_x^2} - 1$) where σ_x^2 is a function of the level of atmospheric turbulence for a system operating at a given wavelength and over a given path length. This SNR decrementing factor (or relative irradiance variance) is derived using a straightforward mathematical analysis unlike the complex works of Tatarskii and Shapiro.

The theoretical analysis shows that large system margins are needed for a given error rate to be maintained if worst case turbulence is likely to be experienced. Such increases will severely limit the range of operation of terrestrial optical communication systems.

The measurements of the atmospheric refractive index structure parameter, C_n^2, over the test program period of some 18 months have generated some considerable data which has been found to be most interesting. The data obtained is generally supportive of theories which have been developed regarding the behaviour of C_n^2 with time, temperature etc. In particular it has been found that the magnitude of turbulence varies considerably during the course of a day and throughout the year, and is dependent on the nature of the ground surface. Interestingly it has been shown that over path lengths of up to around 500 m the value of C_n^2 is about the same throughout the path provided that the ground surface is uniform and that there are no abnormal causes of localised increased levels of turbulence ie heat sources such as air conditioning vents etc.

The results from the systems part of the measurement program show a clear relationship both theoretically and in practice between the system bit error rate and the level of atmospheric turbulence. This correlation suggests that the theory proposed in Chapter 6 can be endorsed and in particular that the proposed signal to noise ratio decrementing factor ($\exp(4\sigma_x^2) - 1$) appears to be fully valid.

The systems data obtained during the course of the 18 month measurement program shows significant variations both during the course of a day and throughout the year. Since the data spans two summers it can be concluded from the data obtained that, for systems installed in the UK, the times of greatest degradation of system error rate performance are in the summer months of July and August (and sometimes June) and during a 4-5 hour period around midday during these months. Graphs have been produced which clearly show the relationship between air temperature, the magnitude of turbulence and system error rate. The colder winter months would not appear to present any major degradation of system performance.

System performance becomes severely degraded when the path length exceeds a certain limit due to the cumulative effect of high levels of turbulence. The degradation can be overcome to varying extents by using aperture averaging techniques, increasing the transmitted power, improving the receiver sensitivity and by the use of error-correcting codes. Nevertheless despite these counter-active measures it would seem that low-speed (eg 2 Mbit/s) terrestrial optical communication systems operating in the near infra-red region and using semi-conductor opto-electronic devices are unlikely to be able to operate satisfactorily over path lengths much in excess of about 1 km. Systems operating at lower bit rates will be less affected by turbulence than higher speed systems. The theoretical predictions supported by the experimental data suggests that designs of optical communication system should employ effective lens diameters of not less than 0.1 m and source powers of not less than $10^5 W/m^2/sr$ if an acceptable overall performance is to be achieved over any respectable path length (ie 500 m or more).

Although turbulence in the atmosphere severely restricts the use of line of sight optical communications systems for terrestrial applications, such systems can offer significant benefits for extra-terrestrial communication

links where turbulence does not present any problems, for instance between geo-stationary satellites. Notwithstanding the above constraints regarding the terrestrial use of optical line of sight communication systems, it is concluded that, owing to the fact that there is currently no spectrum regulation at non-visible optical frequencies, optical communication systems can be used with advantage in various applications where excessive path lengths are not required (ie less than about 1km), since they can be rapidly deployed and are not excessively expensive when used as either temporary expedients or when there is no suitable alternative.

CHAPTER 10

RECOMMENDATIONS AND AREAS JUSTIFYING FUTURE RESEARCH

CHAPTER 10

RECOMMENDATIONS AND POSSIBLE FURTHER WORK AREAS

10.1 RECOMMENDATIONS

As a result of the work culminating in this thesis it is recommended that the following points be taken into account when designing and/or using optical line of sight systems.

a. One or more of the techniques for minimising the effects of scintillation should be employed (Chapter 4). In particular the use of the largest possible receive lens diameter is recommended in order to benefit from the effects of aperture averaging and to facilitate initial link line-up. Background radiation can be minimised by utilising spatial and wavelength filters.

b. The line of sight link should be located as high above ground as possible and as far away from any localised source of heat which might generate turbulence in order to minimise the efects of turbulence - induced scintillation.

c. The transmitter power should be maximised for the best overall system performance.

d. Systems should not be designed to operate at unnecessarily high bit rates unless maximum performance is not a major criterion.

10.2 FURTHER WORK AREAS

During the course of this study a number of research areas have been identified which were not part of the mainstream research activity for this thesis and which it was not possible to pursue if the main objectives of the research work were to be met. These areas are listed below with the object of providing guidance to other researchers wishing to study this fascinating subject:

i The effect of different coding arrangements on the error rate performance due to turbulence-induced scintillation.

ii Measurements relating to the improvement in error probability due to turbulence induced scintillation as a result of the aperture averaging effect at the receiver.

iii More detailed study of the physical processes involved in the saturation region of the log irradiance variance/path length characteristic.

iv Theoretical analysis of the nature of errors due to turbulence induced scintillation ie single errors/burst error behaviour etc.

v A more detailed and varied analysis of the effect on magnitude of C_n^2 of different ground surfaces.

vi Measurements of C_n^2 using temperature sensors having much faster response times.

ACKNOWLEDGEMENTS

The author is indebted to the support and valuable advice of Dr Paul Hensel of British Telecom, and of Dr Mike Meade of The Open University who acted as supervisors throughout this project.

Thanks are also due to the management of British Telecom who assisted by agreeing to the provision of various items of test equipment etc for the practical measurement program, and by providing the necessary typing and reprographic resources needed to produce both the interim typescripts and the final thesis.

REFERENCES

Abbreviations:

JOSA	Journal of the Optical Society of America
CLEO	Conference on Lasers and Electro-Optics (USA)
ECOC	European Conference on Optical Communication
OQE	Optical and Quantum Electronics

Sequence: Author; Publication; Volume No.; Page No.; Year

CHAPTER 1

[1.1]	Bell Alexander G	US Patent 325, 199, December 1880
[1.2]	Huxford W S et al	JOSA 38, 3, pp 253-268, 1945
[1.3]	Maiman T H	Nature, 187, p 493, 1960
[1.4]	Nathan M I	Applied Physics Letters, 1, 63, 1982
[1.5]	Kao C & Hockham G	Proc IEE, 113, 7, p 1115, 1966
[1.6]	Lilly C J	Electronics and Power, pp 630-634, Sept 1981
[1.7]	Lilly C J	'The design and performance of digital optical fibre systems', Electronic & Radio Engineer, Vol 54, No. 4, pp 179-191, April 1984
[1.8]	ITU Journal	Special Issues on Optical Fibre Communication Vol 48, No. 11, Nov 1981 Vol 49, No. 2, Feb 1982
[1.9]	Lilly C J	Proc 8th ECOC, pp 17-24, Cannes, 1982
[1.10]	Lilly C J et al	Proc 7th ECOC, pp 15.4.1-15.4.4, Copenhagen, 1981
[1.11]	Lilly C J	'Optical Fibres in the Trunk Network, ITU Journal, Vol 49, No. 2, pp 107-117, Feb 1982
[1.12]	Maynard J et al	'Space Communications Test Program' CLEO '82, Phoenix, 1982
[1.13]	Mooradian G et al	'Submarine laser communications', ibid
[1.14]	Titterton P J et al	'System and technology trade-offs for all-weather atmospheric optical communications', ibid

[1.15] Bylanski P & Ingram D — 'Digital Transmission Systems', Peter Peregrinus, 1978

[1.16] Gagliardi R & Karp S — 'Optical Communications', Wiley Interscience, 1976

[1.17] ITT — 'Reference Data for Radio Engineers', ITT, Howard Sams & Co, NY, 1977

[1.18] Kennedy R S — 'Fading Dispersive Communication Channels', John Wiley, NY, 1969

[1.19] Jamieson J et al — 'Infra-red Physics & Engineering', McGraw-Hill, NY, 1963

[1.20] Fried D L — JOSA, Vol 57, pp 169-174, Feb 1967

[1.21] Chernov L A — 'Wave propagation in a random medium', Dover Publications, NY, 1967

[1.22] Brookner E — IEEE Trans, Commun Tech, COM-18, 396, Aug 1970

[1.23] Kipeika N et al — Proc IEEE, Vol 58, No. 10, Oct 1970

[1.24] Fried D — Proc IEEE, Vol 55, No. 1, pp 57-67, Jan 1976

[1.25] Karp S et al — Proc IEEE, Vol 58, No. 10, pp 1611-1626, Oct 1970

[1.26] Brain M C — OQE, Vol 13, pp 353-367, 1981

[1.27] Smith D R et al — Proc 6th ECOC, York, Sept 1980

[1.28] Gower J — "Optical Communication Systems", Pentice Hall, 1984

CHAPTER 2

[2.1] Strohbehn J W — IEEE Trans Comm, Feb 1974

[2.2] Tatarskii V I — 'Wave propagation in a turbulent medium', McGraw-Hill, NY, 1961

CHAPTER 3

[3.1] Chiba T — Applied Optics, November 1971

[3.2] Dowling et al — JOSA, July 1973

[3.3] Buck A — Applied Optics, 6, 703, 1967

[3.4] Ochs G R et al — US Gov ESSA Tech Report ERL 154 WPL 10, 1970

[3.5] Cordray D M et al — SPIE Vol 305, pp 273-281, 1981

CHAPTER 4

[4.1] Maiman T H — Nature, 187, 493, 1960

[4.2] Chernov L A — "Wave Propagation in a Random Medium", McGraw-Hill, New York, 1960

[4.3] Tatarskii V I — "Wave Propagation in a Turbulent Medium", McGraw-Hill, New York, 1961

[4.4] Mikesell A H et al — JOSA, 41, 689, 1951

[4.5] Nettlebald F — Observatory, 71, 111, 1951

[4.6] Butler H E — Proc Royal Inst Acad A, 54, 321, 1954

[4.7] Butler H E — Qtly J Royal Met Soc, 80, 241, 1954

[4.8] Ellison M A et al — Mthly Notices Royal Astron Soc, 112, 73, 1952

[4.9] Protheroe W M — Contrib Perkins Observ Ser 2, 127, 1955

[4.10] Kolchinski I G — Astron Zh, 29, 350, 1952

[4.11] Kolchinski I G — Astron Zh, 34, 638, 1957

[4.12] Dainty J C — Topics in Applied Physics, Vol 9, Springer, New York, 1975

[4.13] Obukhov A M — Doklady Akad Navk, SSSR 30, 611, 1941

[4.14] Krasilnikov V A — ibid 47, 486, 1945

[4.15] Krasilnikov V A — ibid 58, 1353, 1947

[4.16] Bergmann P G — Phys Rev, 70, 486, 1946

[4.17] Ellison T H — J Atmos Terr Phys, 2, 14, 1951

[4.18] Tatarskii V I — Zh Eksp Teor Fiz, 25, 74, 1953

[4.19] Mintzner D — J Acoust Soc Am, 25, 922, 1953

[4.20] Mintzner D — ibid 25, 1107, 1953

[4.21] Mintzner D — ibid 26, 186, 1954

[4.22] Obukhov A M — Izv Akad Nauk SSSR Ser Geograf Geofiz, 2, 155, 1953

[4.23] Tatarskii V I — Zh Eksp Teor Fiz, 25, 74, 1953

[4.24] Rytov S M — Izv Akad Nauk SSSR (Ser Fiz), 2, 223, 1937

[4.25] Gracheva M E et al — Izv VUZ Radiofiz, 8, 717, 1965

[4.26]	Gracheva M E	ibid 10, 775, 1967
[4.27]	Tatarskii V I	'Propagation in a Turbulent Atmosphere' Moscow: Nauka, 1967
[4.28]	Strohbehn J W	Proc IEEE, Vol 56, pp 1301-1318, Aug 1968
[4.29]	Kolmogorov A	'Turbulence Classic Papers on Statistical Theory' Eds: S K Friedlander and L Topper. New York: Interscience, p 151, 1961
[4.30]	Owens J C	Applied Optics, Vol 6, No. 1, pp 51-59, 1967
[4.31]	Lane J A	J Atmos Terr Phys, Vol 27, pp 969-978, 1985
[4.32]	Richter J H	Radio Science, Vol 4, No. 12, pp 1261-1269, 1969
[4.33]	Ludlum F H	Quartly. J Royal Met Soc, Vol 93, pp 419-435, 1967
[4.34]	Lawrence R S et al	Proc IEEE, Vol 38, No. 10, Oct 1970
[4.35]	Fante R L	Proc IEEE, 63, 1669, 1975
[4.36]	Strohbehn J W	"Laser Beam Propagation in the Atmosphere" Chap 3, Ed: J W Strohbehn, 1976
[4.37]	Bourret R C	Nuovo Cimento, 26, 1, 1962
[4.38]	Bourret R C	Can J Phys, 40, 782, 1962
[4.39]	Tatarskii V I	"The Effects of the Turbulent - Atmosphere on Wave Propagation" National Technical Info Service, Springfield, Va, p 42, 1971
[4.40]	Tatarskii V I	Sov Phys JETP, 29, 1133, 1969
[4.41]	Klyatskin V I	ibid 31, 332, 1970
[4.42]	Klyatskin V I	ibid 31, 834, 1970
[4.43]	Klyatskin V I	Radio Phys Quant, Electron, 13, 834, 1970
[4.44]	Clifford S F	'Laser Beam Propagation in the Atmosphere', Ed: Strohbehn J W, Topics in Applied Physics, Vol 25, Springer, NY, 1975
[4.45]	Clifford S F et al	JOSA, 64, 148, 1974

[4.46] Gagliardi R M & Karp S — 'Optical Communications', Wiley Interscience, 1976

[4.47] Philips R L et al — Proc SPIE, Vol 410, pp 60-66, 1983

[4.48] Shapiro J H — SPIE, Vol 295, 1981

[4.49] Brookner E et al — IEEE Spectrum, Vol 4, pp 75-82, Jan 1967

[4.50] Bylanski P et al — 'Digital Transmission Systems' Peter Peregrinus Ltd, 1978

CHAPTER 5

[5.1] US Air Force — 'Handbook of Geophysics', MacMillan, NY, 1960

[5.2] Owens J C — Applied Optics, 6, 51, 1967

[5.3] Batchelor G K — 'The Theory of Homogenous Turbulence', Cambridge Univ Press, London, 1953

[5.4] Lumley J L et al — 'The Structure of Atmospheric Turbulence', Interscience, NY, 1964

[5.5] Morris A S et al — 'Statistical Fluid Mechanics: Mechanics of Turbulence, Vol 1, MIT Press, Cambridge, Mass, 1971

[5.6] Tennekes H et al — 'A First Course in Turbulence', MIT Press, Cambridge, Mass, 1972

[5.7] Kolmogorov A — 'Turbulence Classic Papers on Statistical Theory', Eds: Friedlander S K & Topper L, Interscience, NY, 1961

[5.8] Wolfe W L et al — 'The Infra-red Handbook', Office of Naval Research, US Navy, 1978

[5.9] Myrop L O — Tellus, 21, 341, 1969

[5.10] Kaimal J C et al — Qtly J Royal Met Soc, 98, 563, 1972

[5.11] Clifford S F — 'Laser Beam Propagation in the Atmosphere', Topics in Applied Physics, Vol 25, Ed: Strohbehn J W, Springer, 1975

[5.12] Tatarskii V I — 'The effects of the turbulent atmosphere on wave propagation', Chap 4, Section 54, Israel Program for Scientific Translations, Jerusalem, 1971

[5.13] Lawrence R S et al — JOSA, 60, 826, 1970

[5.14] Neff W D — NOAA Tech Report ERL 322-WPL 39, 1975

[5.15] Ochs G R et al — ibid ERL 251-WPL 22, 1972

[5.16] Frisch A S et al — J Appl Meteorology, 14, 415, 1974

[5.17] Bufton J L et al — JOSA Vol 62, No. 9, 1972

[5.18] Fink D G & Beaty H W — Electrical Engineers Reference Handbook, McGraw-Hill, 11th Edition, 1978

[5.19] Hewlett Packard — Hewlett Packard Technical Data Sheet for HP 2804A Temperature Sensor

[5.20] Lawrence R S — JOSA Vol 60, No. 6, 826, 1970

[5.21] Tatarskii V I — 'Wave Propagation in a Turbulent Medium' McGraw-Hill, New York, 1961

[5.22] Dowling J A et al — JOSA Vol 63, No. 7, 846, 1973

[5.23] Ochs G R et al — JOSA Vol 59, 231, 1969

[5.24] Wesely M L et al — Applied Optics Vol 14, No. 4, 847-853, 1975

[5.25] Wang et al — JOSA Vol 68, 334, 1978

[5.26] Hill R J et al — Applied Optics, Vol 17, 22, 3608, 1978

[5.27] Chernov L A — 'Wave Propagation in a Random Medium' McGraw- Hill, New York, 1960

[5.28] Beckman P — Radio Science J Res NBS/USNC-URSI 69D, 629, 1965

[5.29] Hodara H — Proc IEEE, 54, 368, 1966

[5.30] Chiba T — Applied Optics, 10, 11, 1971

[5.31] Ochs G R et al — JOSA, 59, 231, 1969

CHAPTER 6

[6.1] Frieden B R — 'Probability, Statistical Optics and Data Testing', Springer - Verlag, 1983

[6.2] Tatarskii V I — 'The effects of the turbulent atmosphere on wave propagation', Chap 4, Section 54, Israel Program for Scientific Translations, (Orig: Russian) Jerusalem, 1971

[6.3] Shapiro J H et al — Nat Telecoms Conf Paper 27.5, IEEE, Nov 1980

[6.4] Shapiro J H et al — JOSA, 65, 1218A, 1975

[6.5] Shapiro J H — 'Laser Beam Propagation in the Atmosphere', Topics in Applied Physics, Vol 25, Ed: Strohbehn J W, Springer, 1975

[6.6] Dainty J C (Ed) — 'Laser speckle and related phenomena', Topics in Applied Physics, Vol 9, Springer 1975

[6.7] Gagliardi R M & Karp S — 'Optical Communications', Wiley Interscience, Chap 5, NY, 1976

[6.8] Smith D R et al — ITU Journal, Vol 48, 11, pp 680-685, Nov 1981

[6.9] Bennett W R & Davey J R — 'Data Transmission', McGraw-Hill, 1965

[6.10] Bylanski P & Ingram D G — 'Digital Transmission Systems', Peter Peregrinus, 1976

[6.11] Shapiro J H — SPIE, Vol 295, 'Control and communication technology in laser systems', 1981

[6.12] Schwartz M, Bennett W and Stein S — 'Communication Systems and Techniques', McGraw Hill, 1966

[6.13] Middleton D — 'An Introduction to Statistical Communication Theory', McGraw Hill, 1960

[6.14] Lilly C J — Signal to noise ratio computer program, Author's archives, 1984

CHAPTER 7

[7.1] Clifford S F et al — JOSA, 64, 148, 1974

[7.2] Tatarskii V I — 'The effects of the turbulent atmosphere on wave propagation', Chap 4, Section 54, Israel Program for Scientific Translations, (Orig: Russian) Jerusalem, 1971

CHAPTER 8

[8.1] Hewlett Packard — Measuring Equipment Handbooks for HP 3781A, HP 3782A, HP 9915, HP 5150A, Hewlett Packard, 1983

- END -

Appendices follow:

SYMBOLS USED IN PAPERS

(Greek symbols are shown together at the end of the appendix)

A_{im}	image area
A_p	photodetector sensitive area
A_R	effective receiver lens area
A_S	effective optical emitting area of source
A_T	effective transmitter lens area
B	electrical bandwidth (measured in Hz)
B_o	optical bandwidth (measured in microns)
B_s	signal bandwidth (measured in Hz)
C_n^2	atmospheric refractive index structure parameter
C_T^2	temperature structure parameter
$D_n(r)$	refractive index structure function
$D_R(r)$	structure function for random variable R(r)
$D_T(r)$	temperature structure function
DR	dynamic range
d	temperature sensor spacing
d_T	effective transmitter lens diameter
d_R	effective receiver lens diameter
d_w	wire diameter
E	photon energy
e(= q)	electronic charge
F	aperture averaging smoothing factor
f	focal length of lens
G	instantaneous channel gain
G_a	antenna gain
G_c	normalised channel gain = G/G_o; random channel gain factor
G_o	channel gain in absence of turbulence
g	detector gain
g_m	transconductance of first amplifier stage

h	Planck's constant
I	irradiance
I_a	amplifier noise current
I_b	background noise current
I_{ba}	first stage semiconductor base current
I_{coll}	first stage semiconductor collector current
I_D	photodiode dark current
I_o	radiant intensity
I_p	signal current at photodetector
I_{sh}	shot noise current
I_t	thermal noise current
K	degrees Kelvin
k	Boltzmann's constant; also wavenumber = $\frac{2\pi}{\lambda}$
L	path length
L_o	outer scale of turbulence
L_{sc}	optical path loss due to scattering
L_t	total optical path loss
l_o	inner scale of turbulence
N	refractivity
$N(f)$	spectral radiance function
$N(\lambda)$	background optical noise power
n	refractive index
P	power; atmospheric pressure (in millibars)
P_b	average background power incident on detector
$P(e)$	probability of error
P_{ISO}	power density of an isotropic antenna
P_R	average signal power incident on detector
P_T	transmitter power
$P_{TX_{max}}$	maximum power density of the transmitted radiation pattern
q	electronic charge released per electron

R	resistance
R_a	source radiant intensity
R_L	photodiode load resistance
SNR	signal to noise ratio
s	specific resistance
T	absolute temperature (degrees Kelvin)
T_a	atmospheric transmittance
T_{RX}	transmittance of receive optics
t	time
u	distance between optical source and centre of lens
V	voltage
v	optical frequency
W	wavelength (used in computer programs in lieu of λ)
x	log-amplitude fluctuation
y	standard deviation factor for determining cumulative probability
α	attenuation coefficient; detector conversion factor
α_{fs}	free space attenuation coefficient
β	thermal conductivity
η	photodetector quantum efficiency
Ω	solid angle
Ω_a	solid beam angle
Ω_{fv}	field of view
Ω_R	field of view of receiver
σ_x^2	log-amplitude variance
σ_l^2	log-irradiance variance
σ_p^2	beam wander variance
θ	beam spread; also temperature co-efficient of resistance
θ_a	planar angle beam width/beam angle
$< >$	ensemble average

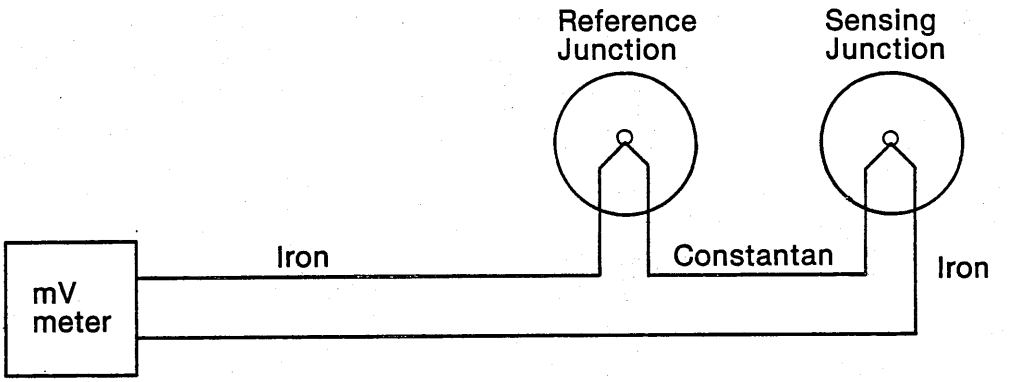

Figure A2.1 A basic thermocouple sensing circuit

A COMPARISON OF TEMPERATURE SENSORS/TRANSDUCERS

1 THERMOCOUPLES

A thermocouple is formed by joining (welding) two dissimilar metals. The resulting junction gives rise to an electric potential, the precise magnitude of which is dependent on the temperature of the junction. Various alloys are used to construct the junction such that various temperature ranges can be conveniently measured, for instance, the temperature coefficient for a typical Type J thermocouple consisting of iron and constantan is 54.14 microvolts/°C. Table A2.1 gives the coefficients for various metal combinations.

TABLE A2.1 TEMPERATURE COEFFICIENT FOR VARIOUS THERMOCOUPLE MATERIALS

MATERIALS	THERMOCOUPLE TYPE	TEMPERATURE COEFFICIENT μV/°C
Chromel - Constantan	E	68
Iron - Constantan	J	54
Copper - Constantan	T	45
Chromel - Alumel	K	38
Platinum - Platinum/Rhodium	S	10

Thermocouples would be configured as shown in Figure A2.1. The reference junction thermocouple is highly desirable since otherwise there would be, in effect, additional thermocouples formed at the junction of the thermocouple wires with the millivolt meter terminals, resulting in possibly erratic and inaccurate measurements. Even with reference and sensor thermocouples additional thermocouples are still formed where the leads join the metal meter terminals, although as long as the terminals are at the same temperature the effect can be largely ignored, since any potential produced in the junctions will be of opposite polarity and will therefore cancel out.

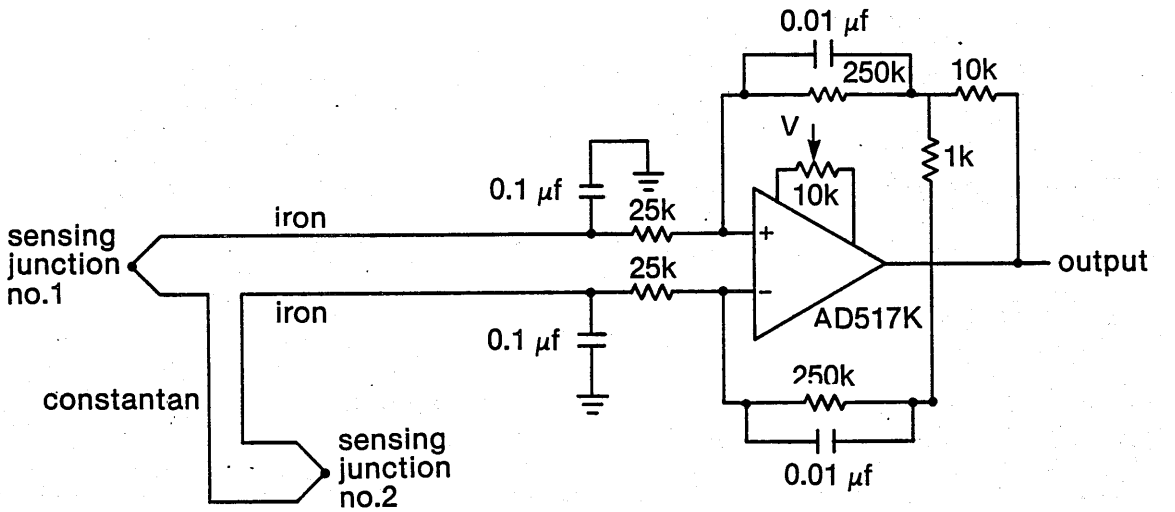

Figure A2.2 A balanced thermocouple amplifier

The readings obtained on the voltmeter are proportional to the difference between the reference and sensor thermocouple temperatures. In normal thermocouple temperature sensing instruments the reference thermocouple is held at a fixed reference temperature. For measurement of C_n^2 the difference reading is all that is required.

The voltmeter used for measuring the difference voltage must be sensitive enough to detect changes of the order of 1 microvolt. It follows therefore that the voltmeter must be highly sensitive, have a stable differential gain, have a moderately high input impedance, which is large compared with the resistance value of the thermocouple leads, and must have good common mode rejection at 50 Hz and good radio frequency immunity.

The circuit of Figure A2.2 is a practical realisation of a thermocouple sensing arrangement. With this particular arrangement and using a low-offset op-amp a drift of less than 1 microvolt/°C should be attained. The thermal noise due to the assumed amplifier input resistance of 1 megohm and assuming a temperature of 293°K and a bandwidth of 1 kHz is of the order of 0.016 nanovolt, where rms thermal noise voltage = $(4k\ TBR)^{\frac{1}{2}}$.

From the above it would appear that the use of thermocouples having as they do an inherent temperature differential measurement capability are ideally suited for the measurement of C_n^2. Thermocouples having high temperature coefficients (ie types J, K, T and E, all of which are in excess of 40 microvolts/°C) would in principle give an adequate sensitivity for the purposes of C_n^2 measurements. The biggest problem with thermocouples is their inherent time constant which is generally of the order of a few seconds. For this reason thermocouples are not ideal for use in C_n^2 measurements, although they might be acceptable if some compromise can be made in respect of the response time.

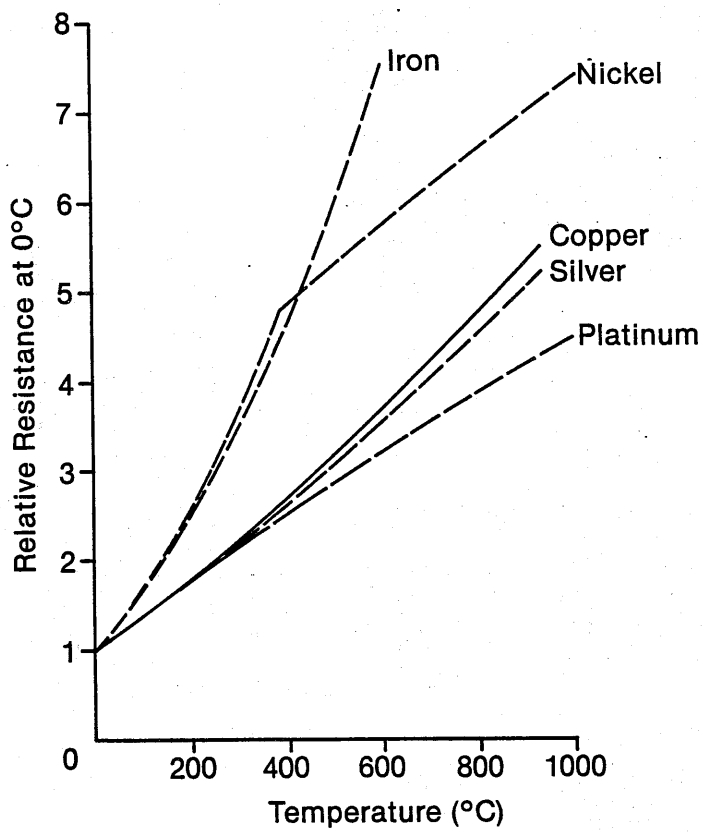

Figure A2.3 Relative resistance (R_t/R_{ref}) versus temperature for some pure metals

2 WIRE RESISTANCE THERMOMETERS

Platinum is the commonest metal to be used in wire resistance temperature sensors mainly due to its linear temperature/resistance coefficient of about 0.4%/°C which is applicable over a wide temperature range, (ie -200 to +1000°C) and its supreme stability with time.

For the purposes of C_n^2 measurement the superb qualities of platinum over such a wide temperature range are actually unnecessary and other metals such as tungsten, iron, nickel, copper and silver are fully acceptable.

Figure A2.3 shows the relative resistance of various commonly available metals which might be used for this purpose.

Wire resistance temperature sensors have the advantage that, provided the diameter of the wire is small enough, the response time can be of the order of a few milliseconds.

It can be calculated that wires having a diameter of less than 20 microns are needed in order to provide adequate temporal sensitivity for the needs of a C_n^2 measurement apparatus.

3 CONCLUSIONS

In addition to thermocouples and resistance thermometers, thermistors, integrated circuit bandgap temperature sensors and quartz crystal sensors were all considered. Of all these options thermocouples were conceptually the most suitable although they do not have the high response times of fine wire resistance thermometers. Table A2.2 summarises the main features of each method. It was concluded that the best option in theory was the use of a fine-wire resistance sensor with the use of thermocouples as a practical alternative should any difficulties be experienced in obtaining platinum wire of the requisite diameter.

TABLE A2.2 COMPARISON OF VARIOUS TEMPERATURE SENSORS

SENSOR TYPE	TEMP COEFF	TIME CONSTANT (99% OF CHANGE)	TEMP RANGE	OTHER FEATURES	SUITABILITY FOR C_n^2 MEASUREMENT
Thermocouple (Fe/Con)	+54 μV/°C	1-2s	-200 to +1000°C	Small size	Almost ideal in that temperature difference measurement is an inherent feature. Response time is not ideal but can be tolerated
Thermistors	-4%/°C (ie typically 100 ohms/°C)	>5s	-80 to +300°C	Suffers from self-heating Extremely sensitive Simple to use Highly accurate	Not suitable due to very large time constant
Metal/film resistance					
a. Platinum wire	+0.3%/°C	)	-200 to +1000°C	Extremely stable with time; not cheap	Theoretically ideal in all respects. In practice very difficult to obtain thin enough wire in order for the requisite response time to be achieved. Platinum wire is optimum for good long-term stability
b. Copper wire	+0.4%/°C	) <<2s	-250 to +100°C		
c. Nickel wire	0.47%/°C	)	0 to +70°C	High linearity, sensitivity	
Integrated circuit bandgap temperature sensor (eg RS 590 kH)	(3 ppm/°C (1 μA/°C	>5s	-55 to +125°C	1% accuracy; Being a current source is suited to remote sensing	Inadequate response time
Quartz crystal sensor	1 kHz/°C	typ 9s	-50 to +150°C	Accuracy of better than 0.0001°C	Although extremely accurate response time is wholly inadequate

THE MEASUREMENT OF C_n^2 USING FINE-WIRE RESISTANCE SENSORS

1 INTRODUCTION

Appendix No. 2 discussed the various sensors which might be used for measuring the atmospheric refractive index structure parameter, C_n^2. In the case of the fine wire option it was calculated that in order to obtain the fast response time of 0.5 ms or less, a Platinum resistance wire having a diameter of 20 μm or less was required. This appendix discusses the problems associated with obtaining Platinum resistance wire having such a small diameter. The work discussed in this appendix formed a fundamental part of the practical part of this research work.

2 PLATINUM RESISTANCE WIRE

2.1 GENERAL

Obtaining Platinum resistance wire having a very small diameter is far from easy. Two approaches were considered viz:-

i To obtain wire having a nominal diameter of say 1 mm and drawing it down to the required diameter.

ii To use Woolaston wire which consists of fine Platinum wire coated in Silver to bring the overall diameter up to a handleable 125 μm.

Approach (i) whilst feasible in principle was thought to be difficult in that close control of the diameter was likely to be a problem. In addition it was thought that it would not be possible to apply an adequate tension to the drawn wire for the purposes of diameter control because the wire diameter of interest would be such as to be incapable of withstanding the required tension.

Approach (ii) appeared to be, in principle, a fairly viable approach although it was recognised that some care would be required in handling such a fine wire.

2.2 WOOLASTON WIRE

The procurement of Woolaston wire was not found to be at all easy. It transpired that it is in fact a highly specialised type of wire which is little used. Eventually the following supplier of specialist materials for research and industry was discovered:-

Goodfellow Metals Ltd

Cambridge Science Park

Milton Road

Cambridge CB4 4DJ

This supplier offers Woolaston wire having diameters as little as 0.001 mm. All the sizes below 0.02 mm were expensive and in excess of £150/m.

After some consideration of the available data a compromise between technical requirements and cost resulted in the choice of the 0.010 mm Woolaston wire for use in this work (Order Code PT005102).

2.3 REMOVAL OF SILVER OUTER LAYER FROM WOOLASTON WIRE

A number of different approaches were tried:-

i Use of concentrated nitric acid

The Woolaston wire was bonded to two copper posts using silver loaded epoxy adhesive such that there was 10 mm of wire between the posts. Note that it was not possible to coil the wire without a former and since it was thought that a former would upset the results the Woolaston wire was kept straight. The copper posts were nominally 50 mm in length and were soldered to the pins of a connector at one end.

The Woolaston wire between the copper posts was then inserted in a small pool of concentrated nitric acid. Unfortunately the wire broke each time this technique was tried even when no attempt was made to remove the wire from the acid. Clearly the use of concentrated nitric

acid resulted in the etching process occurring so rapidly that, even though the wire was under minimal tension, it snapped every time.

ii Use of dilute nitric acid

As in (i) above but dilute nitric acid was used instead of concentrated nitric acid. As was to be expected the etching process took considerably longer with the dilute nitric acid but still the Woolaston wire snapped as soon as all the silver had been etched away. Again this occurred without any movement of the wire or the supporting structure.

It was concluded that the etching process did not yield adequate control and that although there was minimal tension on the wire, the tension was still sufficient to result in the wire being snapped.

iii Electrolytic removal of the silver from Woolaston wire

An electrolytic solution was formed by dissolving 10 gm of silver nitrate ($Ag\ NO_3$) in 50 mls of water. The Woolaston wire element was immersed in the electrolyte and constituted the anode. A 2.5 mm^2 copper wire was employed as the cathode. A 6v dc supply was employed resulting in a current flow of approximately 1A. The silver coating from the Woolaston wire was rapidly removed within about one minute. However the high current flow resulted in the Platinum wire fusing. In fact calculations indicated that the electrolytic current must not exceed 0.022 μA in order to avoid fusing of the wire and that the time needed for the silver to be fully removed from the Woolaston wire with this current would not be less than 19×10^6 hours, or approximately 2146 years. This was calculated using the formula:-

$$\text{Time for silver to dissolve} = \frac{\text{weight of silver}}{\text{current x electro-chemical equiv for silver}}$$

It is therefore concluded that electrolysis is not a practicable means for obtaining ten micron platinum wire from Woolaston wire.

2.4 CALCULATION OF CONDUCTOR DIMENSIONS

The thermal response characteristic as heat passes from the outer surface to the centre of the wire follows an exponential curve of the form:-

$$T_2 - T_1 = 1 - e^{(-2t\beta/d_w)} \qquad \text{(A3.1)}$$

where $T_2 - T_1$ = change in temperature at outer surface

t = response time of wire to 99% of temperature change

β = thermal conductivity of wire in watts/second

$d_w/2$ = radius of wire

Now the equivalent change in resistance due to the temperature change $T_2 - T_1$ is given by:-

$$R_2 - R_1 = \theta(T_2 - T_1) \qquad \text{(A3.2)}$$

where $R_2 - R_1$ = change in resistance of wire per unit length

θ = temperature coefficient of resistance of wire

Combining Expressions (A4.1) and (A4.2) results in:-

$$R_2 - R_1 = \theta(1 - e^{(-2t\beta/d_w)}) \qquad \text{(A3.3)}$$

Equation (A3.3) is the characteristic which relates the change in resistance to wire diameter. This expression can be re-arranged to make determination of wire diameter easier as follows:-

$$\log (R_2 - R_1) = \log \theta + \frac{2t\beta}{d_w} \log e$$

$$\frac{2t\beta}{d_w} \log e = \log (R_2 - R_1) - \log \theta$$

$$d_w = 2t\beta \frac{\log e}{\log (R_2 - R_1) - \log \theta} \qquad \text{(A3.4)}$$

$$= \frac{0.88\ t\beta}{\log (R_2 - R_1) - \log \theta} \qquad \text{(A3.5)}$$

As an example Platinum wire has the following characteristics:-

$\beta = 0.69$ watts/cm/°C

$\theta = 0.385$ ohms/°C

If in practice we have a 2°C temperature change and a required response time of 2 ms then:-

$R_2 - R_1 = \theta \times 2°C = 0.77$ ohms

and $t = 2 \times 10^{-3}$ seconds

Hence the maximum wire diameter in this instance is given by:-

$$d_w = \frac{0.88 \times 2 \times 10^{-3} \times 0.69}{\log 0.77 - \log 0.385}$$

$$= 17.5\ \mu m$$

2.5 CONCLUSIONS REGARDING USE OF WOOLASTON WIRE

It is concluded that although in principle the use of Woolaston wire appeared to be very attractive, in that it meets the various prescribed requirements, in practice it is not a viable proposition due to:-

- the considerable difficulty in exposing the bare platinum wire
- the difficulty in overcoming the inherent fragility of micron size platinum wire.

It is concluded therefore that, for the purposes of this research work, thermocouples are in fact a more practical approach and provide an acceptable level of performance.

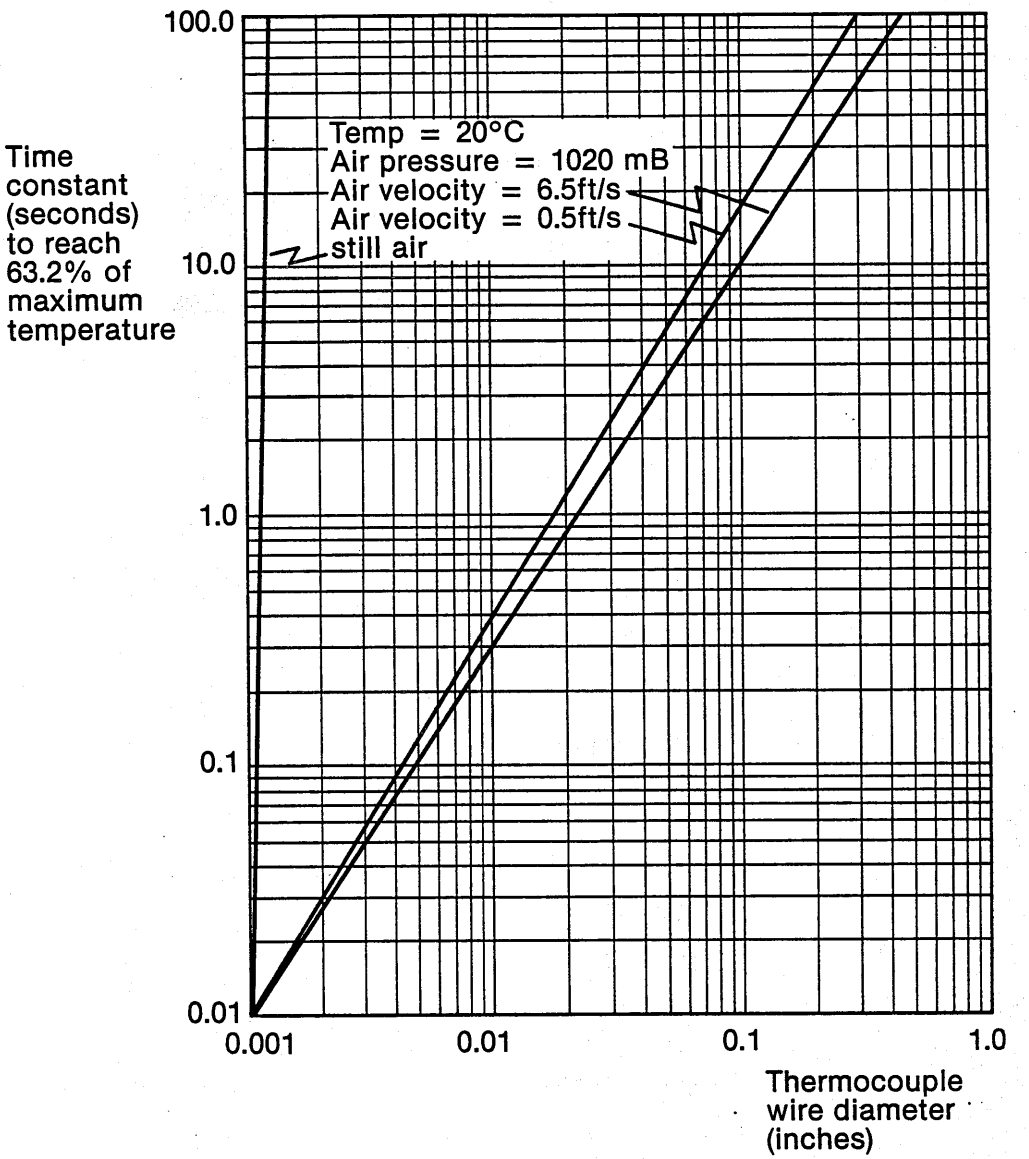

Figure A4.1 Time constant for various diameters of thermocouple wire

THE MEASUREMENT OF C_n^2 USING THERMOCOUPLE SENSORS

1 GENERAL

Appendix 2 discussed the various options for a temperature sensor having the prescribed performance characteristics. In view of the lack of success with Woolaston wire (see Appendix 3) the use of thermocouples is considered to be the most practical approach for the majority of C_n^2 measurements.

2 EVALUATION OF COMMERCIALLY AVAILABLE THERMOCOUPLES

Thermocouples are commercially available in the following ranges:

i

Temperature range	Type	
Copper/Constantan	T	All these thermocouples are adequate for the nominal ambient range 0- + 30°C
Iron/Constantan	J	
Chromel/Constantan	E	
Chromel/Alumel	K	
Platinum with Rhodium/ Platinum	S/R/B	
Tungsten/Tungsten with Rhenium	C/G/D	

ii Sensitivity

The following four types have the best sensitivities:-

Chromel/Constantan	E	68 μV/°C
Iron/Constantan	J	54 μV/°C
Copper/Constantan	T	45 μV/°C
Chromel/Alumel	K	38 μV/°C

iii Time Constant vs Diameter of Bare Thermocouple Wire

A graph of time constant vs diameter of bare thermocouple wire has been prepared using empirically derived data from manufacturers' literature and is given in Figure A4.1 for bare butt welded

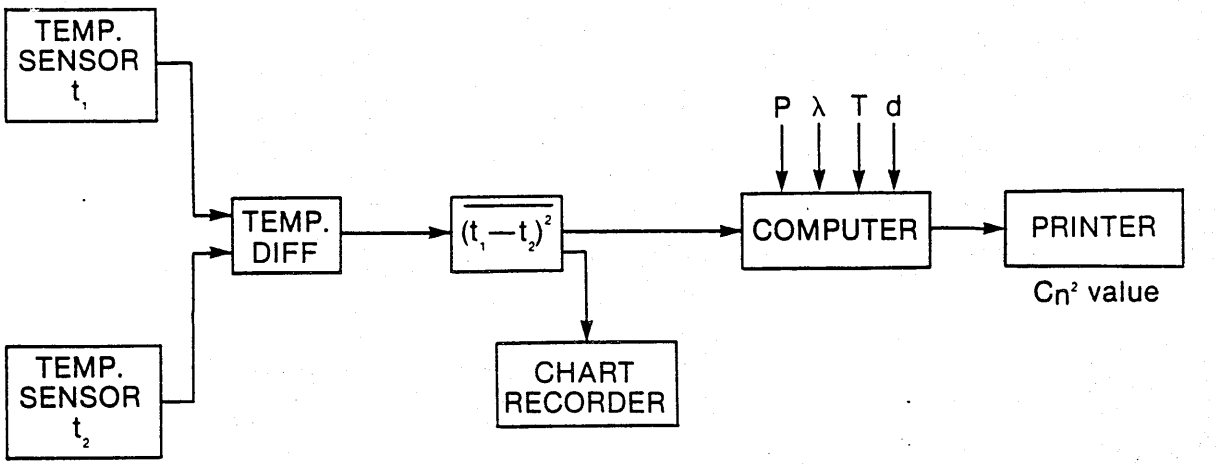

Figure A4.2 Block schematic of C_n^2 measuring equipment

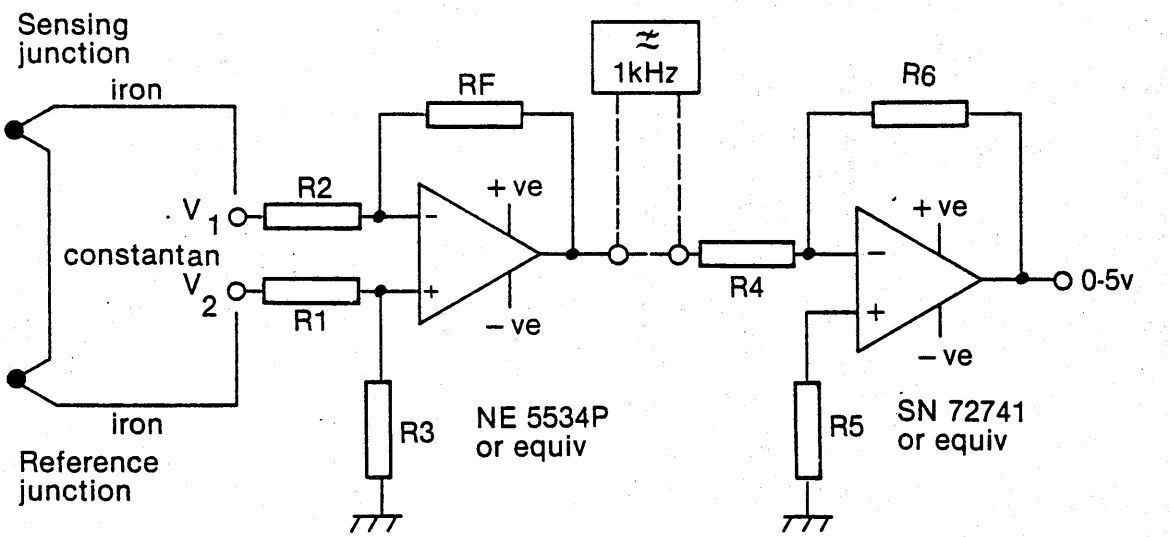

Figure A.4.3 Basic C_n^2 measuring circuit configuration

thermocouples. As would be expected the time constant for a given wire diameter decreases as the velocity of the air surrounding the thermocouple increases. The time constant shown is for a 63% change of the total measured output voltage for a given change in temperature. Inspection of the graph shows that to obtain a time constant of less than 100 ms requires a thermocouple wire diameter of less than 0.005 inches.

3 PREFERRED TYPE OF THERMOCOUPLE

Given the data in Para 2 above the requirements for a preferred type of thermocouple for the measurement of the atmospheric refractive index structure parameter using temperature sensors are:-

Type :	exposed butt welded
Metal:	Chromel/Constantan (Type E) (for maximum sensitivity)
Size:	0.005 inches (for minimum time constant)

A suitable thermocouple meeting these requirements is the Omega Engineering Inc Type SCPSS-020E-6.

4 DESIGN OF THERMOCOUPLE AMPLIFIER AND ASSOCIATED ELECTRONICS FOR MEASUREMENT OF ATMOSPHERIC REFRACTIVE INDEX STRUCTURE PARAMETER

A block diagram showing the configuration of the amplifier and associated electronics is shown in Figure A4.2.

Input Data:

Thermocouple sensitivity	50 μV/°C
Expected max temp change	2°C
Max I/P voltage at amp I/P	50 μV
Thermocouple impedance	c. 25 ohms

Output Data:

Voltage for full scale defection	5V
Amplifier O/P impedance	50/75 ohms

Required Amplifier Characteristics:

$$\text{Closed Loop Voltage Gain} = \frac{5V}{50\ \mu V} = 10^5 = 100\ dB$$

Power Gain = 50 dB

Input impedance >> thermocouple impedance (25 ohm)
= say 1 kohm

Output impedance = 50 ohms

First Stage Design:

Basic circuit configuration - see Figure A4.3.

Calculation of resistor values for first stage:-

$$Vo = -\frac{R_F}{R_1}(V_2 - V_1)$$

$$5V = -\frac{R_F}{R_1}(50\ \mu V)$$

$$\frac{R_F}{R_1} = 10^5$$

$$Zin = R_1 + R_F$$

if $R_F >> R_1$

$$Zin = R_F$$

if $R_1 = 1$ kohm

then $R_F = 10^8$ ohm

This value of R_F is impractically high and suggests that a two stage amplifier is required.

Let each stage have equal voltage gain of 3×10^2

thus if $R_1 = R_2 = 1$ kohm

then $R_F = R_3 = 300$ kohm

and Zin = 300 kohm

Equivalent Input Noise Voltage:

If op. amp has equiv I/P noise voltage of $5nV/(Hz)^{\frac{1}{2}}$ and 3 dB bandwidth of 10 kHz then:

$$\text{noise voltage} = 5 \times 10^{-9} \times 10^{2} = 0.5\ \mu V$$

$$\text{Thus max signal to noise} = \frac{50\ \mu V}{0.5\ \mu V} = 100 = 40\ dB$$

$$\text{min signal to noise} = \frac{\text{say } 1\ \mu V}{0.5\ \mu V} = 2 = 6\ dB$$

Note: The latter is clearly somewhat lower than is desirable hence consideration will be given to reducing effective noise bandwidth to c. 1 kHz.

Second Stage Design

Basic Circuit Configuration - See Figure A4.3.

Calculation of resistor values for second stage:-

$$\frac{R_6}{R_4} = 300 \qquad \text{(ie required voltage gain)}$$

if $R_4 = 1$ kohm

then $R_6 = 300$ kohm

$$R_5 = \frac{R_4 R_6}{R_4 + R_6} = \frac{300.10^6}{301.10^3} = 1 \text{ kohm}$$

Choice of Operational Amplifier

First Stage

Requirements for first stage:-

- Low noise (equivalent I/P noise voltage 5n $V/(Hz)^{\frac{1}{2}}$)
- Good temperature stability (I/P offset voltage temp coeff)
- Internal compensation

Suitable type = NE 5534P

Second Stage

Requirements for second stage:-

- Good temperature stability (I/P offset voltage temp coeff)
- Internal compensation

Suitable type = SN 72741 or equiv

Mean Square Circuit

The output from the second stage operational amplifier is fed to a mean square circuit in order to generate the electrical analogue of $\overline{(t_1-t_2)^2}$. The mean square circuit used was a standard design, with the mean value of the squared signal being generated over a time constant which could be adjusted in steps within the range 1-100 seconds.

Miscellaneous Points

Supply Voltage min $\pm$ 5V

max $\pm$ 15V

battery supply (to avoid noise from power unit)

5 CONCLUSIONS

This appendix has given practical details for the design of an instrument for the measurement of C_n^2 using thermocouples as the temperature sensing elements. The instrument was constructed as part of this project in line with this appendix and used to obtain the measurements of C_n^2 reported in Chapters 7 and 8.

MISCELLANEOUS EXPRESSIONS USED IN EQUATIONS -
(See Appendix 1 for meaning of symbols)

Detector conversion factor $\alpha = \frac{\eta}{h\nu}$

Photocurrent $I_p = \frac{\eta q P}{h\nu}$

Av. no. of photons $= \frac{P}{h\nu}$

Av. no. of electrons $= \frac{I_p}{q} = \frac{\eta P}{h\nu}$

$$\text{SNR} = \frac{\langle I_p^2 \rangle}{\langle I_t^2 \rangle + \langle I_{shot}^2 \rangle + \langle I_a^2 \rangle}$$

SNR @ O/P of detector (amp. noise negligible) $= \dfrac{\langle I_p^2 \rangle}{\frac{4kTB}{R} + 2qBI_{shot}}$

Log-irradiance variance, $\sigma_1^2 = 4\sigma_x^2$

or $\sigma_1 = 2\sigma_x$

$$\sigma_1^2 = \langle [\ln I - \langle \ln I \rangle]^2 \rangle$$

$$= 4 \langle [\ln A - \langle \ln A \rangle]^2 \rangle$$

Log-amplitude variance, $\sigma_x^2 = \langle [\ln A - \langle \ln A \rangle]^2 \rangle$

Log-amplitude fluctuation, $x = \ln A - \langle \ln A \rangle$

$$\langle x^2 \rangle = \langle [\ln A - \langle \ln A \rangle]^2 \rangle$$

Standard deviation $\sigma = \left[\frac{\sum x^2}{n} \right]^{\frac{1}{2}}$

NORMAL VARIABLES
(after Middleton [A6.1])

Given a random variable x, we can define the characteristic function, $F_x(j\nu)$, to be the mean value:

$$F_x(j\nu) = \langle e^{j\nu x} \rangle \qquad \text{(A6.1)}$$

Provided that x is normal with mean $\langle x \rangle$ and variance σ_x^2, then we can use the following standard result [A6.1]:

$$F_x(j\nu) = e^{j\langle x \rangle \nu} e^{-\sigma_x^2 \nu^2/2} \qquad \text{(A6.2)}$$

If we evaluate expression (A6.1) for the case $j\nu = 1$, we obtain

$$\langle e^x \rangle = F_x(1) \qquad \text{(A6.3)}$$

Hence, using expression (A6.3) and with $j\nu = 1$ and $\nu^2 = -1$ inserted in expression (A6.2) we obtain the standard result for a normal variable:

$$\boxed{\langle e^x \rangle = e^{\langle x \rangle} e^{\sigma_x^2/2}} \qquad \text{(A6.4)}$$

Reference: [A6.1] Middleton D 'Introduction to statistical communications theory', McGraw-Hill, 1960

DERIVATION OF RECEIVED POWER P_R

It is assumed that the source is an LED and is therefore diffuse and has a radiating area A_s. It is further assumed that A_s is large enough such that the transmitter is not diffraction limited. Furthermore it is assumed that the radiant intensity I_o is constant for all the light collected by the transmitter lens. The latter has an effective aperture area A_T and a focal length f. The receiver is located a distance L from the transmitter and has an effective aperture area A_R. It is further assumed that all the received light is focussed onto the active region of the photo-detector.

Using basic optical theory the distance between the LED source and the centre of the transmitter lens, u, is given by:-

$$\frac{1}{u} = \frac{1}{f} - \frac{1}{L} \simeq \frac{1}{f}$$

In order to maximise the received power an image of the source should be formed in the plane of the received aperture and the image area A_{im} is given by:-

$$A_{im} = \frac{A_s L^2}{u^2} \simeq \frac{A_s L^2}{f^2}$$

The power collected by the transmitter lens P_T is given by:-

$$P_T = \frac{I_o A_T}{u^2} \simeq \frac{I_o A_T}{f^2}$$

Now assuming that the image of the source more than fills the receive aperture area, the fraction of P_T which reaches the detector is $\frac{A_R}{A_{im}}$.

The received power P_R is given by:-

$$P_R = \frac{P_T A_R}{A_{im}} = \frac{P_T A_R f^2}{A_s L^2} = \frac{I_o A_T A_R}{A_s L^2}$$

$$= \frac{R_a A_T A_R}{L^2}$$

where $R_a = \frac{I_o}{A_s}$ is the radiance of the source

Typically for $R_a = 0.1$ W/mm^2/sr $= 10^5$ W/m^2/sr

$A_T = A_R = 7.9 \times 10^{-3}$ m^2 (ie d = 0.1 m)

$L = 1$ km

in which case $P_R = \frac{10^5 \times (7.9 \times 10^{-3})^2}{10^{-6}}$

$= 6.2 \times 10^{-6}$ W

$= 6.2$ μW

Now the above does not take into account atmospheric losses due to absorption etc. To allow for such losses the atmospheric attenuation coefficient, α, needs to be included in the above expression; the factor being given by (as per standard transmission theory) $e^{-\alpha L}$.

Thus the expression for P_R now becomes:-

$$P_R = \frac{R A_T A_R}{L^2} \cdot e^{-\alpha L}$$

Typically α is 0.1 per km for the atmosphere at sea level and with no precipitation (ie rain or snow) at a wavelength in the near infra red region ie c.1 μm. The factor $e^{-\alpha L}$ is therefore typically 0.9 for L = 1000 m.

Reference:

[A7.1] Gower J "Optical Communication Systems", Prentice Hall, 1984

CALCULATION OF LED RADIANT INTENSITY

Total optical power produced by LED = 70 mW @ 100 mA

Total optical power emitted into air = $P_T = \eta(I/q)E$

For a typical example where

$\eta = 0.012$

$E = 1.4$ eV (photon energy = hv/λ)

$I = 0.53$ mW/sr

$q = 1.6 \times 10^{-19}$ Coulombs

Now if $A_s = 6.25 \times 10^{-10}$ m^2 (corresponding to a diameter of 50 μm)

Then $R_a = \dfrac{I}{A_s} = 0.27$ W/mm^2/sr

Then $P_T = \dfrac{0.012 \times 0.53 \times 2.2 \times 10^{-19}}{1.6 \times 10^{-19}}$

$= 8.7$ mW

and radiant intensity $R_a = \dfrac{P_T}{A_s} = \dfrac{8.7 \times 10^{-3}}{\pi \times (25 \times 10^{-6})^2}$

$= 1.0 \times 10^5$ W/m^2/sr

CALCULATION OF BACKGROUND OPTICAL NOISE POWER

As discussed in Chapter 1 background noise is of two main types, diffuse and point source. The former is represented by the sky, and stars and the sun are representative of the latter.

The background noise power for a diffuse background is calculated as follows:

Kerr [A9.1] has established that the background noise power, P_b, is given by:-

$$P_b = A_R \ \Omega_R \ B_o N(\lambda)$$

The background shot noise current, I_b, is given by:-

$$I_b = \frac{2q^2 \ \eta \ B_o P_b}{hv}$$

and hence $I_b = 2q^2 \ \eta \ A_R \ \Omega_R \ B_o^2 \ N(\lambda)/hv$

For a typical example where:-

$q = 1.6 \times 10^{-19}$

$\eta = 0.6$

$A_R = 7.9 \times 10^{-3} m^2$ (for d = 0.1 m)

$\Omega_R = 10^{-6}$ rad

Optical BW = $B_o = 0.5$ μm

$N(\lambda) = 30 \ W/m^2/sr/\mu m$ BW

Then typically $P_b = A_R \ \Omega_R . B_o . N(\lambda)$

$= 7.9 \times 10^{-3} \times 10^{-6} \times 0.5 \times 10^{-6} \times 30$

$= 1.2 \times 10^{-13}$ Watts

Reference:

[A9.1] Kerr J R Proc IEEE Vol 55 pp 1686-1700 Oct 1967

CALCULATION OF SHOT NOISE TERM

Shot noise has been well documented [A10.1] and the mean square shot noise current for a PIN diode is given by:-

$$\langle I_{sh}^2 \rangle = 2q\bar{I}\,\Delta f \qquad \text{(A10.1)}$$

where $\bar{I} = I_p + I_D$ (A10.2)

therefore $\langle I_{sh}^2 \rangle = 2q\,[I_p + I_D]\,\Delta f = 2q\,(I_p + I_D)\,B$ (A10.3)

where I_p = signal photocurrent

I_D = photodiode dark current

Now $$I_p = \frac{\eta q}{h\nu} \cdot P_R \qquad \text{(A10.4)}$$

where P_R is the received optical signal power at the detector.

Typically $I_D = 10^{-7}$ A for PIN diodes.

But background radiation will also contribute to shot noise and hence the term I_B must be included in equation (A10.3) where

$$I_B = \frac{\eta q}{h\nu} \cdot P_B \qquad \text{(A10.5)}$$

Thus the complete expression for shot noise in a 2 Mbit/s direct modulation optical line of sight system using a PIN photodiode in the receiver is given by:-

$$\langle I_{sh}^2 \rangle = 2qB \left(\frac{\eta q}{h\nu} \cdot P_R + \frac{\eta q}{h\nu} \cdot P_B + I_D \right) \qquad \text{(A10.6)}$$

$$= 2qB \left(\frac{\eta q}{h\nu} (P_R + P_B) + I_D \right) \qquad \text{(A10.7)}$$

Reference:

[A10.1] Gower J "Optical Communications Systems", Prentice Hall, 1984

CALCULATION OF SHOT NOISE LIMIT

Equation (A10.7) in Appendix 10 gives the expression for shot noise. In a shot noise limited system, the shot noise is, by definition, the dominant noise source and the other noise sources may be ignored hence:-

$$SNR = \frac{\langle I_p \rangle^2}{\langle I_{sh} \rangle^2} \qquad \text{(A11.1)}$$

$$= \frac{\langle I_p \rangle^2}{2qB \left(\frac{\eta q}{h\nu} (P_R + P_b) + I_D \right)}$$

$$\langle I_p \rangle^2 = SNR \times 2qB \left(\frac{\eta q}{h\nu} (P_R + P_b) + I_D \right)$$

$$\frac{\eta q P_R}{h\nu} = (SNR)\, 2qB \left(\frac{\eta q}{h\nu} (P_R + P_b) + I_D \right)$$

$$= (SNR)\,(2qB) \left(\left(\frac{\eta q}{h\nu} \right) P_R + \left(\frac{\eta q}{h\nu} \right) P_b + I_D \right)$$

$$1 = \frac{(SNR)\,(2qB)}{P_R} \left(\frac{h\nu}{\eta q} \right) \left[\left(\frac{\eta q}{h\nu} \right) P_R + \left(\frac{\eta q}{h\nu} \right) P_b + I_D \right]$$

$$= (SNR)\,(2qB) \left[1 + \frac{P_b}{P_R} + \frac{I_D}{P_R} \cdot \left(\frac{h\nu}{\eta q} \right) \right]$$

$$\frac{1}{(SNR)\,(2qB)} = 1 + \frac{P_b\, \eta q + I_D\, h\nu}{P_R\, \eta q}$$

$$SNR = \frac{1}{2qB} \cdot \frac{P_R \eta q}{(P_b \eta q + I_D h\nu + P_R \eta q)}$$

$$= \frac{1}{2qB \left(\frac{P_b}{P_R} + \frac{I_D h\nu}{P_R \eta q} + 1 \right)} \qquad \text{(A11.2)}$$

If P_R is much greater than P_b then this expression reduces to:-

$$\text{Shot noise limited} \quad SNR = \frac{1}{\frac{2qB}{P_R} \cdot \frac{h\nu}{\eta q} \left(I_D + \frac{\eta q}{h\nu} P_R \right)} \qquad \text{(A11.3)}$$

Moreover if the photodiode dark current I_D is negligible then the expression reduces still further to:

$$\text{Shot noise limited SNR} = \frac{1}{2qB} \qquad \text{(A11.4)}$$

Thus for a typical system where B = 10^6 Hz then the shot noise limited signal to noise ratio will be:

$$\text{Shot noise limited SNR} = \frac{1}{2 \times 1.6 \times 10^{-19} \times 10^6}$$

$$= \frac{1}{3.2} \; 10^{13} = 3.1 \times 10^{12}$$

$$= 125 \text{ dB}$$

CALCULATION OF QUANTUM NOISE LIMIT

From Melchior [A12.1] the minimum received power level corresponding to the quantum noise limit for a given SNR and bandwidth B is:-

$$P_{R\ min} = 4 \frac{hv}{\eta} B\ SNR$$

Typically for B = 2 MHz and SNR = 12 then:

$$P_{R\ min} = \frac{4 \times 6.63 \times 10^{-34} \times 3 \times 10^{14} \times 2 \times 10^{6} \times 12}{0.6}$$

$$= 1591.2 \times 10^{-20} \times 2 \times 10^{6}$$

$$= 1.6 \times 10^{-17} \times 2 \times 10^{6}$$

$$= 3.2 \times 10^{-11} = 32\ pW$$

Reference:

[A12.1] Melchior J. Proc IEEE, Vol 58, 10, Oct 1970

SYSTEM PARAMETERS FOR MEASUREMENT PROGRAM

1 2 MBIT/S DIGITAL OPTICAL LINE OF SIGHT SYSTEM

1.1 TRANSMITTER

Source	Burrus type led
Peak wavelength	900 nm
Optical power into air	1.7 mW
Optical irradiance	0.53 mW/sr
Source emission area	2.5×10^{-9} m^2
Source radiance	2.7×10^{5} $W/m^2/sr$
Av drive current	100 mA
Modulation	On/off keying; amplitude modulation
Input interface	HDB 3
Nominal bit rate	2.048 Mbit/s
Lens type	Fresnel (plastic)
Effective lens diameter	0.1 m
Focal length of lens	0.1 m

1.2 RECEIVER

Photodiode	PIN
Min Sensitivity	10 nW @ P(e) = 10^{-10}
First stage amplifier	High impedance FET
Output interface	HDB 3
Lens type	Fresnel (plastic)
Effective lens diameter	0.1 m
Focal length of lens	0.1 m

2 MEASURING EQUIPMENT USED FOR ERROR MEASUREMENT

Pattern Generator	Hewlett Packard Type HP 3781A
Error Detector	Hewlett Packard Type HP 3782A

Computer/Controller	Hewlett Packard Type HP 9915 with tape drive (Option 002)
Programming Computer	Hewlett Packard Type HP 85 series
Printer	Hewlett Packard Thermal Type HP 5150A
Relevant settings:	
Pseudo-random pattern	$2^{15}-1$
Interface	HDB 3
Nominal bit rate	2.048 Mbit/s
Averaging period	30 minutes (see note)

Note: The 30 minute averaging period was selected for the measurements since it was found to be the optimum setting in order that meaningful error rate measurements could be recorded. Settings of less than 30 minutes yielded results which still followed the same trend but the fluctuations in error rate were much greater giving rise to some difficulty in recording a particular error rate at any particular instant which would make it more difficult to discern the correlation between error rate and C_n^2. This is especially true at low error rate levels when only one error might be measured over quite a long period (ie tens of minutes). Chapter 8 addressed this problem in connection with the choice of system bit rate of operation.

THE COMPLEMENTARY ERROR FUNCTION (ERFC) AND THE RELATIONSHIP BETWEEN ERROR RATE AND SIGNAL TO NOISE RATIO

The normal distribution is given by:-

$$p(x) = \frac{1}{\sqrt{2\pi}\,\sigma} \cdot e^{(x-x_o)^2/2\sigma^2} \qquad \text{(A14.1)}$$

where $-\infty < x < \infty$

The cumulative distribution or the probability that the random variable x is less than some value x is given by:-

$$p(x<\chi) = \int_{-\infty}^{x} p(x)\,dx = \int_{-\infty}^{x} \frac{e^{-(x-x_o)^2/2\sigma^2}}{\sqrt{2\pi}\cdot\sigma}$$

$$= \tfrac{1}{2}\,(1 + \text{erf}\,(x-x_o)/\sigma) \qquad \text{(A14.2)}$$

where $\text{erf}\ u = \frac{2}{\sqrt{2\pi}} \int_{o}^{u} e^{-t^2/2}\,dt$

is known as the error function. The complementary error function erfc is given by:-

$$\text{erfc}(x) = 1 - \text{erf}(x) \qquad \text{(A14.3)}$$

It can be shown [A14.1] that the possibility of an error in the presence of gaussian noise is given by:-

$$Pe = \tfrac{1}{2}\,(1 - \text{erf}\ Q)$$

$$= \tfrac{1}{2}\,\text{erfc}\ Q \qquad \text{(A14.4)}$$

$$= \tfrac{1}{2}\,\text{erfc}\ \tfrac{1}{2}\,(S/N)^{\frac{1}{2}} \qquad \text{(A14.5)}$$

where $S/N = 4\,Q^2$

Expressions (A14.4) and (A14.5) have been computed and the relationships between the different parameters are shown in Table A14.1.

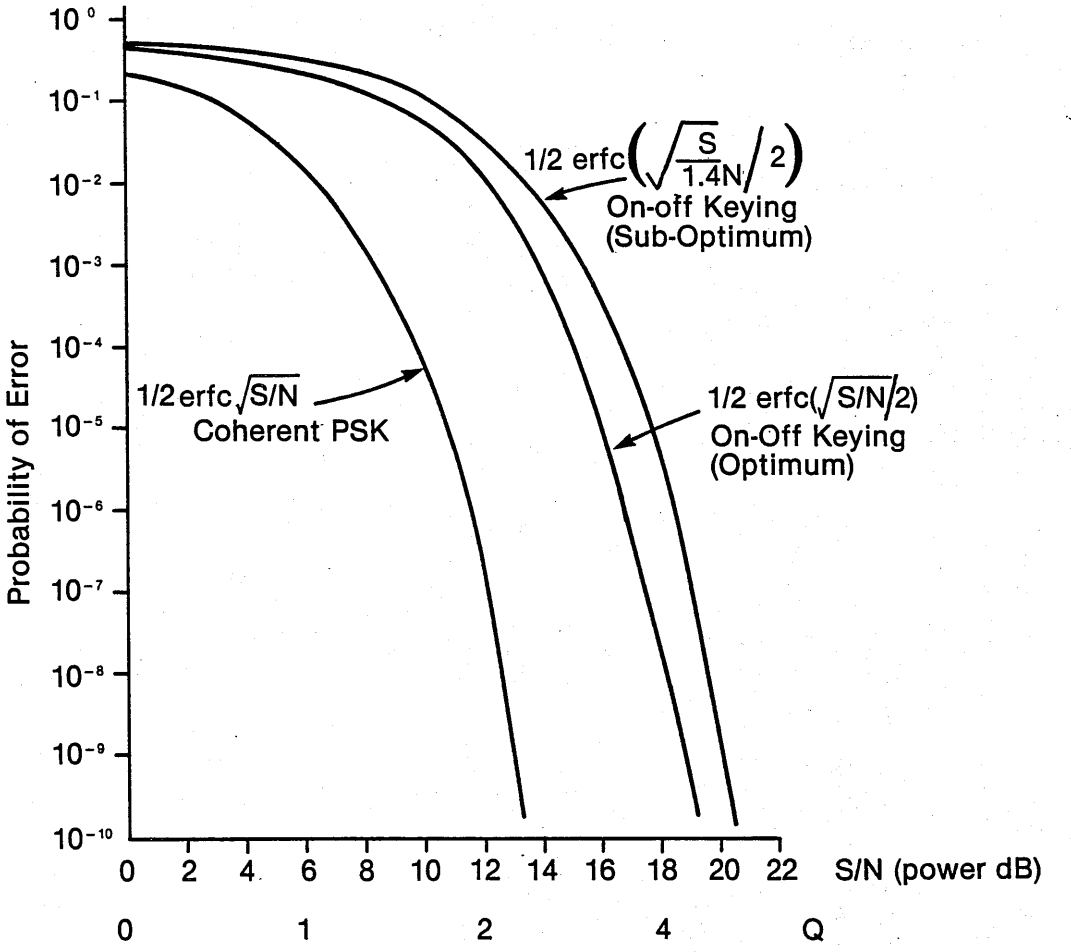

Figure A14.1 Error rate versus signal/noise ratio characteristic. (reference [A14.4])

Q	$S/_N$ RATIO	$S/_N$ dB	P(e)
2	16	12	2.28 E-2
3	36	15.6	1.35 E-3
4	64	18	3.17 E-5
5	100	20	2.87 E-7
6	144	21.6	9.90 E-10
7	196	22.9	2.58 E-12

Table A14.1 Relationship Between Q, SNR and P(e)

$Q = \frac{1}{2}\sqrt{S/_N}$ is a factor employed by Personick [A14.2] and Smith et al [A14.3] in computations of signal to noise ratio and error rate.

Figure A14.1 plots the results for on-off keying and coherent PSK systems.

[A14.1] Bylanski P & Ingram D 'Digital Transmission Systems', Peter Peregrinus, 1976

[A14.2] Personick S · BSTJ 52, pp 843-886 (1973)

[A14.3] Smith D R et al OQE 10, pp 293-300 (1978)

[A14.4] Schwartz M., Bennett W. and Stein S. 'Communications Systems and Techniques' McGraw-Hill, 1966

TERMS AND DEFINITIONS

The terms and definitions used in this thesis are in accordance with those prepared for the International Electro-technical Vocabulary by the Joint Co-ordinating Group (JCG Working Group '0') of the International Electro-technical Commission (IEC) and the International Consultative Committee on Telephones and Telegraphs (CCITT) under the Chairmanship of Mr C J Lilly, British Telecom UK.

In order to facilitate a ready understanding of the contents of this thesis some basic optical terms and their corresponding definitions have been extracted from the above-mentioned vocabulary and included in this Appendix as follows:

1 Radiant energy:

Energy that is transferred via electromagnetic waves, expressed in joules.

2 Radiant power; Optical power; Optical flux; Radiant flux:

The time rate of flow of radiant energy, expressed in watts.

3 Radiant intensity:

Radiant power, in a given direction, per unit solid angle, expressed in watts per steradian.

4 Radiance:

Radiant power, in a given direction, per unit solid angle per unit of projected area of the source, as viewed from that given direction. Radiance is expressed in watts per steradian per square meter.

Note: Previously known as brightness.

5 Irradiance; Power density

Radiant power incident per unit area upon a surface, expressed in watts per square meter.

6 Intensity:

The square of the electric field amplitude of a light wave.

Note: Intensity is proportional to irradiance and may be used in place of the term "irradiance" when only relative values are important. See also: Radiant intensity.

7 Radiant emittance; Radiant exitance:

The total power emitted by a unit area of a source, expressed in watts per square meter.

8 Spectral radiance:

Radiance per unit wavelength interval at a given wavelength, expressed in watts per steradian per unit area per wavelength interval.

9 Spectral irradiance:

Irradiance per unit wavelength interval at a given wavelength, expressed in watts per unit area per unit wavelength interval.

10 Geometric optics; Ray optics:

The treatment of propagation of light as rays.

Note: Rays are bent at the interface between two dissimilar media or may be curved in a medium in which refractive index is a function of position. See also: Physical optics.

11 Physical optics; Wave optics:

The treatment of propagation of light as a wave phenomenom rather than a ray phenomenon, as in geometric optics.

12 Gaussian beam:

A beam of light whose electric field amplitude distribution is gaussian.

Note: When such a beam is circular in cross section, the amplitude is:

$$E(r) = E(0) \exp [-(r/w)^2]$$

where r is the distance from beam centre and w is the radius at which the amplitude is 1/e of its value on the axis; w is called the beamwidth.

13 Beam diameter; Beamwidth:

The distance between two diametrically opposed points at which the irradiance is a specified fraction of the beam's peak irradiance; most commonly applied to beams that are circular or nearly circular in cross section.

14 Beam divergence:

i For beams that are circular or nearly circular in cross section, half the angle subtended by the far-field beam diameter.

ii For beams that are not circular or nearly circular in cross section, half the far-field angle subtended by two diametrically opposed points in a plane perpendicular to the optical axis, at which points the irradiance is a specified fraction of the beam's peak irradiance. Generally, only the maximum and minimum divergences (corresponding to the major and minor diameters of the far-field irradiance) need be specified.

15 Log normal distribution:

A normal distribution in which the logarithms of the variable is used rather than the basic variable.